Interactions between commensal obligate anaerobes and human intestinal cells

A thesis presented in partial fulfilment of the requirements for the degree of

Doctor of Philosophy

Massey University

Manawatu, New Zealand

Dulantha Ulluwishewa

2013

ABSTRACT

The human intestinal epithelium is formed by a single layer of epithelial cells which regulates intestinal barrier permeability. Increased permeability can result in the entry of potentially harmful compounds into the body, and is implicated in autoimmune, inflammatory and atopic diseases. The intestinal tract is inhabited by an estimated 10^{14} microbes and it is increasingly evident that they affect intestinal barrier function. However, over 90% of commensal intestinal bacteria are obligate anaerobes, making it difficult to co-culture them with oxygen-requiring mammalian cells *in vitro*.

To investigate the interactions between obligate anaerobes and epithelial cells that regulate the intestinal barrier, an apical anaerobic model of the human intestinal epithelium, which utilises a dual-environment co-culture chamber, was developed and validated. The chamber allowed for polarised monolayers of the intestinal cell line Caco-2 to be grown such that the apical (luminal) side was exposed to an anaerobic environment, while maintaining an aerobic basal side. The cell viability and barrier function of Caco-2 monolayers was unaffected by culture in the apical anaerobic model for at least 12 hours. Global gene expression analysis predicted upregulation of cell survival and proliferation in Caco-2 cells cultured in the apical anaerobic model, compared to Caco-2 cells grown under conventional conditions, suggesting an adaptation of the Caco-2 cells to a lower supply of oxygen.

The apical anaerobic model was used to co-culture the commensal obligate anaerobe *Faecalibacterium prausnitzii* with Caco-2 cells. The survival of *F. prausnitzii* was improved in the anaerobic apical environment compared to when cultured in an aerobic atmosphere. Live *F. prausnitzii*, but not non-viable (UV-killed) *F. prausnitzii*, were shown to increase permeability across Caco-2 monolayers. Furthermore, global gene expression analysis suggested that live *F. prausnitzii* cells have more profound effects on Caco-2 cells than non-viable *F. prausnitzii*, illustrating the importance of maintaining viability of obligate anaerobes in an *in vitro* co-culture system.

The apical anaerobic model can be used to gain insights into the mechanisms of crosstalk between commensal obligate anaerobic bacteria and intestinal cells, and new knowledge generated using this model will assist in the development of strategies to improve intestinal barrier function.

Dedicated to aththamma, seeya, and 'big' aththamma.
My greatest inspirations. Love always.

ACKNOWLEDGEMENTS

It is with immense gratitude that I acknowledge the guidance and support of my supervisors: Prof Warren McNabb, Dr Nicole Roy, Dr Rachel Anderson, Prof Jerry Wells, and Prof Paul Moughan. To Warren and Paul, thank you for taking me under your wing and making me part of AgResearch and the Riddet Institute. Rachel, thank you for always being available to answer my questions; I have truly appreciated your help and advice. Jerry, thank you for sharing your wisdom and enthusiasm, and imparting some of your expertise to me, it was my privilege to have you as a supervisor. Nicole, it has been my pleasure to study under your guidance - thank you for your kindness and unwavering support. I also acknowledge AgResearch and the Riddet Institute, a Centre of Research Excellence, for funding this research and my PhD fellowship, and providing me with excellent research facilities.

I am indebted to many people for their support and assistance in the completion of this thesis. The co-culture chamber, instrumental for achieving the aims of this thesis, was designed based on the concept conceived by Prof Denise Kelly (University of Aberdeen), and built by Steve Gebbie, Scott Sevier, Hong Zhang, Russel McAuliffe, Paul Lovejoy and Jason Peters. I am most grateful for the technical assistance of Kelly Armstrong (microarrays), Eva Maier (co-culture experiments), Dr Dmitry Sokolov (from the Manawatu Microscopy and Imaging Centre, Massey University; confocal microscopy) and Cécile Mourette (model validation experiments). I share the credit for the microarray analysis with Dr Wayne Young who processed the raw microarray data and generated the heatmaps presented in this dissertation. The imaging of cells by transmission electron microscopy was carried out by Dr Duane Harland and James Vernon at AgResearch Lincoln Research Centre.

I owe my deepest gratitude to Dr John Koolaard for his invaluable advice on most of the statistical analysis carried out in this project. I would also like to acknowledge Dr Mark McCann (cell culture, flow cytometry, qPCR), Graham Naylor (anaerobic microbiology), Dr Adrian Cookson (microbiology), Dr Jurgen Karczewski (confocal microscopy and cell viability assay), Bruce Sinclair (dissolved oxygen assays), Dr Peter van Baarlen (microarray analysis) and Catherine Lloyd-West (statistical analysis) for their valuable advice and sharing their expertise. My thanks also

go to Dr Anna Russ for proof-reading this dissertation and providing me with valuable feedback.

I would also like to thank my many colleagues in AgResearch, especially the PhD students I shared an office with during the course of this project, for their friendship, support and help over the past few years. Thank you for listening and encouraging me through the triumphs and trouble of this study, and providing valuable and entertaining discussions on matter related (or not) to my research. Thank you also to the AgResearch support staff including Denise Martin and Information Services, whose help has been invaluable in carrying out many of the tasks and activities along the road to completing this thesis.

Finally, to my family and friends, especially my parents and sister, thank you for your love and support, and the sacrifices you made to create opportunities for me that you never had. To my wife Neranjala, thank you for your constant encouragement and making me see the positive in every situation - you have brightened up my life in a way I never knew possible. This dissertation is a testament to your unyielding faith in me during my PhD journey.

TABLE OF CONTENTS

LIST OF FIGURES

LIST OF TABLES

LIST OF ABBREVIATIONS

ANOVA	Analysis of variance
ATCC	American Type Culture Collection
BHI	Brain-heart infusion
BLASTN	NCBI nucleotide Basic Local Alignment Search
CAR	Coxsackie and adenovirus receptor
cDNA	Complementary DNA
CFU	Colony-forming units
cIAP	Cellular inhibitor of apoptosis protein
CLA	Conjugated linoleic acids
CRE	cAMP response element
CREB	CRE-binding protein
cRNA	Complementary RNA
DC	Dendritic cells
ddNTPs	Dideoxynucleotides
DGGE	Denaturing gradient gel electrophoresis
DHA	Docosahexaenoic acid
DMSO	Dimethyl sulfoxide
DNA	Deoxyribonucleic acid
dNTP	Deoxyribonucleotide
DO	Dissolved oxygen
DSMZ	Deutsche Sammlung von Mikroorganismen und Zellkulturen (German Collection of Microorganisms and Cell Cultures)
EDTA	Ethylenediamine tetra-acetic acid
EGCG	Epigallocatechin gallate

EHEC	Enterohemorrhagic *Escherichia coli*
EIEC	Enteroinvasive *Escherichia coli*
EPA	Eicosapentaenoic acid
EPEC	Enteropathogenic *Escherichia coli*
ERK	Extracellular signal regulated kinases
FBS	Foetal bovine serum
FSH	Follicle stimulating hormone
GFP	Green fluorescent protein
GLA	γ-linolenic acid
GO	Gene ontology
hCGΔ	Choriogonadotropin
HIF	Hypoxia-inducible factor
IBD	Inflammatory bowel disease
IEC6	Intestinal epithelial cell line 6
IFN	Interferon
Ig	Immunoglobulin
IKK	IκB kinase
IL	Interleukin
IPA	Ingenuity Pathway Analysis
IRAK	IL-1-receptor-asociated kinase
IRF	IFN-regulatory factor
IκB	Inhibitor of NF-κB
JAM	Junctional adhesion molecules
KEGG	Kyoto Encyclopaedia of Genes and Genomes
Lh	Luteinising hormone
LOESS	Locally weighted smoothing spline

LSD	Least significant difference
M199	Medium 199
MAMPs	Microbe-associated molecular patterns
MAPK	Mitogen activated protein kinases
MDCK	Madin Darby canine kidney
MLC	Myosin II regulatory light chain
MLCK	Myosin light chain kinase
MOI	Multiplicity of infection
mRNA	Messenger RNA
MRS	Man, Rogosa and Sharpe
MyD88	Myeloid differentiation primary response gene
NCBI	National Center for Biotechnology Information
NEAA	Non-essential amino acids
NF-κB	Nuclear factor kappa B
NOD	Nucleotide-binding and oligomerisation-domain
NRF2	NF-E2-Related Factor 2
OD	Optical density
PAMPs	Pathogen-associated molecular patterns
pamr	Prediction Analysis for Microarrays
PC	Polycarbonate (Transwell® cell culture inserts)
PCA	Principal component analysis
PCR	Polymerase chain reaction
PDZ	PSD95–DlgA–ZO-1 homology
PEPT1	H+/di-tripeptide transporter
PET	Polyester (Transwell® cell culture inserts)
PGE2	Prostaglandin E2

PI	Propidium iodide
PKC	Protein kinase C
PLA2	Group IIA phospholipase A2
PPAR	Peroxisome-proliferator-activated receptor
PRRs	Pathogen recognition receptors
PTFE	Polytetrafluoroethylene (Transwell® cell culture inserts)
q	False discovery rate
REML	Restricted maximum likelihood
RICK	Receptor-interacting serine/threonine kinase
RNA	Ribonucleic acid
RNase	Ribonuclease A
ROCK	Rho kinases
ROS	Reactive oxygen species
rRNA	Ribosomal RNA
SCFAs	Short chain fatty acids
SDS	Sodium dodecyl sulphate
SEM	Standard error of the mean
SULTs	Sulfotransferases
TAK-1	Transforming growth factor-β-activated kinase-1
TEER	Transepithelial electrical resistance
TGF	Transforming growth factor
TJ	Tight junction
TLR	Toll-like receptor
TNF	Tumour necrosis factor
TNFR	Tumour necrosis factor receptor
TRAF6	TNF-receptor-associated factor 6

TREM	Triggering receptor expressed on myeloid cells
TSLP	Thymic stromal lymphopoietin
UV	Ultraviolet
VegF	Vascular endothelial growth factor
ZO	Zonula occludens

INTRODUCTION

Around 400 B.C., Hippocrates is quoted as saying that "death sits in the intestines"[1]. With an estimated surface area of 200-400 m^2, the intestine is the largest interface between the human body and the outside environment[2,3]. The intestinal surface is continuously exposed to large amounts of food, chemicals, bacteria, and potentially harmful antigens. Thus, in addition to its role in food digestion and nutrient absorption, the intestine also functions as a barrier, preventing unwanted compounds from entering the body.

Proper regulation of the intestinal barrier is vital for optimal health. Usually only small amounts of antigens enter the mucosa and interact with the local and systemic immune systems, thus allowing for controlled activation of the immune system. However, when barrier function is compromised, abnormal antigen exposure results in disruption of the balance between antigen exposure and immune activation, which leads to local or systemic inflammatory disorders[4,5,6]. A leaky barrier is a critical determinant in the predisposition to intestinal inflammation and a number of intestinal diseases, such as coeliac disease[7] and inflammatory bowel disease (IBD)[8], and functional intestinal disorders such as irritable bowel syndrome[9]. A leaky barrier is also a major contributing factor in predisposing to autoimmune disease and inflammatory disease in other parts of the body such as type I diabetes[10], and multiple sclerosis[11], further illustrating the importance of a functional intestinal barrier in human health.

The human intestinal barrier is a complex ecosystem combining the intestinal epithelium, immune cells of the lamina propria and the commensal microbiota[12]. The commensal microbiota is made up of an estimated 10^{14} microbes, composed of about 500-1000 bacterial species[13]. It is becoming increasingly evident that these microbes, and their metabolites, are key mediators of the 'crosstalk' between the epithelium and other cell types in the mucosa, and that their interactions with the epithelium influence aspects of intestinal barrier function[14]. In several disorders where the intestinal barrier integrity is known to be compromised, it has also been shown that the intestinal microbiota composition is altered[15,16,17].

Whilst an understanding of the mechanisms involved in some host-microbe interactions in the intestines is emerging, there are important aspects that have been neglected to date. For example, the majority of the published research investigating

intestinal host-microbe interactions focuses on oxygen-tolerant bacterial species; however, most (over 90%) of the 1.5-3 kg of bacteria resident in the human intestine are obligate anaerobic bacteria that cannot survive in the presence of oxygen[18,19]. This knowledge gap is due to the technical difficulty in co-culturing oxygen-requiring mammalian cells with oxygen-intolerant obligate anaerobic bacteria. Efforts into further understanding the mechanisms of crosstalk between anaerobic commensal bacteria and intestinal cells could have a major impact on human health.

Chapter 1:

Review of literature[†]

[†] Selected material from this section was published as a critical review in the Journal of Nutrition: Ulluwishewa D, Anderson RC, McNabb WC, Moughan PJ, Wells JM & Roy NC. Regulation of tight junction permeability by intestinal bacteria and dietary components. *J Nutr*. 2011 May;141:769-76.

1.1 THE HUMAN INTESTINAL BARRIER

In addition to food digestion and nutrient absorption, the intestine also functions as a barrier between the external environment and the human body. The human intestine, as the largest interface between a host and its external environment (> 300 m^2), is exposed to a large number of pathogenic and commensal microbiota as well as other luminal antigens.

The human intestinal barrier is a complex ecosystem combining the intestinal epithelium, immune cells of the lamina propria and the commensal microbiota[12]. Further, the epithelial surface is covered by a layer of mucus, which together with the commensal microbiota provides the first layer of defence against pathogens[20] (Figure 1.1).

Immunological tolerance is maintained by the ability of the epithelial barrier to restrict the penetration of microbes and antigens to low levels, and the distinctly anti-inflammatory tone of the mucosa[21]. Additionally the specialised antigen sampling sites of the mucosal associated lymphoid tissue are adapted to induce local protective mucosal antibody responses without the induction of systemic immunity and inflammation. When the barrier function is compromised, abnormal antigen exposure results in disruption of the balance between tolerance and immune activation, which leads to inflammatory disorders. Conversely, immune activation has been shown to lead to barrier dysfunction, so it is unclear whether the loss of barrier function is a cause or an effect of inflammatory disorders[22]. While restoration of barrier function has been shown to have beneficial effects, barrier dysfunction alone is unlikely to cause disease[23]. Nevertheless it is evident that the integrity of the intestinal epithelial barrier is crucial for the balance between health and disease.

Increased intestinal permeability is associated with chronic inflammatory diseases of the intestine, such as IBD[8] and coeliac disease[7]. In type I diabetes, an autoimmune disease, patients have increased small intestinal permeability[10]. The incidence of diabetes can be reduced in diabetes-prone rats by preventing an increase in epithelial permeability[24]. Breakdown of the intestinal barrier is also implicated in immune reactions that target organs outside the digestive tract, leading to diseases such

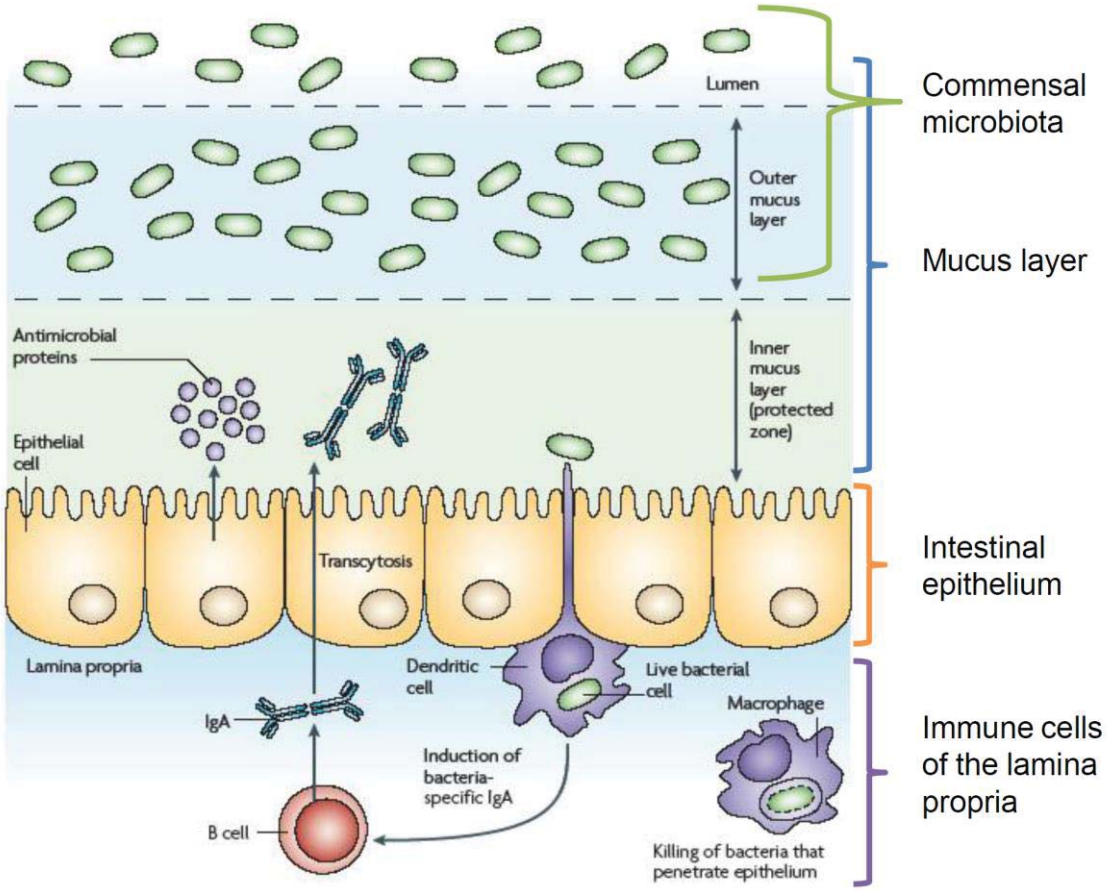

Figure 1.1 Components of the intestinal barrier.

The intestinal epithelium is a single layer of epithelial cells which separates the intestinal lumen from the internal milieu. A layer of mucus protects the epithelium and retains a high concentration of antimicrobial compounds close to the epithelium. Immune cells of the lamina propria help in the defence against pathogens and the maintenance of tolerance towards commensal bacteria. Commensal bacteria protect against pathogens by secretion of bacteriocins and competing for binding spaces and nutrients with pathogens. Figure adapted from Hooper (2009)[25].

as IgA nephropathy[26], non-alcoholic hepatic steatohepatitis[27], and multiple sclerosis in the brain[11]. Furthermore, entry of unwanted antigens through a dysregulated intestinal barrier can lead to systemic inflammatory response syndrome, characterised by a whole-body inflammatory state, and multiple organ failure[5].

The intestinal barrier can also be compromised in individuals with no predisposing conditions. For example, transepithelial permeability of the colon has been shown to increase with age in rats[28,29], suggesting that intestinal barrier integrity may decrease in healthy individuals as they age (though this has not been proven in humans[30]). Physiological conditions, such as stress, have also been shown to increase epithelial permeability[31].

1.2 THE INTESTINAL EPITHELIAL BARRIER

The physical component of the intestinal barrier is the epithelium, made up of a single layer of columnar epithelial cells that separates the intestinal lumen from the underlying lamina propria[5]. The intestinal epithelial cells are mainly absorptive enterocytes (over 80%) but also include enteroendocrine, goblet and Paneth cells[32]. Enteroendocrine cells and goblet cells secrete hormones and mucus respectively. Paneth cells defend against pathogenic bacteria by synthesising antimicrobial peptides and proteins.

Intestinal epithelial cells are polarised cells that have multiple extensions, known as microvilli, on the apical pole[33]. Microvilli are membrane protrusions that form the 'brush border', and their main role is to increase the apical surface area for greater nutrient absorption. In the small intestine the epithelium folds to form many finger-like projections known as villi, which further increases the surface area[32]. The epithelium also folds to form a number of invaginations called crypts embedded in the underlying connective tissue. Near the base of the crypts reside the pluripotent stem cells, which regenerate the intestinal epithelium.

An important component of the epithelium is the intracellular junctional complex, consisting of tight junctions (TJ), adherens junctions, desmosomes and gap junctions[34]. TJ are located at the luminal aspect of the lateral membranes and are the most apical structures of the junctional complex. They seal the paracellular space between the epithelial cells, thus preventing paracellular diffusion of microorganisms and other antigens across the epithelium[34]. However, TJ are not static barriers but rather

highly dynamic structures that are constantly being remodelled due to interactions with external stimuli such as food residues, and pathogenic and commensal bacteria[35]. They can regulate the entry of luminal nutrients, ions and water while restricting pathogen entry and thus regulate the barrier function of the epithelium. Adherens junctions are located beneath the TJ and are involved in cell-cell adhesion and intracellular signalling[36]. Both TJ and adherens junctions (together known as the 'apical junctional complex') are associated with the actin cytoskeleton[36,37]. Desmosomes and gap junctions are involved in cell-cell adhesion[38] and intracellular communication[39], respectively. The cytoskeleton is an intricate structure of protein filaments that extends throughout the cytosol and is essential for maintaining the structure of all eukaryotic cells. Disruption of the cytoskeleton is linked to the loss of intestinal barrier integrity[40].

There are two main routes of entry though the epithelium. Molecules can either be transported across the cells (transcellular pathway), or between the cells of the epithelium (paracellular pathway)[41]. While small molecules such as sugars and amino acids are transported via the transcellular pathway, larger hydrophilic molecules such as bioactive peptides, hormones and vaccines need to be absorbed via the paracellular pathway to enter systemic circulation from the intestinal lumen[42]. It has been estimated that under normal conditions the paracellular pathway is restricted to molecules with molecular radii of less than 11 Å [42], while charge selective pores within the TJ restrict molecules greater than 4 Å [43]. The intercellular junctional complexes, and their interactions with the actin cytoskeleton, regulate the paracellular permeability, and are crucial for the integrity of the epithelial barrier.

1.2.1 Tight junction structure and regulation of intestinal permeability

TJ are complex structures comprising over 50 proteins. They include a series of transmembrane proteins, which form fibrils that cross the plasma membrane and interact with proteins in the adjoining cells[44]. The transmembrane proteins interact with the actin cytoskeleton within the cell through plaque proteins, which act as cytoplasmic adaptors[45]. Plaque proteins are also involved in the clustering and stabilisation of transmembrane proteins. TJ, along with the adherens junctions, are intimately linked to the perijunctional acto-myosin ring, a belt like structure formed by actin and myosin II that encircles the apical pole of epithelial cells[37]. This belt projects actin filaments that

interface with the TJ, and thus circumferential contractions of the perijunctional actomyosin ring regulate TJ structure and paracellular permeability (Figure 1.2). While this section of the review of literature gives an overview of TJ structure and regulation, comprehensive reviews on the complex molecular structure of TJ are available (e.g. Furuse (2010)[46]).

Transmembrane proteins mediate cell-to-cell adhesion and seal the paracellular space between epithelial cells. They can be divided into tetra-span and single-span proteins. The tetra-span proteins are occludin, the claudin family of proteins, and tricellulin. Tetra-span proteins contain four transmembrane domains, and two extracellular loops, with the N and C terminals in the cytoplasm[47,48,49]. Single span transmembrane proteins are mostly junctional adhesion molecules (JAM)[50].

The claudin proteins are considered to be the structural backbone of TJ[51]. In the intestine, claudin-1, -3, -4, -5 and -8 tighten TJ (decrease paracellular permeability), while claudin-2 forms charge-selective paracellular pores (reviewed in Bücker *et al.* (2010)[52]). The function of claudins-7, -12 and -15 is unclear because their effects on intestinal barrier function vary depending on the model system studied[52]. Occludin has also been linked to the regulation of intermembrane diffusion and paracellular diffusion of small molecules[53]. Compared with cultures of Madin Darby canine kidney (MDCK) cells expressing wild-type occludin, cultures expressing truncated occludin mutants exhibit increased paracellular flux of small molecule markers, while transepithelial electrical resistance (TEER), a measure of paracellular ion permeability, is unaffected[53]. While claudin seals the space in between two adjacent cells, the barrier at the junctions between three epithelial cells is reinforced by tricellulin. Suppression of tricellulin gene expression impairs epithelial barrier integrity[49].

The JAM family consists of a transmembrane domain and a C-terminal cytoplasmic domain[54]. JAM-A and coxsackie and adenovirus receptor (CAR), two examples of JAM proteins, have been shown to regulate epithelial barrier function, as expression of either protein leads to a reduction in paracellular permeability[55,56]. These proteins are also implicated in TJ assembly. JAM-A and CAR recruit specific TJ proteins and promote their localisation at cell boundaries[56,57]. Inhibition of JAM-A also prevents TJ reassembly and recovery of TEER after disruption by calcium depletion in cultured T84 epithelial monolayers[58].

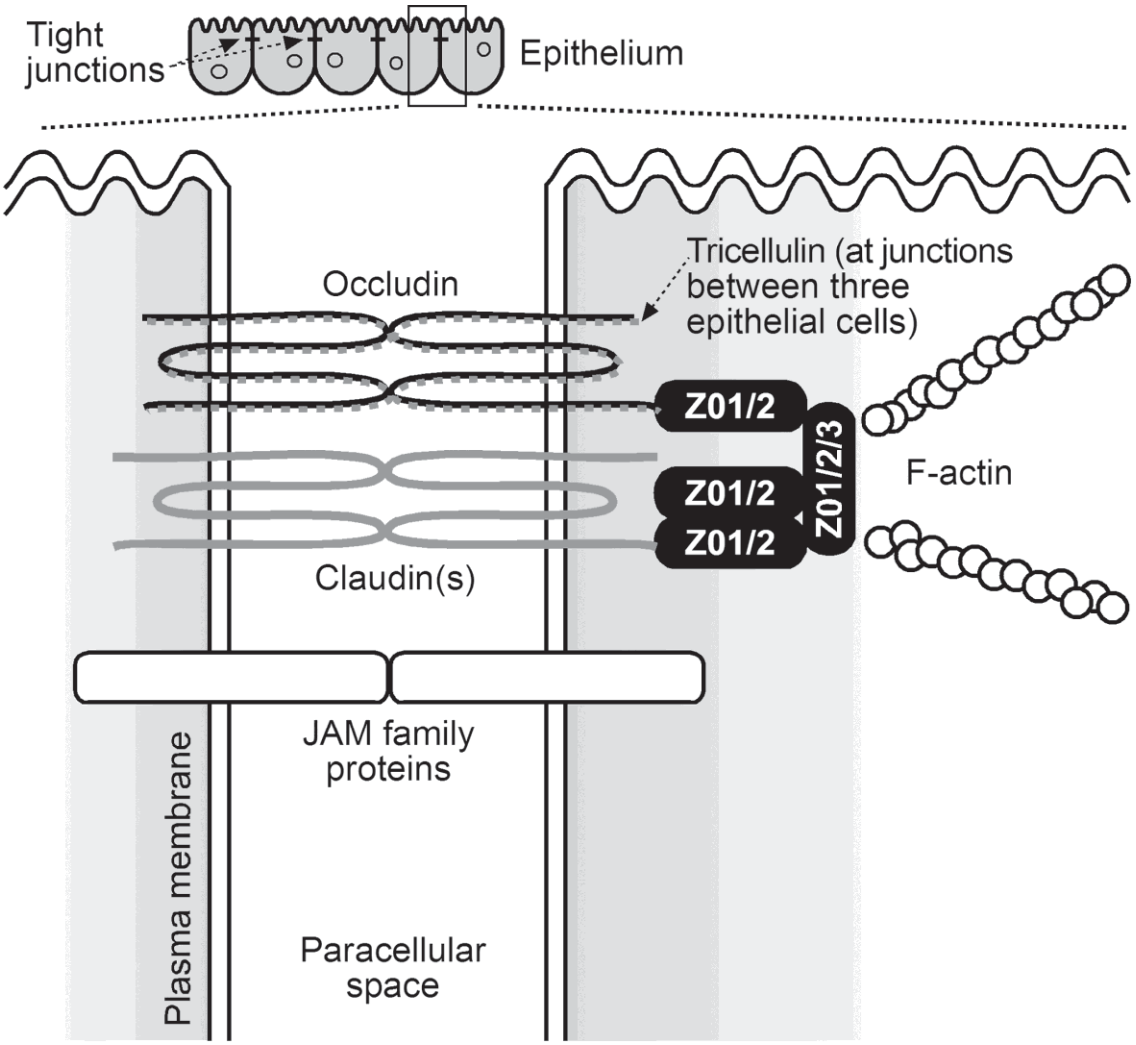

Figure 1.2 Structure of tight junctions.

Transmembrane proteins such as occludin and claudin (tetra-span) and JAM (single span) seal the paracellular space between adjacent epithelial cells. Plaque proteins, such as the ZO family proteins, act as adaptors which connect transmembrane proteins to the perijunctional actomyosin ring. Figure: Ulluwishewa *et al.* (2011)[59].

Plaque proteins are characterised by PSD95–DlgA–ZO-1 homology (PDZ) domains. The PDZ domains of plaque proteins bind to PDZ domains of other proteins forming a scaffold, or interact with specific C-terminal sequences of transmembrane proteins to anchor them to the cytoplasm[60]. Several PDZ proteins have been identified, including the zonula occludens (ZO) proteins, ZO-1, ZO-2 and ZO-3, that all possess three PDZ domains. The first PDZ domain of ZO-1 interacts with the claudin proteins[61], the second domain of ZO-1 interacts with other ZO proteins to form dimers[62], while the third PDZ domain of ZO-1 interacts with JAM-A[63]. Plaque proteins potentially play a central role in TJ regulation as they can cause reorganisation of the cytoskeleton. ZO-1, for example, binds directly to F-actin[64], while AF-6 (another binding partner of JAM-A) is an effector of the Rho-family of small GTPases, signaling proteins involved in TJ regulation[65].

1.2.2 Regulation of tight junctions

Regulation of the assembly, disassembly and maintenance of TJ structure is influenced by various physiological and pathological stimuli. Signalling pathways involved in TJ regulation, and interactions between transmembrane proteins and the actomyosin ring are controlled by several signalling proteins, including protein kinase C (PKC), mitogen activated protein kinases (MAPK), myosin light chain kinase (MLCK), and the Rho family of small GTPases. Phosphorylation of TJ proteins has also been shown to affect epithelial barrier function. For example, in MDCK epithelial cell monolayers with a high TEER, ZO-1 is less phosphorylated than in monolayers with a low TEER[66]. Phosphorylation of claudin proteins has been linked to both increases and decreases of TJ permeability (reviewed in Findley and Koval (2009)[67]). Also, the association of occludin with TJ is thought to require its phosphorylation[68].

Intestinal epithelial cells express a range of PKC isoforms, involved in various signal transduction pathways. Comprehensive reviews describing the role of the various isoforms are available (e.g. Farhadi *et al.* (2006)[69]). Specific PKC isoforms have also been shown to increase or decrease TEER in intestinal epithelial cell monolayers[70]. PKC has also been implicated in the toll-like receptor (TLR)2 pathway, which as discussed in section 1.7, plays a key role in microbial recognition and immune modulation[71]. Stimulation of the TLR2 pathway leads to activation of PKCα and PKCδ, which in turn leads to an increase in TEER and a redistribution of ZO-1.

MAPK responds to stimuli such as growth factors and various stresses[72]. The MAPK pathway is based on a 'phosphorelay' system where protein kinases phosphorylate and activate one another[73]. Epithelial growth factor, which prevents TJ disruption caused by hydrogen peroxide, does so via a MAPK pathway[74]. Extracellular signal regulated kinases (ERK), a group of MAPK, have been shown to interact directly with the C-terminal region of occludin to prevent hydrogen peroxide-induced disruption to TJ[74].

Contractions in the actomyosin ring are largely regulated by phosphorylation of myosin II regulatory light chain (MLC) by MLCK. In the human colon carcinoma cell line Caco-2, initiation of Na^+-glucose co-transport is followed by increased phosphorylation of MLC[75]. Inhibition of MLCK prevents increases in TJ permeability. MLCK mediated regulation of TJ permeability is also a crucial intermediate step in a variety of pathways employed by other extracellular stimuli, such as cytokines and bacteria, to regulate the TJ barrier (e.g. Scott *et al.* (2002)[76]).

MLC phosphorylation is also implicated in the assembly and regulation of TJ. In a study by Shen *et al.* (2006) [77], a Caco-2 cell line expressing a constitutively active MLCK mutant under the control of an inducible promoter was produced. Inducing MLCK in fully differentiated Caco-2 cell monolayers led to a reduction in TEER and redistribution of ZO-1 and occludin.

The Rho family of small GTPases, RhoA, Rac and Cdc42, are implicated in the regulation of TJ structure and function, and the perijunctional actomyosin ring[78]. Downstream effectors of Rho (known as Rho kinases (ROCK)), phosphorylate MLC, induce contraction of the actomyosin ring[79]. Further demonstrating its importance in TJ regulation, inhibition of ROCK prevents proper localisation of TJ proteins during TJ assembly in cultured T84 monolayers[80].

Rho GTPase mediated regulation of TJ is complex, as there are multiple interactions between the different Rho proteins. For example, inactivation of Rho leads to redistribution of ZO-1 and occludin away from the cell membrane, and reorganisation of perijunctional F-actin, which leads to reduced TEER and increased paracellular flux[78]. Increased activation of Rho, however, can also lead to increased TJ disassembly via contraction of the actomyosin ring induced by increased Rho/ROCK signalling and increased MLC phosphorylation[81].

1.2.3 Effects of dietary components on tight junction integrity

TJ can be regulated by dietary components. In patients with coeliac disease, pathogenesis is induced by gliadin, a glycoprotein present in wheat. When rat small intestinal epithelial cell line 6 (IEC6) and Caco-2 cells are exposed to gliadin *in vitro*, interaction between occludin and ZO-1 is compromised and the cytoskeleton is rearranged, leading to increased monolayer permeability[82]. The mechanism for this has been linked to zonulin, the human homologue of the ZO toxin from *Vibrio cholera* that is known to modulate TJ[83]. Gliadin induces zonulin release, leading to PKC-mediated cytoskeletal reorganisation[84]. *Ex vivo* human intestinal samples from coeliac patients in remission also showed zonulin release when exposed to gliadin, causing cytoskeletal rearrangement and ZO-1 reorganisation, leading to increased permeability[82]. Gliadin causes zonulin release by binding to the CXCR3 receptor in intestinal cells[85].

Most food components have not been studied in this way. However, in a screening of vegetable extracts, an extract of sweet pepper was found to decrease TEER in Caco-2 cell monolayers after a 10 minute incubation period[86]. In another study, *Solanaceae* spices, such as cayenne pepper (*Capsicum frutescens*) and paprika (*Capsicum anuum*), were found to cause an immediate decrease in TEER *in vitro* in the ileocecal adenocarcinoma cell line, HCT-8[87]. In the case of paprika, this is accompanied by an increase in small molecule permeability and reorganisation of ZO-1 protein. Conversely, black pepper (*Piper nigrum*), green pepper, nutmeg and bay leaf extracts caused an increase in TEER, although small molecule permeability and ZO-1 organisation were not affected. The active compound in sweet pepper was identified as capsianoside, and this was shown to reorganise actin filaments and decrease TEER[88]. The increase in TEER caused by black and green pepper can be attributed to piperine[87]. While the authors speculated that the decrease in ion permeability was caused by cell swelling, the possible involvement of TJ was not investigated.

In a more recent screening of over 300 food extracts, galangal (*Alpinia officinarum*), marigold (*Tagetes erecta*), *Acer nikoense*, and hops (*Humulus lupulus*) were found to decrease TEER and increase paracellular flux of Lucifer yellow across Caco-2 cell monolayers, without having any cytotoxic effect on the cells[89]. Extracts of linden (*Tilia vulgaris*), star anise (*Illicium anisatum*), *Arenga engleri*, and black tea (*Camellia sinensis*), on the other hand, were found to decrease paracellular flux and increase TEER.

Surfactants are known to affect TJ permeability. The food-grade surfactant sucrose monoester fatty acid caused a decrease in TEER and an increase in the permeability to the egg white allergen, ovomucoid, across Caco-2 cell monolayers[90]. Furthermore, the perijunctional rings of the surfactant treated cells are partially disbanded when examined under fluorescence microscopy. Similarly, when Caco-2 cell monolayers are exposed to *Quillaja* saponin at non-toxic levels, TEER decreases and paracellular flux increases[91].

Some dietary proteins and amino acids alone modulate intestinal permeability. For example, protamine (an arginine-rich protein) decreases paracellular flow of lactulose *in vivo* in rat small intestines[92]. In contrast, TJ permeability is shown to increase following L-alanine perfusion in rats[93]. The casein peptide Asn-Pro-Trp-Asp-Gln increases TEER in Caco-2 cells in a dose dependent manner, which correlates with increased levels of occludin gene and protein expression[94]. Feeding diabetes-prone rats hydrolysed casein decreased intestinal permeability as demonstrated by reduced lactulose uptake[95]. This correlated with an increased level of ileal claudin-1 gene expression, and increased TEER in *ex vivo* ileal samples. β-lactoglobulin (from skim milk) increases TEER across Caco-2 cell monolayers when the TJ are destabilised by culturing in serum free medium[96]. The putative mechanisms of action involve PKC mediated signal transduction pathways, as treating the Caco-2 cell monolayer with a PKC inhibitor before adding β-lactoglobulin reduces the TEER increase. The authors also concluded that β-lactoglobulin-induced increases in TEER may be caused by modifications to the cytoskeletal structure, as treating the cells with cytochalasin D (known to disrupt the cytoskeleton) also inhibits β-lactoglobulin-induced increases in TEER. This could be further verified by immunostaining cytoskeletal structures of Caco-2 cells both untreated and treated with β-lactoglobulin.

At supraphysiologic levels, tryptophan disrupts TJ in hamster small intestinal epithelia, shown by visible perturbations in TJ (transmission electron microscopy), decreased TEER and increased insulin flux[97]. In contrast, glutamine can restore stress-induced loss of barrier integrity[98]. With Caco-2 cell monolayers where maturation was achieved by treatment with sodium butyrate (compared with spontaneously matured Caco-2 cell monolayers), exposure of cells to the atmosphere during media change led to a temporary decrease in TEER. The speed of TEER recovery was improved if the cells were exposed to glutamine before the stress. Furthermore, when Caco-2 cells were

deprived of glutamine via inhibition of glutamine synthetase, occludin, claudin-1 and ZO-1 protein expression was decreased[99]. Studies have shown that treatment with glutamine leads to activation of the MAPKs, ERKs and JNKs[100], thus glutamine could potentially modulate TJ via a MAPK-dependent signal transduction pathway.

As well as having nutritional value, trace elements such as zinc may also assist with the maintenance of intestinal barrier integrity. Caco-2 cells grown in a zinc-deficient medium had reduced TEER and altered expression of ZO-1 and occludin (localised away from the cell boundaries, less homogenous) compared to Caco-2 cells grown in zinc replete medium[101]. This was accompanied by a disorganisation of the F-actin filaments.

Other dietary components such as fatty acids, polysaccharides and flavonoids are also known to alter TJ. The medium-chain fatty acids capric acid and lauric acid increase paracellular flux and cause a rapid decrease in TEER in Caco-2 cells[102]. Docosahexaenoic acid (DHA), γ-linolenic acid (GLA), and eicosapentaenoic acid (EPA) are also shown to decrease TEER and increase paracellular permeability of fluorescein sulfonic acid, in a concentration dependent manner[103,104]. Caco-2 cells exposed to sodium caprate had irregular expression of ZO-1 and occludin at the cell boundaries. While the decrease in paracellular permeability was observed within 3 minutes of capric acid exposure, reorganisation of TJ proteins took at least 60 minutes. Sodium caprate is known to increase TJ permeability in rat ileum *ex vivo*, reducing TEER, increasing paracellular flux and inducing dilations in TJ visible by transmission electron microscopy[105]. Conjugated linoleic acids (CLA) have also been shown to modulate paracellular permeability in epithelial cells[106]. Caco-2 cells grown in medium supplemented with the *trans*-10 isomer of CLA have a slower rate of TEER increase, increased paracellular flux and altered distribution of occludin and ZO-1. Chitosan, a polysaccharide widely used in the food industry is also known for its absorption enhancing properties[107]. Caco-2 cells treated with chitosan have altered distribution of ZO-1 and F-actin leading to increased paracellular permeability[108]. Quercetin, the most common flavonoid in nature, increases TEER[109,110] and reduces paracellular flux of Lucifer yellow[110] across Caco-2 cell monolayers in a dose dependent manner. This was accompanied by an increase in claudin-4[109,110]. While the overall expression of claudin-1, occludin, and ZO-2 were not affected[109,110], these proteins were redistributed and associated with the actin cytoskeleton[110]. Furthermore there was greater localisation of

claudin-1 and -4 at TJ in Caco-2 cells treated with quercetin[109,110]. Quercetin also inhibited activity of PKCδ, TJ regulation by quercetin is likely PKCδ-dependent[110].

While dietary components may regulate TJ permeability by directly targeting signal transduction pathways involved in TJ regulation, certain dietary components have been identified which influence cytokine signalling, thereby modifying TJ permeability. For example, epigallocatechin gallate (EGCG), the predominant polyphenol in green tea, when incubated with T84 monolayers did not affect epithelial permeability. When treated concomitantly with interferon (IFN)-γ, however, EGCG prevented the IFN-γ-induced decrease in TEER and increase in paracellular flux[111]. Similarly, the isoflavonoid genistein prevents TNF-α-induced decreases in TEER in the colonic cell line HT-29/B6, but does not affect TEER itself[112].

1.3 THE MUCUS LAYER

The mucus layer, a viscoelastic gel layer that overlays the intestinal epithelium, is the first anatomical site at which the host encounters intestinal bacteria. The mucus layer forms a semi-permeable protective barrier that traps bacteria by interacting with the bacteria cell surface polysaccharides and protein appendages. Once trapped, the bacteria can be washed away by peristalsis[113]. The mucus layer also helps in intestinal defence by retaining a high concentration of antimicrobial compounds close to the epithelium[114]. In the colon it has two distinct layers, an inner layer, which is seemingly sterile and attached to the underlying mucosa[115,116,117], and an upper layer, which contains mucins, cell debris and bacteria[115].

Mucus is secreted by specialised epithelial cells known as goblet cells[20]. Mucus is predominantly composed of mucin proteins, which provide a matrix, and other compounds including phospholipids. Goblet cells are polarised epithelial cells, similar to enterocytes, with a brush border and TJ connecting to adjacent cells[2]. Below the brush border, these cells contain numerous secretory granules with packaged mucins. While mucins are constitutively secreted by goblet cells (known as baseline secretion), exposure to certain compounds, including inflammatory mediators, such as cytokines, leads to an acute release of mucin granules (known as compound exocytosis)[118].

The mucus layer varies in thickness throughout the intestinal tract (reviewed in Deplancke and Gaskins (2001)[20], and Barnett *et. al.* (2012)[119]). It is thickest in the

stomach (estimates as high as 450 μm thick) to protect the epithelium from pepsin, while it is thin and discontinuous in the small intestine (estimates less than 20 μm thick). Peyer's patches are thought to not be covered with mucus to aid bacterial sampling by M cells. The mucus layer again increases in thickness from the start of the colon, reaching an estimated 250 μm thickness in the rectum[120]. Furthermore, the mucus layer is structurally altered in intestinal diseases such as Crohn's disease (thin mucus layer) and Ulcerative Colitis (thick mucus layer)[121]. It is difficult to estimate the thickness of the mucus layer through histochemical studies because the mucus layer can be easily lost during tissue handling and fixing[114]. Imaging in live rodents has shown the mucus layer in the colon to be about 800 μm thick. Consistent with human histochemical studies (e.g. Matsuo (1999)[115]), this includes both an inner (100 μm) and outer (700 μm) layer[120].

The mucus layer is a dynamic barrier. Mucus-related indexes such as the thickness of the mucus layer, and its protein composition, are affected by the commensal intestinal bacteria[122,123,124,125]. For example the mucus layer is twice as thick in conventionally raised mice compared with germ-free mice[122].

1.4 IMMUNE CELLS AND SIGNALLING IN THE INTESTINAL BARRIER

The intestinal immune system is the largest and most complex part of the immune system[126]. The intestinal barrier encounters more antigens than any other part of the body, and the immunological barrier needs to remain unresponsive to commensal bacteria and food antigens while defending against pathogens. In cases where the immune system fails to make this differentiation, homeostasis in the intestine breaks down leading to chronic intestinal inflammatory disorders.

The lamina propria contains specialised lymphoid structures, including Peyer's patches in the ileum, and isolated lymphoid follicles distributed through the small intestine and colon, containing antigen presenting cells such as dendritic cells (DC) and macrophages[126]. Luminal antigens are sampled via specialised epithelial cells known as M cells which overlie Peyer's patches and other lymphoid follicles[127]. Further, DC can extend dendrites through the epithelial TJ into the lumen and directly sample luminal antigens[128]. DC also express TJ proteins, and thus possibly form TJ with the epithelial

cells, preserving the integrity of the intestinal barrier during this process. Epithelial cell and immune cells in the lamina propria recognise microbes by means of pathogen recognition receptors (PRRs), the activation of which can lead to an inflammatory response against pathogens[129].

The mechanisms of defence employed by the innate immune system are aimed at preventing microorganisms from gaining access to the apical surface of the cell layer[130]. In the innate immune response, host cells detect pathogens by means of TLR and other pattern recognition molecules. This leads to the recruitment of inflammatory leukocytes such as neutrophils and the production of antimicrobial peptides, which results in an acute antimicrobial response. The mucosal adaptive immune system provides an additional line of defence and works synergistically with the innate immune system[3]. It actively samples luminal antigens and provides an antigen specific immune response.

1.4.1 Host recognition of bacteria

The innate recognition of microbes in the intestine is achieved through PRRs, which specifically recognise pathogen-associated molecular patterns (PAMPs). PAMPs are invariant molecular constitutions of microbes, essential for microbe survival. These structures are not unique to pathogens and are produced by all microorganisms, and thus are also referred to as microbe-associated molecular patterns (MAMPs); however they are not produced by the host, allowing the host to distinguish 'non-self' from 'self'[129]. The PRRs can be membrane bound, cytosolic or secreted. Membrane bound PRRs sense extracellular MAMPs, while cytosolic receptors detect intra-cytoplasmic MAMPs. Secreted PRRs bind to microbes and mark them for destruction.

In the intestinal tract there are two classes of PRRs: the membrane-bound TLRs and the cytosolic nucleotide-binding and oligomerisation-domain (NOD) proteins. When these receptors identify bacterial structures they trigger several signal transduction cascades, such as the nuclear factor kappa B (NF-κB) pathway. Unbalanced activation of these pathways, usually due to host genetic predisposition, however can lead to chronic inflammation and promote tissue damage.

1.4.2 Pro-inflammatory pathways

The various PRRs present in the host trigger several different signalling pathways when they recognise pathogens. However, all these pathways induce the expression of pro-inflammatory genes, usually driven by the transcription factor NF-κB, leading to the production of cytokines and chemokines and causing inflammation at the site of infection[113]. The underlying molecular mechanisms are well characterised and several key pathways have been identified.

The transcription factor NF-κB is considered a master switch for many of the genes involved in the innate immune response. For example activation of NF-κB leads to increased secretion of cytokines, which attracts macrophages, neutrophils, and various growth factors that aid proliferation of immune cells. In addition, NF-κB induces expression of genes which encode anti-apoptotic factors and defensins[130,131].

Under homeostatic conditions, localisation of NF-κB from the cytoplasm into the nucleus is prevented by a binding partner known as inhibitor of NF-κB (IκB). However, under pathological conditions, a protein known as IκB kinase (IKK) phosphorylates IκB, targeting it for degradation by means of ubiquitination (Figure 1.3). This in turn frees NF-κB to enter the nucleus and initiate transcription of NF-κB responsive genes[132]. This pathway can be triggered by both the TLR and NOD systems[131,133].

When TLRs recognise their respective antagonist, they recruit adaptor proteins such as MyD88[134]. This leads to the formation of a protein complex containing the IL-1-receptor-asociated kinase (IRAK) proteins IRAK-1 and IRAK-4. TNF-receptor-associated factor 6 (TRAF6) binds to this complex then dissociates to bind to transforming growth factor-β-activated kinase-1 (TAK-1), which in turn activates the IKK complex which phosphorylates IκB. NOD1 and NOD2 activate the NF-κB pathway by recruiting receptor-interacting serine/threonine kinase (RICK) which in turn activates IKK.

Also triggered by the TLR system is the IFN-regulatory factor (IRF) pathway. The IRF family of transcription factors is involved in regulating the expression of IFNs, a family of cytokines. Members of this family are divided into type I (which includes

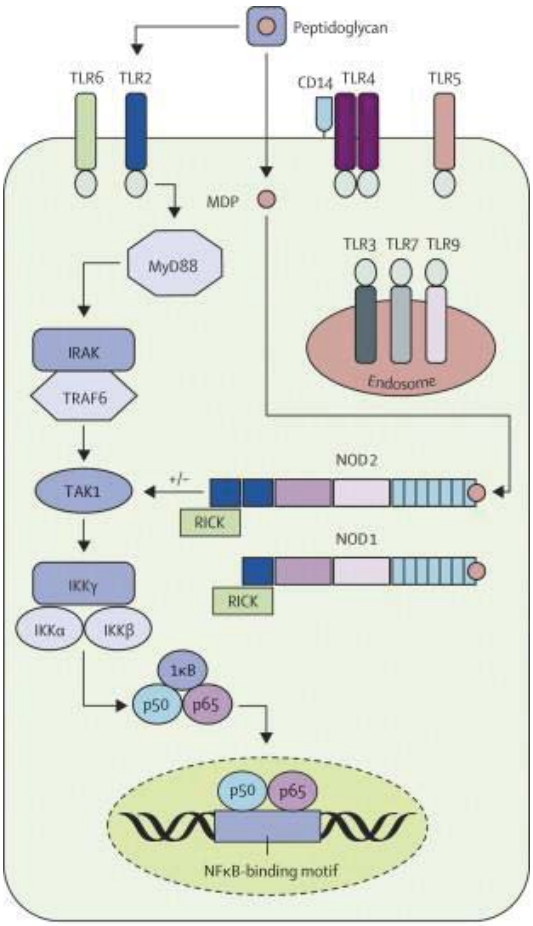

Figure 1.3 TLR and NOD signalling in the NF-κB pathway.

The schematic depicts activation of NF-κB transcription factor by a bacterial stimulus (peptidoglycan) via TLR or NOD signalling pathways. MyD, myeloid differentiation primary response protein; IRAK, interleukin-1 1-receptor receptor-associated kinase; TRAF, TNF-receptor-associated factor; TAK, transforming growth factor-β-activated kinase; IKK, inhibitor of NF-κB (IκB)-kinase; RICK, receptor-interacting serine/threonine kinase. Figure adapted from Baumgart & Carding (2007)[133].

IFN-α and IFN-β) and type II (represented by IFN-γ) IFNs[135]. IFN-γ mediates macrophage activation while IFN-α and -β have been shown to defend against viruses by preventing viral replication. They also have a potential key role in adaptive immunity, as they can stimulate co-stimulatory molecules in antigen presenting cells.

1.4.3 Dendritic cells

DC are antigen presenting cells that, in the intestinal tract, have been implicated both in the maintenance and tolerance towards commensals and the generation of immune response against pathogens[136]. These cells have two major functions, which are to acquire antigens and stimulate lymphocytes. Antigens are acquired by 'immature' DC, which are cells optimised for antigen uptake. These cells express low levels of major histocompatibility complex (MHC) class II and co-stimulatory molecules (such as CD80 and CD86) and are weak stimulators of lymphocytes. However, inflammatory stimuli induce the maturation of DC and upregulate the expression of MHC class II and co-stimulatory molecules. Mature DC present antigens to naïve T cells in mesenteric lymph nodes and Peyer's patches, and thereby drive the clonal expansion and shape the differentiation of these T cells[137,138]. Furthermore, DC in the Peyer's patch have been shown to differentiate B cells into IgA secreting cells[139]. DC are thought to have a large influence on the immune response, with one DC influencing the function of 300-1000 T cells[138].

DC are present at various levels throughout different organs and tissues. Within the intestinal barrier, these cells are found in cryptopatches, Peyer's patches, isolated lymphoid follicles and the mesenteric lymph nodes[140]. Depending on their surface marker expression, DC can be grouped into several different sub populations. The largest subpopulation of DC is characterised by the receptor for CX3CL1/fractalkine, CX3CR1; and these cells populate the entire lamina propria of the small and large intestine[141].

DC appear to utilise several different mechanisms to sample antigens that are encountered by the intestinal barrier. Lamina propria DC, for example, are positioned to sample antigens that may leak through a compromised epithelial barrier; while Peyer's patch DC sample antigens which transcytose across M-cells[142]. Furthermore, myeloid lamina propria DC are able to extend dendrites through the TJ of the epithelium and directly sample the lumen[128]. Studies in which mouse DC were labelled with green

fluorescent protein (GFP) reporter DNA, showed transepithelial DC extensions along the small intestine[141,143,144]. The proportion of DC extensions observed along each region of the intestine however varies depending on the study. This discrepancy can be attributed to the method of detection used. In studies where $CX3CR1^{+}$ was used, the terminal ileum was shown to have the highest number of extensions[141,144], while when $CD11c^{+}$ or MHC class II^{+} were used, the terminal ileum had the lowest proportion of extensions[143]. It is thus possible that CXC3CR1 labelled DC[141] are a distinct population from CD11c or MHC CII labelled DC[143],

Protein and mRNA analyses have shown that DC express the transmembrane TJ proteins occludin, claudin-1, and JAM, as well as the cytoplasmic adaptors ZO-1, E-cadherin and β-catenin which are required for TJ formation and localisation[128,145]; and the expression of these proteins is regulated during DC maturation. During the process of extending their dendrites through the epithelium, occludin and claudin-1 expressed by the DC are thought to interact with the epithelial cells, opening the existing TJ and forming new junction-like structures to maintain the integrity of the epithelial barrier[128].

The generation of these transepithelial dendrites has been shown to require both the presence of bacteria[143] and CX3CR1[141] (the receptor for CX3CL1), a chemokine expressed at the surface of intestinal epithelial cells. DC were observed in mice by replacing either one or both copies of *cx3cr1* with GFP reporter cDNA, which resulted in heterozygous mice ($cx_3cr1^{GFP/+}$) that express the receptor, and homozygous mice ($cx_3cr1^{GFP/GFP}$) that are CX3CR1-deficient. Visualisation of intestinal tissue by confocal microscopy showed intraepithelial dendritic extensions in $cx_3cr1^{GFP/+}$ mice, but not in CX3CR1-deficient mice[141]. Demonstrating that this process is also influenced by the presence of bacteria, $cx_3cr1^{GFP/+}$ mice (but not CX3CR1-deficient mice) infected with the pathogen *Salmonella typhimurium* showed an increase in transepithelial dendrite formation, a potential mechanism for increased luminal sampling by the immune system. Furthermore, in a different study, treatment of mice with broad spectrum antibiotics to reduce the intestinal microbial load, led to a significant decrease in transepithelial dendritic extensions. Introducing live *Salmonella* by means of oral gavage led to a substantial increase in the number of extensions in the terminal ileum, which under steady state had the lowest proportion of transepithelial extensions[143].

DC in all peripheral tissue are usually found in an ‘immature’ state. Immature DC are optimised for antigen uptake; they express low levels of MHC class II and co-

stimulatory molecules (such as CD80 and CD86), and thus are weak stimulators of lymphocytes. Upon activation however, DC mature and upregulate the expression of MHC class II and co-stimulatory molecules. The co-stimulators 'flag' the antigen presented by the DC as being microbe-derived. Activation and maturation can occur when DC are exposed to bacteria or pro-inflammatory mediators, such as TNF-α, IL-1 and type I IFNs, which are recognised by DC via PRRs.

Once DC acquire antigens they migrate from the lamina propria and/or Peyer's patches to the mesenteric lymph nodes. This was shown using fluorescently labelled non-pathogenic *Escherichia coli*, which could be detected in DC that extend dendrites through the epithelium, and DC in the interfollicular regions, as well as in DC that were cultured from Peyer's patches and mesenteric lymph nodes in $cx_3cr1^{GFP/+}$ mice[141]. As this occurs even during the steady state, it can be postulated that DC induce tolerance towards commensal bacteria and other harmless antigens. However, once activated, the DC migrate to the mesenteric lymph nodes much more rapidly, and also migrate within Peyer's patches to T cell zones. This process also seems to require CX3CR1, as *E. coli* could be cultured from the Peyer's patches, but not from the mesenteric lymph nodes of CX3CR1-deficient mice[141].

DC influence the T cell response via the production of pro-inflammatory (e.g. IL-12, IL-18 and IL-23) or anti-inflammatory (e.g. IL-4 and IL-10) cytokines[138]. During steady state, myeloid DC in the colon secrete IL-10, but fail to secrete IL-12 even in response to inflammatory stimuli such as lipopolysaccharide or CpG[146]. Thus lamina propria DC, while able to respond to inflammatory stimuli, do not initiate an inflammatory response, and are probably important in tolerance towards commensal bacteria and maintaining intestinal homeostasis[147,148].

1.5 COMMENSAL INTESTINAL MICROBIOTA

The intestinal tract is inhabited by 10^{14} microbes, over tenfold the number of cells that make up the human body[18]. The intestinal microbiota is dominated by bacterial species (but species of archaea and eukarya are also found)[149]. The majority of studies estimate that the intestinal tract is colonised by 400 to 500 different species of commensal bacteria, while other studies report up to 1000 species[13]. If the gastrointestinal tract is assumed to be inhabited by 1000 bacterial species, and *E. coli* is taken as a

representative of the intestinal microbiota, then the genomes of the bacterial species (collectively known as the microbiome), will contain over 100 times the number of genes in the human genome[149]. Bacteria in the intestine can adhere to the mucosal surface or remain unattached in the lumen; however, surface-adherent bacteria are generally found to be a subset of the luminal bacteria[19,150]. It is becoming increasingly evident that the intestinal microbiota is involved in molecular 'crosstalk' with the intestinal cells, and play functional roles in the development of the intestine and the maturation of the intestinal immune system, as well as regulation of the intestinal barrier[151]. More than 90% of the intestinal bacteria are composed of obligate anaerobes[19,150]. Due to the difficulty in culturing obligate anaerobic bacteria with intestinal cells, the mechanisms that enable the intestinal microbiota to influence intestinal barrier integrity are largely unknown.

1.5.1 Establishment of intestinal microbiota

It is generally believed that the human intestinal tract is sterile *in utero*, and that colonisation by bacteria starts immediately after birth. However, recent studies have identified bacteria in umbilical cord blood and the placenta, suggesting that the developing foetus may be exposed to the maternal commensal microbiota during pregnancy[152,153]. Faecal bacterial counts of the newborn reach approximately 10^9 per gram of faeces after the first week[19]. Initially the intestine is colonised by aerobic species[133], followed by facultative anaerobes consisting of Enterobacteria, *Streptococcus*, and *Staphylococcus*[154]. During weaning however, these are replaced by obligate anaerobes such as *Bacteroides* and *Clostridium*[155]. The timing of colonisation and the composition of bacteria depends on the mother as well as on several other environmental and genetic factors. For example, studies have shown differences in intestinal colonisation between neonates delivered by caesarean section and vaginally delivered neonates[156157], and between breast-fed and bottle-fed infants[158].

Host genetic factors also seem to contribute to the composition of intestinal bacteria. Denaturing gradient gel electrophoresis (DGGE) profiles of the intestinal contents were shown to be more similar between identical twins than unrelated individuals[159]. Similarly, the host diet also has an effect. In a study of faecal bacterial diversity in vegetarians, the *Bacteroides* made up only 6% of the population. Other studies have also failed to identify any *Faecalibacterium prausnitzii*, normally a major

component of the intestinal microbiota, in people with vegetarian diets[160,161]. Furthermore, in a comparative study of faecal bacteria among different European populations, the highest numbers of *F. prausnitzii* were identified in a group whose diet was characterised by high consumption of fish and meat[162].

The establishment of the intestinal microbiota is a complex process that is not fully understood. While initial colonisation of the bacteria is thought to be due to chance encounters, nutrient supply and immune surveillance, the sequence in which these bacteria settle a niche in the colon has been suggested to affect the ability of other bacteria to colonise[163]. Once established, the microbiota remains stable over a long period of time[19]. However, a cross-sectional European study showed the elderly to have higher proportions of *Enterobacteria* compared with young adults regardless of geographic location[162]. The elderly in Asia have also been shown to harbour higher levels of *Enterobacteria* and reduced numbers of anaerobic bacteria[164].

1.5.2 Distribution of microbiota in the intestinal tract

There are geographical differences in the bacterial colonisation along the intestinal tract of the adult human. Bacterial cell densities are usually quite low in the stomach and the proximal small intestine (duodenum); but there is a continuous gradient of increasing numbers of bacteria from the duodenum to the ileum, where the bacterial counts reach 10^8 per gram in the ileum (Figure 1.4). The colon contains the majority of the commensal bacteria with a density of 10^{11}-10^{12} cells per gram[19,151]. Several factors regulate the intestinal microbiota and many are not well understood. Important physiological factors include gastric acid, and intestinal transit time. Acid, bile and pancreatic secretions, and low pH, in the stomach prevent the survival of most bacteria; and rapid transit in the duodenum and ileum leads to a small bacterial population in this region, while the colon, with slow transit, allows for a larger bacterial population[19].

Molecular analyses of the gastrointestinal microbiota have shown that the same bacterial phyla predominate in the stomach, small intestine, caecum and colon; however, the relative abundance of subgroups vary with anatomical location[165]. For example, the stomach contains considerably more quantities and strains of *Helicobacter* spp. than the rest of the gastrointestinal tract[166]; the ileum contains higher proportions of *Streptococcaceae* (23%) compared with the colon (5%)[17]; and in almost all humans

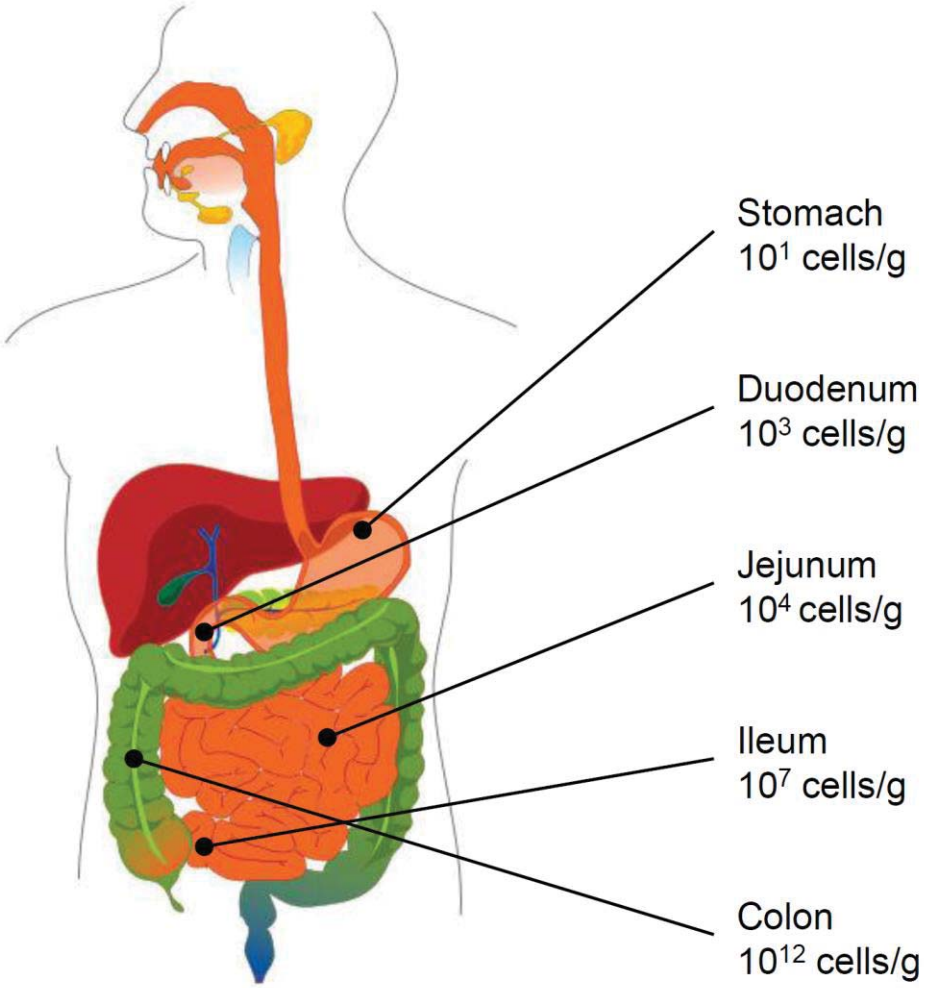

Figure 1.4 Variation in numbers of bacteria along the intestinal tract.

The commensal intestinal microbiota is not homogenous. The bacterial density increases from the proximal to the distal segments of the intestinal tract. Data taken from Sekirov *et al.* (2010)[1] and O'Hara & Shanahan (2006)[151]. Figure adapted from Wikimedia Commons[167].

studied so far, *Bacteroides* and *Firmicutes* predominate in the colon[168]. The ileum is also dominated by *Bacteroidetes* and *Firmicutes*, but it differs from the colon in the relative proportions of the subgroups of these phyla are present[17]. For example, members of class *Bacillus* (predominantly *Lactobacillales* clade) are more abundant in the small intestine than colon, while several members of *Bacteroidetes* and the family *Lachnospinaceae* are less abundant in the small intestine than the colon[17].

The bacteria in the intestine can be either attached to the mucus layer or reside in the lumen without attachment. These two populations of bacteria may be distinct with different roles within the ecosystem, and the surface-adherent bacteria may have a greater influence on the intestinal barrier function than the luminal bacteria[19]. For example the surface-adherent bacteria form a "biofilm" (a dense cohesive community of microbes that embed themselves within a matrix and able to resist hydrodynamic shear forces), which in close contact to the epithelium can promote nutrient absorption and induce host immunity[169]. However, a study of multiple colonic mucosal sites from three individuals showed that the surface-adherent bacteria were a subset of the luminal bacteria[150]. Authors of this study also postulate that the faecal microbiota represents a combination of shed mucosal bacteria and a separate nonadherent luminal population.

The proportion of obligate anaerobes increases from the proximal to the distal regions of the intestine. Obligate anaerobes are first observed in the lumen of the ileum, and in the colon the anaerobes outnumber the aerobic bacteria by a factor of 100 to 1000[19,130]. Facultative anaerobes tend to associate with epithelial cells to gain access to an oxygen source[130].

1.5.3 Diversity of the commensal bacteria

Over 90% of the commensal bacteria are obligate anaerobes, while the facultative anaerobes and aerobes are present in smaller numbers. The growth requirements for obligate anaerobes are largely unknown and therefore the majority of bacterial species cannot be cultured *in vitro*[130]. The reported proportion of cultivable bacteria depends on the study and has ranged from 20%[150] to 46%[170]. In 2005 GenBank consisted of 1822 rRNA gene sequences annotated as being derived from the human intestine; of these 1689 represented uncultured bacteria. Backhed *et al.* (2005)[171] clustered these sequences into groups based on percentage sequence identity, with 98% used to delimit species, and determined ~800 species to be present. Since then at least 3 large-scale culture-

independent studies of the human gastrointestinal tract have been carried out[17,150,172], which collectively surveyed over 45000 rRNA gene sequences. These sequences represent at least 1800 genera, and between 15000 and 36000 species (when delimited at 99% and 97% sequence similarity respectively)[17]. These sequences, at most, are thought only to represent 50% of the predicted sequence diversity (collector's curves do not plateau); thus much diversity remains uncharacterised[17].

While there are over 50 known bacterial divisions, the bacteria identified in the human gastrointestinal tract belong to only one of 11 bacterial divisions[168]. Two divisions, namely the *Cytophaga-Flavobacterium-Bacteroides*, and the *Firmicutes*, dominate in the gastrointestinal tract. The majority of the *Firmicutes*, which make up about 40-65% of the colonic microbiota[173], fall into two major groups; *Clostridial cluster IV* (the *Clostridium leptum* group) and *Clostridial cluster XIVa*, each of which makes up about 25% of the colonic microbiota[173]. *Clostridial cluster IX* is another group of the *Firmicutes*, which is common (makes up ~7% of the faecal microbiota[173]). The *Cytophaga-Flavobacterium-Bacteroides* division is dominated by the *Bacteroides* which make up about 25% of the colonic bacteria. Together, the *Bacteroides* and *Firmicutes* make up 60-80% of the total faecal community, and over 90% of the colonic bacteria[150]. The *Proteobacteria* and *Actinobacteria* are also commonly found in the gastrointestinal tract, making up 8% and 3 to 5% of the colonic bacteria respectively[17]. Bacteria from the remaining divisions are very rarely found. These divisions are *Spirochaeates, Fusobacteria, Cyanobacteria, Deferribacteres, Deinococcus-Thermus, Verrucomicrobi* and *VadinBE97*.

1.6 FUNCTIONS OF THE COMMENSAL BACTERIA

The human intestinal microbiota play a crucial role in the function and development of the intestine, and are also implicated in the metabolism and normal development of the mucosal immune system. This is demonstrated in germ-free animals which are more susceptible to infection, have reduced digestive enzyme activity, reduced muscle wall thickness, reduced cytokine production, reduced serum immunoglobulin levels, smaller Peyer's patches and fewer intraepithelial lymphocytes[174]. It is possible to restore normal immune function in such animals by reconstituting them with normal intestinal bacteria.

The intestinal microbiota ferment non-digestible dietary residue (such as resistant starches, cellulose, pectins and some oligosaccharides) allowing for the recovery of metabolic energy and absorbable substrates for the host. For example, while the human genome contains only one predicted enzyme for the degradation of xylan-, pectin-, and arabinose-containing polysaccharides, *Bacteroides thetaiotaomicron*, a prominent member of the human intestinal microbiota contains 64 predicted enzymes. Similarly, while the human genome has 98 glycoside hydrolases, *B. thetaiotaomicron* has 226 glycoside hydrolases[171]. Studies have also found the enrichment of genes involved in carbohydrate and amino acid transport and metabolism in the intestinal ecosystem[175]. Colonisation of the intestine with commensal bacterial species has also been shown to affect the host's capacity to metabolise xenobiotics and endogenous toxins[176]. Intestinal bacteria also play a role in the synthesis of vitamins[177], absorption of ions[178], and hormonal regulation of the host[179].

Germ-free rats have a reduced rate of intestinal crypt cell production and fewer cells in the crypts than conventionally bred rats, which suggests that the intestinal microbiota affect proliferation of epithelial cells[180]. The fatty acid chains derived from the bacterial fermentation of non-digestible dietary residues have also been shown to stimulate epithelial cell proliferation and differentiation *in vitro*[181].

Commensal bacteria are also thought to play an instructive role in postnatal intestinal maturation. Maturation changes observed during postnatal intestinal development, such as reductions in ileal epithelial lactase, are also apparent when adult germ-free mice are colonised with *B. thetaiotaomicron*[176]. Similarly, the construction of the submucosal capillary network of germ-free animals, which is less complex than that of their conventional counterparts, can be completed by colonising adult germ-free mice with *B. thetaiotaomicron*. This is evidence that commensal microbiota also regulate angiogenesis[182].

Commensal bacteria are crucial in helping limit pathogen colonisation of the intestinal barrier by the production of antimicrobial compounds, known as bacteriocins[183], and through competition for mucosal binding sites. By adhering to the epithelium, commensal bacteria prevent pathogen attachment, inhibiting pathogen-host interactions and pathogen-induced cell injuries[184]. Commensals also compete for nutrients, and in the case of *B. thetaiotaomicron*, the bacterium is involved in crosstalk with the host such that the host does not over-produce nutrients[185].

In several intestinal disorders, such as coeliac disease or IBD, where the intestinal barrier integrity is known to be compromised [7,8], it has also been shown that the intestinal microbiota composition is altered. For example, there is a reduction in the proportion of the obligate anaerobe *F. prausnitzii* in the mucosa-associated microbiota of patients with IBD [15] and coeliac disease [16]. Similarly, in a culture-independent study characterising bacterial communities in patients with IBD, sequences representative of *B. thetaiotaomicron*, *F. prausnitzii* as well as several other cultured commensal anaerobes, were found to be depleted in patients with IBD [17]. It is therefore plausible that these and other commensal anaerobic bacteria are important in the regulation of intestinal barrier integrity.

1.7 INTERACTIONS BETWEEN INTESTINAL CELLS AND BACTERIA

1.7.1 Barrier enhancement by commensals and probiotic bacteria

Improvements in barrier integrity are associated with changes in TJ structure via changes in TJ protein expression and distribution. Commensal bacteria and probiotics have been shown to promote intestinal barrier integrity both *in vitro* and *in vivo*. Some probiotics preserve the intestinal barrier in mouse models of colitis[186], and reduce intestinal permeability in human patients with Crohn's Disease[187]. Probiotic treatment has also been shown to reduce epithelial barrier dysfunction following psychological stress in rats[188]. Treatment of epithelial cells with *E. coli* Nissle 1917, a human faecal isolate and widely used probiotic, leads to increased expression of ZO-2 protein and redistribution of ZO-2 from the cytosol to cell boundaries *in vitro*[189]. A similar effect is observed in intestinal epithelial cells isolated from germ-free mice treated with *E. coli* Nissle 1917[190]. Similarly, treating T84 cell monolayers with metabolites secreted by *Bifidobacterium infantis* Y1 from the probiotic product VSL#3, leads to an increase in ZO-1[191]. This also leads to an increase in occludin protein expression, while reducing claudin-2, thus demonstrating the ability of bacteria and bacterial products to modify TEER and ion selectivity of TJ[191]. Furthermore, treatment of Caco-2 cells with the probiotic *Lactobacillus plantarum* MB452 (also from the probiotic product VSL#3), results in increased transcription of occludin and cingulin genes, suggesting that

bacteria induced improvements to intestinal barrier integrity may also be regulated at the gene expression level[192].

Recently, *L. plantarum* has been shown to regulate human epithelial TJ proteins *in vivo* and to confer protective effects against chemically induced disruption of the epithelial barrier[193]. Administration of *L. plantarum* into the duodenum of healthy human volunteers was shown to increase ZO-1 and occludin in the vicinity of TJ structures[193]. Pre-treatment of Caco-2 cell monolayers with *L. plantarum* significantly attenuated the effects of phorbol ester induced dislocation of ZO-1 and occludin and the associated increase in epithelial permeability[193]. This protection was also seen with an agonist of TLR2. This supports previous studies showing that oral treatment of colitis with the TLR2 ligand PCSK suppressed mucosal inflammation *in vivo* and provides a plausible mechanism for the use of probiotics in colitis prevention and reduction[194].

Some probiotics and commensals have also been shown to prevent, and even reverse, the adverse effects of pathogens on intestinal barrier function. When cultured simultaneously with enteroinvasive *E. coli* (EIEC) strain O124:NM, *L. plantarum* strain CGMCC No.1258 maintains TEER and molecule permeability in cultured Caco-2 cell monolayers by preventing EIEC-induced loss of expression and redistribution of TJ associated proteins[195]. EIEC infection leads to the disruption and disorganisation of the actin cytoskeleton, but these effects can then be reversed by incubating the epithelial cells with *L. plantarum*, which leads to a high density of actin filaments at the perijunctional regions and TJ proteins being more closely associated with the cytoskeleton. Co-culture of Caco-2 cells with *L. plantarum* DSM 2648 has also been shown to prevent Enteropathogenic *E. coli* (EPEC)-induced reduction in TEER, possibly because *L. plantarum* reduces EPEC adherence to Caco-2 cells[196].

Pre-treatment with metabolites from probiotic bacteria may also be protective against pathogen-induced changes in intestinal barrier function. Treating Caco-2 cells with the cell-free supernatant of *Bifidobacterium lactis* 420 before adding the supernatant of enterohemorrhagic *E. coli* (EHEC) strain O157:H7 increased TEER, while adding the supernatant of EHEC alone decreased TEER[197]. The increase in TEER was not seen, however, if the supernatant was added with or after EHEC treatment; only pre-treatment with the bacterial metabolites was effective.

Live probiotic bacteria and their cell-free supernatants, therefore, differ in their ability to protect against pathogen-induced changes to barrier function. This may be attributed to the fact that live probiotic bacteria are able to compete with pathogens for nutrients for growth and adhesion, whereas metabolites secreted by probiotic bacteria may strengthen intestinal TJ via a cell signalling pathway that needs to be initiated before treatment with metabolites secreted by pathogenic bacteria. It is conceivable that promotion of TJ integrity prevents pathogenic bacteria and their effectors from entering via the paracellular pathway to cause further damage.

Some specific bacterial effectors have been shown to improve the integrity of the intestinal barrier. One example is AvrA, secreted by *Salmonella enterica serovar* Typhimurium[198]. While infection with *Salmonella* lacking AvrA leads to the disruption of TJ (by reduced expression of TJ proteins and disorganised expression), *Salmonella* strains expressing AvrA stabilise TJ despite the presence of effectors known to disrupt TJ[199]. AvrA seems to target the expression of ZO-1 and occludin, but not claudin, as claudin abundance is reduced and its localisation limited to the cytosol, even if AvrA is present. The mechanisms through which ZO-1 and occludin expression and distribution are altered is yet to be elucidated.

Bacteria also utilise epithelial cell signalling proteins involved in TJ regulation, including Rho family GTPases, PKC and MAPK to enhance barrier integrity. For example, the ability of the probiotics *Streptococcus thermophilus* and *Lactobacillus acidophilus* to preserve phosphorylation of occludin in EIEC infected cells can be reduced by treating the cells with ROCK inhibitors[200], suggesting these bacteria employ Rho family GTPases to protect against EIEC-induced TJ disruption.

E. coli Nissle 1917, uses a PKCζ dependent signalling pathway to reduce epithelial barrier disruption caused by EPEC [189]. PKCζ is the only PKC isotype located in the TJ complex, and activation of PKCζ leads to phosphorylation of ZO-2 resulting in its removal from the TJ and cytoskeleton. *E. coli* Nissle 1917 is thought to reduce the PKC phosphorylation caused by EPEC, and redistribute PKCζ away from the cell boundaries to the cytosol, reducing ZO-2 - PKCζ co-localisation and thus allowing proper formation of TJ and association of ZO-2 with the cytoskeleton.

Metabolites secreted by *B. infantis* Y1, which increase the TEER in cultured epithelial monolayers, have been shown to promote MAPK dependent pathways. *B.*

infantis-induced TEER-increases can be prevented by inhibiting ERK, and treating epithelial cells with *B. infantis* metabolites leads to a transient phosphorylation (hence activation), of ERK1/2, and a decrease in phosphorylation of p38[191]. However, it has also been shown that the ability of *S. thermophilus* and *L. acidophilus* to protect against EIEC infection (which is reduced by ROCK inhibitors), does not seem to be affected by inhibition of ERK1/2 or p38 [200]. This suggests that different species of bacteria may use different pathways to modulate TJ integrity.

Commensals and probiotics are also known to decrease intestinal barrier dysfunction caused by cytokines. Treatment of cell monolayers with the cytokines TNF-α or IFN-γ leads to a decrease in TEER and an increase in epithelial permeability [201]. This TEER decrease can be prevented by pre-incubating with the probiotics *S. thermophilus* ATCC19258 and *L. acidophilus* ATCC4356, or the commensal *B. thetaiotaomicron* ATCC29184[201]. DNA from the commensal bacteria *Lactobacillus rhamnosus* GG and *Bifidobacterium longum* SP 07/3 have also been shown to induce a signal transduction cascade via an epithelial cell surface receptor, which reduces TNF-α-induced p38 phosphorylation[202].

1.7.2 Modulation of intestinal epithelial cell function by commensal bacteria

As the intestinal barrier is in constant contact with commensal bacteria, it is vital that the innate immune system can distinguish between commensal and pathogenic bacteria, so as to prevent continuous activation of inflammatory systems. An important difference between pathogenic and commensal bacteria is the presence of pathogenicity genes, usually organised in clusters known as pathogenicity islands[203]. These genes allow pathogens to express pathogenicity factors, such as adherins and invasins, which allow the pathogens to adhere to the epithelial barrier. Commensals lack these pathogenicity factors, and are usually trapped in the mucus layer and washed away by peristalsis[113,130]. Pathogenic bacteria are, however, able to hijack host signalling pathways and biological functions, allowing them, for example, to remodel the host cytoskeleton, resulting in enhanced adhesion or allowing the bacterium to penetrate into the cell[204]. In line with this, it has been shown that enteric bacteria penetrate the mucus layer and attach directly to the epithelium in IBD patients[205].

However, as previously mentioned, epithelial cells express a wide range of PRRs that recognise bacterial factors from both commensal and pathogenic bacteria. It has been proposed that PRRs are distributed such that only pathogens, which have evolved to gain access to compartments within the host, are detected. For example TLR4 is expressed intracellularly (in golgi apparatus) in the epithelium[206] and TLR5 is confined to the basolateral side of epithelial cells[207]. Nonetheless, commensal *E. coli* has been shown to stimulate TLR5 in epithelial cells *in vitro*, even when applied to the apical side[208]. Intestinal cells are thus able to recognise and respond to commensal bacteria, hence creating a need for the commensals to actively modulate intestinal epithelial function to maintain immune homeostasis.

Examples of commensal bacteria modulating intestinal immune pathways exist. Non-virulent species of Salmonella are able to prevent activation of the NF-κB pathway by inhibiting the ubiquitination of IκB[209]. This is likely achieved by the bacteria inhibiting E3-SCF$^{\beta\text{-TrCP}}$, a multiprotein complex where the β-TrCP functions as an IκB-specific ubiquitin ligase. This in turn prevents NF-κB translocating to the nucleus (Figure 1.5). *B. thetaiotaomicron* has also been shown to attenuate the NF-κB pathway in the epithelium by targeting the nuclear hormone receptor, peroxisome-proliferator-activated receptor (PPAR)-γ. In the presence of *B. thetaiotaomicron*, PPAR-γ associates with the P65 (RelA) subunit of NF-κB, and the complex is retro-transported from the nucleus back to the cytoplasm (Figure 1.5)[210]. Similarly, *L. plantarum*, a common food bacterium, induces intestinal immune tolerance by regulating expression of genes involved in the NF-κB pathway. Transcriptomic analysis of human duodenum tissue showed only basal amounts of the P65 subunit and increased expression of negative regulators of NF-κB such as A20, BCL3, IκBα and SOCS3 in response to *L. plantarum*[211]. It is possible that other commensal bacteria have also evolved similar mechanisms to prevent intestinal inflammation.

1.7.3 Modulation of intestinal-dendritic cell crosstalk

While DC directly sample antigens from the intestinal lumen[141], and transport bacteria to the mesenteric lymph nodes[21], they do not initiate an undesired immune reaction in response to commensal bacteria. This can be attributed, at least in part, to intestinal epithelial cells, which have been shown to modulate the function of immune cells such

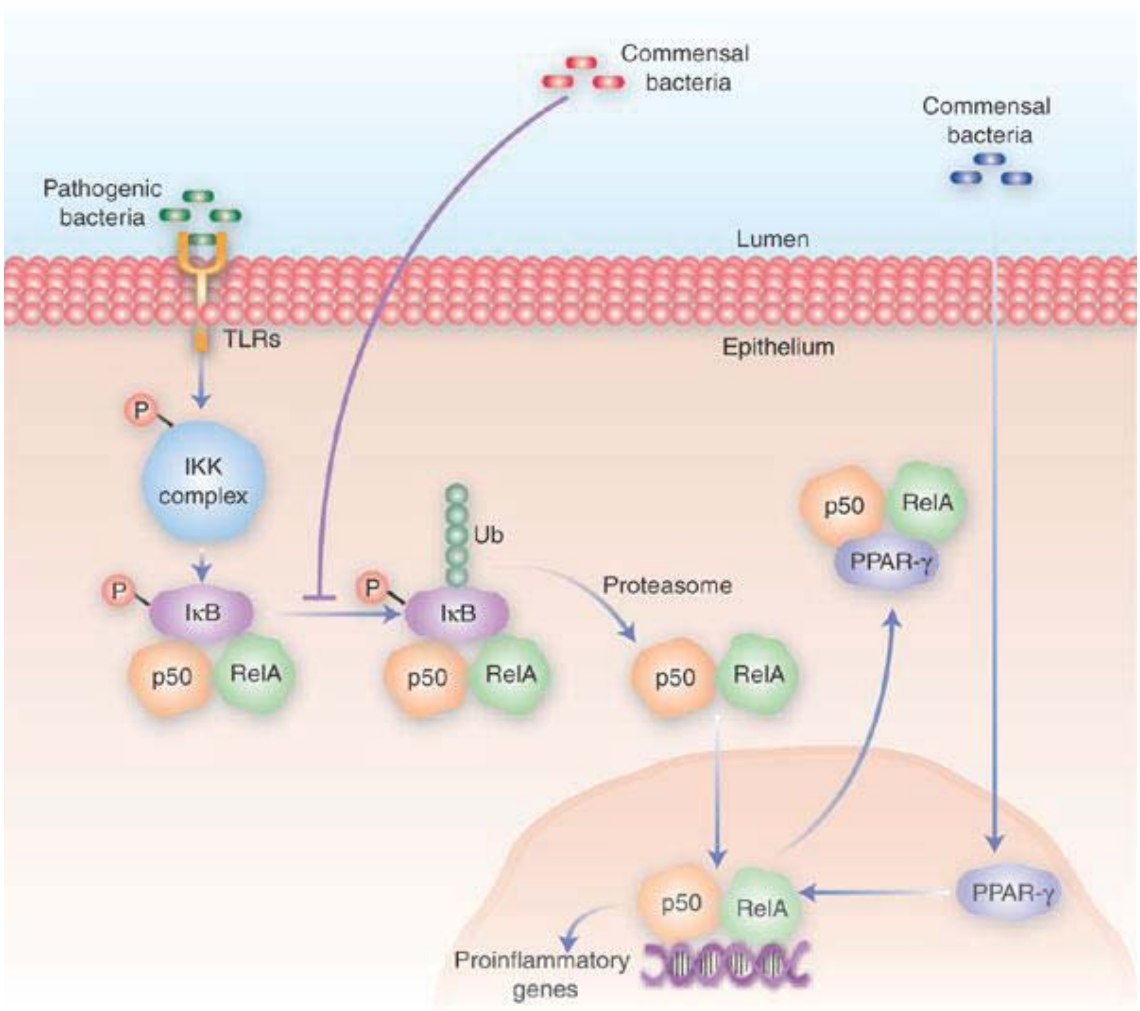

Figure 1.5 Modulation of the NF-*κ*B pathway in epithelial cells by bacteria.

The NF-*κ*B pathway is activated by pathogenic bacteria (green); and can be inhibited by the ubiquitination (red) and PPAR-γ (blue) pathways. P, phosphorylation; Ub, ubiquitin. Figure: Beg (2004)[212].

as macrophages and DC. As previously mentioned, pathogenic bacteria stimulate epithelial cells to release proinflammatory cytokines that can activate DC. In contrast, commensal bacteria are unable to stimulate epithelial cells, but are still able to directly activate DC that translocate dendrites to the apical side[213]. Epithelial cells are able to 'condition' these DC such that they do not induce an immune reaction. Furthermore, intestinal epithelial cells are implicated in the transepithelial DC extension[143].

Because CX3CR1 has been shown to be necessary in the generation of transepithelial dendrites[141], it implies that the expression of the ligand fractalkine (CX3CL1) on epithelial cells is also necessary for this process. In line with this, expression of transepithelial dendrites in CX3CR1 labelled DC (in *cx$_3$cr1$^{GFP/+}$*mice) were limited to the terminal ileum, which correlates with the localisation of fractalkine[141]. A later study however, that found an increase in transepithelial dendrites in the terminal ileum on exposure to non-invasive *Salmonella*, showed that fractalkine mRNA levels remained unchanged during this process[143]. While this suggests that fractalkine on epithelial cells is not involved in inducing transepithelial dendritic migration, it should be pointed out that the latter study[143] observed only a minimal amount of transepithelial dendrites in the terminal ileum prior to adding bacteria, while the terminal ileum of *cx$_3$cr1$^{GFP/+}$*mice contained the highest proportion of transepithelial dendrites[141]. This discrepancy could be attributed to the labelling of DC; and it is thus possible that CXC3CR1 labelled DC[141] are a distinct population from CD11c or MHCII labelled DC[143], which utilise different mechanisms of interaction with epithelial cells to form dendritic extensions to the lumen.

MyD88-dependent signalling by intestinal epithelial TLRs has also been implicated in transepithelial dendrite formation. Mice lacking MyD88 do not show transepithelial dendrites in response to *Salmonella*, unlike their control counterparts. Similarly, mice lacking either TLR2 or TLR4 in their intestines, also fail to induce transepithelial dendrites in response to their respective ligands, while control mice show DC extensions in the peri-caecal region after administration of the same ligands. Thus it can be conceived that epithelial cells, which detect bacteria or MAMPs through TLRs, induce transepithelial DC migration through MyD88 dependent signalling. However, transepithelial dendritic extensions are also present (at a reduced level), during the steady state in mice lacking MyD88, suggesting that this process can also occur independently of MyD88 signalling[143].

When stimulated with a T_H1 inducing pathogen *in vitro*, DC isolated from human colon induce a T cell response polarised towards T_H2, while human monocyte-derived DC induce a T_H1 response[148]. A similar discrepancy can be observed when comparing DC isolated from the Peyer's patch to those isolated from the spleen. Peyer's patch DC, which are in close contact with epithelial cells, drive T_H2 immune responses, even when exposed to T_H1 stimuli, while spleenic DC do not, suggesting that the epithelial cells condition the DC to initiate a non-inflammatory response[142]. When monocyte-derived DC are cultured with supernatants from Caco-2 cell monolayers or primary epithelial cells, they release IL-10 and IL-6 but not IL-12, and induce a T_H2 response even after exposure to a T_H1-inducing pathogen[148].

Epithelial cells seem to condition DC through the release of specific immunoregulatory molecules. Thymic stromal lymphopoietin (TSLP), transforming growth factor (TGF)-β, and metabolites such as prostaglandin E_2 (PGE_2), secreted by epithelial cells, have been shown to directly influence the pro-inflammatory cytokine expression in DC. PGE_2 is a metabolite of the cyclooxygenase-2 enzyme, expressed by intestinal epithelial cells, and has been shown to modulate the function of multiple immune cells[214]. It has also been shown to influence T cell function both directly and indirectly, either by inhibiting production of T_H1 cytokines by T cells[215], or inhibiting the expression of IL-12 by DC[216].

TSLP is a potent activator of DC, and is constitutively expressed by intestinal epithelial cells[148]. By culturing DC in the supernatant of a Caco-2 cell line in which *Tslp* expression is abrogated, it has been shown that TSLP is responsible for limiting IL-12 expression by DC, and thereby its ability to drive a T_H1 response. The expression of TSLP at mucosal surfaces can be upregulated by a range of stimuli (e.g. infection, inflammation), suggesting a role for TSLP in preventing an uncontrolled immune response[217]. Furthermore, TSLP was not detected in the majority of Crohn's disease patients tested, suggesting that the lack of TSLP-mediated control of DC could lead to the observed intestinal inflammation in these patients[148].

TGF-β is an immunoregulatory cytokine produced by epithelial and stromal cells in the intestine[218]. DC cultured in TGF-β have limited expression of pro-inflammatory cytokines and fail to respond to bacterial stimuli[219]. Epithelial cell conditioned DC have also been shown to produce increased levels of TGF-β, which could lead to self regulation of DC immune function. Furthermore, TGF-β can diminish

the ability of intestinal macrophages to secrete inflammatory cytokines in response to bacterial stimuli[220], and inhibit NF-κB dependent gene expression[216], implicating multiple pathways through which epithelial cells utilise TGF-β to modulate intestinal immune function.

1.7.4 Modulation of intestinal function by dietary components and intestinal bacteria

Interactions between dietary components and the microbiota are also crucial in the regulation of barrier integrity. The intestinal microbiota in the large intestine ferments substances that cannot be digested in the small intestine (such as digestion resistant starches, cellulose, pectins and some oligosaccharides), allowing for the recovery of energy and absorbable substrates for the host. Soya milk fermented by *L. plantarum*, *Lactobacillus fermentum*, and *L. rhamnosus* is also able to prevent IFN-γ-induced decrease in TEER in the Caco-2 cell line[221]. This effect, however, cannot be seen with non-fermented soya milk. The protective effect of soya milk is attributed to isoflavone aglycones synthesised in the fermented milk; thus demonstrating the importance of food-bacteria interactions in the regulation of intestinal barrier function. Intestinal microbiota can also indirectly affect intestinal barrier function via fermentation of undigested carbohydrates in the intestine. An example of this is the production of butyrate by colonic bacteria, which enhances the intestinal barrier by facilitating TJ assembly[222]. Some dietary carbohydrates, on the other hand, are able to shift the commensal community towards a more advantageous composition by selectively stimulating the growth and/or activity of specific bacteria within the gastrointestinal system, which in turn can affect TJ integrity[223]. Dietary components have also been shown to negate the effects of pathogenic bacteria, and thereby protect the integrity of the intestinal barrier. For example, human milk oligosaccharides inhibit the adhesion of intestinal pathogens EPEC O119, *Vibrio cholerae*, and *Salmonella fyris* to Caco-2 cells[224]. Thus it is important to consider the interactions between the different components of the intestinal barrier when developing strategies for enhancing barrier integrity using food and/or bacteria.

1.8 *IN VITRO* EPITHELIAL MODELS OF THE INTESTINAL BARRIER

In vitro intestinal epithelial cell models are widely used, not only in the study of host-microbe interactions, but also to study bioavailability, nutrient absorption, drug delivery and toxicity. Advantages of *in vitro* models over *in vivo* models include cost effectiveness, availability of automation techniques, the possibility of mass screening, and inter-lab reproducibility due to the clonal origin of cell lines[225]. However, arguably the greatest advantage of an *in vitro* system is that it provides a platform for using a reductionist approach to elucidate mechanisms by which the intestinal barrier is regulated.

1.8.1 *In vitro* cell lines as models of the intestinal epithelium

Much of the development of culturing intestinal cells *in vitro* took place in the 1980s, and main approaches included the *in vitro* culturing of normal enterocytes (primary cells)[226] or the differentiation of cancer-derived intestinal cells to enterocyte-like cells[227,228,229]. While several functional models of the intestine have been developed using normal cell lines prepared from primary cells[230,231], most of the established models of the intestinal epithelium are immortalised cancer-derived cell lines[225,232,233,234] because primary cells, due to their short lifespan, have inherent limitations with repeatability[225], and are relatively more difficult to culture than immortalised cells[226,234].

There are many examples of immortalised epithelial cell lines. These include non-intestine derived cells such as MDCK cells isolated from a dog kidney[235], which is an accepted model of intestinal epithelial transport[236], and human intestinal epithelial cell lines such as Caco-2[228], HT-29[237], T84[238], HCT-8[239], HCT-15[240] and DLD-1[240]. Many however do not express important *in vivo* features such as a well-defined brush border, TJ on the apical surface, or do not possess the ability to undertake transepithelial ionic transport[232]. The human adenocarcinoma cell lines HT-29, Caco-2 and T84, however, reproducibly express morphological and functional characteristics of the intestinal mucosa and are widely used in studies of transport and toxicity[241].

Of these, Caco-2 cells are considered the best characterised and most widely used cell line[220,225,233]. In a study comparing 20 human colon carcinoma cell lines, only Caco-2 cells spontaneously differentiated into enterocyte-like cells, characterised by

polarisation of the cell layer, development of a brush border with brush border-associated hydrolases, and the formation of domes[242]. In culture, Caco-2 cells form a confluent monolayer and spontaneously differentiate into polarised small intestine enterocyte-like cells, characterised by an apical brush border and TJ between adjacent cells[228]. Although HT29 cells can by induced to differentiate by means of various chemicals, unlike Caco-2 cells they do not differentiate spontaneously under normal culture conditions[229]. While T84 cells do differentiate spontaneously, their brush border is not as well developed as in Caco-2 cells and their features are characteristic of colonic crypt cells[238].

However, the disadvantages of using tumour-derived cells over primary cells should not be overlooked. Caco-2 and other cancer-derived cell lines, despite their extensive detailed study and extensive use, due to their tumoral origin, have inherent limitations. For example, Caco-2 cells, while of colonic origin, mainly express characteristics of small intestinal cells[243]. Further, as with all *in vitro* models, these cells are grown in an artificial environment, and thus it is difficult to extrapolate data to the *in vivo* (physiological) situation.

1.8.2 Transepithelial models to study host-bacteria interactions

Polarising epithelial cells such as Caco-2, T84 and MDCK can be grown on microporous membranes on cell culture inserts allowing them to become fully polarised[244] (Figure 1.6a). The microporous membrane allows separation of the apical compartment, which represents the intestinal lumen, from the basal compartment. In this configuration, cells receive nutrients via basal feeding, similar to the *in vivo* situation where cells receive nutrients from the underlying capillary bed[244].

It is possible to co-culture epithelial cells with bacteria and examine the interactions between the two cell types in terms of epithelial barrier integrity, bacterial cell attachment and epithelial cell apoptosis, among other functional and biological characteristics[232]. As exemplified by many of the studies described in this review, examination of host-microbe interactions using co-culture models have shown that bacteria affect a large number of epithelial functions *in vitro*, including cell permeability[245], ion conductivity[246], and the production of immune mediators[247].

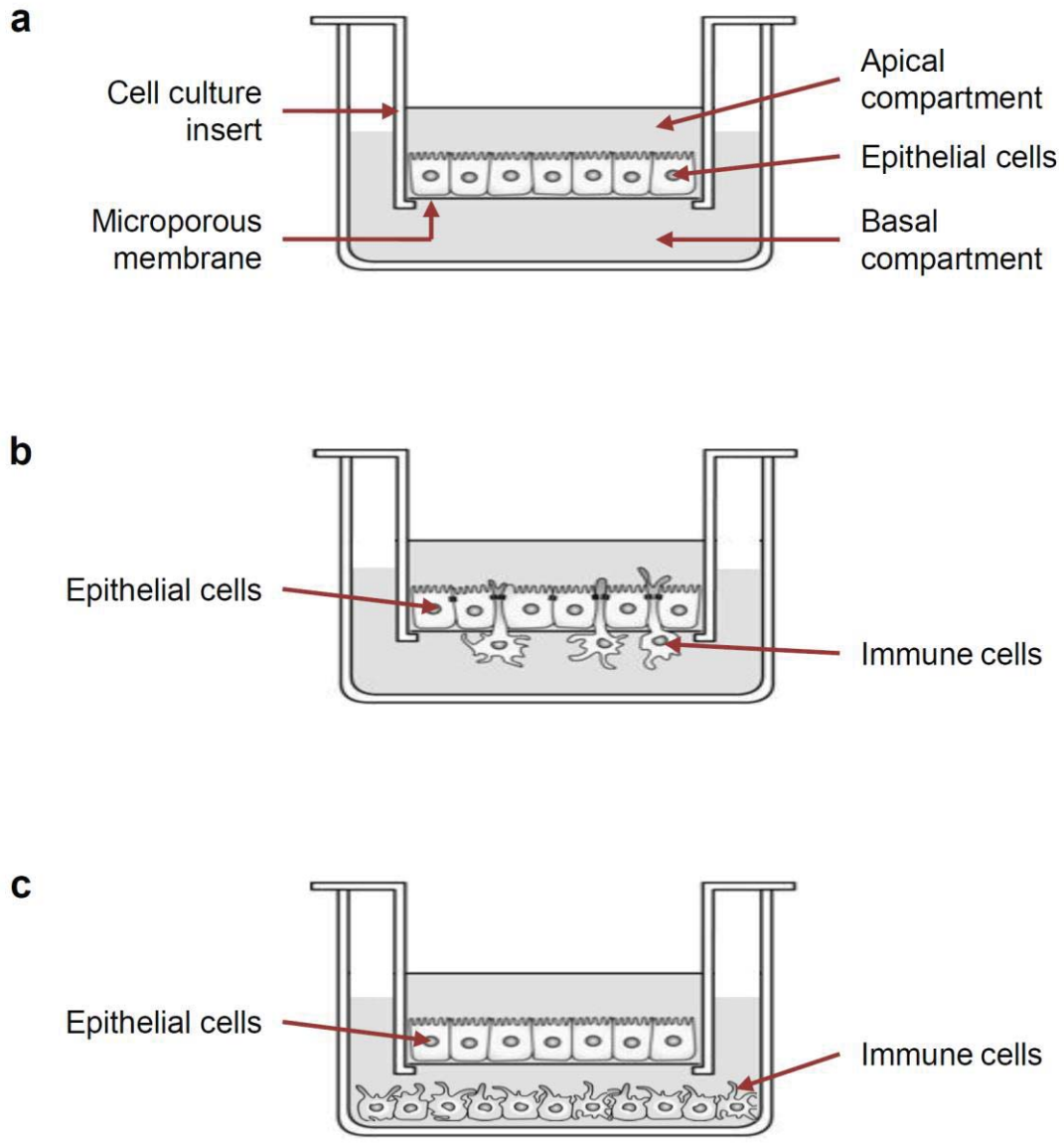

Figure 1.6 Representation of transepithelial models.

(a) Polarising epithelial cells grown on microporous membranes on cell culture inserts. The microporous membrane separates of the apical compartment, which represents the intestinal lumen, from the basal compartment. (b) Immune cells grown in the basal compartment of the transepithelial model such that epithelial-immune cell contact does not occur. (c) Immune cells seeded on the opposite side of the microporous membrane to the epithelial cells. Figure modified from the drawings by Peter Vullings.

As previously described, the intestinal epithelium is composed of several other cell types in addition to absorptive enterocytes[32]. To better mimic the intestinal barrier it is possible to co-culture enterocyte-like cells with a more specialised cell type, such as mucus secreting goblet cells. An example of this is the co-culture of Caco-2 cells with goblet-like HT29-MTX cells[248,249,250,251]. Compared with pure Caco-2 cell monolayers, Caco-2/HT29-MTX co-cultures have an altered permeability and a layer of mucus secreted by the HT29-MTX cells, better mimicking the *in vivo* situation.

Immune cells of the lamina propria, as previously discussed, are known to influence various aspects of intestinal epithelial cell function, either through direct contact of the epithelial cells or secretion of immune mediators. Epithelial-immune cell co-cultures can be established to mimic the intestinal barrier. In some studies, immune cells are purified from peripheral blood mononuclear cells retrieved from blood[252,253], while other studies utilise intestine-derived lymphocytes[142]. Immune cells can either be grown in the basal compartment of the transepithelial model such that epithelial-immune cell contact does not occur[253,254] (Figure 1.6b), or seeded on the opposite side of the microporous membrane to the epithelial cells[128] (Figure 1.6c), or together with epithelial cells in the apical compartment[253]. Such reductionist models allow for the dissection of intercellular signalling pathways, and are a convenient means of screening bacteria which impart a beneficial effect on intestinal barrier function. As illustrated in the studies discussed in this review, the direct effects of immune mediators or activated immune cells on epithelial cells are difficult to study *in vivo* due to the complexity of the intestine, and much of our current knowledge on epithelial cell immunomodulation has been derived from *in vitro* cell models.

1.8.3 *In vitro* models to study interactions between obligate anaerobes and intestinal epithelial cells

A major disadvantage of using transepithelial models to study interactions between intestinal bacteria and the intestinal epithelium is that while epithelial cells require an aerobic atmosphere for survival *in vitro*, the intestinal commensal microbiota is composed mainly of obligate anaerobic bacteria. This makes it especially difficult to co-culture intestinal cells with commensal obligate anaerobes *in vitro*.

Several *in vitro* studies have investigated interactions between obligate anaerobic bacteria and human intestinal cells, but not without inherent limitations. For

example, in a recent study in which the adherence of the obligate anaerobe *Clostridium difficile* to human intestinal cells was evaluated using the Caco-2 cell line, the Caco-2 cells were exposed to an anaerobic environment[255]. However this meant that the duration of the assay was only 3 hours and hypoxia may have affected the physiology of the cells. Conversely, another study analysed immune responses of HT29 cells to the commensal obligate anaerobe *B. infantis*[256] under aerobic conditions. However, after 6 hours of co-culture, less than 0.02% of the bacteria were viable.

In a study evaluating the immunomodulatory properties of the commensal obligate anaerobe *F. prausnitzii*, it was shown that the bacterial supernatant, but not UV-killed bacterial cells, was able to inhibit the NF-κB pathway in Caco-2 cells[257]. It was also found that while the supernatant was able to reduce secretion of the pro-inflammatory cytokine IL8 by Caco-2 cells, UV-killed bacteria and bacterial cell fractions were not. This disparity may have occurred because the bacterial cells were non-viable; if the cells were co-cultured in an environment where viability of neither the Caco-2 nor bacterial cells was compromised, the bacteria would be expected to have produced the active components in the supernatant, and the results might have been comparable.

Other studies have utilised dual-environment systems to co-culture oxygen-requiring mammalian cells with microbial cells that require microaerophilic or anaerobic conditions for optimal growth. One example is a vertical diffusion chamber developed by Cottet *et al.* (2002)[258] where Caco-2 cells were grown on a microporous membrane mounted between two chambers. One of the chambers contained cell culture medium continuously perfused with air, while the other chamber contained bacterial culture medium continuously perfused with a microaerophilic gas mixture. A similar model was used in other studies to investigate the invasion and adherence of pathogenic intestinal bacteria to intestinal epithelial cells[259,260]. Another example is a two-chamber system developed by Laube *et al.* (2000)[261] for the purpose of co-culturing hepatocytes with faecal microbiota. Similar to the previously described model, hepatocytes were cultivated as a monolayer on a microporous membrane mounted between two chambers. The chamber containing the hepatocytes was perfused with an aerobic gas mixture, while the chamber containing the faecal microbiota was perfused with an anaerobic gas mixture.

It should be noted that the above described dual-environment systems were not optimised for the co-culture of obligate anaerobes and intestinal epithelial cells.

However, Kelly *et al.* (2004)[210] utilised a dual-environment system that allowed for anaerobic bacteria and oxygen-requiring Caco-2 cells to be co-cultured, to investigate the immune modulation of Caco-2 cells by the commensal anaerobe *B. thetaiotaomicron*. This system included a custom built chamber which was used inside an anaerobic workstation. Although immune assays, immunoblotting and transcriptomic analysis were possible in this system, direct measurements of the effects of bacteria on barrier integrity of the Caco-2 cell monolayer were not reported. Nonetheless, it may be possible to utilise this concept to develop a dual-environment system for the comprehensive investigation of the effects of obligate anaerobes on intestinal barrier integrity. These improvements could include the addition of electrodes for measuring TEER, and the addition of sampling port to aid intestinal barrier permeability measurements.

1.9 CONCLUSIONS AND FUTURE PERSPECTIVES

The intestinal barrier is a complex ecosystem combining the intestinal epithelium, coated with a protective mucus layer, immune cells of the lamina propria, and an estimated 500-1000 species of commensal bacteria, and thus the regulation of barrier function cannot be easily elucidated. Commensal bacteria are instrumental in modulating the interactions between intestinal epithelial and immune cells, and regulating the barrier. Many of the studies on the beneficial effects of bacteria on intestinal barrier function and the underlying mechanisms of regulation have focused on probiotic strains. This may reflect a greater interest in understanding the beneficial effects of probiotics due to their commercial applications, but it may also be due to difficulties in culturing commensal bacteria, the vast majority of which are obligate anaerobes. Some probiotics were isolated from humans, such as *E. coli* Nissle 1917, a human faecal isolate. Not all commensal bacteria may be able to modulate epithelial barrier functions as shown in a study comparing commensal and probiotic strains (e.g. Resta-Lenert and Barrett (2006)[201]).

While immune modulation of the human intestinal cells in response to anaerobic commensal bacteria has been investigated both *in vitro* and *in vivo*[210,257], the regulation of intestinal barrier function by anaerobic bacteria has been poorly studied. This may be due to the lack of a suitable system to co-culture, and investigate the effect of anaerobic

bacteria on intestinal cell barrier function. The use of a reductionist *in vitro* model, which allows the co-culture of obligate anaerobic bacteria with intestinal epithelial cell lines, would facilitate comparison of mechanisms employed by probiotics and commensals to regulate the intestinal barrier function. An understanding of the mechanisms underlying the regulation of the epithelial barrier of the intestinal tract is important in the future development of novel and improved strategies to improve intestinal barrier function and health.

1.10 AIMS OF WORK REPORTED IN DISSERTATION

It is becoming increasingly evident that the commensal intestinal microbiota and their metabolites are key mediators of the 'crosstalk' between the epithelium and other cell types in the intestinal mucosa, and that their interactions with the epithelium influence aspects of the intestinal barrier function. However, as over 90% of the commensal bacteria are obligate anaerobes that are difficult to culture, especially in the presence of oxygen-requiring epithelial cells, the mechanisms that enable the intestinal microbiota to influence intestinal barrier integrity are largely unknown.

A novel *in vitro* model of the intestinal epithelium, where the apical surface of the cells, which represents the luminal aspect of the epithelium, is exposed to an anaerobic environment, will address this important gap. This model is likely to be more representative of *in vivo* intestinal conditions (of the ileum and colon, which harbours the greatest number of commensal bacteria) than intestinal epithelial cell models in a solely aerobic environment. As the luminal side is anaerobic, the model will allow for the intestinal cells to be co-cultured with species of commensal obligate anaerobic bacteria. Once the model is developed, experiments would be carried out to validate the model and identify differences between intestinal cells cultured under conventional or apical anaerobic conditions. Ultimately the model would be used to co-culture intestinal cells together with obligate anaerobic bacteria, and determine the effects of the bacteria on intestinal cells, specifically with regard to barrier function. This model, henceforth referred to as the apical anaerobic model, could be used to gain insights into the mechanisms of crosstalk between the epithelium and commensal anaerobic bacteria, and subsequently this knowledge could be used to improve intestinal barrier function, and hence health.

The overall aim of this study was to develop and demonstrate the use of an apical anaerobic model of the human intestinal barrier to allow study of the interactions between intestinal cells, which require oxygen for survival, and obligate anaerobic bacteria, which die in the presence of oxygen. The main hypotheses of this study, couched in the context of an *in vitro* apical anaerobic model, were: (i) intestinal epithelial cells in an apical anaerobic environment remain viable and form an intact barrier, (ii) intestinal epithelial cells in an anaerobic apical environment have altered biological and functional characteristics compared to intestinal epithelial cells in a solely aerobic environment, and (iii) viable obligate anaerobic bacteria and non-viable cells of the same strain exert differential effects on intestinal epithelial cells, and thus could potentially modulate the intestinal barrier function through different mechanisms.

1.11 APPROACH AND STRUCTURE OF THE DISSERTATION

The aims of this study will be achieved through the following objectives:

- Development: Culture polarised intestinal epithelial cells such that the apical (luminal) side is exposed to an anaerobic environment (Chapter 2).
- Validation: Compare the characteristics of intestinal epithelial cells grown in an anaerobic apical environment to intestinal epithelial cells grown in a solely aerobic environment (Chapters 3-4).
- Application: Use the model to co-culture epithelial cells with viable commensal anaerobic bacteria (Chapter 5).

The apical anaerobic model of the intestinal barrier utilises a dual-environment co-culture chamber, which when placed inside an anaerobic workstation allows polarised intestinal epithelial monolayers to be exposed to an anaerobic environment on the apical side. Chapter 2 of this dissertation describes the concept and the development of the apical anaerobic model, as well as the design and optimisation of the custom-built co-culture chamber.

The work described in Chapter 3 investigates the validity of the apical anaerobic model. Firstly the dissolved oxygen (DO) levels were measured to ensure the apical and basal atmospheres were anaerobic and aerobic respectively as intended. Secondly cell viability and morphology of intestinal cells exposed to the apical anaerobic environment

were examined and compared to cells grown under conventional conditions. Finally barrier function assays and confocal microscopy were used to examine the barrier integrity of the intestinal cell monolayer, as a well formed barrier is not only integral to maintaining a dual-environment, but also necessary to study regulation of barrier function by intestinal bacteria.

In Chapter 4 results of global gene expression analysis, carried out to identify key differences in gene expression between intestinal cells with an anaerobic apical side compared to those grown in conventional cell culture conditions, are reported. Based on these differences, changes in biological functions and pathways were predicted and compared with the phenotypic data reported in Chapter 3.

The work described in Chapter 5 demonstrates how the apical anaerobic model can be used to study interactions between live obligate anaerobes and intestinal cells. An obligate anaerobic strain of the commensal intestinal microbiota was co-cultured with intestinal cells, and its viability measured in the apical anaerobic model. The effects of the live obligate anaerobe on intestinal barrier function and epithelial cell gene expression was studied and compared with that of non-viable bacterial cells of the same strain.

A summary and discussion of the main findings of the thesis is given in Chapter 6. A flowchart describing the structure of the dissertation is presented in Figure 1.7.

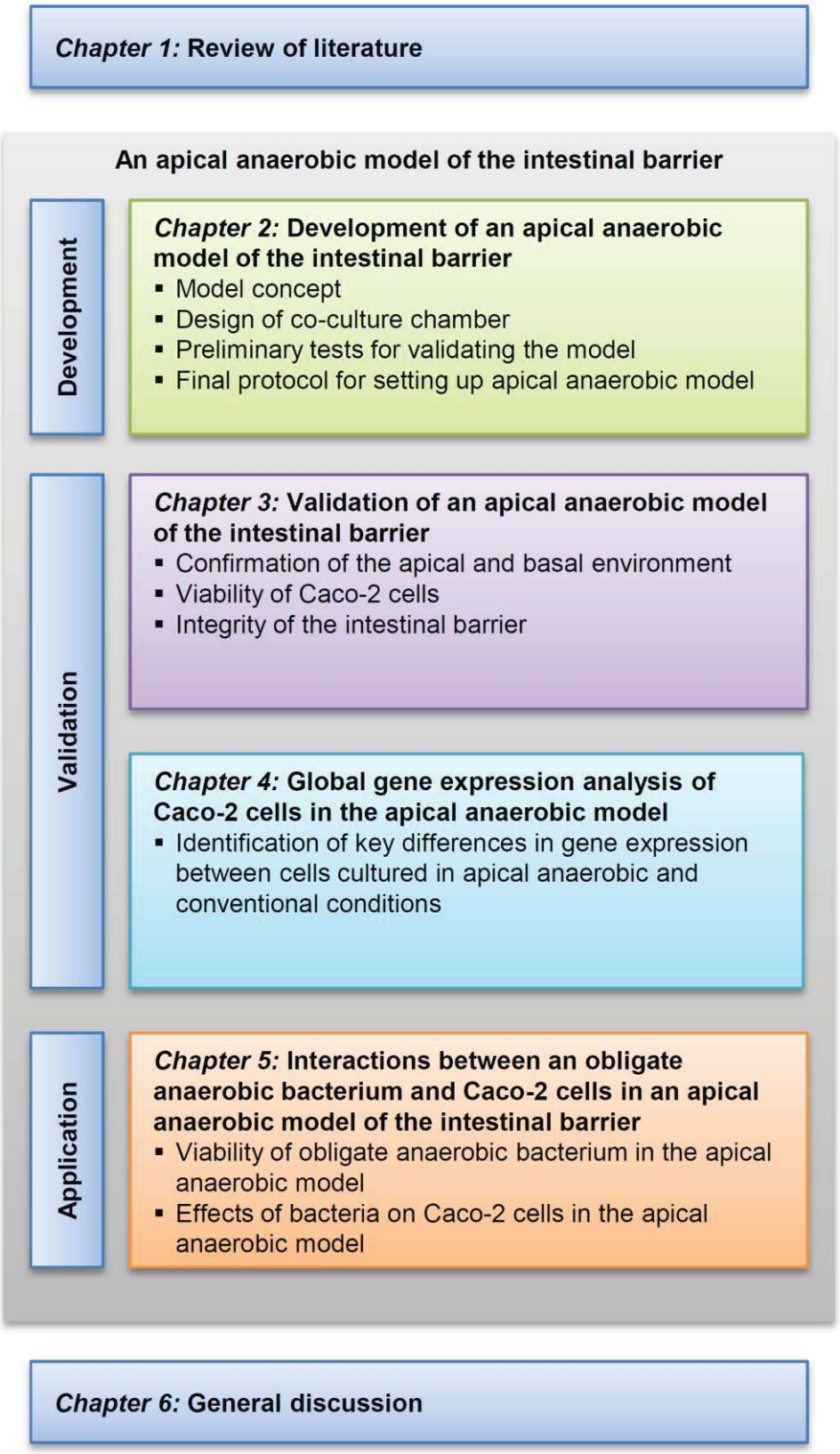

Figure 1.7 Structure of the dissertation.

A flow chart describing the outline of the dissertation and its experimental chapters.

Chapter 2:

Development of an apical anaerobic model of the intestinal barrier

2.1 INTRODUCTION

The human intestine is crucial for the digestion of food and the absorption of nutrients and water but also functions as a barrier to prevent commensals, pathogens and excessive amounts of antigens from entering the mucosal tissues. The most important physical barrier is a single layer of epithelial cells which separates the luminal contents from the inside of the body. TJ seal the paracellular space between epithelial cells with selective permeability to fluids, electrolytes and small molecules. Increased permeability can result in the entry of unwanted antigens and pathogens into the body and is implicated in autoimmune[10], inflammatory[8] and atopic diseases[262]. It is becoming increasingly evident that microbes, including their metabolites, are key mediators of the 'crosstalk' between the polarised epithelium and other cell types in the mucosa, and that their interactions with the epithelium influence aspects of intestinal barrier function[14]. However, over 90% of the estimated 10^{14} microbes[18] that inhabit the intestinal tract are obligate anaerobes[19,150], making it difficult to study their interactions with oxygen-requiring mammalian cells commonly used in *in vitro* models of the intestinal barrier.

Several *in vitro* studies have investigated interactions between obligate anaerobic bacteria and human intestinal cells, but not without inherent limitations. For example, one study exposed Caco-2 cells to an anaerobic environment to study the adherence of the obligate anaerobe *Clostridium difficile* to human intestinal cells[255]. However this meant that the duration of the assay was only 3 hours and hypoxia may have affected the physiology of the cells. Conversely, another study exposed the obligate anaerobe *B. infantis* to aerobic conditions to analyse its effect on the immune responses of HT29 cells[256]. However, after 6 hours of co-culture the bacterial cell viability had dropped to less than 0.02%. It has been shown that metabolites secreted by viable anaerobic bacteria, compared to non-viable bacteria cells of the same strain, have different immunomodulatory effects on Caco-2 cells[257]. This demonstrates the need for a co-culture system where the viability of neither the intestinal epithelial cells nor the anaerobic bacteria is compromised.

Thus several studies have utilised dual-environment systems to co-culture oxygen-requiring mammalian cells with microbial cells that require microaerophilic or anaerobic conditions for optimal growth[258,261]. Several of these models were optimised

for the co-culture of microaerophilic pathogens with intestinal epithelial cells[258,259,260], or the co-culture of anaerobic bacteria with hepatocytes[261]. Conversely, Kelly *et al.* (2004)[210] utilised a dual-environment system that allowed for commensal anaerobic bacteria and oxygen-requiring Caco-2 cells to be co-cultured, to investigate the immune modulation of Caco-2 cells by the commensal anaerobe *B. thetaiotaomicron*. Although immune assays, immunoblotting and transcriptomic analysis were possible in this system, direct measurements of the effects of bacteria on barrier integrity of the Caco-2 cell monolayer were not reported. Nonetheless, it may be possible to utilise this concept to develop a dual-environment system for the comprehensive investigation of the effects of obligate anaerobes on intestinal barrier integrity.

2.2 AIM

The aim of the research reported in this chapter was to develop, optimise and establish protocols for the use of an *in vitro* model of the human intestinal epithelium, known as the apical anaerobic model, designed to allow investigation of the interactions between obligate anaerobic bacteria and the intestinal epithelium. The apical anaerobic model utilised a dual-environment co-culture chamber, which when placed inside an anaerobic workstation, allows polarised intestinal cell monolayers to be exposed on the apical (luminal) side to an anaerobic environment while maintaining an aerobic basal side to prevent hypoxia. In this configuration, the intestinal cells can be co-cultured with obligate anaerobic bacteria in the anaerobic apical environment.

2.3 METHODS

2.3.1 Model concept

Caco-2 cells develop morphological and functional characteristics similar to small intestine enterocytes and thus are a useful model of the intestinal epithelium[243]. In culture these cells form a monolayer and undergo spontaneous differentiation, characterised by polarisation of the cell monolayer, and the presence of an apical brush border and TJ between adjacent cells[33,228]. Caco-2 cells undergo similar differentiation when grown on a microporous membrane, allowing separation of the apical compartment, which represents the intestinal lumen, from the basal compartments[234,243].

The apical anaerobic model utilised a custom built co-culture chamber used inside an anaerobic workstation (Concept Plus, Ruskinn Technology Ltd, Pencoed, Bridgend, UK) which maintained a temperature of 37°C and an atmosphere of 10% CO_2, 10% H_2 in N_2. The co-culture chamber contained an apical and a basal compartment separated by a microporous membrane. Caco-2 cells were grown on the microporous membrane. The basal compartment of the co-culture chamber, sealed off from the external anaerobic atmosphere, contained an aerobic cell culture medium, and is also known as the aerobic compartment. The apical compartment of the co-culture chamber, exposed to the oxygen-free atmosphere of the anaerobic workstation contained anaerobic cell culture medium, and is also known as the anaerobic compartment. In this configuration the DO in the basal compartment was predicted to diffuse through the microporous membrane to the cells, thereby ensuring survival of the Caco-2 cells. The apical anaerobic co-culture model is illustrated in Figure 2.1.

2.3.2 Culture of intestinal epithelial cells

The Caco-2 cell line (HTB37) was obtained from the American Type Culture Collection (ATCC) at Passage 18 and used in experiments at Passage 26-35. It was critical to use the cells within a defined interval of passages, as phenotypes of Caco-2 cells taken from high and low passage intervals can differ[263,264]. Caco-2 cells and cell culture medium and reagents were handled using aseptic techniques in a laminar flow hood (class II biological safety cabinet).

2.3.2.1 Maintenance of Caco-2 cells

Caco-2 cells were cultured in cell culture medium (Table 2.1) under standard culture conditions (37°C; 5% CO_2 incubator). The cell culture medium described in Table 2.1 was used as it was shown to have a higher buffering capacity against pH change in the presence of bacteria, than the culture medium recommended by ATCC (Dr Rachel Anderson, unpublished data). The cells were maintained in 75 cm² rectangular canted-neck cell culture flasks with vent caps (Corning, Lindfield, New South Wales, Australia) containing approximately 20 mL of cell culture medium. The cell culture medium in the flask was replaced every 3-4 days, and the cells passaged weekly at a 1:5 dilution as described in section 2.3.2.3. Cell culture medium and other reagents were pre-warmed to 37°C to reduce undue stress on the cells.

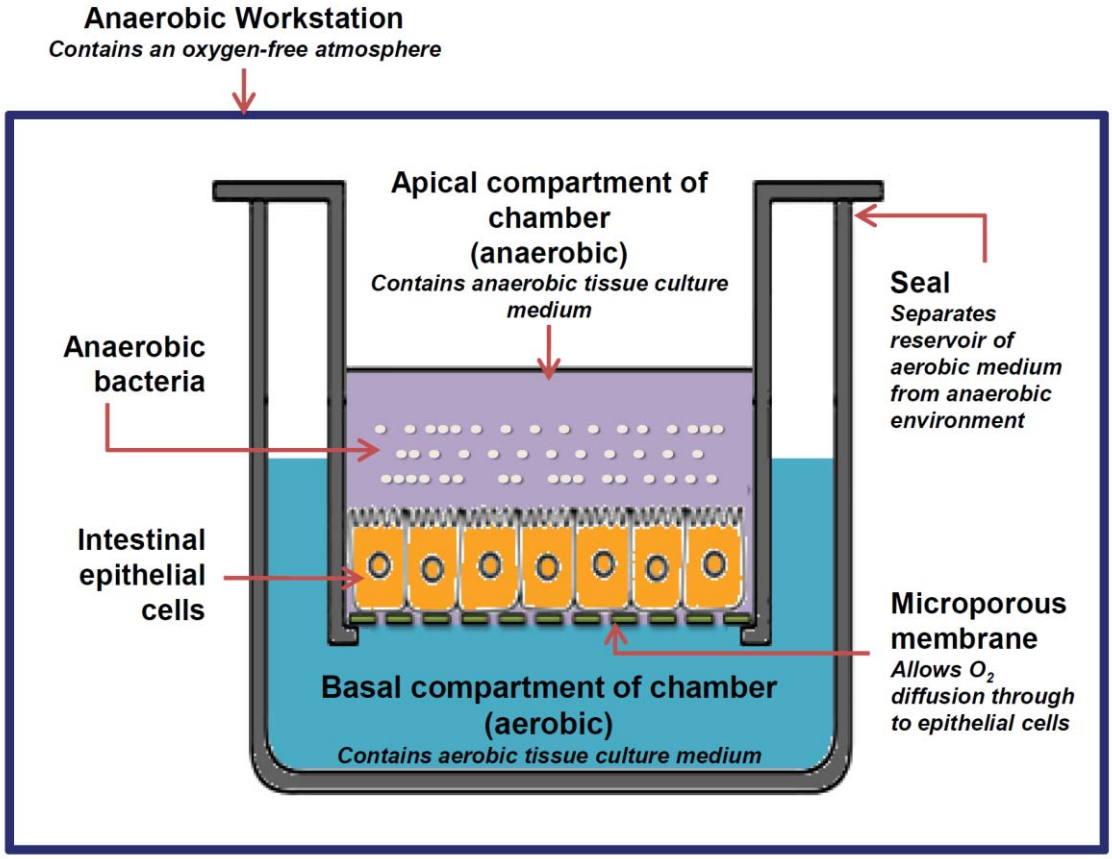

Figure 2.1 The apical anaerobic co-culture model.

The model utilised a co-culture chamber placed inside an anaerobic workstation, which had an oxygen-free atmosphere. Intestinal epithelial cells were grown on a microporous membrane in a well containing aerobic cell culture medium. This reservoir of aerobic medium constituted the anaerobic basal compartment of the chamber, and was sealed off from the external environment. The compartment above the microporous membrane was thus exposed to an anaerobic atmosphere and constituted the apical anaerobic compartment of the co-culture chamber. Obligate anaerobic bacteria can be co-cultured with intestinal epithelial cells in an anaerobic cell culture medium in the apical compartment of the co-culture chamber. Oxygen is predicted to diffuse through the microporous membrane to the epithelial cells ensuring their survival. Figure modified from the drawing by Peter Vullings.

Table 2.1 Composition of cell culture medium.

Media components and volumes required to prepare 50 mL of cell culture medium.

Media component	*Volume*
Medium 199 (M199; Life Technologies)	44 mL
Foetal bovine serum (FBS; Life Technologies)	5 mL
Penicillin-Streptomycin (10 000 units/mL penicillin and 10 mg/mL streptomycin; Sigma-Aldrich)	500 µL
MEM Non-Essential Amino Acids (NEAA; 100 x solution; Life Technologies)	500 µL

2.3.2.2 Harvesting Caco-2 cells

Cells were dissociated from the flask using 2.5 mL (25 cm^2 flask) or 5 mL (75 cm^2 flask) TrypLE express (Life Technologies, Penrose, Auckland, NZ) and incubating at 37°C for 5-12 minutes. The flask was inspected under a light microscope to ensure that the cells had detached, and the side of the flask tapped to aid detachment of loosely adhered cells. The cell suspension was mixed with an equal volume of cell culture medium to inactivate the TrypLE express enzyme, and the cells pelleted by centrifugation for 3 minutes at 240 x g, and resuspended in 5 mL of fresh cell culture medium.

2.3.2.3 Passaging of Caco-2 cell line

Passaging refers to the transfer of cells between flasks (with or without dilution)[265]. The biochemistry of confluent cells can be different from that of exponentially growing cells so they should be passaged before they become confluent. Cultures of Caco-2 cells were passaged weekly, when they reached approximately 90% confluence. Cells were harvested as described in section 2.3.2.2. For a 1:5 dilution, 1 mL of the cell suspension was added to a new cell culture flask containing pre-warmed cell culture medium.

2.3.2.4 Long term storage of Caco-2 cells

Frozen stocks of Caco-2 cells were maintained in liquid nitrogen in cryopreservation medium. Cryopreservation medium was prepared by adding 1 mL of dimethyl sulphoxide (DMSO; Sigma-Aldrich, St. Louis, Missouri, USA) to 9 mL of FBS. DMSO is a cryoprotective agent that increases dehydration of the cells, lowers the freezing point and reduces the risk of damage to cells by ice crystal formation[266]. Caco-2 cells were harvested from 75 cm^2 flasks which were approximately 90% confluent as described in section 2.3.2.2, but resuspended in 4 mL cryopreservation medium per flask. The cell suspension was transferred to cryogenic vials (Corning) in 1 mL aliquots and stored overnight at -80°C inside a Nalge Nunc Cryo 1°C Mr. Frosty Freezing Container (Thermo Fisher Scientific, Scoresby, Victoria, Australia) filled with 100% isopropyl alcohol, following which the vials were transferred into a liquid nitrogen Dewar. The freezing container facilitated a cooling rate of approximately 1°C per minute, thus promoting a greater loss of water from the cells and reduced ice crystal formation and thereby minimising the potential for cell damage[266].

Frozen stocks were recovered by thawing the contents of the cryogenic vial at 37°C and mixing with 9 mL of cell culture medium following which the cells were centrifuged at 240 x g for 3 minutes. The cell supernatant, which contained DMSO, toxic to cells at warm temperatures, was discarded, and the cells were resuspended in fresh 10 mL cell culture medium and added to a 25 cm^2 rectangular canted-neck cell culture flask (Corning). After 24-48 hours at 37°C in a 5% CO_2 incubator, the cells were examined under a microscope to ensure that they had adhered to the flask, had normal morphology, and lacked contamination. The media in the flask was replaced with fresh cell culture medium. When the cells reached approximately 90% confluence they were passaged without dilution to a 75 cm^2 flask as described in section 2.3.2.3.

2.3.2.5 Cell counting

Cells were harvested as described in 2.3.2.2, and a 10 µL sample of the cell suspension was removed for cell counting and mixed with 90 µL of Trypan Blue (0.4% solution, Life Technologies). Trypan Blue is a non-permeable dye taken up by only non-viable cells. Thus non-viable cells appear blue, while healthy cells are refractory to the dye and appear rounded under the microscope. The stained cell suspension was loaded on to a counting chamber in an improved Neubauer haemocytometer. The counting chamber was 0.1 mm deep and divided into nine large squares, each of which had a volume of 0.1 mm^3. Thus to determine the number of cells per mL of stained cell suspension, the number of viable cells in each of four squares was averaged and multiplied by 10^4. This number was multiplied by 10 to take into account the 1:10 dilution with Trypan Blue to calculate the concentration of cells in the undiluted cell suspension.

2.3.3 Growth of Caco-2 cells on microporous membranes

The use of cell culture inserts with microporous membranes is a standard method for culturing cells, where human intestinal cell lines can be grown and allowed to differentiate[241] (Figure 2.2). In this system the cell monolayer formed a dual compartment system where the apical medium in the insert was separated from the basal medium in the cell culture well. Caco-2 cells were seeded on the cell culture inserts at

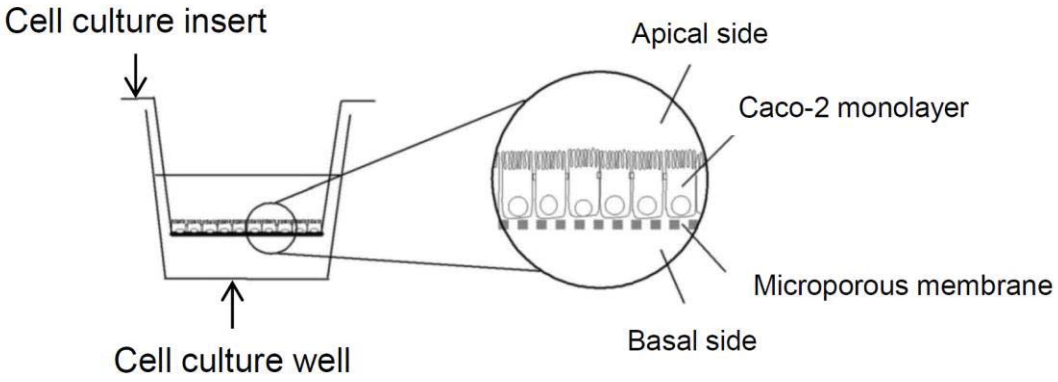

Figure 2.2 Cell culture insert configuration.

Caco-2 cells were seeded on a cell culture insert in a cell culture well. Cell culture media were added to both the insert (apical side) and well (basal side). Figure adapted from Hubatsch *et al.* (2007)[264].

passage 26-35, maintained under standard culture conditions and the cell culture medium replaced three times a week. The growth of Caco-2 cells was tested on several types of cell culture inserts of varying sizes, membranes and pores (Table 2.2), to determine the best type of insert to use in the apical anaerobic model.

Cell culture medium was added to the cell culture well, following which the cell culture insert was added to the well, and cell culture medium added to the insert. Cell culture medium was added at the volumes indicated in Table 2.3, and the multiple-well cell culture plate was incubated under standard culture conditions for 1 hour to equilibrate the microporous membranes and thus aid improved cell attachment.

Caco-2 cells were harvested from a 75 cm^2 flask as described in section 2.3.2.2. The concentration of cells in the suspension was determined (section 2.3.2.5), and diluted to the appropriate amount as indicated in Table 2.3. The medium in the cell culture insert was removed and replaced with the cell suspension. After an overnight incubation in standard cell culture conditions, the cell culture medium in the insert was replaced following examination under a microscope to ensure cells had adhered and had normal morphology.

2.3.4 TEER measurements

The TEER assay is one of the simplest and least invasive methods of measuring intestinal barrier integrity. It is an inverse measure of ion permeability across the epithelium, and reflects the 'tightness' of the barrier[244,267].

TEER across Caco-2 cell monolayers grown on culture inserts was measured using an STX-2 electrode (World Precision Instruments, Sarasota, Florida, USA; section 2.3.4.1), or an EndOhm culture cup (World Precision Instruments; section 2.3.4.2) connected to an EVOM voltohmmeter (0-20000 Ω range; World Precision Instruments). The resistance read by the voltohmmeter was converted to TEER ($\Omega.cm^2$) using the following equation: $((R)-(R_{background})) \times (A)$ where R is the resistance (Ω) across the Caco-2 cell monolayer, $R_{background}$ is the resistance (Ω) across the microporous membrane (without the Caco-2 cell monolayer), and A is the area (cm^2) of the membrane.

Table 2.2 Cell culture membranes selected to test the growth of Caco-2 cell monolayers.

The membrane types included polyester (PET), polycarbonate (PC), and collagen-coated polytetrafluoroethylene (PTFE) in small (S) and large (L) sizes (Membranes were manufactured by Corning Transwell, except for 'Cellagen', which was manufactured by MP Biomedicals).

Membrane name	*Membrane material*	*Diameter (mm)*	*Pore size (μm^2)*	*Pore density (pores/cm^2)*	*Growth area (cm^2)*
1. PET-S	Polyester	12	3.0	2×10^6	1.12
2. PET-L	Polyester	24	3.0	2×10^6	4.67
3. PTFE-S	Collagen-coated polytetrafluoroethylene	12	3.0	undefined	1.12
4. PTFE-L	Collagen-coated polytetrafluoroethylene	24	3.0	undefined	4.67
5. PC-S	Polycarbonate	12	3.0	2×10^6	1.12
6. PC-L	Polycarbonate	24	3.0	2×10^6	4.67
7. Cellagen	Collagen	14	unavailable	undefined	1.54
8. PET	Polyester	24	0.4	4×10^6	4.67

Table 2.3 Volume of medium and number of Caco-2 cells added to cell culture inserts.

Details for three different insert sizes are shown. 'Cells per insert' denotes the number of cells seeded in the insert of the given size. 'Cells per cm^2' is the number of cells seeded divided by the surface area of the microporous membrane. 'Volume per insert' and 'Volume per well' denotes the volume of cell culture medium added to the insert and well respectively. 'Cells per mL' indicates the concentration of Caco-2 cells in the cell culture medium added to the insert when seeding the cells.

Membrane type	*Cells per insert*	*Cells per cm^2*	*Volume per insert*	*Volume per well*	*Cells per mL*
Cellagen	1×10^5	6.5×10^4	250 µL	500 µL	4×10^5
Transwell (12 mm)	0.7×10^5	6.5×10^4	500 µL	1500 µL	$\sim 1.5 \times 10^5$
Transwell (24 mm)	3×10^5	6.5×10^4	1500 µL	2500 µL	2×10^5
Transwell (24 mm)	1.2×10^6	2.6×10^5	1500 µL	2500 µL	8×10^5

2.3.4.1 STX-2 electrodes

An STX-2 electrode was sterilised by spraying with 70% ethanol. The electrodes were allowed to air dry and rinsed with cell culture medium, and connected to an EVOM voltohmmeter as per the manufacturer's instructions. The electrode was placed vertically in the cell culture well as illustrated in Figure 2.3a, so the tip of the longer electrode touched the bottom of the well, and the shorter electrode was above the membrane of the Transwell insert. The TEER was measured by pushing the 'R' (resistance) button on the voltohmmeter and holding for 3 seconds until the reading stabilised.

2.3.4.2 EndOhm culture cup

A 24 mm EndOhm culture cup was sterilised with 70% ethanol, and rinsed with 5 mL cell culture medium after air drying. Three mL of cell culture medium was added to the culture cup, and connected to an EVOM Voltohmmeter as per the manufacturer's instructions. The Transwell insert was placed in the culture cup as illustrated in Figure 2.3b, and the top electrode height adjusted so that it was 1 mm above the membrane of the Transwell insert. TEER was measured by pushing the 'R' (resistance) button on the voltohmmeter and holding for 3 seconds until the reading stabilised. Generally the readings given by the EndOhm cup were more stable and consistent compared to those obtained from the STX-2 electrodes because the position of the electrodes relative to the cell monolayer was fixed between different inserts and measurements. With fixed electrodes the variation of reading on the same sample is 1-2 Ω, whereas for the STX-2 electrodes the variation is 5-10 % of the total reading[268].

2.3.4.3 Statistical analysis

Statistical analysis was performed in GenStat (version 13; VSN international Ltd., Hemel Hempstead, Hertfordshire, UK). Treatments were compared using a general analysis of variance (ANOVA), except for when the effect on TEER was measured over time, where treatments were compared using a repeated measurements ANOVA. Statistical difference was declared between two treatments (for a given time point) when the difference in means was greater than the least significant difference (LSD) at 5%. To identify at what point in time after seeding the TEER across Caco-2 monolayers plateaued, a logistic curve was fitted to the TEER data over time using GenStat .

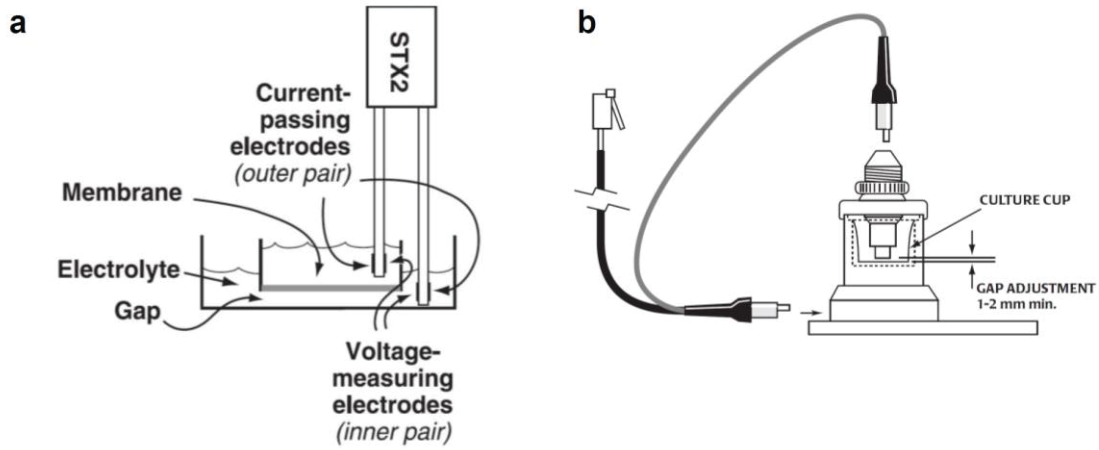

Figure 2.3 Methods of measuring TEER across Caco-2 cell monolayers.

TEER can be measured directly in the cell culture plate using an STX electrode (a), or by transferring the Transwell insert into an EndOhm culture cup (b).

2.3.5 Design of co-culture chamber[‡]

2.3.5.1 Design concept

Two prototype co-culture chambers were built, each containing 6 wells. Figure 2.4 represents a cross section from a single well of the co-culture chamber. Each well was equipped with a lid that acted as an adaptor for 12 mm Transwell inserts. Each chamber well was filled with 50 mL of culture medium, and each lid fitted with a cell culture insert, which sealed off the chamber well (basal compartment of co-culture chamber) from the outside environment. Thus when the co-culture chamber was moved into an anaerobic workstation (Concept Plus), the culture medium in the insert (apical compartment of co-culture chamber) could be replaced with anaerobic culture medium enabling the culture of Caco-2 cells such that the basal side was exposed to (aerobic) culture medium, while the apical side was exposed to the anaerobic environment of the anaerobic workstation.

2.3.5.2 Components of the co-culture chamber

Each chamber consisted of a chamber base with six wells, each equipped with an electrode (Figure 2.5a), six lids which also acted as adaptors to cell culture inserts and contained a sealable sampling port (Figure 2.5b), an electrode plate which encompassed the top electrodes for each chamber well (Figure 2.5c), and a cable to connect the bottom electrodes of the chamber base to the top electrodes of the plate (Figure 2.5d). Figure 2.5e shows an assembled prototype co-culture chamber. Once assembled the co-culture chamber was connected to a voltohmmeter.

2.3.5.3 Chamber size

The size of each well and hence the size of the chamber was determined by the size of the Transwell insert (12 mm in diameter) and the volume of the basal compartment. A large volume (50 mL) of culture medium was required in the basal compartment to ensure that sufficient DO was present to diffuse through to the Caco-2 cells.

[‡] The co-culture chamber was designed based on the concept conceived by Prof Denise Kelly (University of Aberdeen) and built by Steve Gebbie, Scott Sevier, Hong Zhang, Russel McAuliffe (all from AgResearch Lincoln), and Paul Lovejoy and Jason Peters (both from AgResearch Grasslands).

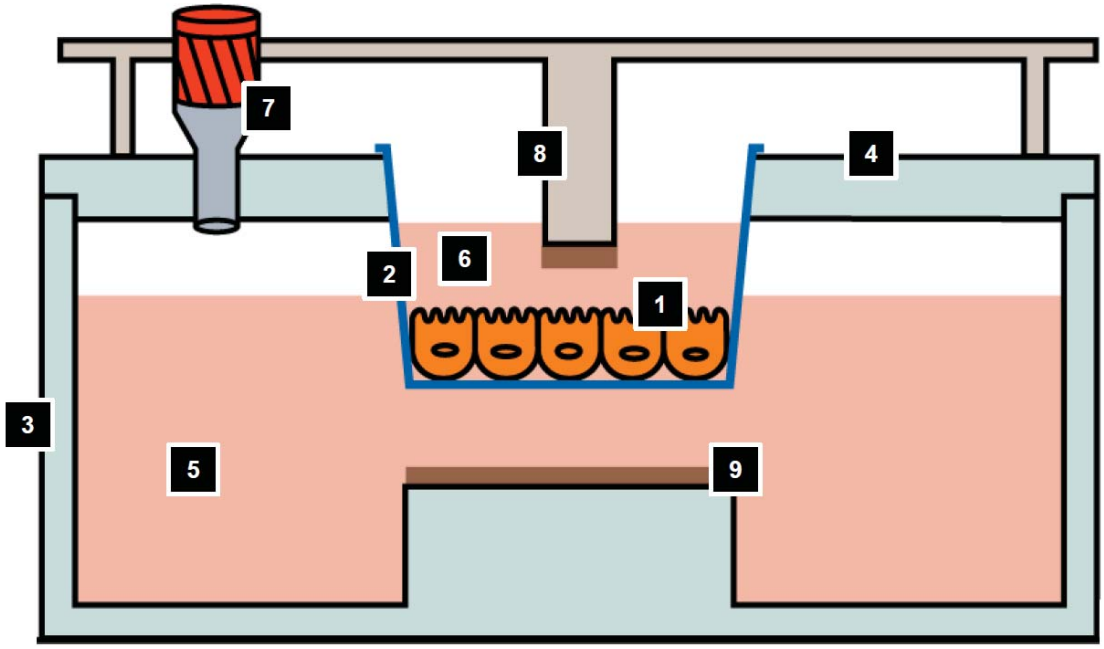

Figure 2.4 Design concept of co-culture chamber

A schematic representing a cross-section of a single well from the co-culture chamber inside the anaerobic workstation is shown. The chamber well was filled with (aerobic) cell culture medium. A Transwell insert with a Caco-2 cell monolayer was fitted on to the chamber lid, thus sealing off the chamber well (basal/aerobic compartment of co-culture chamber) from the anaerobic environment when inside the anaerobic workstation. The insert (apical/anaerobic compartment of the co-culture chamber) was filled with anaerobic cell culture medium. Thus, the apical side of the Caco-2 cell monolayer was exposed to an anaerobic environment, while the basal side was exposed to oxygen which diffuses through the membrane of the insert. The well was equipped with a pair of electrodes (one inside the chamber well, directly beneath the insert, and another directly above the insert) for automated measurement of TEER, and the chamber lid had a port sealed with a septum so that the basal medium could be removed without altering the environment, allowing the monitoring of small molecule flux. 1, Caco-2 cell monolayer; 2, Transwell insert (anaerobic apical compartment); 3, Chamber well (aerobic basal compartment); 4, Chamber lid (adaptor for Transwell insert); 5, Aerobic cell culture medium; 6, Anaerobic cell culture medium; 7, Port sealed with rubber septum for sampling media from the basal compartment; 8, Top TEER electrode; 9, Bottom TEER electrode. Figure modified from the drawing by Pauline Hunt.

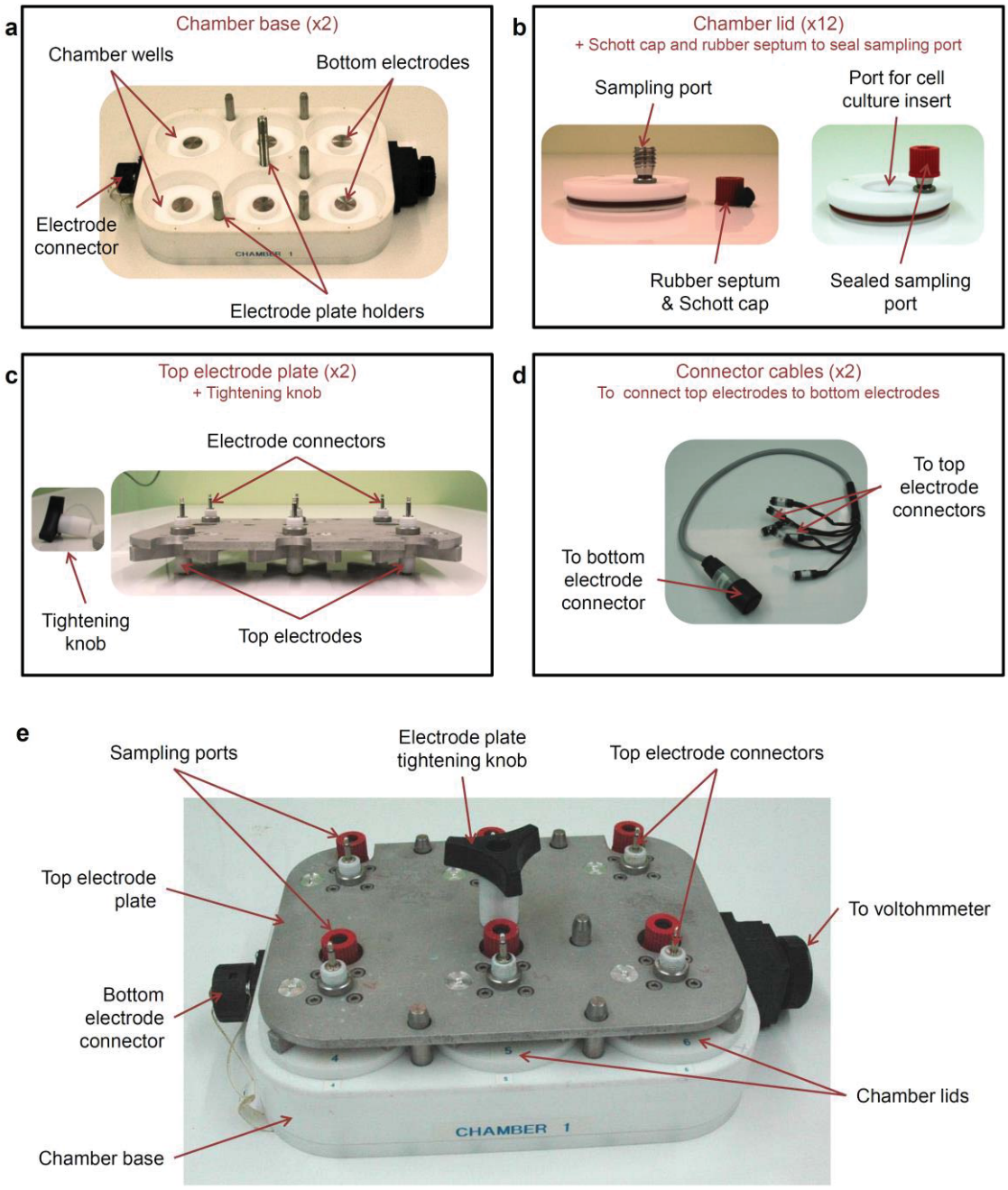

Figure 2.5 Components of the prototype co-culture chamber

Panels (a)-(d) show the individual components of the co-culture chamber; panel (e) shows the assembled co-culture chamber. (a) The chamber base contains 6 wells each equipped with an electrode; (b) Each chamber lid acts as an adaptor for a cell culture insert and contains a sampling port which can be sealed using a rubber septum and Schott cap; (c) The top electrode plate contains 6 electrodes and connectors; (d) A connector cable connects the bottom electrodes of the chamber base to the top electrodes of the electrode plate; (e) When assembled each well is closed with a lid and the top electrodes placed directly above the bottom electrodes and tightened with the tightening knob.

However the size of the chamber was constrained by the size of the interlock chamber in the anaerobic workstation. The interlock chamber was used to move objects into the anaerobic workstation. Objects were moved into the interlock via the 'outer door', the interlock purged with anaerobic gas, following which the object was moved into the anaerobic workstation via the 'inner door'. The dimensions of the interlock doors were 225 mm (width) x 275 mm (height) for the inner door, and 295 mm (width) x 250 mm (height) for the outer door; and the dimensions of the interlock were 320 mm (width), 300 mm (height), 300 mm (depth). Hence, two prototype chambers containing 2 x 3 wells, rather than a single chamber containing 12 wells, were built; each with the dimensions of 284.2 mm (width) x 123 mm (height) x 196 mm (depth). Engineers' drawings of the co-culture chamber are shown in Appendix I.

2.3.5.4 Features

The chamber was machined using Teflon so that it could be autoclaved. Each well of the chamber was equipped with a pair of electrodes, one directly above, and the other directly below the Transwell insert, for automated measurement of TEER (Figure 2.4). The electrodes were built of copper for its conductance properties and connected to an EVOM voltohmmeter. The display of the EVOM voltohmmeter meter was read by a camera which recorded 10 frames/second for a maximum of 5 seconds. Blocks of 10 frames were analysed, and where the greatest difference between two frames was less than 5 Ω, the average of the 10 frames was taken. When the minimum variability was greater than 5 Ω, the reading was flagged as unstable, and not considered for further analysis.

Each chamber lid was equipped with a port sealed with a septum (Figure 2.4). This allowed for the medium in the basal compartment of the chamber to be sampled using a needle and syringe without compromising the aerobic basal environment. The chamber lids also contained two O-rings: an inner O-ring to create a seal between the Transwell insert and chamber lid, and an outer O-ring to seal the chamber well from the outside environment.

2.4 RESULTS

2.4.1 Choice of microporous membrane and cell seeding density

The use of cell culture inserts with microporous membranes is a standard method for culturing cells. These membranes are manufactured in various sizes, using various materials and various pore-sizes.

Seven types of cell culture inserts (Table 2.2, membranes 1-7) were tested for the ability of Caco-2 cell monolayers to maintain TEER over time (n = 6). Caco-2 cells were seeded on the microporous membranes at a density of 6.5 x 10^4 cells/cm^2, and TEER was measured every 2-3 days using an STX2 electrode as described in section 2.3.4.1 (Figure 2.6). Except Transwell PET, all membranes tested displayed a drop in TEER across the Caco-2 cell monolayer (significant at the 5% LSD level) from day 9 onwards. While this drop in TEER was not observed with Caco-2 cell monolayers grown on 12 mm Transwell membranes, Caco-2 cell monolayers grown on 24 mm PET membranes had a higher TEER than those grown on 12 mm PET membranes from day 9 onwards.

Based on the above results, the TEER across Caco-2 cell monolayers over time was further tested in triplicate on 24 mm PET membranes with pore sizes of either 3.0 μm^2 (Table 2.2, membrane 2) or 0.4 μm^2 (Table 2.2, membrane 8) using an EndOhm culture cup as described in section 2.3.4.2. Caco-2 cells were seeded at the previous cell density of 3 x 10^5 cells/insert (6.5 x 10^4 cells/cm^2) or an increased cell density of 1.2 x 10^6 cells/insert (2.6 x 10^5 cells/cm^2). Caco-2 cell monolayers grown on membranes with a pore size of 0.4 μm^2 achieved a higher TEER than those grown on membranes with a pore size of 3.0 μm^2 (Figure 2.7). When viewed under a microscope, Caco-2 cell monolayers grown on membranes with a pore size of 3.0 μm^2 were not well-formed compared to those grown on membranes with a pore size of 0.4 μm^2, displaying a discontinuous monolayer with many empty patches on the microporous membrane. While differences were observed in TEER between membranes of the same pore size seeded with Caco-2 cells at a high or low density, these differences were not at pronounced as those observed between membranes of different pore-sizes, nor were they observed at every time point (Figure 2.7). Based on these results TEER across 24 mm Transwell PET inserts with 0.4 μm^2 pores (henceforth referred to as Transwell inserts), were selected for all future experiments.

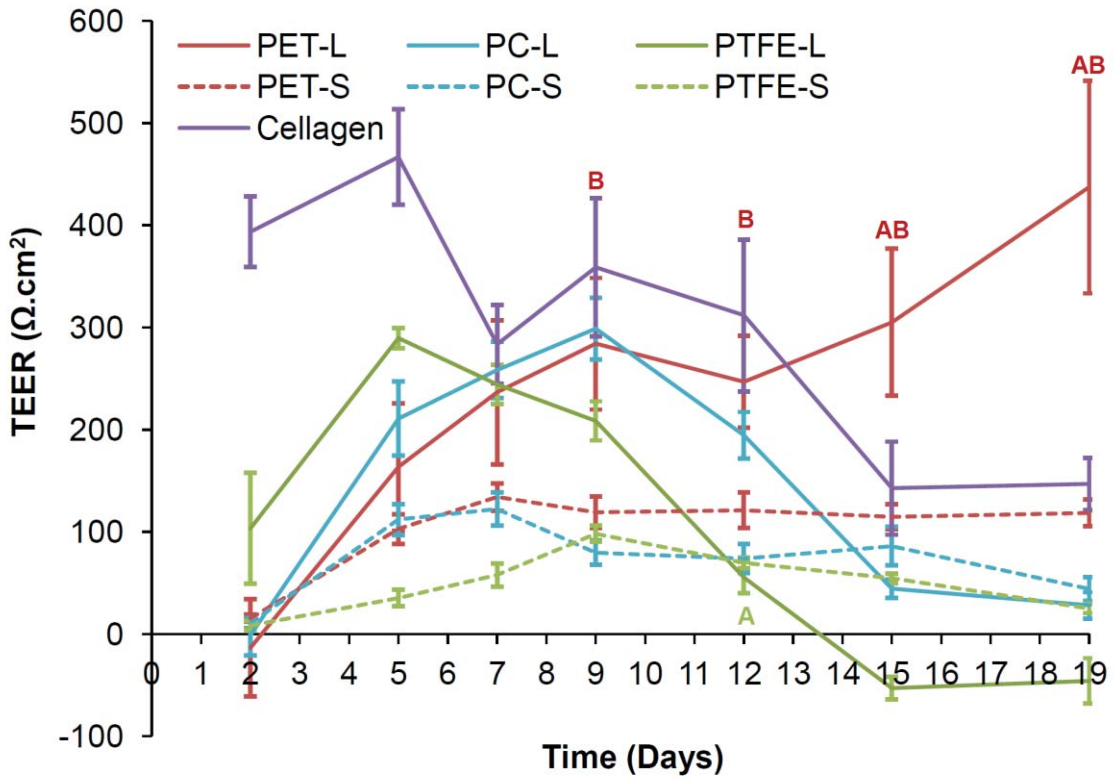

Figure 2.6 TEER across Caco-2 cell monolayers grown on selected cell culture membranes.

Caco-2 cells seeded at a density of 6.5 x 10^4 cells/cm^2 on Transwell PET, Transwell PC or Transwell PTFE membranes with a diameter of 24 mm (large; L) or 12 mm (small; S), or Cellagen membranes. Graphs show mean (+/- SEM; n = 6) TEER across time. 'A' denotes that TEER was different to that of all other Transwell membranes of the same size at that time point ($P < 0.05$). 'B' denotes that TEER across large Transwell PET was different to that of small Transwell PET at that time point ($P < 0.05$).

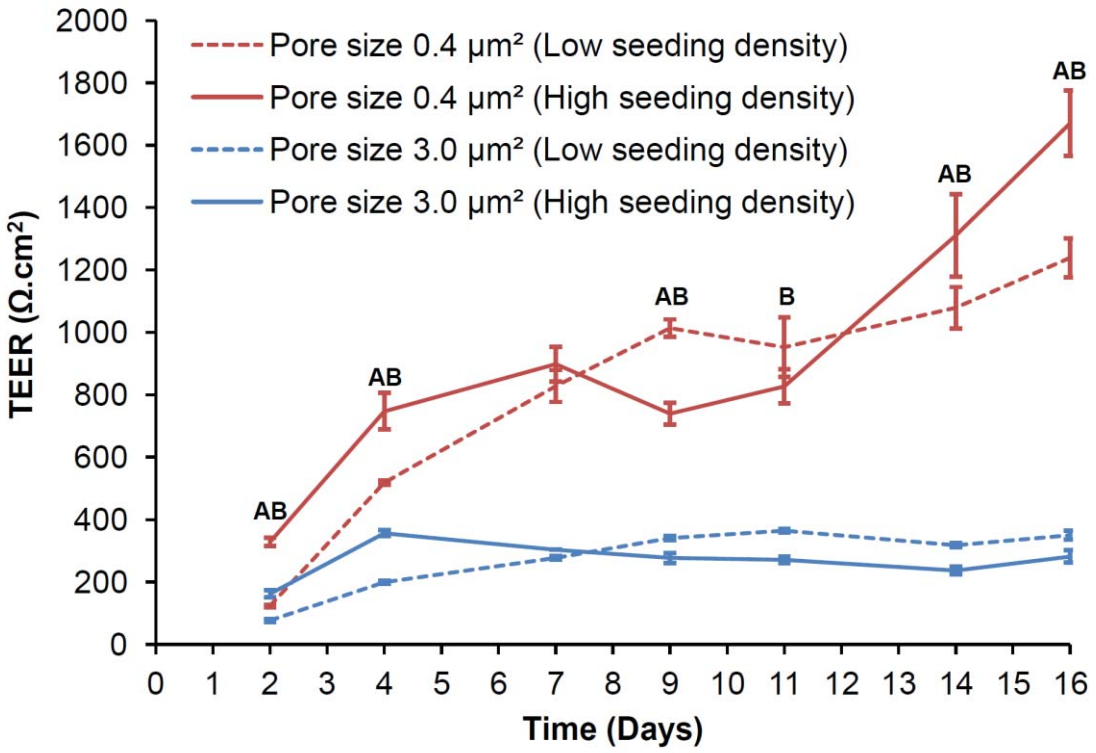

Figure 2.7 TEER across Caco-2 cell monolayers grown Transwell PET membranes.

Caco-2 cell monolayers seeded at a density of 3 x 10^5 cells/insert (low seeding density) or 1.2 x 10^6 cells/insert (high seeding density) on Transwell PET inserts with pore sizes of 0.4 µm^2 or 3.0 µm^2. Graphs show mean (+/- SEM; n =3) TEER across time. The TEER across Caco-2 monolayers grown on membranes with a pore size of 0.4 µm^2 was different to that of Caco-2 monolayers grown on membrane with a pore size of 3.0 µm^2 ($P < 0.05$) at every time point. 'A' denotes that TEER across 0.4 µm^2 inserts with a low seeding density was different to that of 0.4 µm^2 inserts with a high seeding density at the given time point ($P < 0.05$). 'B' denotes that TEER across 3.0 µm^2 inserts with a low seeding density was different to that of 3.0 µm^2 inserts with a high seeding density at the given time point ($P < 0.05$).

To identify at what point in time after seeding the TEER plateaued, an EndOhm 24 mm culture cup (refer to section 2.3.4.2) was used to measure TEER across Caco-2 monolayers grown on Transwell inserts, seeded at a density of 3 x 10^5 cells/insert. The Caco-2 cell monolayers showed a rapid increase in TEER over the first 3 days following seeding, after which the TEER plateaued (Figure 2.8a). Previously, when TEER was shown to continually increase beyond 10 days, cells were only handled 3 times per week, rather than daily. Thus the experiment was repeated and TEER measured 3 times per week. TEER increased until day 11, and reached a maximum TEER greater than that observed on the previous run of the experiment (Figure 2.8b). With the exception of a drop in TEER on day 18, which can be attributed to a loss of CO_2 in the 5% CO_2 incubator, the TEER plateaued 11-13 days after seeding.

2.4.2 Co-culture chamber set-up

Cell culture inserts containing 14-day-old Caco-2 cell monolayers were fitted on to the chamber lids which were then used to seal the chamber wells filled with 50 mL of cell culture medium (Figure 2.9a). The sampling ports of the lids were sealed with rubber septa and Schott caps (Schott, Hattenbergstrasse, Mainz, Germany), and the top electrode plate was placed on to the chamber base and tightened using the electrode plate tightening knob. This method proved to be gentler on the microporous membrane and Caco-2 cell monolayer than fitting the insert into a lid that had already been fitted on to a well and sealed (Figure 2.9b). When the co-culture chamber was set up as described in Figure 2.9b, more pressure needed to be applied on the insert to fit it into the lid, which could potentially have a detrimental effect on the Caco-2 cell monolayer.

2.4.2.1 Effect of co-culture chamber set-up on TEER

Immediately prior to setting up the co-culture chamber, the TEER across the Caco-2 cell monolayers was measured as described in section 2.3.4.2. Immediately following the setting up of the co-culture chamber, the inserts were gently removed from the co-culture chamber and the TEER measurements were repeated. In most instances the TEER had dropped from a normal TEER of 200-400 $\Omega.cm^2$ prior to incubation, to a negligible TEER immediately after the incubation.

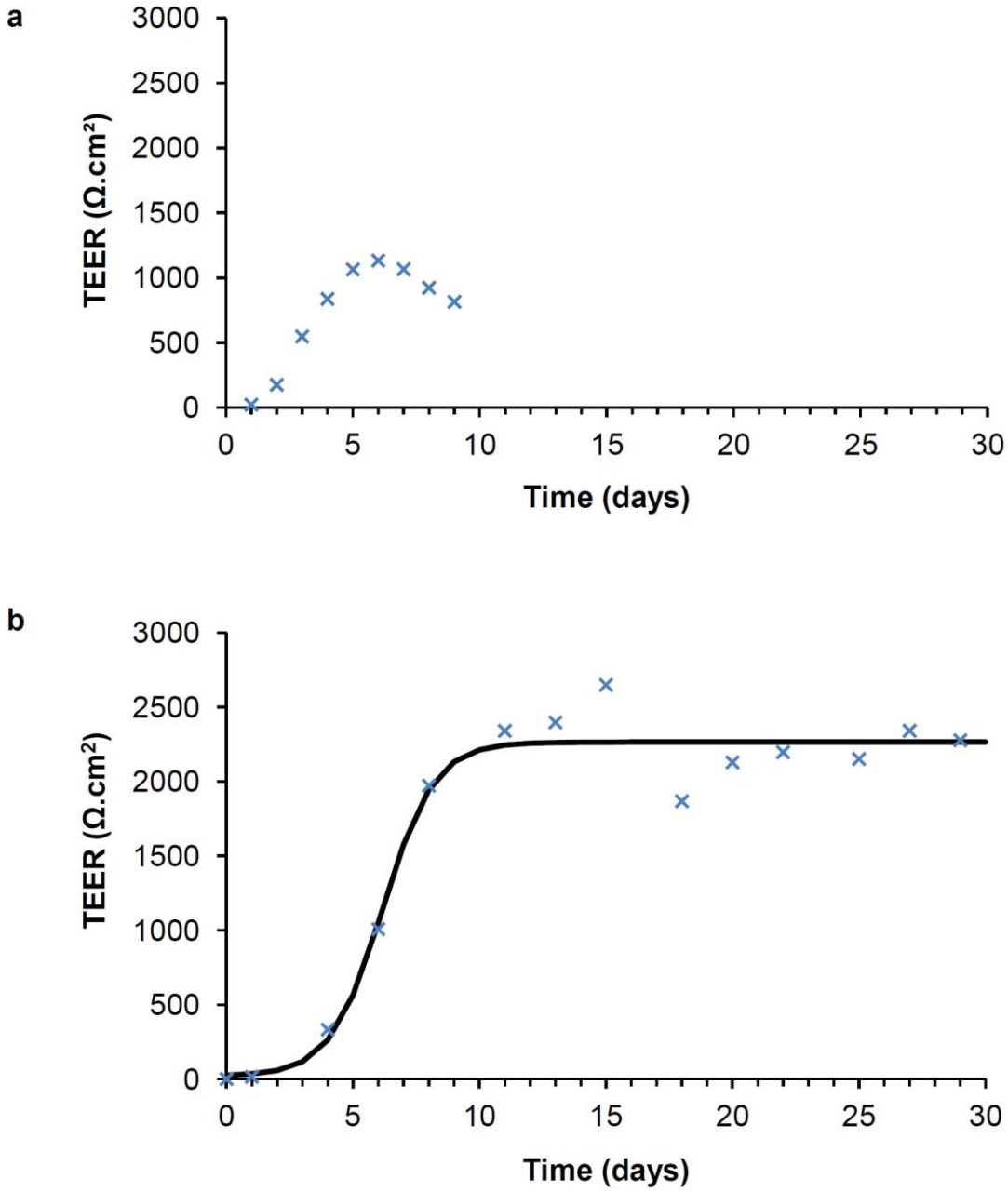

Figure 2.8 TEER over time across Caco-2 cell monolayers seeded on Transwell PET membranes with 0.4 µm pores.

Each cross denotes the mean TEER at the given time point, while the solid line indicates the logistic curve fitted to the TEER values. (a) When measured daily, TEER (n = 5) stopped increasing after 3 days post seeding, and hence measurements were discontinued after 9 days. (b) When measured 3 times/week, TEER (n = 6) increased until day 11 post seeding, and plateaued between days 11-13.

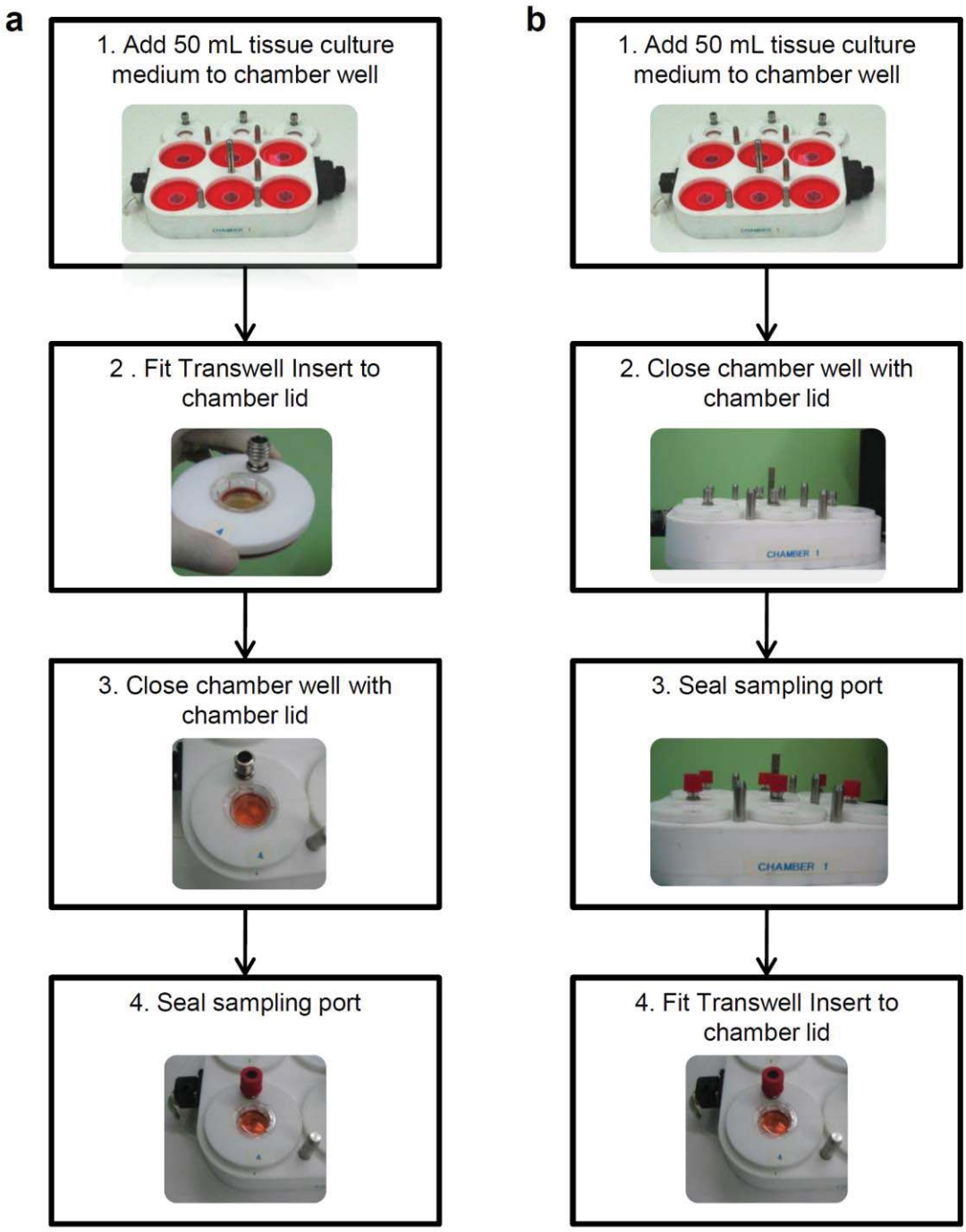

Figure 2.9 Alternative methods of setting up co-culture chamber.

The flow chart depicts main steps involved in setting co-culture chamber in 2 alternative methods: (a) Cell culture insert fitted to the chamber lid prior to sealing the chamber base; (b) Chamber well closed with chamber lid prior to fitting cell culture insert.

A typical result is shown in Figure 2.10a, where with the exception of inserts fitted on to wells 2 and 11 of the co-culture chamber, all inserts had negligible TEER following incubation in the co-culture chamber. Inspection under a light microscope indicated that the monolayer integrity was compromised. Large gaps within the Caco-2 cell monolayer, and many detached cells and cell debris were commonly visible.

In addition to the above mentioned 'manual' TEER measurements, 'automatic' TEER measurements were also taken periodically during the incubation period using the built in TEER electrodes within the wells of the co-culture chamber (Figure 2.10b). The final automatic TEER reading for each well was comparable to the manual TEER reading taken immediately after the incubation, indicating that the automatic TEER readings were likely accurate. However, the 0-2.5 hour TEER readings for well 2 were unstable (variability was over 30 Ω for each reading) based on the criteria described in section 2.3.5.4 and hence were disregarded. With the exception of well 11, and possibly well 2, where the TEER readings gradually decreased over the incubation period, all other wells showed a negligible TEER by the 0 hour time point. This observation led to the hypothesis that the observed disruption of the Caco-2 cell monolayer, as indicated by the sudden drop in TEER, was caused during the setting up of the co-culture chamber, and could be avoided by modifying the method used to fit the Transwell lid into the chamber lid.

2.4.2.2 Optimisation of co-culture chamber set up

To determine which step of the co-culture chamber set up caused the observed detrimental effect on TEER, inserts were removed from the co-culture chamber following each step illustrated in Figure 2.9a and the TEER across the Caco-2 cell monolayer was measured as described in section 2.3.4.2. This experiment indicated that the TEER remained relatively unchanged until the sealing of the sampling port (step 4, Figure 2.9a) at which point monolayer integrity was lost.

It was hypothesised that the tightening of the Schott cap over the rubber septum leads to an increase in pressure inside the chamber well, leading to the escape of air through the microporous membrane thus disrupting the Caco-2 cell monolayer. To rectify this issue, a 21G x 2″ needle (Becton Dickinson, Mt Wellington, Auckland, NZ)

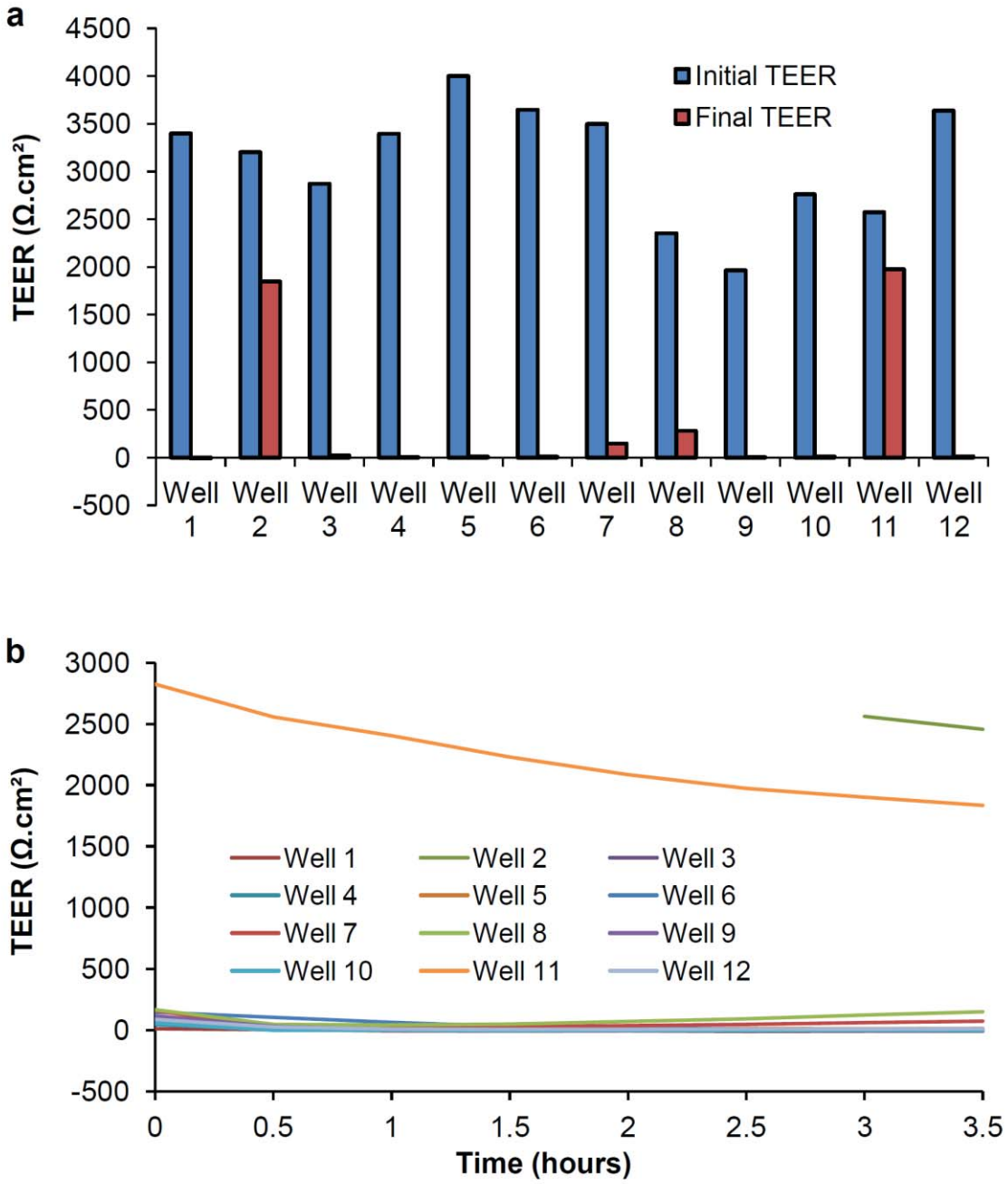

Figure 2.10 Typical TEER profile for Caco-2 cells cultured in the co-culture chamber at 37°C in a 5% CO_2 incubator.

(a) Manual TEER readings for individual cell culture inserts taken prior to (Initial TEER) and immediately after (Final TEER) setting up the co-culture chamber. (b) Automatic TEER measurements for individual inserts taken every 0.5 hours during the incubation period by the built in TEER electrodes of the co-culture chamber. The readings taken for 'well 2' prior to the 3 hour time point were unstable and hence are not displayed on the graph.

was passed through the rubber septum as illustrated in Figure 2.11 prior to tightening the Schott cap. The theory was that the needle would act as an alternative passage for the release of pressure during the sealing of the sampling port, thus preserving the integrity of the Caco-2 cell monolayer.

To test this hypothesis, TEER across the Caco-2 cell monolayers was measured using the built in TEER electrodes of the co-culture chamber, prior to and after sealing the sampling port with or without the use of the needle (Figure 2.12). For both treatments, the TEER prior to sealing the sampling port was not different to that of the initial TEER (prior to transferring the insert to the co-culture chamber, measured manually as described in section 2.3.4.2). Where the sampling port was sealed without the use of a needle, the Caco-2 cell monolayers showed a dramatic reduction in TEER; where the sampling port was sealed with the use of a needle (Figure 2.11), the TEER was unaffected from prior to the sealing of the sampling port. Further, visual inspection under the microscope showed that when the septum was sealed with the use of a needle, the large holes in the monolayer and cell debris, present when the septum was sealed without the use of a needle, were absent.

2.4.3 Analysis of TEER in the co-culture chamber

Caco-2 cells were grown in the co-culture chamber at 37°C inside a 5% CO_2 incubator, and to ensure the integrity of the Caco-2 cell monolayer was preserved, the co-culture chamber was set up using the optimised method (section 2.4.2.2). TEER across the Caco-2 cell monolayers was measured using the built-in TEER electrodes in the co-culture chamber. Figure 2.13 shows a TEER profile from a typical experiment. While the previously observed sudden loss of TEER did not take place, a gradual loss of TEER could be observed. After approximately 20 hours in the co-culture chamber, the TEER across the Caco-2 cell monolayers was negligible. This loss in TEER was also accompanied by increased cell detachment and large gaps in the Caco-2 cell monolayer.

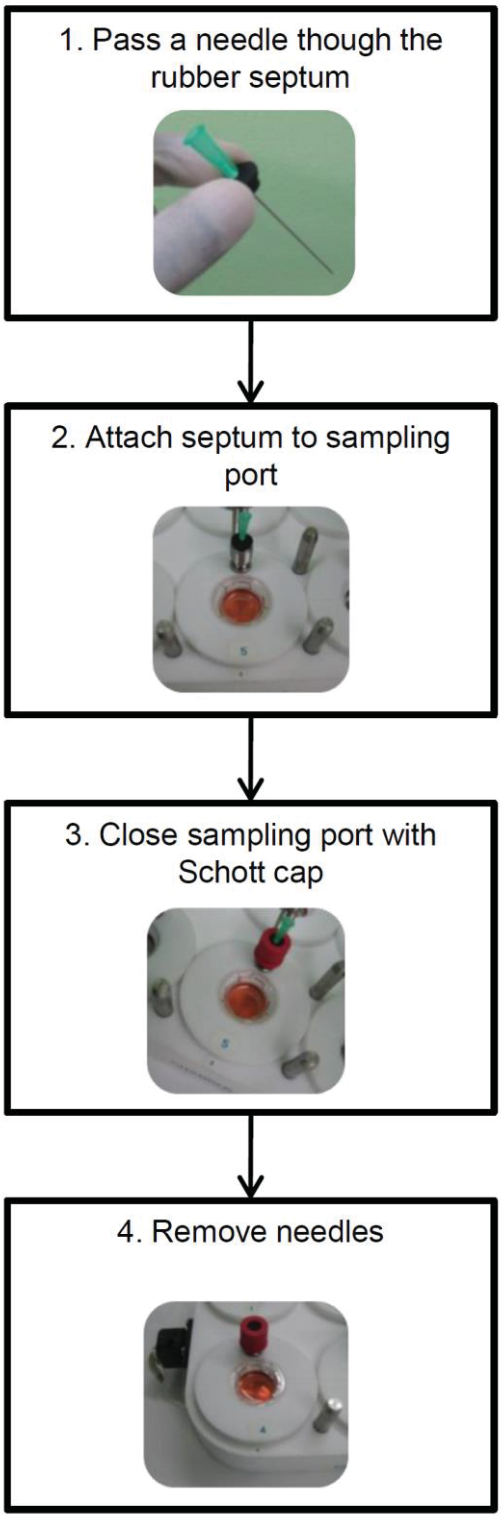

Figure 2.11 Process for the sealing of the sampling port in the co-culture chamber with the use of a needle.

Flow chart depicts main steps involved in sealing the sampling port of the co-culture chamber with the aid of a 21G x 2" needle so as to prevent loss of Caco-2 cell monolayer integrity.

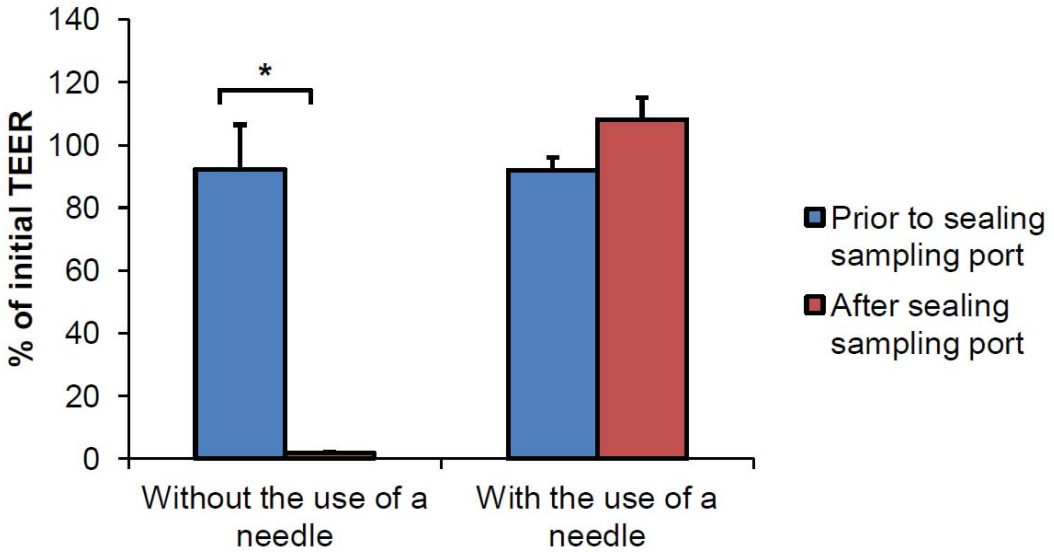

Figure 2.12 Effect of sealing the sealing the co-culture chamber sampling port on TEER across the Caco-2 cell monolayer.

Graphs show mean (+/- SEM; n = 3) TEER across Caco-2 cell monolayers, prior to and after the sampling port was sealed (with or without the use of a needle) as a percentage of the initial TEER. * $P < 0.05$.

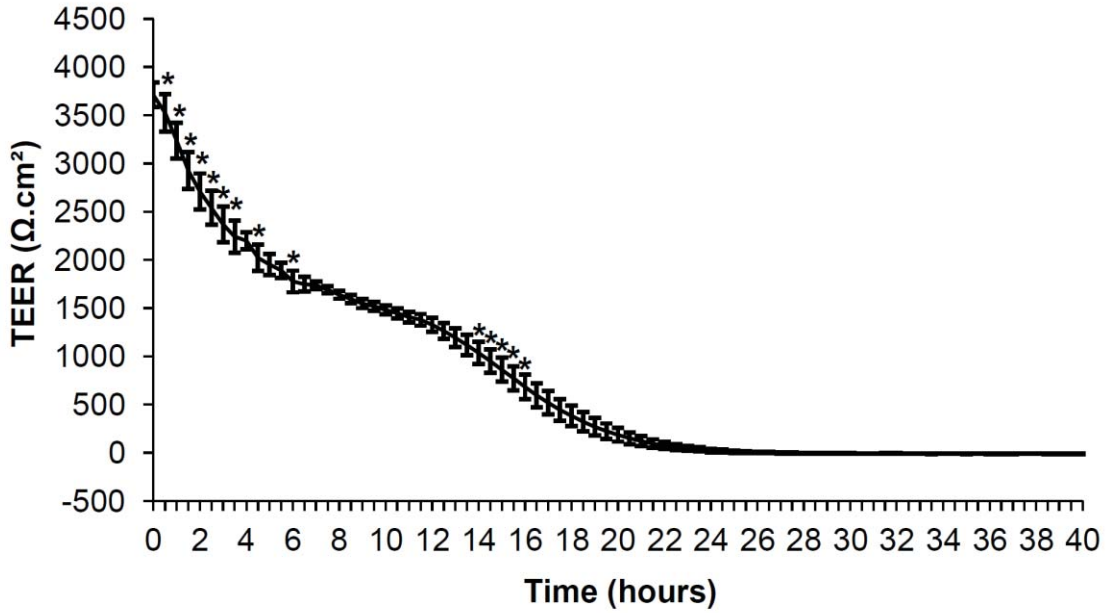

Figure 2.13 TEER across Caco-2 cell monolayers when cultured in the co-culture chamber set up using the optimised method

The sampling ports of the co-culture chamber were sealed with the use of a needle, and co-culture chamber was incubated at 37°C in a 5% CO_2 incubator for 40 hours during which time the TEER was measured every 30 minutes using the built in TEER electrodes. Graph shows mean (+/- SEM; n =6) TEER over time. * $P < 0.05$ compared to previous time point.

2.4.4 Modification of co-culture chamber

2.4.4.1 Determination of the cause of loss in Caco-2 cell monolayer integrity

Several hypotheses were formulated to identify the cause of the gradual TEER loss when Caco-2 cells were grown in the co-culture chamber. To test each hypothesis, a group of co-culture chamber wells were set up (as per section 2.4.2.2) while another group of wells were set up using an alternative method. TEER across the cell monolayers was measured and compared between the two groups. The various hypotheses, the methods used to test the hypotheses, as well as the outcomes from the experiments is summarised in Table 2.4.

One hypothesis was based on the fact that the basal compartment of the co-culture chamber is air-tight. Thus if pressure builds up within this compartment (e.g. due to the basal culture medium warming up from room temperature to 37°C), excess pressure has to be released via the microporous membrane, thus disrupting the Caco-2 cell monolayer. This hypothesis was tested by setting up the co-culture chamber without sealing the sampling port with the rubber septum, thus preventing any build up of pressure within the chamber well.

Another hypothesis was that the process of pushing the cell culture insert into the chamber lid, along with sealing the chamber well with the chamber lid, disrupts the cell monolayer. This was tested by removing the O-rings in the chamber lid to allow for a gentler movement when installing the lid and insert, thus reducing the risk of disruption to the cell monolayer. Furthermore, to test if the decrease in TEER was due to a combination of both of the above mentioned reasons, the co-culture chamber was set up with the O-rings removed, and with the sampling port left unsealed. However, as shown in Table 2.4, all of the above hypotheses were disproved.

An alternative hypothesis (Table 2.4) was that the basal side of the Caco-2 cells were not in contact with the culture medium. This may have been possible due to an insufficient volume of basal medium, or the formation of air bubbles beneath the microporous membrane. This hypothesis was tested by increasing the volume of basal medium such that the chamber well was filled to the rim, not allowing room for any air bubble formation. However, the extra medium pushed through the microporous membrane, abolishing monolayer integrity.

Table 2.4 Summary of hypotheses developed to explain the observed loss of TJ integrity in Caco-2 cell monolayers when cultured in the co-culture chamber set up using the optimised method

	Hypothesis	*Method for testing hypothesis*	*Outcome*
1	Pressure builds up within the chamber well, and escapes through the microporous membrane disrupting the cell monolayer.	Did not seal sampling ports with rubber septa.	TEER decreased at a similar rate in both sealed and unsealed wells.
2	Basal side of the cell culture membrane is not in contact with the cell culture medium (e.g. basal media volume is too low, air bubbles present underneath membrane).	Filled chamber well to rim with cell culture medium (no space for air bubble formation).	TEER plummeted as extra media pushed through membrane disrupting cell monolayer
3	The process of pushing the cell culture insert into the chamber lid and/or sealing the chamber well with the lid disrupts the cell monolayer.	Removed both outer and inner O-rings to allow for gentler movement when installing insert and lid.	TEER decreased at a similar rate in both wells with and without the O-rings.
4	A combination of hypotheses 1 & 3.	Removed O-rings from chamber lid, and did not seal sampling port with rubber septa.	TEER decreased at a similar rate in both wells with or without the O-rings and septa.
5	The top electrode plate isolates the Caco-2 cells from the 5% CO_2 environment of the incubator.	Did not assemble top electrode plate.	TEER dropped by a similar amount in wells both covered and uncovered with the electrode plate.
6	Dark coloured build up on electrodes could be toxic to Caco-2 cells.	Cleaned electrodes using 'Autosol' metal polish.	TEER dropped faster in wells with 'cleaned up' electrodes.

It was also hypothesised that the top electrode plate of the co-culture chamber isolated the apical side of the of the Caco-2 cell monolayer from the atmosphere of the incubator, implying that the Caco-2 cells may be exposed to a non-favourable environment on the apical side. However the TEER across Caco-2 cell monolayers dropped by a similar amount in wells both covered or uncovered by the electrode plate.

It was then hypothesised (Table 2.4) that the observed phenomenon may be inherent to the co-culture chamber and not necessarily due to the method of chamber assembly. It was noted that a dark coloured residue had built up on each of the electrodes, and it was hypothesised that this residue may be toxic to the Caco-2 cells. To test this hypothesis, electrodes were cleaned with metal polish (Autosol). However the TEER dropped faster in Caco-2 cells grown in wells where the electrodes had been cleaned, and the residue had begun to build up again following the incubation period. Nonetheless this did not disprove that the exposure to the electrodes had an adverse effect on the Caco-2 cells.

2.4.4.2 Replacement of electrodes

To determine if exposure to the electrodes had an adverse effect on the Caco-2 cells, copper shavings from the electrodes, approximately 0.1 mm thick and of similar diameter to the electrodes in the chamber, were placed in wells of Transwell plates, and incubated at 37°C for 20 hours. The morphology of the Caco-2 cell monolayers, visually inspected under the microscope, and TEER were compared to Caco-2 cell monolayers not exposed to the electrode shavings (n = 3 per treatment).

No difference was observed in TEER between untreated Caco-2 cell monolayers and those exposed to electrode shavings after 2 hours (Figure 2.14). However by 20 hours the TEER across the Caco-2 cell monolayers exposed to copper electrode shavings was lower than that of the untreated Caco-2 cell monolayers (115.4 ± 14.5 % of initial TEER). Furthermore, by this point in time, the medium in the wells containing copper shavings (3.1 ± 2.3 % of initial TEER) had turned a dark red/ brown colour, and the Caco-2 cells no longer formed a tight monolayer, but rather were ‘rounded’ in shape with several gaps in the monolayer.

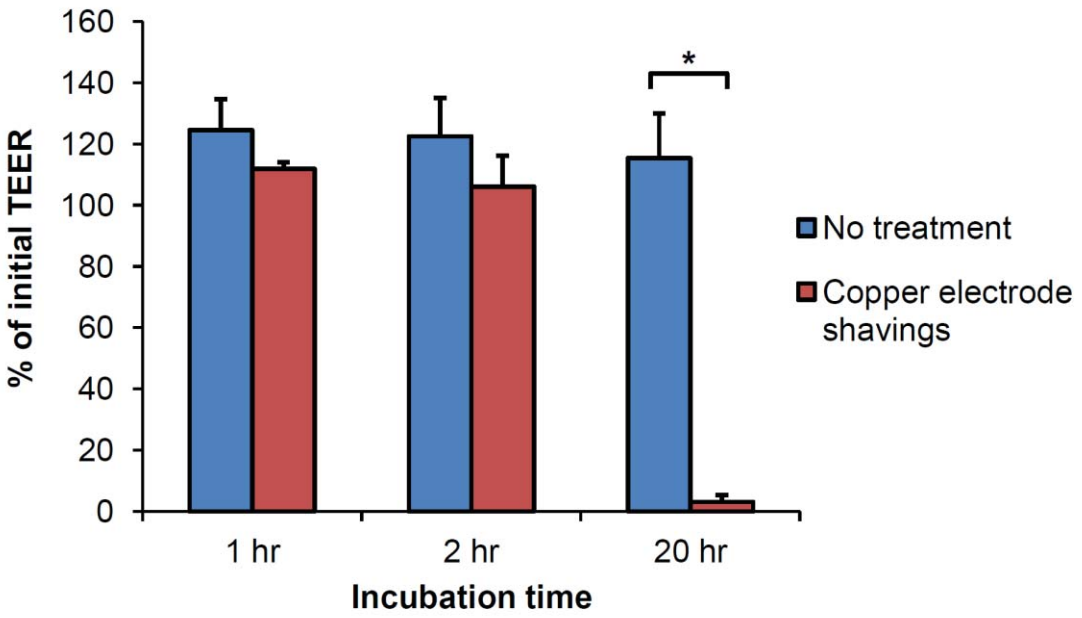

Figure 2.14 Effect of copper electrode shavings on the TEER across Caco-2 cell monolayers cultured at 37°C in a 5% CO_2 incubator.

Graphs show mean (+/- SEM; n = 3) TEER across Caco-2 cell monolayer, either exposed or not to copper electrode shavings, for 1, 2, and 20 hours, as a percentage of the initial TEER. * P <0.05.

To determine if stainless steel electrodes were a suitable alternative, the existing copper electrodes were removed from four wells of one co-culture chamber and replaced with four mock electrodes, two of which were stainless steel, and two 'control' electrodes machined out of the same material as the chamber base, PTFE Teflon. Caco-2 cell monolayers were grown in each well of the co-culture chamber for 24 hours (without assembling the top electrode plate), and TEER across each monolayer was measured using an EndOhm culture cup (section 2.3.4.2) before and after the 20 hour incubation, and the final TEER displayed as a percentage of the initial TEER (Figure 2.15). There was no difference in TEER between the PTFE and stainless steel electrodes, while the copper electrodes had caused a significant reduction in TEER. Based on these results all top and bottom electrodes (originally copper) were removed and replaced with stainless steel electrodes.

2.4.4.3 Introduction of pressure release valves

As an alternative and more convenient method of sealing the sampling ports with a needle (Figure 2.11), the rubber septa were replaced with pressure release valves with a spring pressure of 0.11 psi. For each chamber well, a valve was passed through a Schott cap, and sealed with a modified silicone septum (Figure 2.16). Sampling ports in the co-culture chamber were sealed, while maintaining the integrity of the Caco-2 cell monolayer, by gently screwing on the Schott caps with the pressure release valves. However, for experiments that required the medium in the chamber well to be sampled, sampling ports would need to be sealed with the rubber septa.

2.4.4.4 CellZscope controller

As the TEER electrodes in the co-culture chamber were connected to an EVOM voltohmmeter, where the reading on the voltohmmeter display was converted by means of a camera and custom software, a more direct method of taking TEER measurements was required. Thus the chamber electrodes were connected to a CellZscope controller (nanoAnalytics), a commercially available automated TEER monitoring system, which allowed TEER data to be read and accessed through CellZscope software (version 2.0.0; nanoAnalytics).

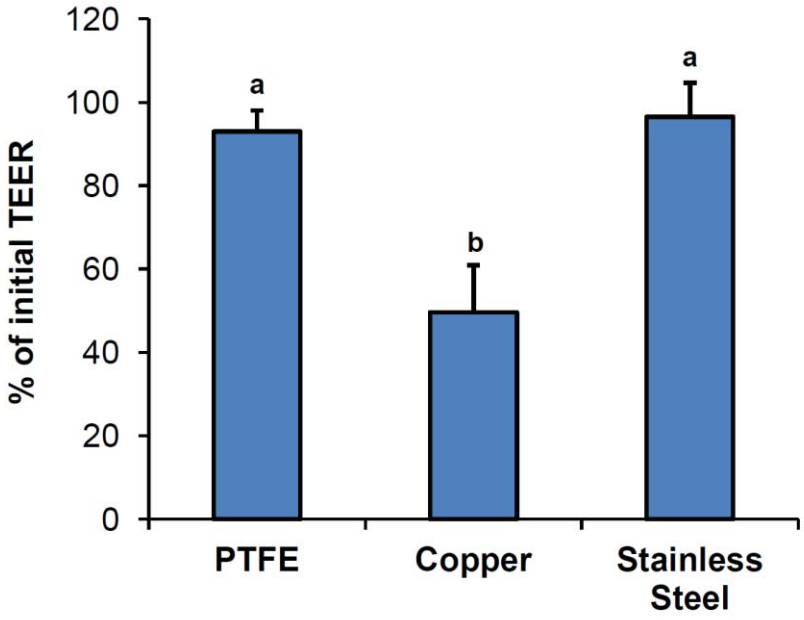

Figure 2.15 Effect of electrodes in the co-culture chamber on TEER across Caco-2 cell monolayers.

Graphs show mean (± SEM; n=2) TEER across Caco-2 cell monolayer at the end of the treatment given as a percentage of the initial TEER. Treatments which do not share the same letter (a or b) are significantly different ($P < 0.05$).

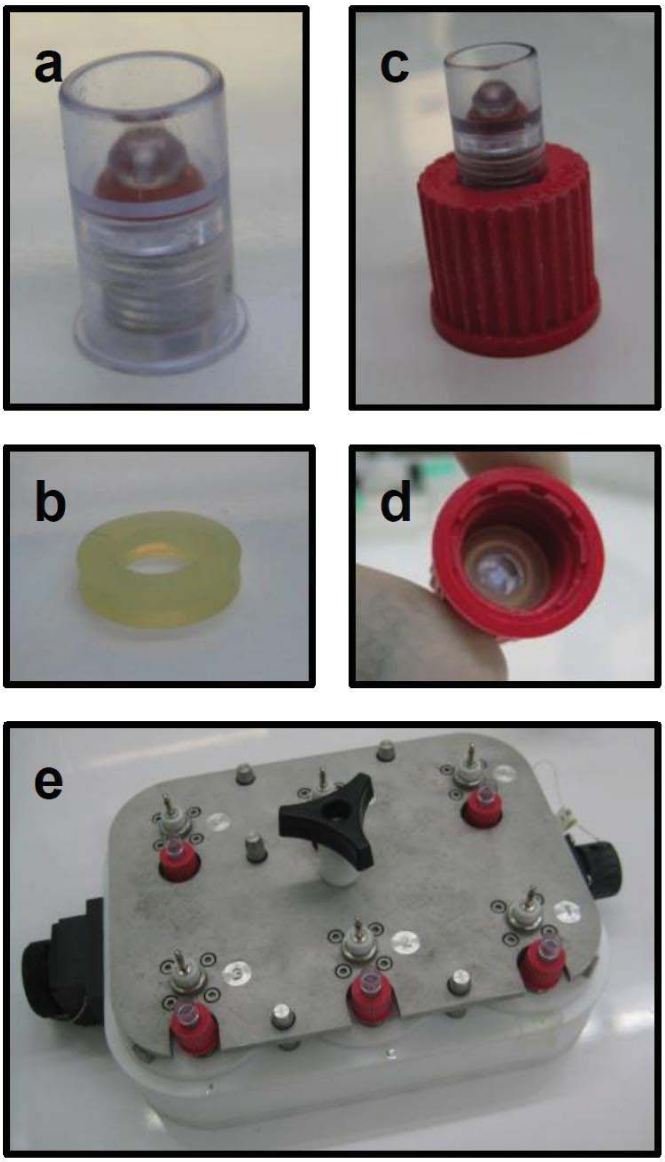

Figure 2.16 Pressure release valves in the co-culture chamber.

As an alternative method of sealing the sampling ports of the co-culture chamber, the rubber septa were replaced with pressure release valves that were passed through the Schott caps and sealed with modified silicone septa. Images show (a) a pressure release valve; (b) a modified silicone septum; (c) a pressure release valve passed through a Schott cap and (d) sealed with modified silicone septum; (e) sampling ports in the co-culture chamber sealed with Schott caps with pressure release valves.

2.4.5 Establishing the apical anaerobic co-culture model

Based on the previous results and observations, the following method, illustrated in Figure 2.17, was proposed for establishing the apical anaerobic model of the intestinal barrier. Firstly, Caco-2 cells were seeded on to 24 mm Transwell cell culture inserts (0.4 μm pores), and cultured for 2 weeks at 37°C in 5% CO_2 (section 2.3.3). Cell culture medium (50 mL) was added to each well of the co-culture chamber, and cell culture inserts were gently fitted into the chamber lids. The chamber wells were sealed with the chamber lids, following which the sampling ports were sealed with Schott caps using either rubber septa (section 2.4.2.2) or pressure release valves (section 2.4.4.3). The chamber was moved into an anaerobic workstation that had an atmosphere of 37°C and 10% CO_2, 10% H_2 in N_2. The cell culture media in the inserts were replaced with anaerobic cell culture medium thus exposing the apical side of the Caco-2 cell monolayer to an anaerobic environment. For experiments that required the TEER across Caco-2 cell monolayers to be measured, the top electrode plate was also assembled. However, as tightening of the top electrode plate led to the chamber lids being pushed further down against the chamber base and thus creating pressure in the basal compartment of the chamber, the sampling ports were momentarily opened during this process. Once the top electrode plate had been tightened, the sampling ports were re-sealed, and the TEER electrodes connected to the control box for TEER measurements.

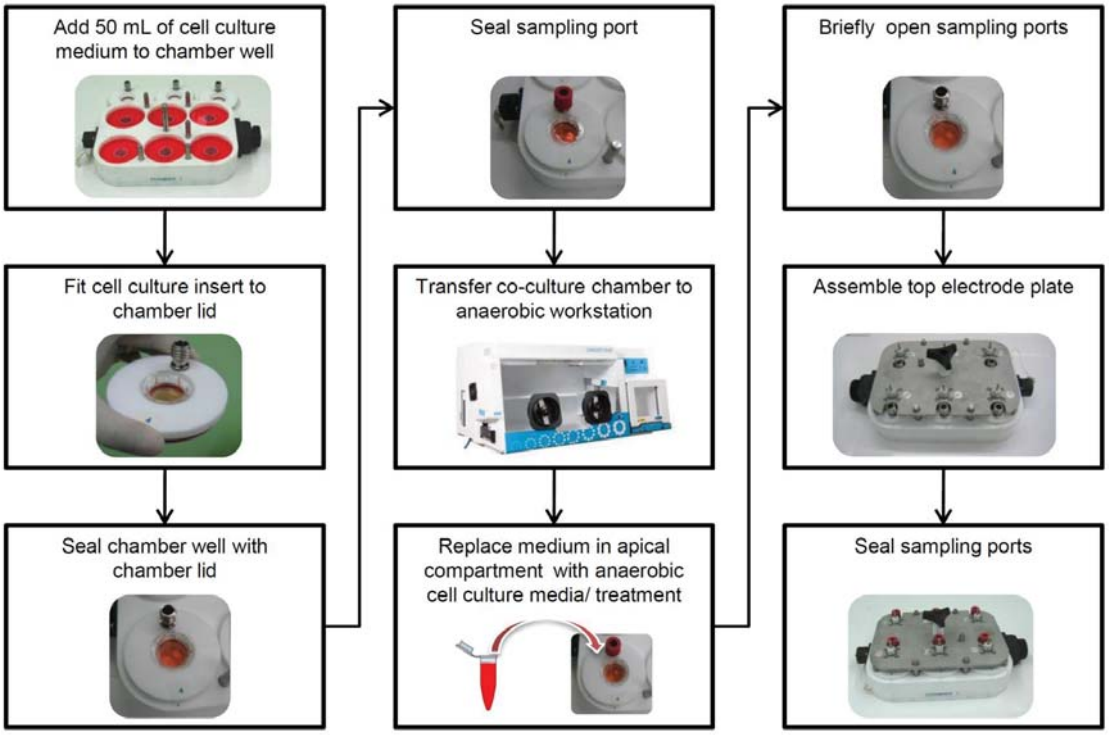

Figure 2.17 Final proposed method for setting up the apical anaerobic co-culture model.

Flowchart depicts main steps required to expose Caco-2 cells to an anaerobic apical environment using the co-culture chamber.

2.5 DISCUSSION

This chapter describes the development of an apical anaerobic model of the intestinal barrier, which utilised a custom built prototype co-culture chamber placed inside an anaerobic workstation. This prototype chamber contained 12 individual wells and each well was equipped with a pair of electrodes for automated measurement of TEER, and a port sealed with a septum for measuring molecule permeability. These features allow for comprehensive investigation of the effects of anaerobic commensals and other bacterial and non-bacterial compounds on intestinal barrier integrity.

Caco-2 cells in this model were grown on 12 mm Transwell PET inserts with a 0.4 μm pore-size, and were cultured for 14 days in standard cell culture conditions prior to being transferred to the co-culture chamber. It is well established that many culture-related factors, including the length of cell culture, and the type of microporous membrane, influence several aspects of the Caco-2 cell monolayer[269]. Thus, as described in this chapter, a standard cell culture protocol was established to minimise variability across experiments.

In this study, the TEER across Caco-2 cell monolayers plateaued around 11-13 days post-seeding. Previous studies have shown that TEER values plateau between days 3-10 post-seeding, while the polarity of the Caco-2 cells continue to develop[243]. Similar to the protocol used in this study, previous studies have also used Caco-2 cells after 14 days in culture[193], while other studies have also used Caco-2 cells after 21 or more days in culture[248]. However, it has been shown that up to 20 days after confluence the Caco-2 cells are only heterogeneously polarised and differentiated, full differentiation can take up to 30 days post-confluence[270]. Nonetheless, TJ are thought to be well formed in Caco-2 cell monolayers after 13 days in culture[271].

While the results presented in this chapter did not show a difference in TEER after 14 days between Caco-2 cell monolayers seeded at difference densities, the seeding density of the Caco-2 cells is thought to influence the rate of cell proliferation and differentiation[272]. Further, differences in expression levels of apical actin and peptide transporters have also been observed depending on the initial seeding density[273].

The type of microporous membrane used has also been shown to influence morphological and biochemical properties of the Caco-2 cell monolayer, including the

rate of cell proliferation and differentiation[272]. Similar to the data reported in this study PET membranes have been shown to result in a higher TEER across Caco-2 cell monolayers than PC membranes[273,274]. Furthermore, the Caco-2 cell density has been shown to be higher in days 4-9 post-seeding (but not days 10-16 post-seeding) on PET membranes compared to PC membranes[274].

Treatment of the membrane with collagen is thought to increase cell attachment compared with membranes not treated with collagen[243,275]. However, TEER of the Caco-2 cell monolayer did not show any improvement when seeded on Transwell PTFE membranes that were pre-treated with collagen, compared with other membrane types. Further, treatment of the membrane with collagen is also thought to increase the rate of cell proliferation and differentiation[272]. However given that the TEER did not improve, it is unlikely that the Caco-2 cells grown on the PTFE membranes proliferated faster than Caco-2 cells grown on the other types of membranes. However, this may have been, at least in part, due to the large pore size of the membrane.

When grown on the basal side of the microporous membrane, DC have been shown to extend projections through to the epithelial cells in the apical side in response to bacteria[128,276]. Thus the growth of Caco-2 cells was initially tested on inserts with 3.0 μm pores, as this pore size permitted the co-culture of Caco-2 cells with immune cells such as DC[128,276]. However, Caco-2 cells did not form a complete monolayer, and produced a relatively low TEER on membranes with 3.0 μm pores compared to membranes with 0.4 μm pores. Previous studies have also shown that cell attachment to be poor in membranes with large pores compared to those with smaller pore sizes[264,277]. Further, larger pore sizes are known to lead to the migration of Caco-2 cells to the basal side of the membrane, and promote the formation of a Caco-2 multilayer[264,277], highly undesirable in this model. Migration of cells through to the opposing side can potentially also lead to the loss of polarity[277].

Copper electrodes were initially built into the co-culture chamber to facilitate the automatic measurement of TEER. These electrodes were replaced with stainless steel electrodes, as the presence of copper electrodes was shown to be detrimental to the TEER and the viability of Caco-2 cells. Copper electrodes were chosen based on their electrical conductivity properties. However, copper has been known to have negative effects on mammalian cells. For example, copper oxide nanoparticles have been shown to induce cytotoxicity in epithelial cell lines[278], while copper chloride and copper wires

have been shown to kill mouse embryos[279]. The dark coloured build-up on the copper electrodes was likely copper oxide, though this was not tested. The commercially available EndOhm culture cups contain silver electrodes plated with silver chloride. While there is little evidence of toxic effects of silver on epithelial cells[280], silver is a commonly used antimicrobial agent[281]. Thus as the co-culture chamber would be used to grow bacteria along with epithelial cells, silver electrodes were not a feasible option. Indeed EndOhm culture cups (with silver electrodes) have been used in studies to measure TEER where epithelial cells are co-cultured with bacteria[196]. However in this case, the cell culture inserts were only placed in the EndOhm culture cups, exposed to the silver electrodes, for a few seconds every 2 hours. On the other hand, bacteria in the apical anaerobic model would be continuously exposed to the electrodes of the co-culture chamber, potentially affecting their viability. Ultimately, stainless steel electrodes were chosen as a suitable replacement for copper. The commercially available CellZscope, which allows the continuous and automated measurement of TEER under cell culture conditions, also uses electrodes made of stainless steel. Several studies have used this device to measure TEER in the presence of bacteria with no obvious cytotoxic effects on the bacteria or epithelial cells[193,282].

The concept for the apical anaerobic co-culture model was derived from a similar model used by Kelly *et al* (2004)[210] to study the immune modulation of Caco-2 cells by the commensal anaerobe *B. thetaiotaomicron* (Prof Denise Kelly, personal communication). In their co-culture chamber, however, the aerobic basal medium was shared by all cell culture inserts, compared to the co-culture chamber described in this chapter which contains a separate well for each insert. Along with the presence of the sampling ports, having independent wells enables the ability to sample basal media for individual replicates from various treatments. This allows, for example, the measurement of small molecule flux across the epithelial monolayer, or measurement of cytokines secreted basally from the epithelium.

Another dual environment co-culture system was developed by Cottet *et al.* (2002)[258] to co-culture Caco-2 cells with the microaerophilic pathogen *Helicobacter pylori*. Here Caco-2 cells were grown on microporous membrane inserts which were mounted between two chambers. The apical chamber contained bacterial culture medium continuously perfused with a microaerophilic gas mixture, while the basal chamber contained cell culture medium continuously perfused with air containing 5%

CO_2. A similar model was recently used in other studies to study *Campylobacter jejuni* and *E. coli* invasion of intestinal epithelial cells under microaerophilic conditions, which better represent the *in vivo* environment[259,260]. The constant flow of gas ensured that the optimal atmospheres for microaerophilic bacteria and Caco-2 cells were consistently maintained in the apical and basal compartments respectively[258]. In the apical anaerobic model described in this chapter, however, the level of oxygen is likely to become depleted, while some oxygen may diffuse through to the apical anaerobic compartment, thus slightly altering both environments during the course of experiments. The study by Cottet *et al.* (2002)[258] showed that microaerophilic bacteria, not only survive, but also grow in their co-culture model[258]. This is likely due to the bacteria being grown under optimal culture conditions in bacterial culture medium. In the apical anaerobic model described in this chapter, because the Caco-2 cells are exposed to an environment completely devoid of oxygen on the apical side, cell culture medium, instead of bacterial medium, was used to support the survival of the Caco-2 cells. Thus, while the anaerobic environment is likely to ensure the survival of obligate anaerobic bacteria, they are unlikely to grow in the apical anaerobic model. In the model of Cottet *et al.* (2002)[258] the Caco-2 cell monolayer lies in a vertical position. In this orientation, bacteria which do not float and settle at the bottom of the vessel are unlikely to interact with the Caco-2 cell monolayer; whereas in the apical anaerobic model, the flow of gravity encourages contact between the Caco-2 cell monolayer and bacteria. Furthermore, the previous models were not designed for the specific purpose of studying intestinal barrier integrity and lack built-in TEER electrodes.

Further modifications have been considered to improve the co-culture chamber used for the apical anaerobic model. Currently each chamber lid can hold either a pressure release valve, or a rubber septum, sealing the sampling port. Future prototypes would allow for both a sampling port sealed with a septum, and a valve which allows for more convenient setting up of the co-culture chamber. Furthermore, while the current design of the chamber includes a top electrode plate, this does not serve the same purpose as the lid of a multi-well cell culture plate. Integration of a secondary lid (over the top electrode plate) could help maintain the sterility in the apical compartment of the chamber when being transferred between the cell culture hood, 5% CO_2 incubator and anaerobic workstation.

Methods of introducing oxygen to the basal compartment of the co-culture chamber were also investigated to ensure that Caco-2 cells received sufficient oxygen from the basal compartment of the chamber. One proposed method included modifying the chamber base with six individual channels each of which allows fresh aerobic medium to flow through and replace the contents of each chamber well. However, a simpler, and more feasible method was drafted which involved converting the existing sampling port to an ‘oxygen port’. A gas line would run through the rubber septum of the sampling port to the basal compartment of the chamber allowing the basal medium to be perfused with aerobic gas. These methods would be further developed if the validation of the model proved that the current method was insufficient to ensure epithelial cell viability in the apical anaerobic model.

The model described in this chapter can be used to grow intestinal epithelial cells in custom-built co-culture such that the apical and basal sides of the cell monolayer are exposed to independent environments. Compared to existing similar models, this model offers the advantages of simplicity, and automated measurements of epithelial barrier integrity. The co-culture chamber can be used to expose the apical environment of the cells to an anaerobic environment, which would allow the co-culture of epithelial cells with commensal obligate anaerobic bacteria. Thus, once validated, this model would be suitable for the study of the regulation of intestinal barrier integrity by anaerobic commensal bacteria.

Chapter 3:

Validation of the apical anaerobic model of the intestinal barrier

3.1 INTRODUCTION

The intestinal epithelium, which comprises the physical component of the intestinal barrier, consists of a single layer of columnar epithelial cells that separates the intestinal lumen from the underlying lamina propria[5]. Intestinal epithelial cells are polarised cells that have multiple extensions, known as microvilli, on the apical pole[33]. Microvilli are membrane protrusions that form the 'brush border', and their main role is to increase the apical surface area for greater nutrient absorption. Enterocytes make up over 80% of intestinal epithelial cells and control the flow of ions and small molecules across the intestinal barrier[32].

An important component of the epithelium is the apical junctional complex, consisting of TJ and adherens junctions[34]. TJ are the most apical structures of the junctional complex, and regulate the entry of luminal nutrients, ions and water while restricting pathogen entry and thus regulating the barrier function of the epithelium[35]. Adherens junctions are involved in cell to cell adhesion and intracellular signalling[36].

TJ are integral for epithelial barrier integrity as they seal the paracellular space between the epithelial cells, thus preventing paracellular diffusion of microorganisms and other antigens across the epithelium[34]. TJ are complex structures comprising over 50 proteins. These include transmembrane proteins, which form fibrils that cross the plasma membrane and interact with proteins in the adjoining cells[44], and plaque proteins, which act as cytoplasmic adaptors, stabilising and anchoring transmembrane proteins to the cytoplasm[45]. Regulation of the assembly, disassembly and maintenance of TJ structure is influenced by various physiological and pathological stimuli. For example, administration of *L. plantarum* into the duodenum of healthy human volunteers has been shown to increase expression of the transmembrane protein occludin, and the plaque protein ZO-1 in the vicinity of TJ structures[193].

The Caco-2 cell line is a well recognised model of the intestinal barrier[269], which forms a confluent monolayer and spontaneously differentiates into polarised small-intestine-like cells expressing morphological and biochemical characteristics similar to enterocytes[228,243]. These monolayers form TJ between adjacent cells at the apical surface, and also show desmosomes when examined through electron microscopy. The

differentiated Caco-2 cell monolayer also grows a brush border which increases in number and organisation over time in culture.

The previous chapter described the development of an apical anaerobic model of the intestinal barrier, where differentiated Caco-2 cells were exposed to an anaerobic environment on the apical side while maintaining an aerobic environment on the basal side. However, with this model, it is critical that sufficient oxygen diffuses to the cells from the basal compartment of the chamber. Where the oxygen supply is diminished, hypoxia has been shown to affect cell physiology. In particular, hypoxia has been shown to lead to a loss of epithelial barrier function[283,284], including increased epithelial permeability and decreased TEER in Caco-2 cells[285]. A well-formed epithelial barrier is integral for the dual environment in the apical anaerobic model, as a 'leaky' barrier could allow oxygen from the basal compartment to diffuse through to the apical compartment.

3.2 HYPOTHESIS AND AIMS

The hypothesis of the research described in this chapter was that Caco-2 cells in the apical anaerobic model receive sufficient oxygen from the basal side to remain viable and maintain an intact barrier for 12 hours. The first aim of this chapter was to determine the DO content in the apical and basal compartments of the co-culture chamber to ensure that oxygen was present basally while the apical side of the Caco-2 cell monolayer remained anaerobic. The second aim of the work described in this chapter was to compare the viability, morphology, and epithelial permeability of the Caco-2 cells in the apical anaerobic model with that in conventional aerobic cultures of polarised Caco-2 cells in a transepithelial model, ensuring that the Caco-2 cells in the apical anaerobic model received sufficient oxygen to sustain their viability and maintain barrier function.

3.3 METHODS

3.3.1 Cell culture

3.3.1.1 Culture of Caco-2 cells

Caco-2 cells were cultured and maintained under standard cell culture conditions as described in section 2.3.2. These cells were seeded onto Transwell cell culture inserts (24 mm diameter, PET membrane, 0.4 μm pores; Corning), as described in section 2.3.3, at a density of 3 x 10^5 cells/insert. Each insert and well contained 1.5 mL and 2.5 mL of cell culture medium respectively and the medium was replaced 3 times/week. The cells were grown on the cell culture inserts for 14 days allowing the Caco-2 cell monolayers to differentiate, following which they were used in the co-culture chamber (section 3.3.1.2).

3.3.1.2 Co-culture chamber set up

Fourteen day old Caco-2 cell monolayers (section 3.3.1.1) were transferred into the co-culture chamber as follows. The resistance across each monolayer was measured using an EndOhm culture cup (section 2.3.4.2) to ensure Caco-2 cells had formed an effective barrier. Only monolayers with a resistance of at least 300 Ω were used. Cell culture medium (50 mL) was added to each well of the co-culture chamber, and cell culture inserts were gently fitted into the chamber lids. The chamber wells were sealed with the chamber lids, following which the sampling ports were sealed with Schott caps using either rubber septa (as described in section 2.4.2.2) or pressure release valves (as described in section 2.4.4.3).

3.3.1.3 Apical anaerobic model

The co-culture chamber (section 3.3.1.2) was moved into an anaerobic workstation (37°C; 10% CO_2, 10% H_2 in N_2; Concept Plus, Ruskinn Technology Ltd), and the cell culture media in the inserts were replaced with anaerobic cell culture medium, thereby exposing the apical side of the Caco-2 cell monolayer to an anaerobic environment. For experiments that required the TEER across Caco-2 cell monolayers to be measured, the sampling ports were momentarily opened, and the top electrode plate was assembled.

Once the top electrode plate had been tightened, the sampling ports were re-sealed, and the TEER electrodes connected to the control box for TEER measurements.

Anaerobic cell culture medium was prepared by placing an open vial of cell culture medium inside an anaerobic workstation overnight. This method was verified to be effective by confirming the DO content in the anaerobic cell culture medium to be 0% using a galvanic DO probe (DO6+, Eutech Instruments, Thermo Fisher Scientific).

3.3.1.4 Alternative cell culture environments

For the purpose of the validation of this model, 14 day old Caco-2 cell monolayers on cell culture inserts were also cultured for 12 hours in a standard cell culture plate inside a 5% CO_2 incubator (conventional cell culture conditions) or inside an anaerobic workstation (a completely anaerobic environment). Where cells were cultured in a completely anaerobic environment, the cell culture medium in the wells of the cell culture plate and the Transwell inserts was replaced with anaerobic cell culture medium (prepared as described in section 3.3.1.3). To control for the effect of the co-culture chamber, Caco-2 cell monolayers were also cultured in the co-culture chamber inside a 5% CO_2 incubator. Cell culture medium in the apical compartment of the chamber was replaced with fresh cell culture medium instead of anaerobic cell culture medium as described in 3.3.1.3. Figure 3.1 illustrates the various cell culture environments under which the Caco-2 cell monolayers were cultured for the research in this chapter.

3.3.2 Measuring dissolved oxygen in the aerobic compartment

DO was measured using a galvanic DO probe (DO6+, Eutech Instruments). The probe was calibrated daily, in air (corresponding to 100% saturation in water), and in a saturated solution of sodium sulphite (0% oxygen solution), as per the manufacturer's instructions. The percent saturation measured by the DO probe was converted to mg/L using the following equation as described by Radtke *et al.*[286]: DO (mg/L) = DO (% saturation) x (DO at 100% saturation (mg/L) / 100) x salinity correction factor. The DO at 100% saturation at 37°C, assuming standard atmospheric pressure (760 mm.Hg), was 6.7 mg/L[286]. The salinity correction factor, where the conductivity of the cell culture medium was approximately 11 µS/cm at 25°C, was 0.967. The salinity of the cell culture medium was measured using a Russell RL060C conductivity meter (Thermo Fisher Scientific).

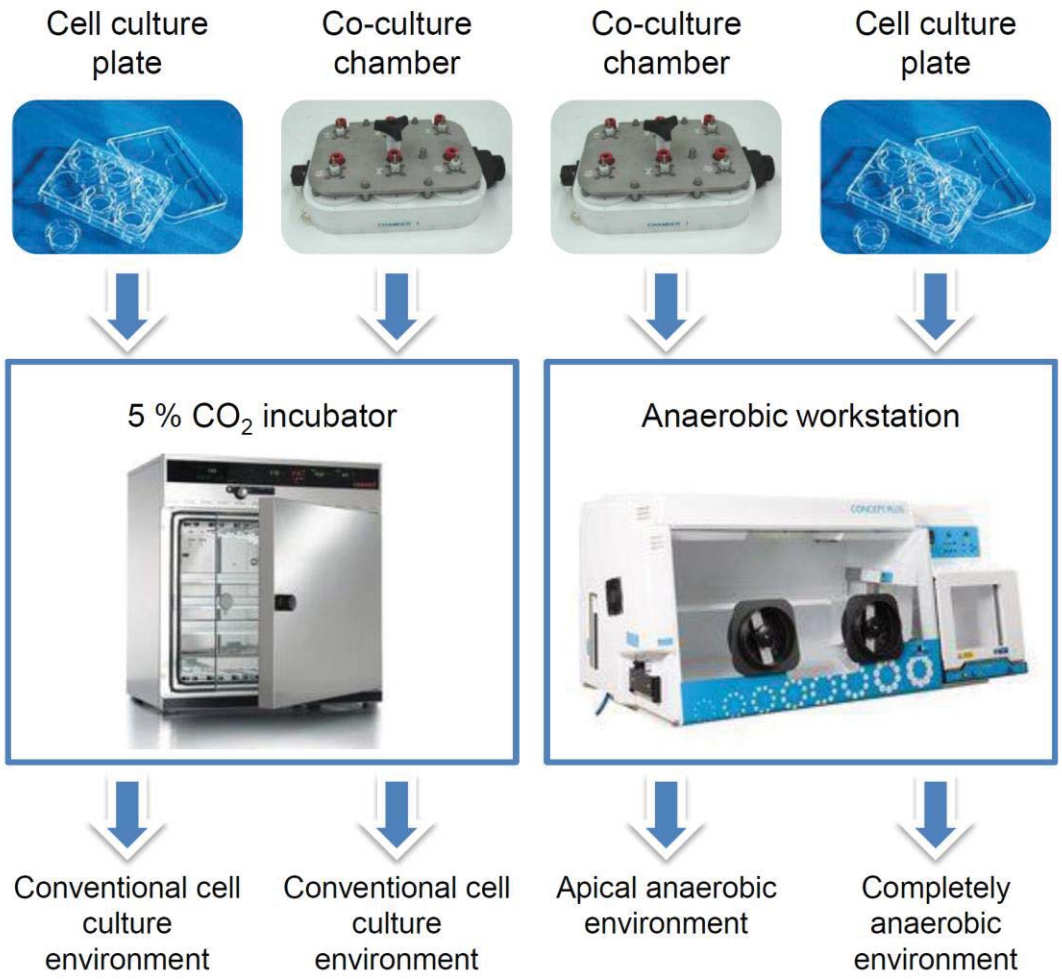

Figure 3.1 Alternative cell culture environments used to compare and validate the apical anaerobic model.

To expose Caco-2 cells to an apical anaerobic environment, Caco-2 cell monolayers on cell culture inserts were cultured in a co-culture chamber inside an anaerobic workstation. Caco-2 cell monolayers on cell culture inserts were also cultured in a cell culture plate inside a 5% CO_2 incubator (conventional cell culture environment) or anaerobic workstation (completely anaerobic environment). To control for the effect of the co-culture chamber, Caco-2 cell monolayers were also cultured in a co-culture chamber inside a 5% CO_2 incubator.

3.3.2.1 Initial methods of measuring basal dissolved oxygen level

Various methods were used to measure DO in the chamber well. In the first method, the chamber lid was opened, the DO probe was submerged in the cell culture medium in the basal compartment, at 0, 4 and 8 hours (n = 2 per time point). As opening the lid compromised the environment in the basal compartment of the chamber, one well could only be used per single time point.

In the second method, 2 mL of medium was removed from the basal compartment of the chamber using a 21G x 2″ needle (Becton Dickinson) attached to a 3 mL syringe (Becton Dickinson), and injected into a 50 mL conical bottom tube (Corning). The medium in the chamber was mixed by gently moving the chamber in a circular motion 5 times prior to each reading. The DO probe was submerged into the 2 mL of medium, which, following the measurement, was injected back into the basal compartment of the chamber via the sampling port. As the chamber lid remained sealed during this process, each well was sampled (n = 3) at multiple time points. Fresh medium was not used to replace the sampled media as this would introduce new oxygen into the basal compartment. However, as the 2 mL samples were exposed to an anaerobic environment during the measurement, they could potentially modify the DO composition of the aerobic medium when reintroduced to the basal compartment of the chamber. Further, it was difficult to guarantee the sterility of the sample medium during this process.

The final method was similar to the second method. However, 1 mL of sample was removed and injected into a 10 mL universal bottle. Due to the shape and diameter of the universal bottle (flat bottom), 1 mL of medium provided a sufficient height to cover the sensing area of the DO probe. Basal medium was sampled (n = 3) at 0, 2, 4, and 6 hours. As only a total of 3 mL of medium was removed prior to the final time point, this medium did not need to be replaced. However, as with the previous methods, the sample was exposed to an anaerobic environment, unlike the medium in the basal compartment which was sealed off from the anaerobic environment; and thus raised the need for an optimised method which did not alter the environment of the basal medium (section 3.3.2.2).

Mean DO for each time point was compared to the initial (0 hour) DO using an ANOVA (in the first method), or a repeated measured ANOVA (in the second and third

methods). Statistical difference was declared where the difference in means was greater than the LSD at 5%.

3.3.2.2 Optimised method for measuring basal dissolved oxygen level

The optimised method for measuring DO in the chamber well utilised a special adaptor/lid containing a port for the DO probe (Figure 3.2). The port was machined such that the sensing area of the probe was submerged in the medium in the chamber well, while sealing the well from the external environment. The level of DO was measured prior to, and immediately after, transferring the co-culture chamber into the anaerobic workstation. DO levels were then measured hourly between 0 and 12 hours in the anaerobic workstation. To ensure accurate measurements, the medium in the chamber was mixed by gently moving the chamber in circular motion 5 times prior to each reading, and 3 readings (technical replicates) were taken for each time point (5 second intervals between readings). DO depletion in the chamber well was measured in a co-culture chamber (i) set up as per normal (insert with Caco-2 cell monolayer), (ii) without Caco-2 cell monolayer (insert only), and (iii) without the insert. Measurements were carried out on 5 separate days for each treatment. The average loss of oxygen per hour was estimated using residual maximum likelihood (REML) analysis in GenStat and statistical difference was declared between two treatments where the difference was greater than the LSD at 5%.

3.3.3 Measuring dissolved oxygen in the anaerobic compartment

The co-culture chambers were set up using inserts with (n = 18) or without (n = 15) Caco-2 cell monolayers. Once inside the anaerobic workstation, the cell culture medium in the insert was replaced with 1.5 mL of anaerobic medium. Due to the low volume of medium in the apical compartment of the chamber, the DO probe could not be submerged to a sufficient depth to yield accurate measurements. Hence, after the cells had been cultured in the co-culture chamber in the anaerobic workstation for 12 hours, the media from the inserts were transferred to a 10 mL universal bottle (Figure 3.3). Media from three cell culture inserts were pooled into one universal bottle. The amount of DO in each of the pools was measured using the DO probe. Measurements were carried out inside the anaerobic workstation, to ensure oxygen was not introduced to the

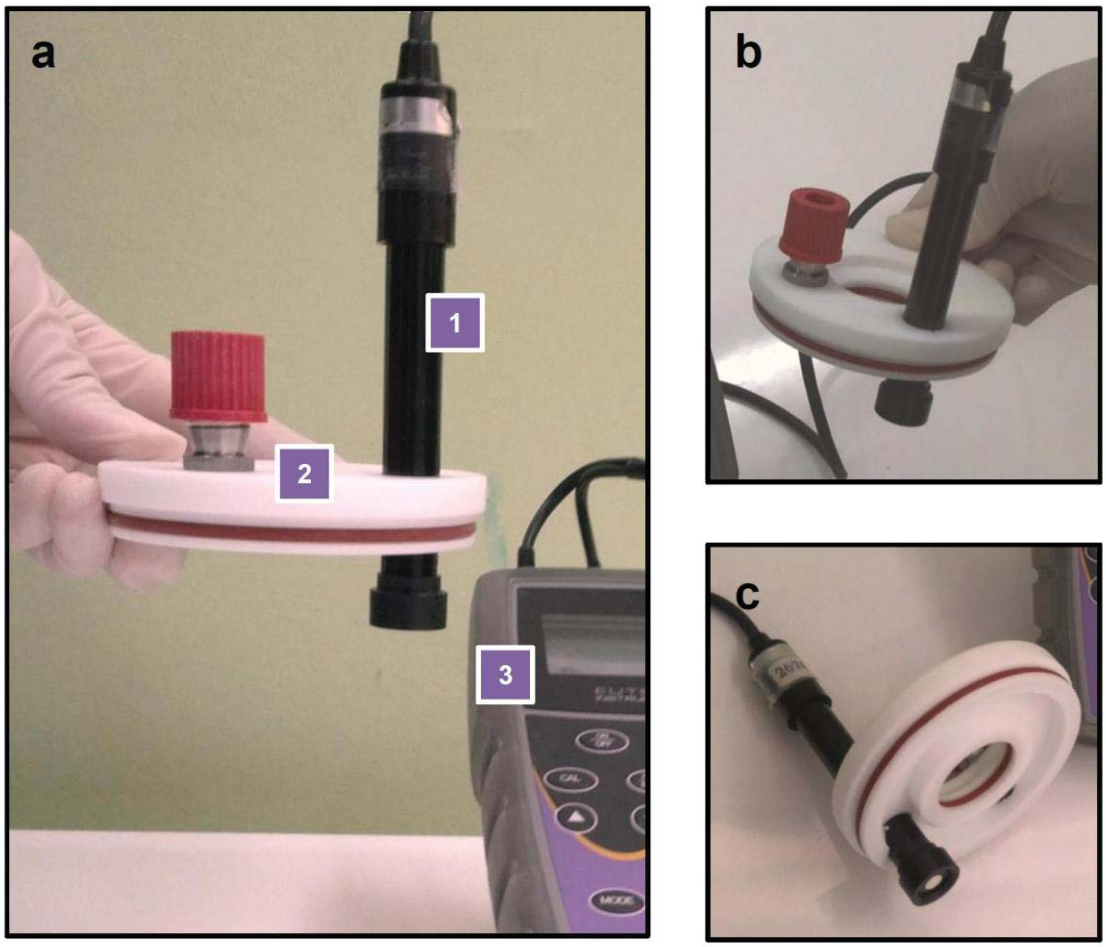

Figure 3.2 Special chamber lid containing a port for the dissolved oxygen probe.

Images show the view from the side (a), top (b) and bottom (c) of the lid. 1, DO probe; 2, chamber lid; 3, DO meter.

Figure 3.3 Measuring dissolved oxygen in the apical compartment of the co-culture chamber.

Media from three cell culture inserts were pooled into a 10 mL universal bottle. The bottles were capped with a plastic lid with an access port for the DO probe to ensure minimal diffusion during the measurement. Under this configuration the sensing area of the probe was submerged at a sufficient depth in cell culture medium. 1, DO probe; 2, Plastic lid with access port for DO probe; 3, DO meter; 4, universal bottle; 5, cell culture medium.

medium, and the bottles were capped with a plastic lid with an access port for the DO probe to ensure minimal oxygen diffusion during measurements. This experiment was carried out in 3 batches. Treatments were compared with a Kruskal-Wallis one-way ANOVA as the dataset contained a high number of zero values, and statistical difference was declared at probability less than 0.05.

3.3.4 Neutral red uptake assay

The neutral red uptake assay is a cell cytotoxicity assay based on the ability of viable cells to incorporate and bind neutral red (3-amino-7-dimethylamino-2-methylphenazine hydrochloride)[287]. Neutral red is extracted from the viable cells using an acidified ethanol solution, and the absorbance of the solubilised dye is quantified using a spectrophotometer. This assay was preferred over commercially available cell cytotoxicity and ATP colourimetric assay kits optimised for microtitre plates[288], as it allowed for the assay to be carried out in the cell culture inserts, minimising disruption to the Caco-2 cells prior to the completion of the assay. A dye exclusion method such as using Trypan blue[289] to distinguish between viable and non-viable cells was also considered inappropriate, as non-viable cells tended to detach from the inserts prior to staining[232], giving an underestimate of the proportion of non-viable cells. Detachment of non-viable cells would not affect the results of the neutral red assay as only viable cells take up the dye.

Caco-2 cell monolayers were cultured in a standard cell culture plate or the co-culture chamber either inside an anaerobic workstation or 5% CO_2 incubator for 12 hours, and cell viability was measured using the neutral red uptake assay (n = 6 per treatment). Following incubation, the inserts were removed from their respective environments and transferred to cell culture plates with fresh cell culture medium. The media in the inserts were removed and replaced with 1.5 mL of 50 μg/mL neutral red (Sigma-Aldrich) in cell culture medium, and incubated at 37°C in 5% CO_2 incubator for 2 hours. The cells were washed twice in phosphate-buffered saline (PBS) pH 7.2 (Life Technologies) to remove unincorporated dye and neutral red was extracted from viable cells by adding a solution containing 1% acetic acid and 50% ethanol in water, and shaking for 3 minutes at 70 rpm. Three 150 μL aliquots were removed from each sample, and the neutral red in each aliquot was quantified by measuring the absorbance at 540 nm (SpectraMax 250, Molecular Devices, California, United States). Background

absorbance was measured at 690 nm and subtracted from the 540 nm measurements, and the corrected values were normalised by dividing by the average corrected value for samples cultured in the cell culture plate in 5% CO_2. The experiment was repeated 3 times. Treatments were compared using restricted maximum likelihood (REML) to allow for analysis of multiple experiments in GenStat. Statistical difference was declared between two treatments where the difference in means was greater than the LSD at 5%.

3.3.5 Transmission electron microscopy[§]

Caco-2 cells were cultured on Transwell inserts in a co-culture chamber in an anaerobic environment for 12 hours. Immediately after removing the inserts from the chamber, the cells were fixed by immersing the Caco-2 cell monolayers in a solution of 2.5% glutaraldehyde, 0.002 M CaCl in 0.1 M cacodylate buffer for 1 hour at 37°C. The cells were then washed twice in 0.1M cacodylate buffer containing 0.002 M CaCl and 6.84% sucrose and transported to the electron microscopy facility in the same buffer. The cells were post-fixed in 0.1M cacodylate buffer containing 1% osmium tetroxide and 1.5% potassium ferricyanide for 1 hour, washed three times with water, and incubated in 1% uranyl acetate for 1 hour in the dark. After dehydration in a graded ethanol series followed by 50:50 ethanol and acetone and 100% acetone, the membrane was embedded in Procure resin. Sectioning was carried out using an Ultracut UCT ultramicrotome (Leica, Germany) fitted with a 45° diamond knife (Drukker, Netherlands). Sections were cut onto ultrapure water and collected on 100-mesh copper carbon- formvar-coated grids. Ultrathin sections (60-80 nm thickness) were examined using a FEI (USA) Morgagni 268D transmission electron microscope, and micrographs captured using a SIS/Olympus Megapixel III digital camera mounted above the phosphor screen.

[§] Preparation of cells for electron microscopy and imaging was carried out by Dr Duane Harland and James Vernon (both from AgResearch Lincoln) at the AgResearch Electron Microscopy Facility, Lincoln Research Centre.

3.3.6 DNA content analysis by flow cytometry

Caco-2 cell monolayers were cultured in a standard cell culture plate or the co-culture chamber either inside an anaerobic workstation or 5% CO_2 incubator for 12 hours, and the proportion of cells in phase of the cell cycle was calculated via DNA content analysis by flow cytometry (n = 3 per treatment). This technique was based on the incorporation of propidium iodide (PI) into nucleic acids and the detection of PI fluorescence[290]. Each fluorescence event equated to a single cell and allows for the proportion of cells in each phase of the cell cycle to be calculated. After the incubation period the inserts were removed from their respective environments, and the cells were rinsed in warm PBS, harvested by trypsinisation, and subsequently pelleted by centrifugation for 5 minutes at 240 x g. The cells were fixed by resuspending each cell pellet in 1 mL of cold PBS before adding 2 mL of cold 70% ethanol and shaking the cells vigorously. The fixed cells were stored at -20°C until further analysis. The fixed cell population from each insert was split into three tubes (equal volume) and RNase treated as follows. Frozen cells were pelleted by centrifugation for 5 minutes at 240 x g, and resuspended in 470 μL of PBS. Twenty five μL of 1 mg/mL RNase A was added to each cell suspension and mixed before incubating at 37°C for 30 minutes. Following RNase treatment, 5 μL of 400 μg/mL of PI was added to each sample and further incubated at 37°C 5 minutes. The samples were run through a FACScalibur (Becton Dickinson; settings shown in Appendix II), and 10000 events were collected three times from each tube. Doublets and cell debris was excluded based on forward and side scatter, and the fluorescence emission spectra of PI was collected. Subsequently the emission spectra were analysed for DNA content using FlowJo (TreeStar, Ashland, Ohio, USA). The fraction of cells in G0/G1, S and M/G2 were identified by fitting the data to the Dean-Jett-Fox model. The experiment was repeated 3 times, and the treatments were compared using a multiple experiments residual maximum likelihood (REML) analysis in GenStat. Statistical difference was declared between two treatments for a stage of the cell cycle, when the difference was greater than the least significant difference at 5% for that particular stage of the cell cycle.

3.3.7 TEER assay

Caco-2 cell monolayers were cultured in the co-culture chamber either inside an anaerobic workstation or 5% CO_2 incubator for 12 hours, during which TEER was

monitored (n = 6 per treatment). TEER of the monolayers was measured every 30 minutes using the built-in electrodes in the co-culture chamber connected to a CellZscope controller (nanoAnalytics) and software (version 2.0.0; nanoAnalytics). The change in TEER for each insert was calculated using the following formula: change in TEER (%) = (TEER ($\Omega.cm^2$) / initial TEER ($\Omega.cm^2$)) x 100 (%). The experiment was repeated two times and the data were combined. Treatments were compared using repeated measurements ANOVA in R (version 2.14.0; R Foundation for Statistical Computing, Vienna, Austria) and statistical difference was declared between two treatments for a given time point when the difference in means was greater than the LSD at 5%.

3.3.8 ^{3}H-mannitol bioassay

Caco-2 cell monolayers were cultured in the co-culture chamber either inside the anaerobic workstation or 5% CO_2 incubator for 12 hours, and paracellular permeability of the Caco-2 cell monolayer was measured during this time (n = 3 per treatment). ^{3}H-mannitol is an accepted marker of paracellular permeability[291]. Prior to the 12 hour incubation, ^{3}H-mannitol in 90% ethanol (American Radiolabelled Chemicals, St. Louis, Missouri, USA) was diluted in cell culture medium (aerobic or anaerobic, as appropriate) to an activity of approximately 9.25×10^4 Bq/mL, and added to the Transwell inserts (apical compartment; 1.5 mL/insert). During the incubation, 500 µL of cell culture medium from each chamber well (basal compartment) was sampled at 0, 3, 6, 9 and 12 hours. All samples were mixed with scintillation fluid (StarScint, PerkinElmer, Waltham, Massachusetts, USA) at a 1:1 ratio and counted using a 1459 Microbeta Trilux scintillation counter (PerkinElmer). The ^{3}H counts in the samples were used to calculate the amount of ^{3}H-mannitol in each chamber well at each time point. The percentage of ^{3}H-mannitol from each Transwell insert that had passed through to the chamber well was calculated for each time point. The experiment was repeated three times and the data combined. Treatments were compared using repeated measurements ANOVA in GenStat. The data were log-transformed to stabilise variance, and predicted means were derived from a generalised linear mixed model analysis and back transformed to estimate the rate of ^{3}H-mannitol increase in the basal compartment assuming a straight line trend. Statistical difference was declared between two

treatments for a given time point where the difference in means was greater than the LSD at 5%.

3.3.9 Confocal laser scanning microscopy

Caco-2 cell monolayers were cultured in either a standard cell culture plate or a co-culture chamber in either anaerobic conditions or 5% CO_2 for 12 hours (n = 3 per treatment). Following incubation, the Transwell inserts were removed from their respective environments and the Caco-2 cell monolayers immediately washed with PBS and fixed in 4% (w/v) paraformaldehyde for 15 minutes. The fixed Caco-2 cells were then rinsed three times with PBS, and permeabilised in PBS containing 0.2% (v/v) triton X-100, 1% (v/v) normal goat serum and 0.1% (w/v) sodium azide. The triton X-100 was used to permeabilise the cells, while the goat serum and sodium azide were used as a blocking agent and preservative respectively. The monolayers were incubated overnight at 4°C in 1 μg/mL of polyclonal rabbit anti-occludin (Life Technologies) and monoclonal mouse anti-ZO-1 (Life Technologies), washed three times in PBS containing 0.1% (v/v) triton-X 100 to remove non-specific binding, and incubated for 2 hours at room temperature in 8 μg/mL of Alexa Fluor 555 conjugated goat anti-rabbit IgG (Life Technologies), and Alexa Fluor 488 goat anti mouse IgG (Life Technologies). The Transwell membranes with the Caco-2 cell monolayers were excised off the plastic supports and mounted on to slides using mounting medium (Prolong gold antifade reagent; Life Technologies). Confocal images were obtained using a Leica SP5 DM6000B with a 63x oil objective (Manawatu Microscopy & Imaging Centre, Massey University). Sequential scanning was used to avoid overlap between the occludin (Alexa Fluor 555) and ZO-1 (Alexa Fluor 488) channels, and the scanner and hardware settings were kept consistent throughout the experiment to allow for comparison between samples (settings shown in Appendix III).

3.3.10 Analysis of abundance and localisation of tight junction proteins

The fluorescent staining of occludin and ZO-1 in the TJ region was quantified using ImageJ software (National Institutes of Health, USA) fitted with the LSM Toolbox plugin. Each image (blindly coded) was overlayed with a grid where each square had an area of 1853.78 μm^2 (Figure 3.4). For each image, a single grid line was chosen where

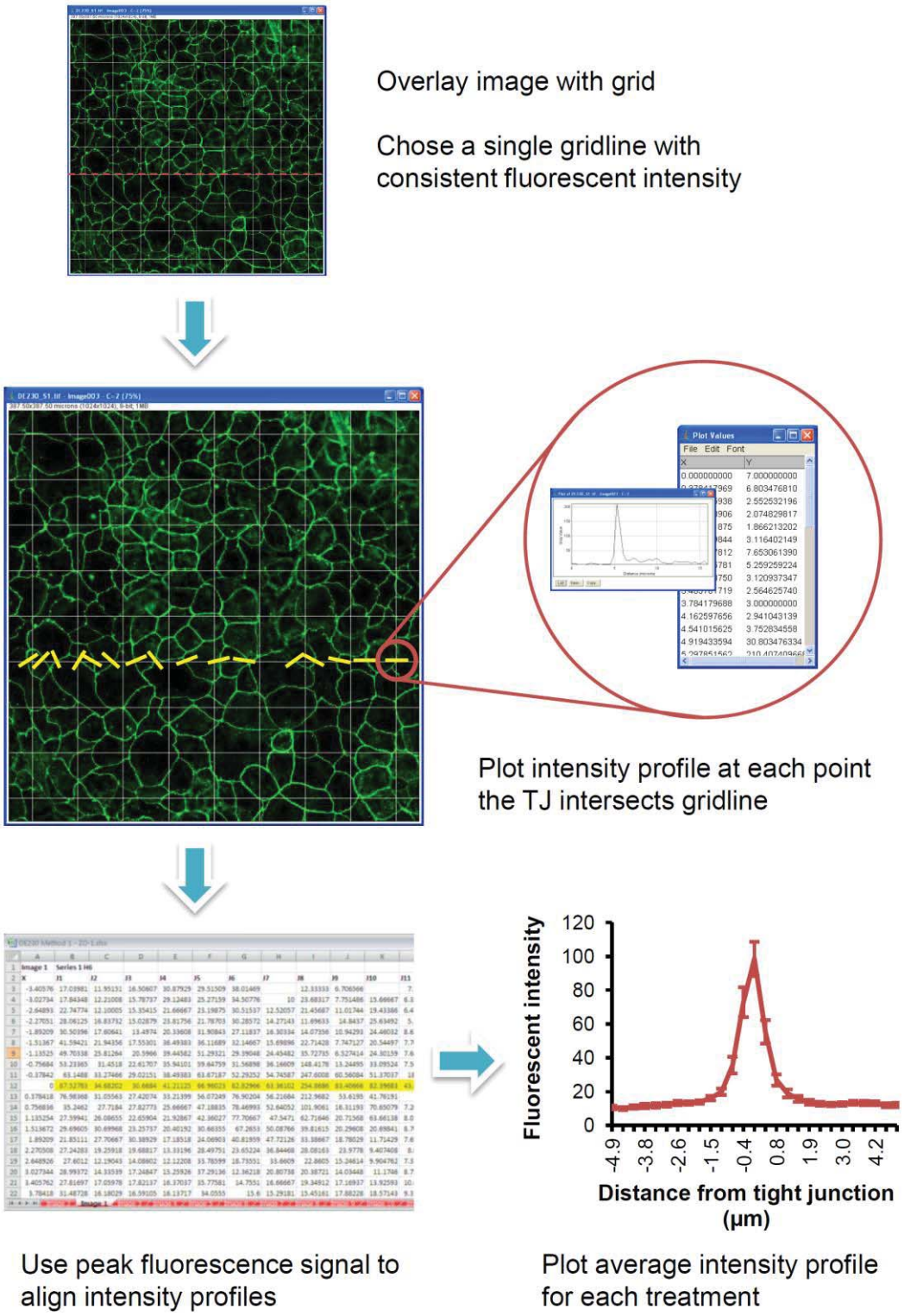

Figure 3.4 Analysing abundance and localisation of TJ proteins.

Using Image J software each image was overlayed with a grid, and a single grid line (red dashed line) was chosen where the fluorescent intensity of TJ was consistent along the entire line. The fluorescent intensity profiles were plotted for each point the TJ intersected this gridline (yellow lines); and using Microsoft Excel, the plot profiles were aligned based on their peak fluorescence signal.

the fluorescent intensity was consistent; and the fluorescent intensity profiles of Alexa Fluor 488 and Alexa Fluor 555 was plotted at each point a TJ intersected this grid line. Intensity profiles for about 45 junctions were plotted for each treatment group (15 junctions plotted per sample). The identification of the images was decoded and the fluorescence intensities plotted as a function of cell location using the peak fluorescence signal to align each intensity profile using Microsoft Office Excel (version 2007; Microsoft Corporation, Redmond, Washington, USA).

The fluorescent intensity profiles were smoothed using a locally weighted smoothing spline (LOESS) model[292] in R to eliminate noise[**]. TJ protein abundance and localisation were evaluated using the peak fluorescent intensity for each profile, and the distance from the TJ at which the intensity dropped to 50% (d50) and 20% (d20) of the peak intensity. Peak fluorescent intensity values were based on the original intensity profiles, while the d50 and d20 values were based on the smoothed intensity profiles. Treatment effect of peak fluorescent intensity, d50 and d20 was compared using a one-way ANOVA in R, and statistical difference was declared between two treatments where the difference in means was greater than the LSD at 5%.

3.3.11 Analysis of internalisation of tight junction proteins

TJ protein internalisation was determined in two ways based on the methods described by Coyne *et al.*[293]. First, internalisation was determined by the relative fluorescent intensity in the cytoplasm for each cell. The fluorescent intensity of a given area was determined by multiplying the size of the area by its average fluorescent intensity as determined using ImageJ software. Relative fluorescent intensity for the cytoplasm was calculated from blindly coded images according to the following equation: $(F_C)/(F_{TOTAL})$ x 100% where F_C is the fluorescent intensity within the cytoplasm, and F_{TOTAL} is the total fluorescence of the cell (including the TJ along the cell boundary). Calculations were based on 30 cells per treatment (10 cells per samples).

Internalisation was also determined by counting the number of cells in each image with internalised TJ protein, and expressing this as a percentage of the total cell number. For this analysis, a cell where fluorescence saturated the cytoplasm was classified as a cell with internalised TJ protein. The image threshold was automatically

[**] Analysis in R was performed by Dr John Koolaard (AgResearch Grasslands).

adjusted using ImageJ software to reduce subjectivity and help determining cells with internalised TJ protein. Three blindly coded images were analysed for each treatment (~175 cells per image). For both methods, treatment effect on protein internalisation was compared using a one-way ANOVA using each individual image as a block in GenStat and statistical difference was declared between two treatments where the difference in means was greater than the LSD at 5%.

3.4 RESULTS

3.4.1 Oxygen depletion in the aerobic compartment of the co-culture chamber

Several methods as described in section 3.3.2.1 were used to measure the amount of DO in the basal compartment at various time points during incubation. The results from these experiments suggested that the oxygen in the basal compartment depleted rapidly, reaching levels of less than 30% saturation by 4 hours (Figure 3.5). However, as described in section 3.3.2.1, these methods were not without inherent limitations, and required the basal medium to be exposed to an alternate environment during the measurement. Further, the readings in the DO meter were highly unstable and variable between samples and time points.

An optimised method (refer to section 3.3.2.2) was used to measure the DO concentration in the medium in the aerobic basal compartment over 12 hours (Figure 3.6). The DO concentration reduced from about 97% saturation at a rate of -1.49% saturation/hour, and the mean (± SEM) DO at 12 hours was 77.4 ± 1.1% saturation. This equates to a loss of 0.10 mg/L/hour, or a total loss of 57.92 mg of DO (in the 50 mL basal medium) over the 12 hour period; and the basal compartment held 5.02 mg/L or a total 3.00 g of DO at the end of the 12 hour period.

The rate of DO depletion was unaffected by the presence or absence of the Caco-2 cell monolayer at the 5% LSD level (0.43) showing that the rate determining factor was the Transwell membrane, rather than the cell monolayer. When the Transwell insert alone (no Caco-2 cell monolayer) was present, the rate of depletion was -1.57% saturation/hour (-0.10 mg/L/hour). However, the rate of oxygen depletion was greater when no Transwell insert was present (-7.09% saturation/hour; -0.46 mg/L/hour).

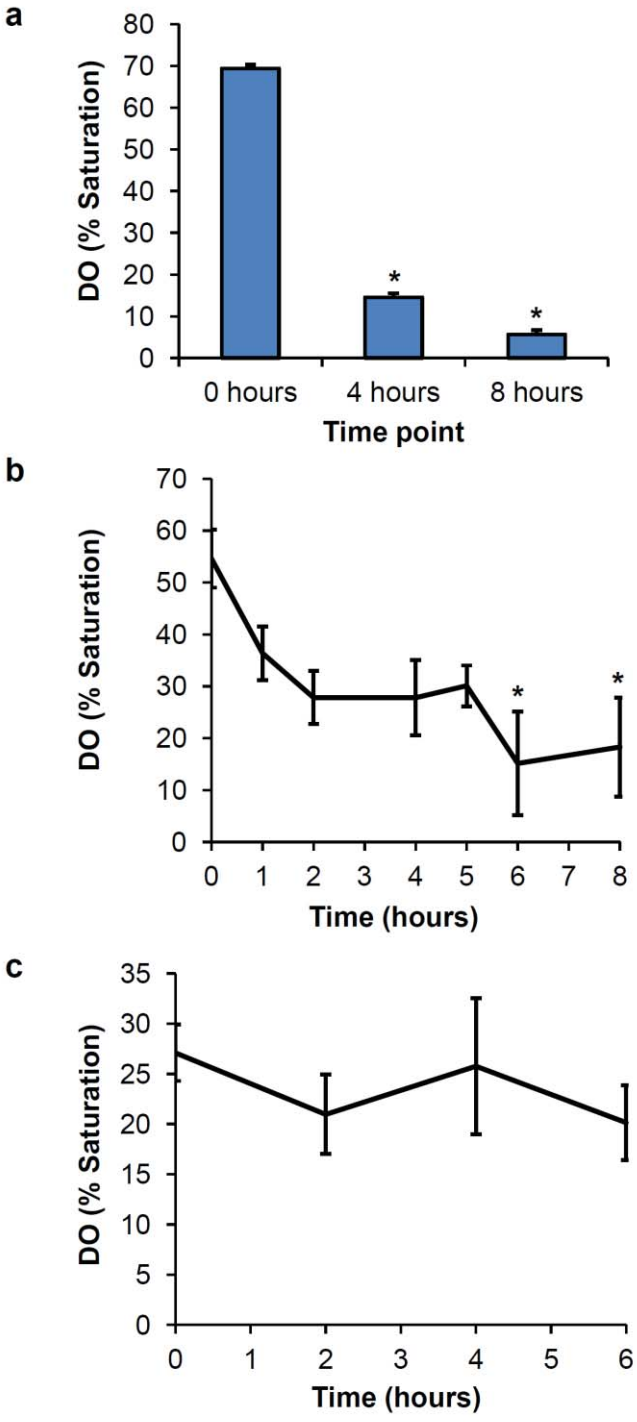

Figure 3.5 Preliminary data on depletion of dissolved oxygen in basal compartment of co-culture chamber.

DO in the basal compartment was measured using various methods which suggested a rapid depletion of oxygen. However all methods were not without inherent limitations. (a) chamber lid removed (n = 2 per time point); (b) 3 mL of basal medium sampled and reintroduced to co-culture chamber (n = 3); (c) 1 mL of basal medium sampled (n = 3). All graphs show mean (+/- SEM) DO for each time point. * $P < 0.05$ compared to 0 hour time point.

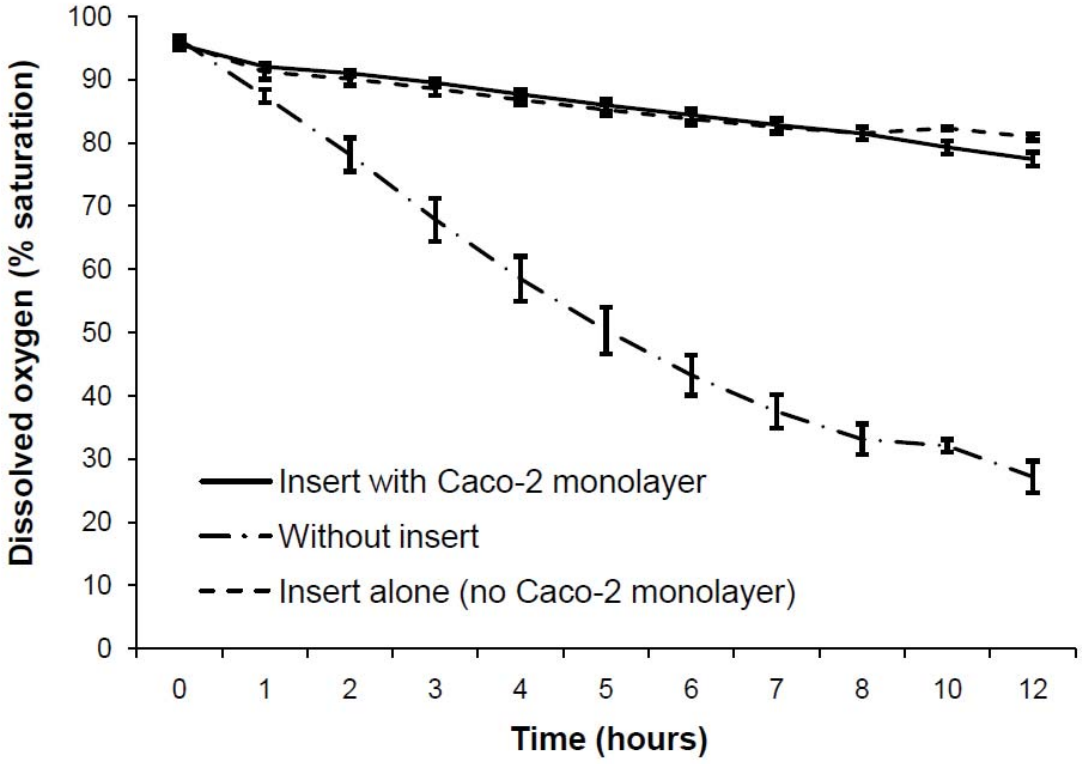

Figure 3.6 Depletion of dissolved oxygen in the basal compartment of the co-culture chamber over 12 hours.

The graph shows the mean (+/- SEM) DO for each hour, when the chamber was set up with an insert with a Caco-2 cell monolayer (n = 5), an insert alone (0-8 hours, n = 5; 10-12 hours, n = 2), and without an insert (0-8 hours, n = 5; 10-12 hours, n = 2). The rate of DO depletion was unaffected by the presence or absence of the Caco-2 cell monolayer, but was greater when no insert was present ($P < 0.05$).

3.4.2 Dissolved oxygen in the anaerobic compartment of the co-culture chamber

After 12 hours of incubation in the anaerobic workstation, DO levels of the apical media in the inserts were measured. DO was undetectable in 5 out of the 6 pools of media collected from the inserts. In one of the pools, DO was detected at 0.9% saturation (which equates to 0.06 mg/L). The mean (± SEM) DO concentration in the anaerobic compartment was 0.15 ± 0.14% saturation (which equates to 0.01 mg/L). When inserts without Caco-2 cell monolayers were used, oxygen was detected in all pools of media tested and the mean (± SEM) DO concentration of 2.38 ± 0.31% saturation was higher than when the Caco-2 cell monolayer was present (P = 0.004). The absence of DO at 12 hours in the apical compartment when the Caco-2 cell monolayer was present suggests that the oxygen which diffused through the Transwell membrane was fully used for cell respiration.

3.4.3 Ultrastructural features of Caco-2 cells cultured in the apical anaerobic model

Caco-2 cells exposed to the apical anaerobic environment were imaged using transmission electron microscopy (Figure 3.7). The ultrastructural features of the cell monolayer consisted of the classic motif of TJ, adhesion belt junction then desmosome, as well as microvilli forming an apical brush border as seen in Caco-2 cells grown in a conventional Transwell model[243].

3.4.4 Effect of anaerobic apical environment on Caco-2 cell viability

The neutral red uptake assay was used to determine Caco-2 cell viability after 12 hours (Figure 3.8). REML analysis showed a treatment effect (P = 0.02), and the 5% LSD was 0.13. There was no difference in viability between Caco-2 cells cultured in a standard cell culture plate in a 5% CO_2 environment, the co-culture chamber in 5% CO_2, or the co-culture chamber in the anaerobic workstation. In contrast, Caco-2 cells cultured in Transwell inserts in a standard cell culture plate in an anaerobic environment had reduced viability.

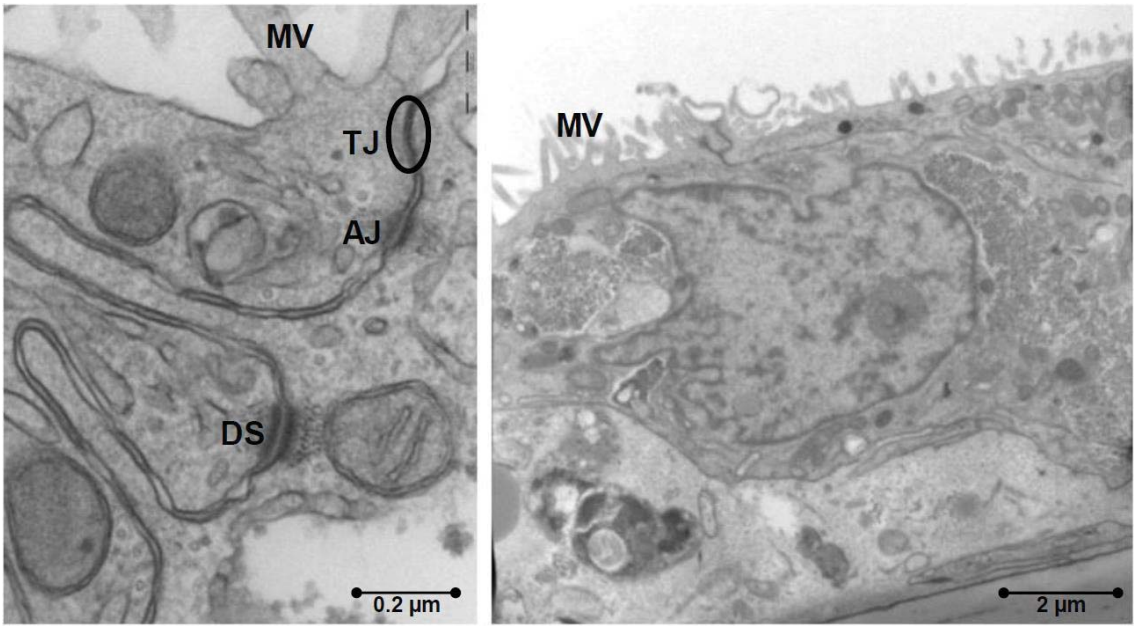

Figure 3.7 Transmission electron micrographs of Caco-2 cells cultured in the apical anaerobic model.

Transmission electron micrographs showing ultrastructural features of a Caco-2 cell monolayer incubated in an apical anaerobic environment for 12 hours. MV, microvilli; TJ, tight junction; AJ, adherens junction; DS, desmosome.

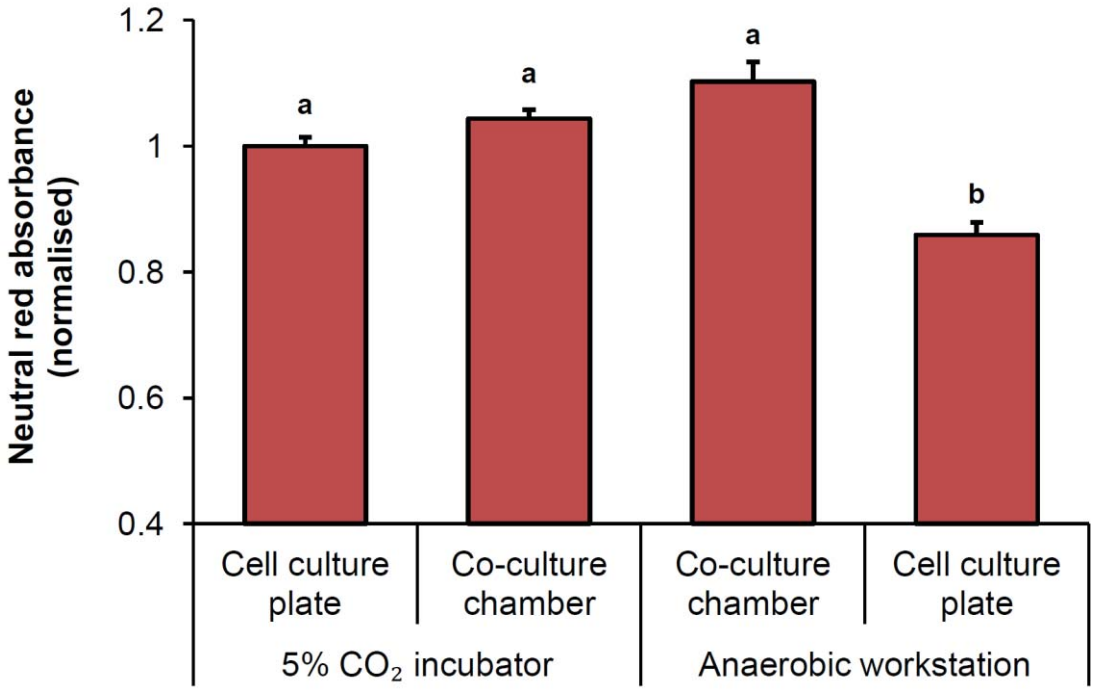

Figure 3.8 Neutral red uptake assay to determine viability of Caco-2 cells cultured in various cell culture environments.

Neutral red uptake by Caco-2 cells cultured in a standard tissue culture plate or co-culture chamber for 12 hours inside an anaerobic workstation or 5% CO_2 incubator. Neutral red absorbance was normalised by adjusting the control cells (tissue culture plate in 5% CO2 incubator) to 1. The graph shows normalised mean (+/- SEM) absorbance for 3 experiments (n = 18; 6 samples per treatment per experiment). Treatments that do not share the same letter (a or b) were significantly different ($P < 0.05$).

3.4.5 Cell cycle analysis

Distribution of cells across the cell cycle was investigated by DNA content analysis using flow cytometry, in cells grown either in a cell culture plate or the co-culture chamber in either an anaerobic environment or 5% CO_2. Figure 3.9 shows a representative dot plot of forward and side scatter with the gating used to exclude cell debris and doublets. The percentage of cells in each phase of the cell cycle did not differ between the various cell culture environments (Figure 3.10). Furthermore, there was no consistent trend across the three experiments.

3.4.6 Effect of apical anaerobic environment on the barrier function of the Caco-2 cell monolayer

The barrier integrity of the Caco-2 cell monolayers cultured in the co-culture chamber, either in 5% CO_2 or an anaerobic environment was measured using the TEER (24 hours) and ^{3}H-mannitol assays (12 hours). The mean TEER dropped initially, but stabilised over time (Figure 3.11). The amount of ^{3}H-mannitol that crossed the Caco-2 cell monolayer from the apical to the basal side was monitored by measuring ^{3}H-mannitol in the chamber well every 3 hours. (Figure 3.12). It was estimated that 0.088% and 0.092% of ^{3}H-mannitol in the insert, crossed over to the chamber well every hour, in the 5% CO_2 incubator and an anaerobic workstation respectively. Neither the mannitol flux nor TEER differed between treatment groups at any time point.

3.4.7 Effect of apical anaerobic environment on the localisation of tight junction proteins

To further ensure the Caco-2 cells in the apical anaerobic model formed an intact barrier, the abundance and localisation of the TJ proteins occludin, a transmembrane protein, and ZO-1, a plaque protein, was visualised using confocal microscopy (Figure 3.13). TJ staining was similar for cell monolayers grown in the co-culture chamber in an anaerobic workstation, compared with cells in a cell culture plate or the co-culture chamber in a 5% CO_2 incubator, with the TJ proteins localised at cell boundaries. However, where cells were grown in a fully anaerobic environment (cell culture plate in an anaerobic workstation), the cell boundaries were not well defined.

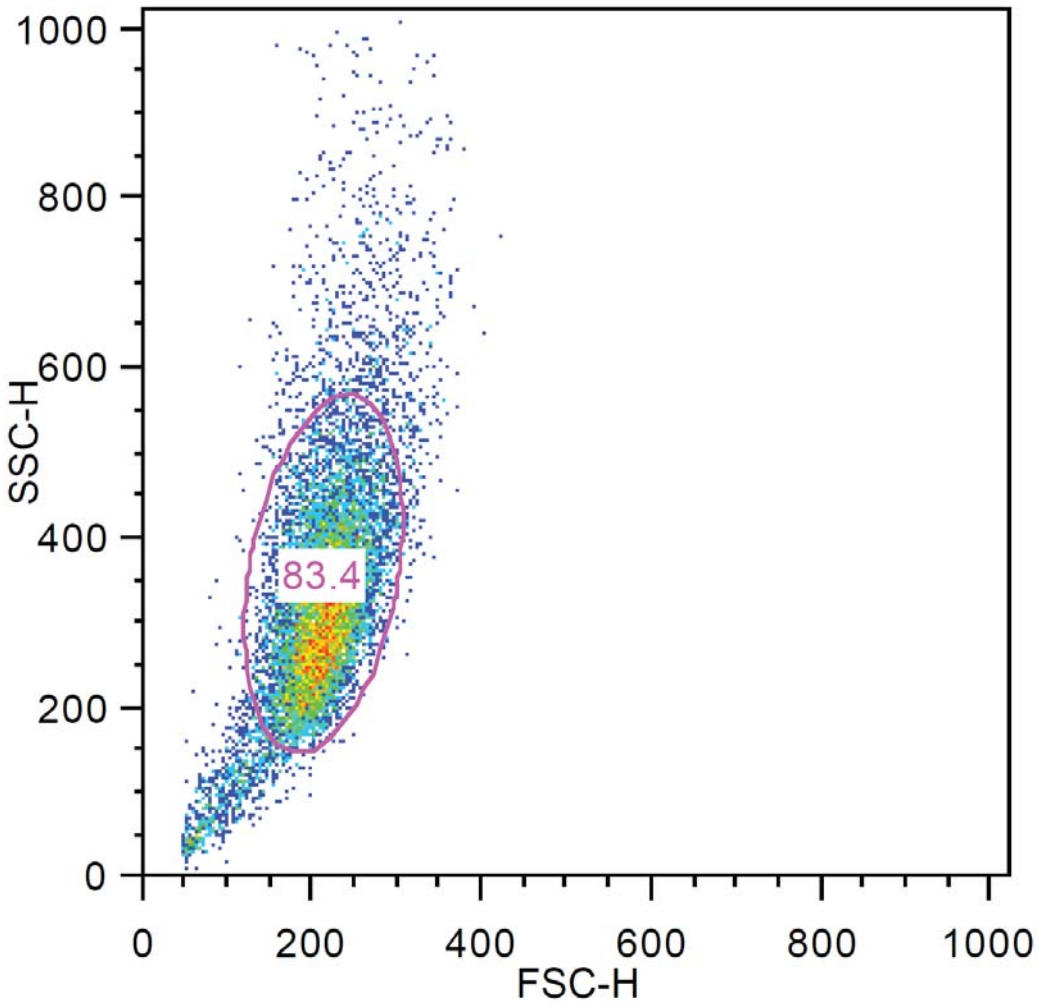

Figure 3.9 Representative dot plot of forward and side scatter of Caco-2 cells harvested for cell cycle analysis.

Caco-2 cells were harvested from a cell culture insert, fixed with ethanol, and stained with propidium iodide. The cells were run through a flow cytometer and the events collected were gated to exclude cell debris and doublets. DNA content analysis was subsequently performed on the gated events. SSC-H, side scatter; FSC-H, forward scatter.

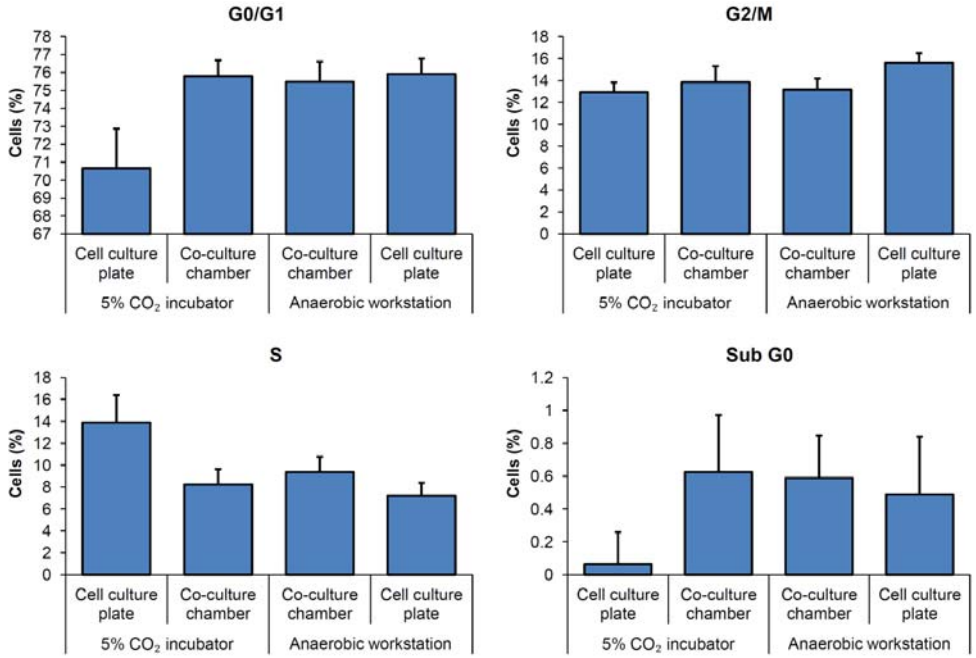

Figure 3.10 Cell cycle analysis for Caco-2 cells cultured in various cell culture environments.

Percentage of Caco-2 cell population in G0/G1, S, G2/M and sub G0 stages of cell cycle for cells cultured in a standard tissue culture plate or co-culture chamber for 12 hours inside an anaerobic workstation or 5% CO_2 incubator. The graphs show mean (+/- SEM) percentages for 3 experiments (n = 9; 3 samples per treatment per experiment). The mean percentage of cells did not differ between treatments for at any phase of the cell cycle.

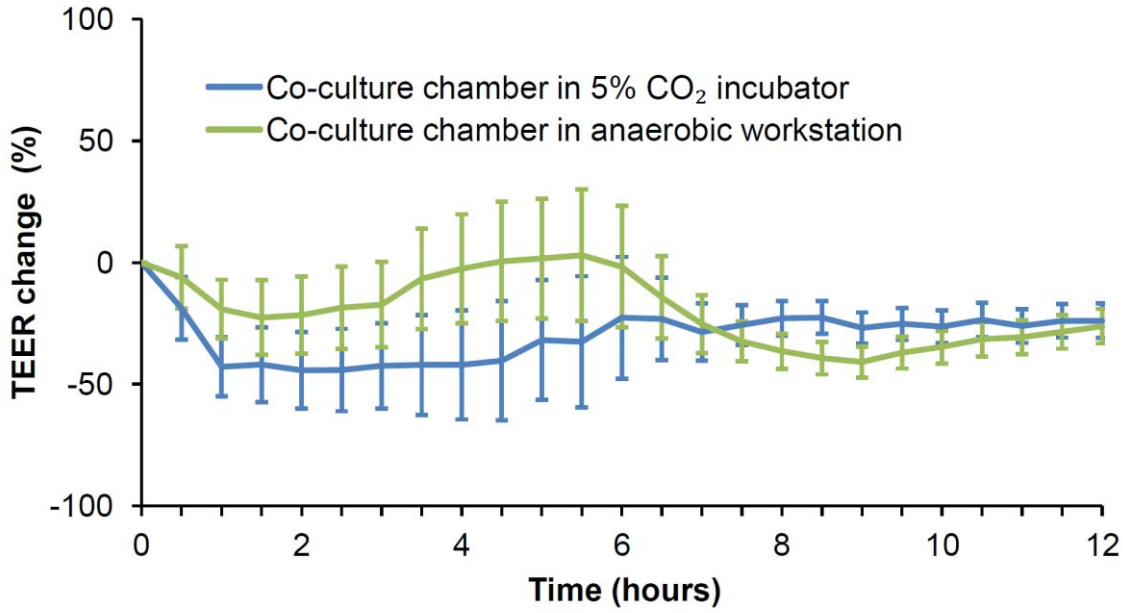

Figure 3.11 TEER over time across Caco-2 cell monolayers cultured in the co-culture chamber.

Change in TEER across Caco-2 cell monolayers in the co-culture chamber inside an anaerobic workstation or 5% CO_2 incubator. The graph shows the mean (+/- SEM) change in TEER (n = 12; 2 experiments, 6 samples per treatment per experiment). The mean TEER did not differ between treatments at any time point.

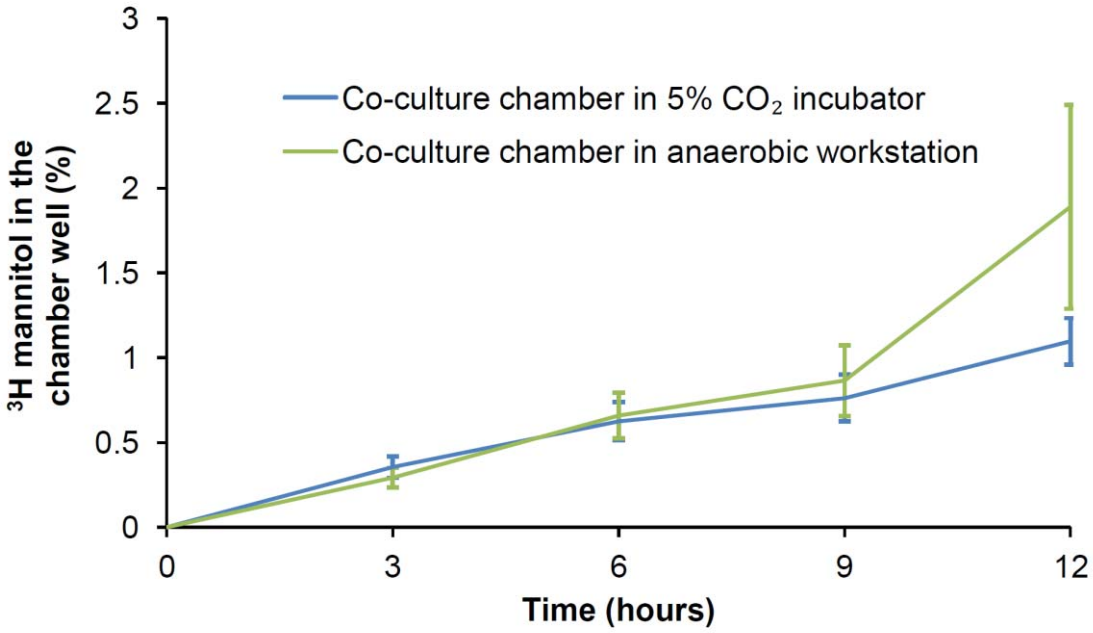

Figure 3.12 ^{3}H-mannitol permeability across Caco-2 cell monolayers cultured in the co-culture chamber.

Permeability of ^{3}H-mannitol across Caco-2 cell monolayers in the co-culture chamber inside an anaerobic workstation or 5% CO_2 incubator. The graph shows the mean (+/- SEM) % of ^{3}H-mannitol in the cell culture insert that crossed the Caco-2 cell monolayer to the chamber well (n = 9; 3 experiments, 3 samples per treatment per experiment). The mean % ^{3}H-mannitol did not differ between treatments at any time point.

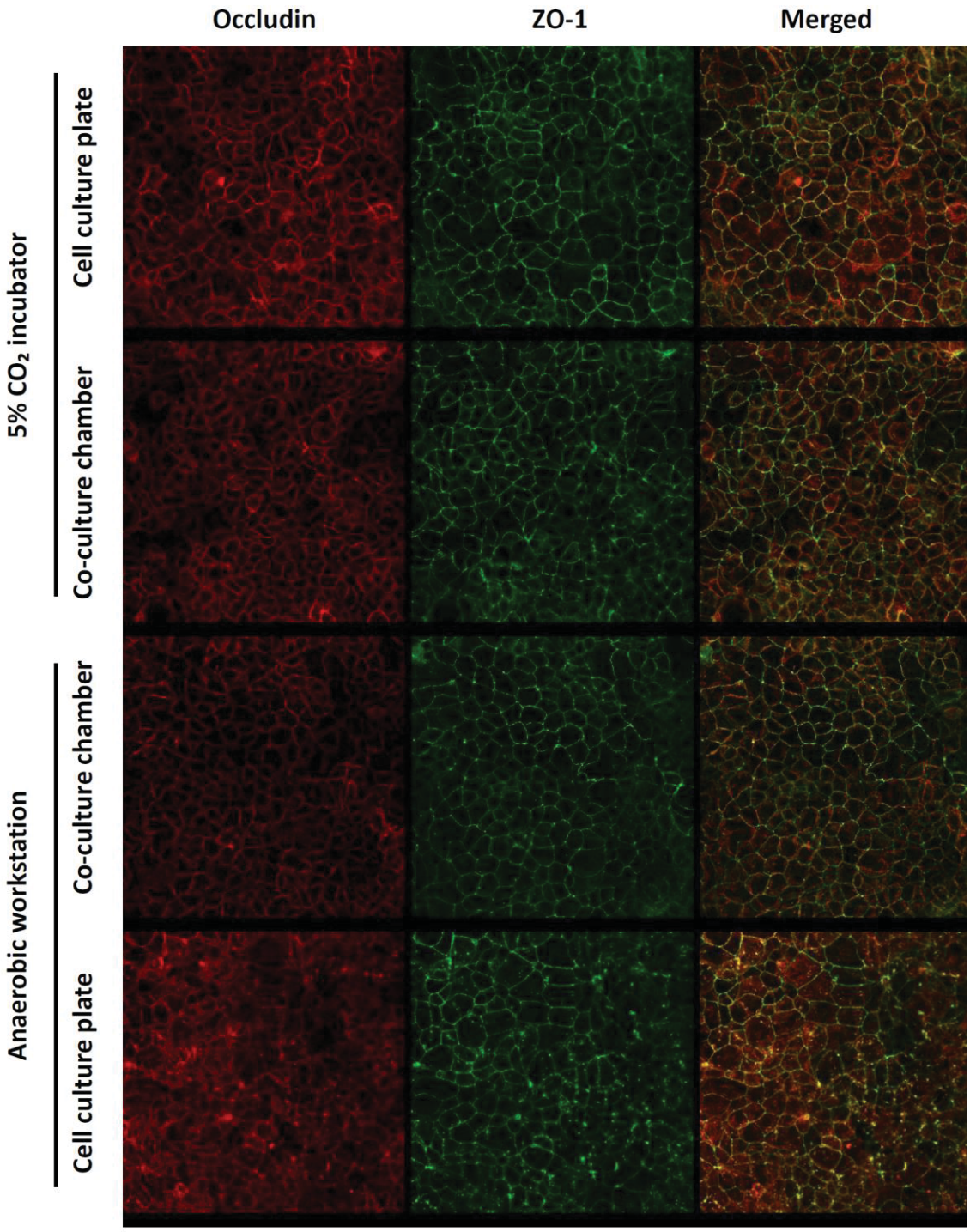

Figure 3.13 Caco-2 cell monolayers stained for TJ proteins and visualised using confocal microscopy.

Typical images of Caco-2 cell monolayers (cultured in a standard cell culture plate or co-culture chamber for 12 hours inside an anaerobic workstation or 5% CO_2 incubator) stained for occludin (red) and ZO-1 (green). Yellow indicates overlap of red and green fluorescence.

Abundance and localisation of occludin and ZO-1 were analysed by plotting the fluorescence intensity profiles of the TJ to determine the peak fluorescence intensity, and the distance over which the intensity drops to 50% (d50) and 20% (d20) of the peak intensity (Figure 3.14). For both occludin and ZO-1, peak fluorescence intensity was reduced in all treatment groups compared to Transwell inserts in a cell culture plate in a 5% CO_2 incubator, suggesting that growing the cells in the co-culture chamber or the anaerobic workstation for 12 hours reduces the TJ integrity (Figure 3.15). In the case of occludin, peak fluorescence was also reduced for Caco-2 cell monolayers grown in the anaerobic workstation compared to cells grown in the 5% CO_2 incubator. Of the Caco-2 cell monolayers grown in anaerobic workstation, those in the co-culture chamber had reduced peak fluorescence compared to those in the tissue culture plate.

The d50 and d20 values for occludin were not different between treatments at the 5% significance level (Figure 3.16). However, there was a trend ($P < 0.1$) for d20 to be increased in cells grown in the anaerobic workstation, suggesting that TJ localisation may be altered. In the case of ZO-1 however, both d50 and d20 differed significantly between treatments. Compared to Caco-2 cells grown in a tissue culture plate in a 5% CO_2 incubator, cells grown in the co-culture chamber in the anaerobic workstation had an increased d50 value. This suggests that TJ localisation was more widely spread.

TJ localisation was also evaluated by determining the amount of staining in the cell cytoplasm. There was no difference between treatments in the fluorescence intensity of the cytoplasm relative to the total fluorescence intensity (Figure 3.17). However, Caco-2 cell monolayers grown in a fully anaerobic environment (cell culture plate in anaerobic workstation) had an increase in the number of cells with occludin staining within the cell cytoplasm (Figure 3.18) compared to all other treatments, while Caco-2 cell monolayers grown in the apical anaerobic model (co-culture chamber in anaerobic workstation), were not different to cells grown in the conventional Transwell system (cell culture plate in 5% CO_2 incubator). No differences were observed between treatments for ZO-1 staining within the cell cytoplasm.

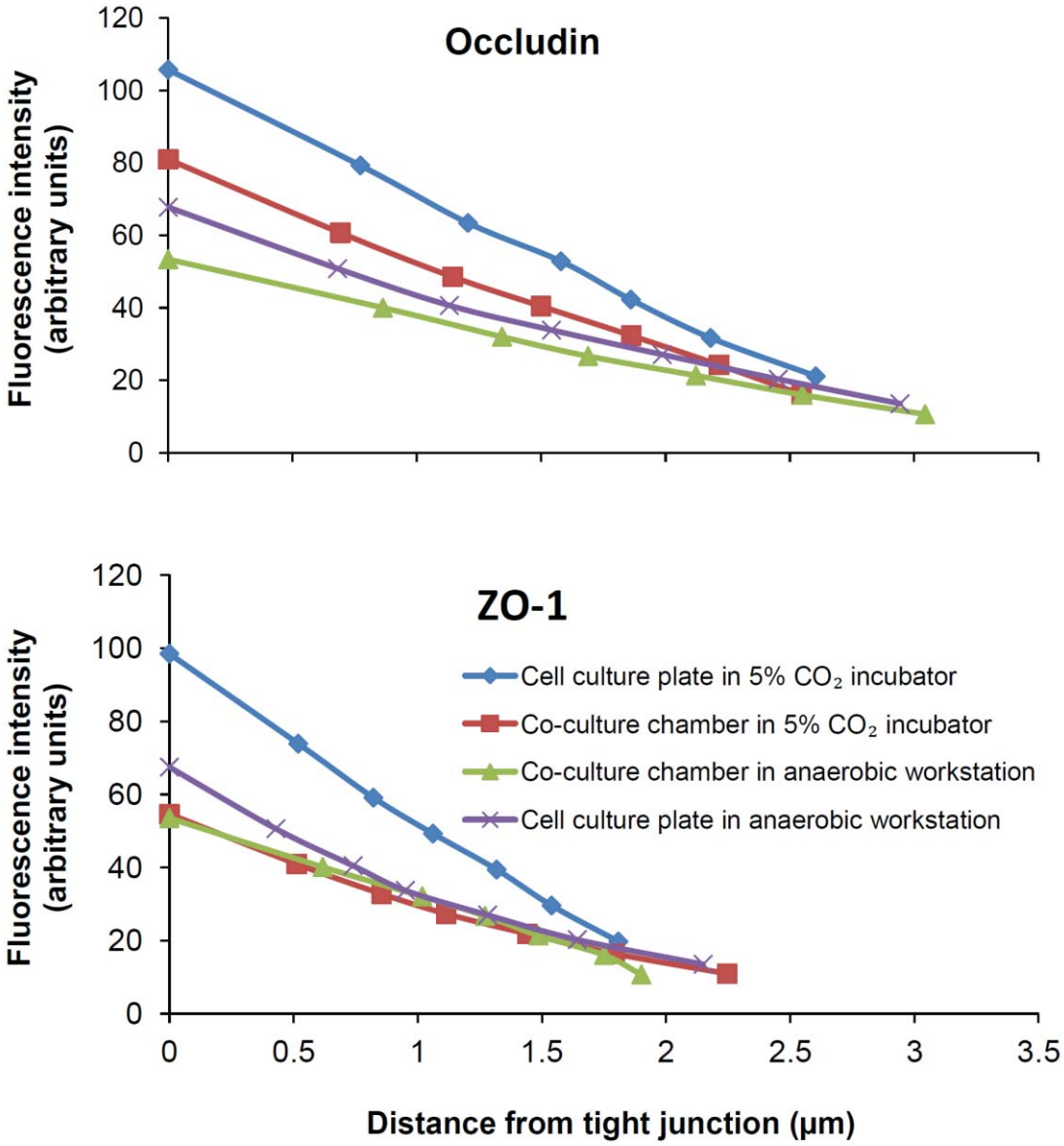

Figure 3.14 Abundance and localisation of TJ proteins in Caco-2 cell monolayers cultured in various cell culture environments.

Abundance and localisation of occludin and ZO-1 were analysed by plotting the intensity profiles of fluorescently labelled TJ. The graphs depict the mean peak fluorescence intensity (assumed to be at 0 µm from the TJ) of occludin or ZO-1 for each treatment, and the mean distance from the TJ at which the intensity drops to 75%, 60%, 50%, 40%, 30% and 20% of the peak intensity. Fluorescence intensity values are based on the actual peak intensity, while the distances from the TJ are based on the intensity profiles that were smoothed using a LOESS model (n = ~45).

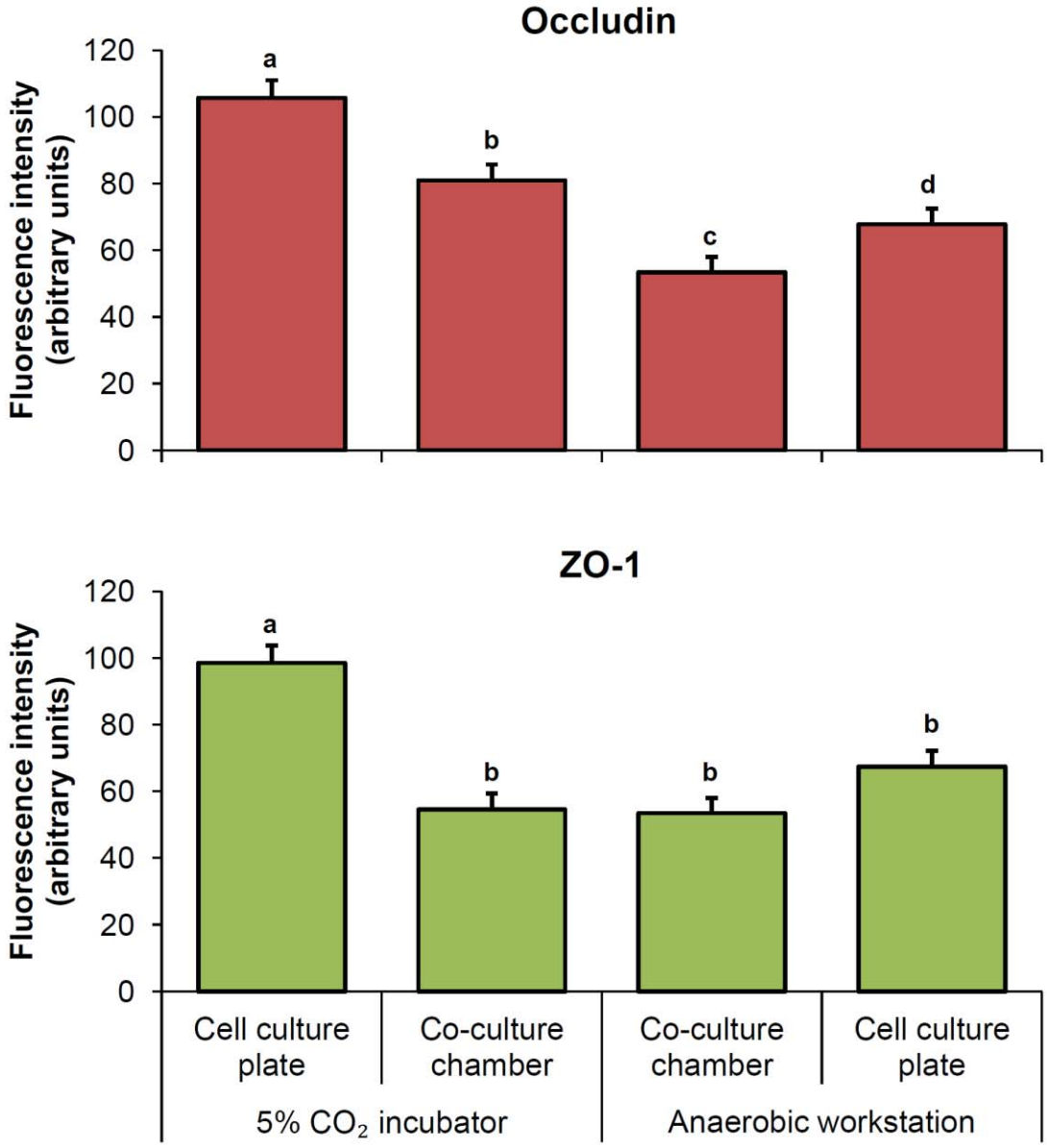

Figure 3.15 Abundance of TJ proteins as measured by peak fluorescence intensity in Caco-2 cells cultured in various cell culture environments.

Abundance of occludin and ZO-1 were analysed by plotting the intensity profiles of fluorescently labelled TJ. The graphs show the mean (+/- SEM) peak fluorescence intensity of occludin and ZO-1 profiles for each treatment (n = ~45). In each graph treatments which do not share the same letter (a, b, c or d) are significantly different ($P < 0.05$).

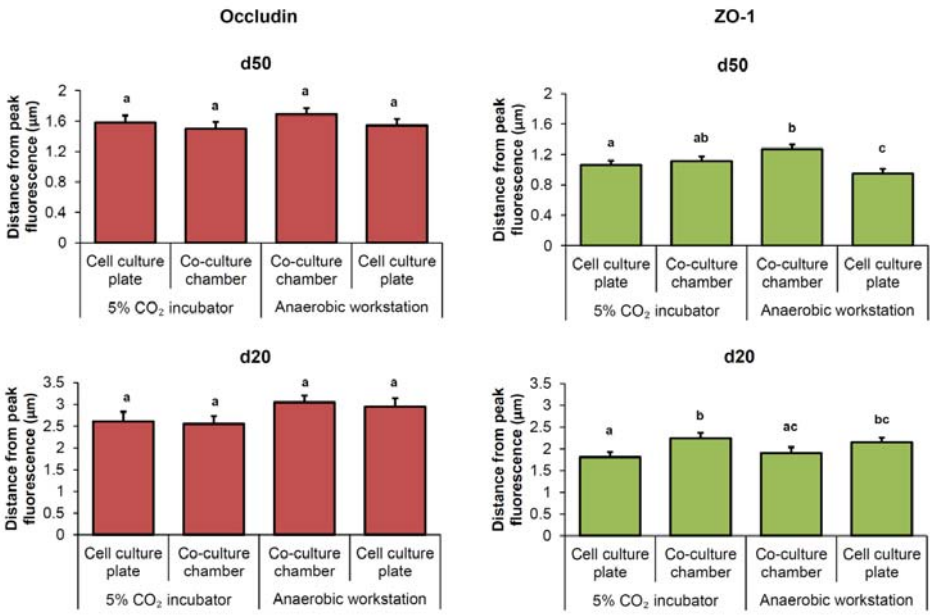

Figure 3.16 Localisation of TJ proteins as measured by distance from TJ at which 50% (d50) and 20% (d20) of peak fluorescence intensity is reached in Caco-2 cells cultured in various cell culture environments.

Localisation of occludin and ZO-1 were analysed by plotting the intensity profiles of fluorescently labelled TJ. The graphs show the mean distance from the TJ (peak intensity of fluorescent profile) at which fluorescence of occludin and ZO-1 drops to 50% and 20% of the peak intensity. In each graph treatments which do not share the same letter (a, b, or c) are significantly different ($P < 0.05$).

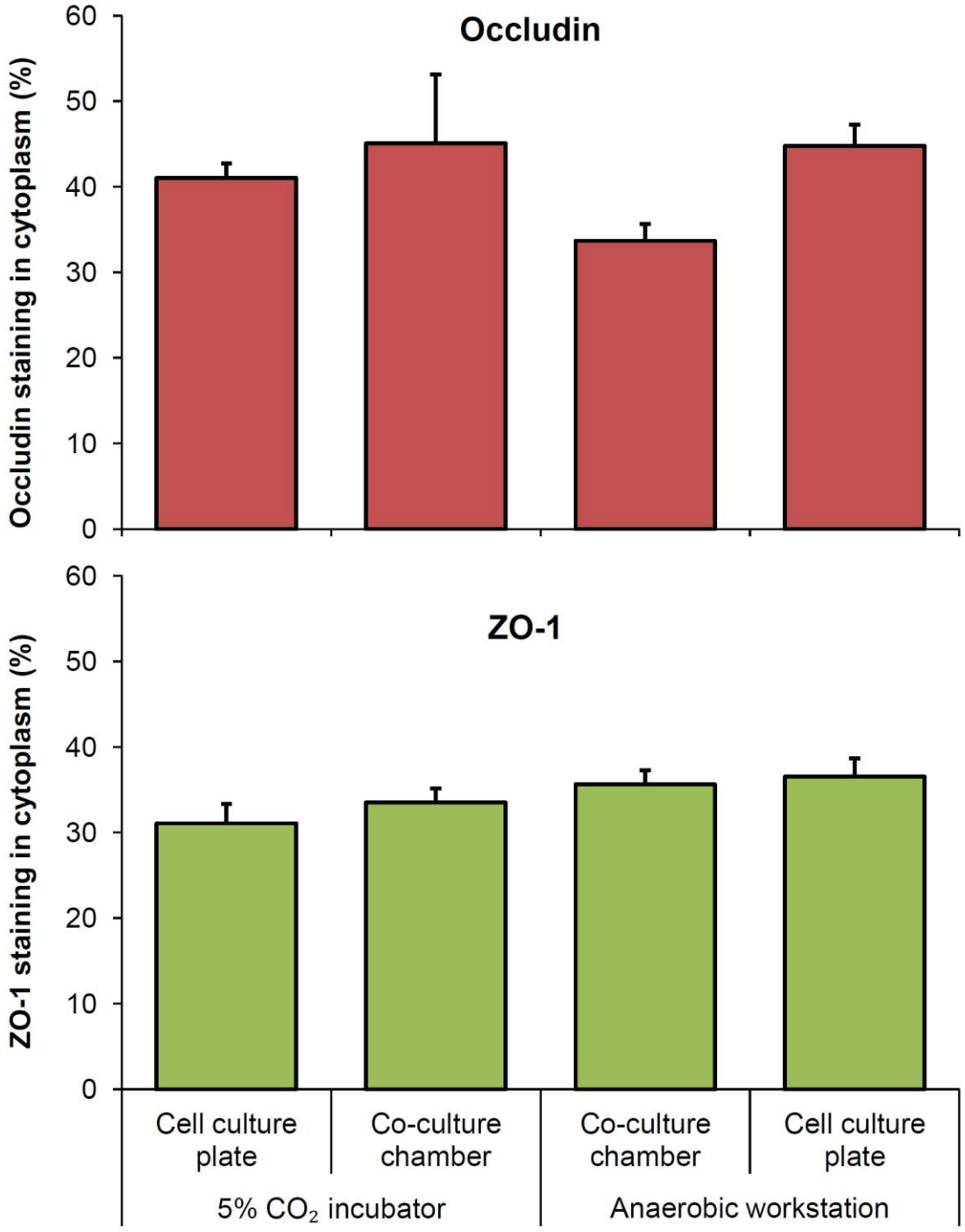

Figure 3.17 TJ staining within the cytoplasm of Caco-2 cells cultured in various cell culture environments.

Graphs show the mean (+/- SEM) fluorescence intensity for occludin and ZO-1 within the cell cytoplasm relative to the total fluorescent intensity of the cell (n = 30). TJ staining did not differ between treatment groups.

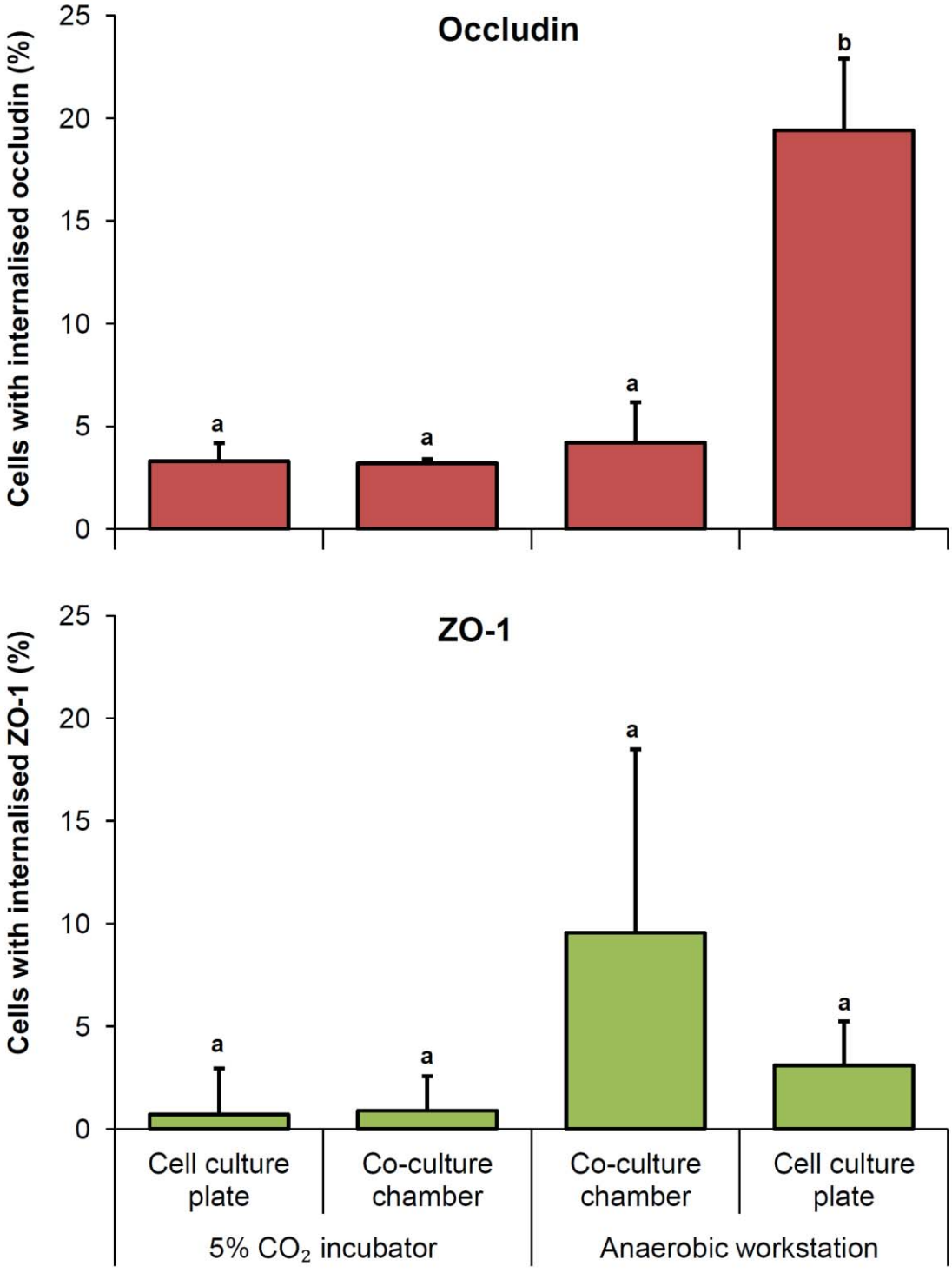

Figure 3.18 Number of cells with internalised TJ protein in Caco-2 monolayers cultured in various cell culture environments.

Graphs show the mean (+/- SEM) number of cells saturated with occludin and ZO-1 staining in the cell cytoplasm as percentage of the total number of cells (n = ~175). In each graph treatment means which do not share the same letter (a, b, or c) are significantly different ($P < 0.05$).

3.5 DISCUSSION

The results of the presently described work show that the Caco-2 cells were viable, had the normal morphology and structure of polarised intestinal cells, and maintained an intact epithelial barrier in the apical anaerobic intestinal barrier model over a 12 hour period. A time frame of 12 hours for validation was based on previous studies where commensal and probiotic bacteria exerted their effects on barrier integrity within this period of time[196,201]. At 12 hours, DO content in the apical compartment of the co-culture chamber was almost undetectable, while in the basal compartment DO was over 75% saturation, showing that oxygen tension in the basal compartment was not depleted, and supporting the validity of the use of this model over 12 hours.

In vivo the epithelial cells of the intestine receive oxygen from the underlying capillary bed, which drains into the hepatic portal vein[294]. The oxygen tension in this vein has been estimated to be 30 mm Hg[295]. Tissue oxygen tension in the intestinal tract of patients that inspired oxygen concentrations of 33% (c.f. standard inspired oxygen concentration of 21%), was between 30-40 mm Hg[296]. An oxygen tension of 40 mm Hg (the upper limit of oxygen tension in the intestinal tract) is equivalent to less than 2 mg/L of oxygen (calculated as described in Colt (1984)[297]). DO saturation in the intestine at 12 hours (equivalent to about 5 mg/L of oxygen), can thus be considered sufficient. Replacing oxygen in the basal compartment of the co-culture chamber was considered risky, as excessive oxygen is known to have toxic or growth inhibitory effects on mammalian cells[298].

There is some evidence that oxygen is present at a low concentration in the apical compartment of the chamber. However, while the intestinal lumen is considered to be devoid of oxygen[299], the intestinal mucosa is thought to be a microaerophilic environment due to oxygen influx from the intestinal epithelium[300]. Hence the apical anaerobic model may resemble the physiological conditions of the human intestine. A microaerophilic environment may still allow for the survival of obligate anaerobes. For example, *Faecalibacterium prausnitzii*, an obligate anaerobe that loses its viability within 2 minutes when exposed to atmospheric conditions[301], is known to be associated with the colonic mucosa where low levels of oxygen exist[300,302], and has been shown *in*

vitro to grow in the oxic-anoxic interphase of a gas tube, and utilise the available oxygen[303].

Further, facultative anaerobic bacteria in the intestine, such as *E. coli*, which are able to survive both in the presence and absence of oxygen, have an altered metabolism and gene expression profile in the anaerobic conditions of the intestine, compared to when cultured in conventional aerobic conditions[304]. Thus if grown in the apical anaerobic model, these bacteria would likely behave as they would in the physiological conditions of the intestine, and their interactions with the host epithelium would likely be more representative of the *in vivo* conditions.

Depletion of ATP is a consequence of cellular hypoxia[305,306]. The amount of neutral red a cell takes up and stores in its lysosomes depends on the cell's capacity to maintain pH gradients, which in turn is dependent on its production of ATP[307]. Neutral red uptake was unaffected in cells grown in the apical anaerobic model over 12 hours, while it was decreased in cells grown in the fully anaerobic environment. This suggests a reduction in ATP synthesis in Caco-2 cell monolayers grown in a fully anaerobic environment, which is consistent with the reduced amount of oxygen available to the cells. As cell viability was unaffected in Caco-2 cell monolayers grown in the apical anaerobic environment, it may be inferred that the amount of oxygen the cells received from the basolateral side was sufficient to maintain normal cell metabolism.

Alterations to the cell cycle may also indicate a reduction in viability. For example where cell damage has occurred, cell cycle is arrested to prevent carcinogenesis, which in turn alters the distribution of cells across the cell cycle. DNA content analysis by flow cytometry did not reveal any differences in cell cycle between treatments. This was largely due to the variation between the different runs of the same experiment. However, the doubling time of Caco-2 cells (HTB37 clone) is approximately 62 hours[308], so differences in cell viability are not likely to be reflected in the distribution of cells across the cell cycle after 12 hours of treatment. Although doublets were excluded from DNA content analysis based on forward and side scatter of the events collected, this does not ensure the gated events are free of clumped cells. Further complex analyses required to exclude clumped cells[290] were not possible with the available flow cytometer. Thus doublets may have been erroneously interpreted during DNA content analysis to be single cell with double the DNA content, which may explain the greater than expected percentage of cells in G2/M phase[309].

The barrier integrity of the Caco-2 cell monolayer in this model is crucial for several reasons. Firstly, a well-formed barrier is an indicator of cell viability, as cells with reduced viability would not be able to form an intact barrier. This barrier is also necessary to limit the amount of oxygen in the apical compartment of co-culture chamber. This is demonstrated by the increased level of DO in the Transwell inserts in the absence of a Caco-2 cell monolayer, compared to when a Caco-2 cell monolayer was present. Further, a properly regulated barrier in the absence of external stimuli, such as bacteria, is a pre-requisite to study the regulation of the barrier by bacteria.

In this study, the barrier integrity was evaluated using several independent measures including TEER and molecule permeability which can indicate several parameters of TJ integrity. TEER, a measure of ion permeability, is altered by the differential expression of claudin isoforms, and expression of claudin-2 is associated with a decline in TEER[310]. Phosphorylation of the TJ protein ZO-1 is also associated with a reduced TEER[66]. Conversely, paracellular permeability (as measured using the mannitol bioassay), seems to be determined by occludin[53]. Expression of occludin is associated with an increase in molecule permeability while at the same time increasing TEER, thus suggesting that distinct molecular mechanisms exist for the two processes[53]. Changes in TJ permeability may also reflect structural changes in the cell cytoskeleton and perijunctional actomyosin ring, also important in maintaining intestinal barrier integrity[311]. Hypoxia has been shown to lead to a loss of epithelial barrier function[283,284], including increased epithelial permeability and decreased TEER in Caco-2 cells[285]. As neither TEER nor molecule permeability assays showed a difference between monolayers in the co-culture chamber inside the anaerobic workstation or 5% CO_2 incubator, it could be inferred that the TJ structure was preserved in the apical anaerobic model. Hypoxia induced loss of intestinal barrier integrity is thought to be, at least partially, due to depletion of cellular ATP[312]. The maintenance of barrier integrity in cells grown in the apical anaerobic model is consistent with this theory as these cells did not show a loss of cell viability as measured by the neutral red uptake assay.

Confocal microscopy was used to further analyse the abundance and localisation of occludin and ZO-1. The TJ staining in the confocal images appeared visually different for cells grown in the anaerobic workstation in a cell culture plate compared to all other treatment groups. Various analyses were carried out in an effort to quantitatively express these differences. These analyses showed differences between all

treatment groups in the peak florescence intensity and the distance over which the intensity drops. However, these differences were not apparent by visual examination of the confocal images. Further, based on other measures of barrier integrity carried out in the studies described in this chapter, it is unlikely these differences are associated with a loss of barrier function. The main reason for the observed difference in the cells grown in a completely anaerobic environment is seemingly due to a larger number of cells with occludin staining within the cell cytoplasm compared to all other treatment groups. This observed cytoplasmic staining may indicate internalisation of occludin protein. Internalisation of occludin and other TJ proteins have been observed following exposure of epithelial monolayers to chemical and pathophysiological stimuli both *in vivo*[313,314] and *in vitro*[315,316], and have been associated with a loss of barrier function[35,313,314,315,316].

The Caco-2 cells in this model remained viable and maintained an intact and well-formed barrier when exposed to an anaerobic environment on the apical side. This demonstrates the model is suitable for co-culture with obligate anaerobic bacteria and is arguably more representative of the physiological conditions in the intestinal tract than traditional models in a completely aerobic environment. This improved model also offers the advantages of simplicity, and automated measurements of epithelial barrier integrity, and as such is suitable for the study of regulation of barrier integrity.

Chapter 4:

Global gene expression analysis of Caco-2 cells cultured in an anaerobic apical environment

4.1 INTRODUCTION

The distal segments of the human intestinal tract are largely anaerobic, especially the colon, where bacterial counts reach 10^{11}-10^{12} per mL, and the obligate anaerobes outnumber the aerobes and facultative anaerobes by a factor of 1000[1,19]. Thus, the intestinal epithelium is exposed to an anaerobic environment on the apical (or luminal) side. These cells, however, receive oxygen from the underlying capillary bed, which drains into the portal vein[294,300] (Figure 4.1).

The Caco-2 cell line seeded on microporous membranes is a well characterised model of the intestinal epithelium[243]. These characteristics include a small intestine enterocyte like phenotype with a microvilli brush border, the formation of TJ between adjacent cells, and expression of small intestinal hydrolase activities[228,242,243]. Caco-2 cells are also known to express many intestinal transporters, such as the H+/di-tripeptide transporter (PEPT1)[317] and Na+ dependent bile acid transporter (ASBT)[318], metabolic enzymes such as cytochrome P450 1A (CYP1A)[319], and sulphotransferases (SULTs)[320], and nuclear receptors such as peroxisome proliferator-activated receptor (PPAR)α and PPARγ[321]. Environmental factors (e.g. exposure to cytokines) however can alter the activity and expression of the transporters and enzymes. For example, the treatment of Caco-2 cells with the synthetic PPARα ligand WY-14643 resulted in enhanced PEPT1 mRNA expression and increased PEPT1-mediated uptake of glycylsarcosine[322]. Furthermore, cell culture related factors, such as passage number and time of culture, can also influence characteristics of the Caco-2 cells[269].

Caco-2 cells are usually cultured under standard cell culture conditions, in air containing 5-10% CO_2, rather than in an anaerobic environment on the apical side as observed *in vivo*. Therefore it could be inferred that Caco-2 cells grown in the apical anaerobic model would have several altered biological and functional characteristics compared with those cultured under standard conditions. For example, cancer cells in the intestine, which due to the tumour environment do not receive sufficient oxygen, have been shown to metabolise glucose through a glycolytic pathway, rather than though the mitochondrial dependent pathway used by intestinal cells that receive a sufficient amount of oxygen[323]. Further, hypoxia has been shown to induce the transcription and translation of TLR2 and TLR6 in Caco-2 and other cell lines[324].

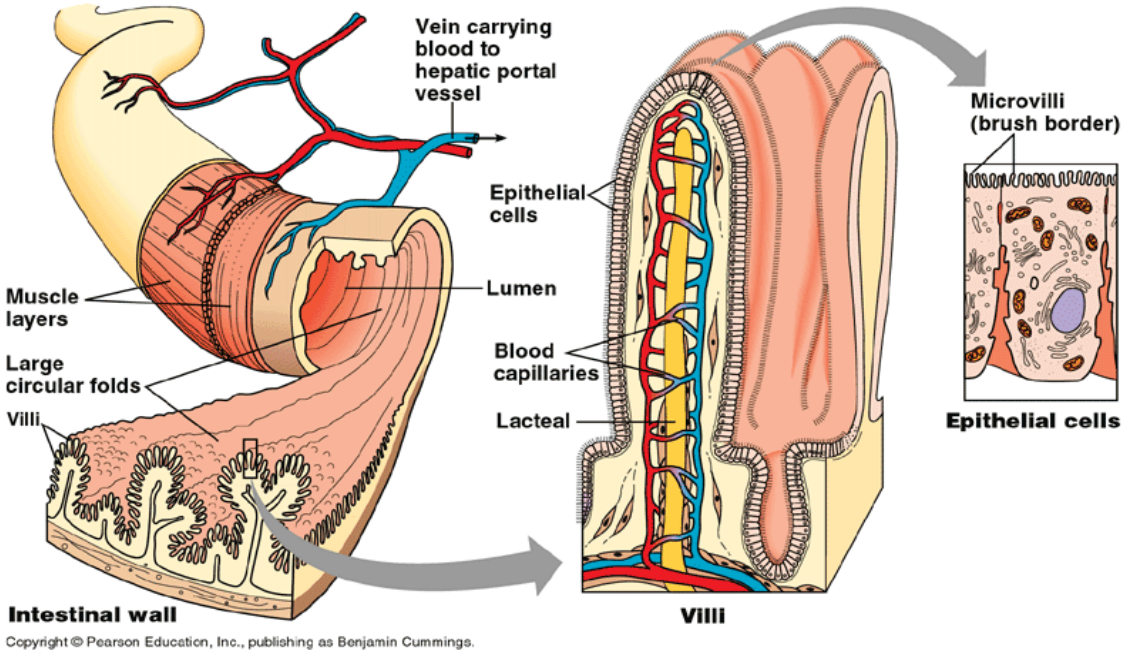

Figure 4.1 Intestinal epithelial cells receive oxygen from the underlying capillary bed.

The figure depicts a three-dimensional view of the small intestine villi. The underlying blood capillaries provide the oxygen to the epithelial cells, and drain into the hepatic portal vein. Figure: the Kennesaw State University website[325].

It is important to identify regulatory differences between Caco-2 cells cultured under conventional and apical anaerobic conditions, as these differences could influence host-bacteria interactions. For example, alteration of TLR expression could influence the recognition of bacteria by epithelial cells in the apical anaerobic model, and in turn alter the epithelial cell response.

4.2 HYPOTHESIS AND AIM

The hypothesis of the research presented in this chapter was that Caco-2 cells in the apical anaerobic model are functionally different to Caco-2 cells cultured under standard cell culture conditions. The aim of this chapter was to identify putative biological and functional differences between Caco-2 cells cultured for 12 hours under apical anaerobic conditions and those cultured under conventional conditions using global gene expression analysis.

4.3 METHODS

4.3.1 Overview

Microarray technology is a tool for monitoring the genome-wide expression levels of genes in a given organism. Microarrays consist of thousands of oligonucleotide probe sequences, each corresponding to a gene, usually fixed on to a glass slide at specific locations called spots[326]. To compare expression of genes from Caco-2 cells exposed to the apical anaerobic conditions (condition B), with that of Caco-2 cells maintained under conventional conditions (condition A), RNA was extracted from the cells, reverse transcribed into cDNA, which was used to synthesise cRNA that was labelled with different fluorescent dyes (cyanine-5 or cyanine-3), and hybridised onto a microarray. The microarray slides were then scanned to detect the fluorescence of each spot, which corresponds to the proportion of bound cyanine-5 and cyanine-3 labelled RNA, thus indicating the relative expression level of that gene. Following quality control, and normalisation, differentially expressed genes are identified and the data analysed using pathway analysis software. The microarray workflow is depicted in Figure 4.2.

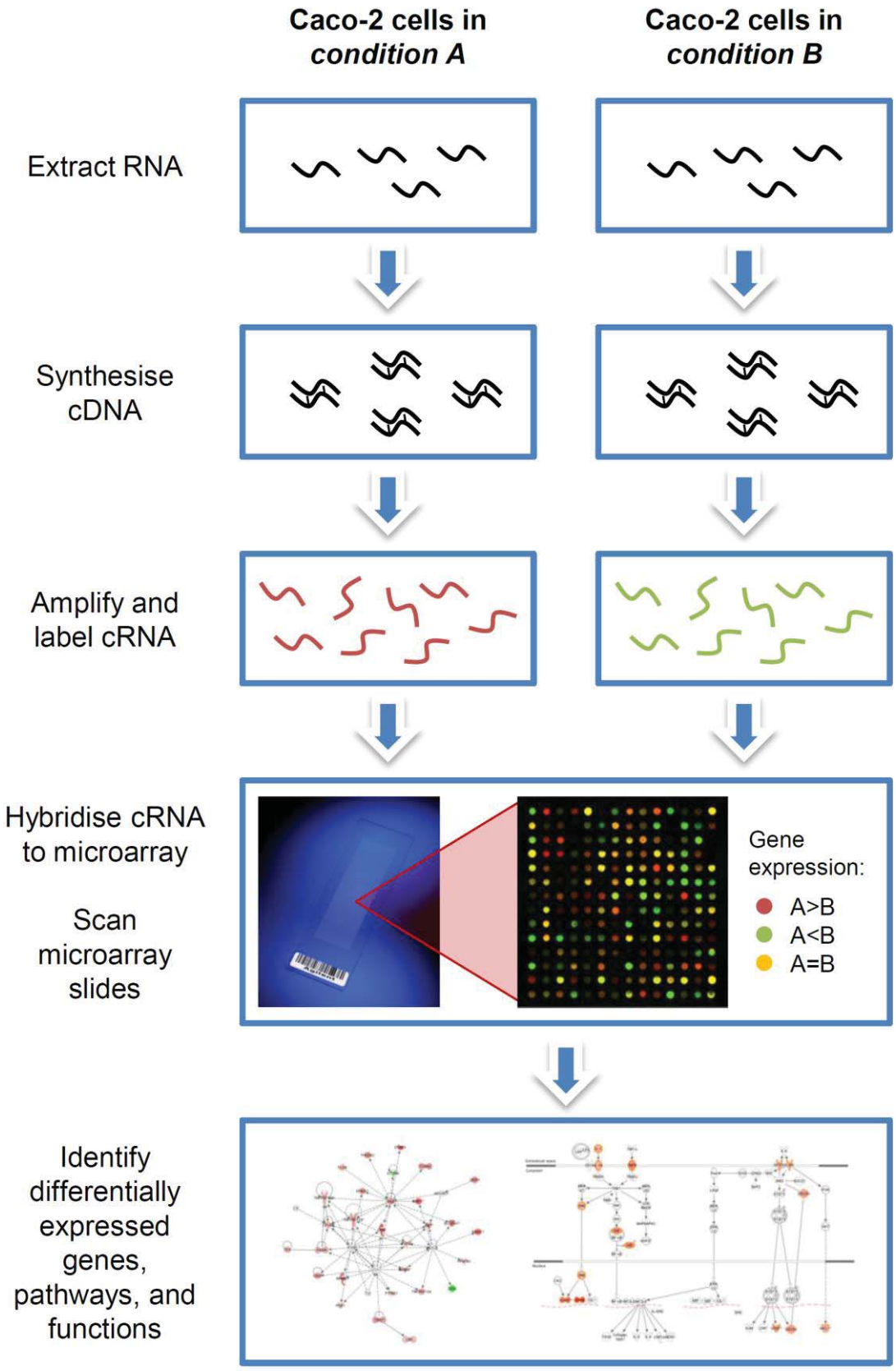

Figure 4.2 Microarray analysis workflow.

The figure depicts the main steps involved in identifying differences in gene expression between Caco-2 cells cultured under different conditions.

4.3.2 Cell culture

Fourteen-day-old Caco-2 cell monolayers (refer to section 3.3.1.1) were transferred into a co-culture chamber as described under section 3.3.1.2. The co-culture chamber was placed inside an anaerobic workstation, thereby exposing the cells to an anaerobic environment (section 3.3.1.3; condition B), or inside a 5% CO_2 incubator (section 3.3.1.4; condition A) for 12 hours (n = 6 per treatment).

4.3.3 RNA isolation

At the end of the incubation period, RNAprotect Cell Reagent (Qiagen, Valencia, California, USA) was added at a volume of approximately 9 times the apical medium to lyse the Caco-2 cells and stabilise the RNA. The cell suspension in the RNAprotect reagent was centrifuged (500 x g for 5 minutes) and the supernatant discarded. The cell pellet was resuspended in buffer RLT (Qiagen) containing 1 µL/mL of β-mercaptoethanol, and homogenised using a homogeniser with a 5 mm probe (Omni International, Kennesaw, Georgia, USA). Total RNA was extracted from the homogenised cell lysate using RNeasy mini kit (Qiagen) as per the manufacturer's protocol.

The RNA quantity and purity were determined using a NanoDrop (ND-1000 UV-Vis Spectrophotometer, Thermo Fisher Scientific) to ensure the 260/230 and 260/280 ratios were above 1.6 and 1.8 respectively. Samples which did not meet these criteria were cleaned up using the RNeasy mini kit (Qiagen) as per the manufacturer's 'RNA cleanup' protocol. The RNA quality of the samples was further assessed using an RNA 6000 NanoLabChip kit with the Agilent 2100 Bioanalyzer (Agilent Technologies, Santa Clara, California, USA), to ensure the samples had an RNA integrity number above 8.0 prior to downstream analysis.

4.3.4 Microarray experimental design

A loop design was used for the microarray experiment, which involved hybridising a sample labelled from one treatment group with cyanine-3, with an experiment sample from the other treatment group labelled with cyanine-5. To account for dye bias, three samples (randomly chosen) from each treatment group were labelled with cyanine-3, while the other three samples were labelled with cyanine-5. The slide and array

positions of cyanine-3 and cyanine-5 labelled samples were systematically chosen such that (i) each slide received two cyanine-3 labelled, and two cyanine-5 labelled samples from each treatment group, and (ii) samples from the same treatment group on the two outside arrays (array 1 and 4) of each slide were labelled with different dyes, to ensure no bias was introduced based on array or slide position (Table 4.1).

4.3.5 Global gene expression analysis

The RNA samples were amplified and labelled with either cyanine-3 or cyanine-5 labelled CTP dye using the Agilent Quick-Amp Labelling Kit (Agilent Technologies), and hybridized onto 44k whole human genome oligonucleotide arrays (Agilent Technologies) according to the manufacturer's instructions (Two-Color Microarray-Based Gene Expression Analysis (Quick Amp Labelling), Version 5.7, March 2008, Agilent Technologies). The microarray slides were scanned using a DNA Microarray Scanner G2565CA (Agilent Technologies) according to the manufacturer's instructions.

Array images (TIFF files) were uploaded to Agilent Feature Extraction software, which generated numerical intensity data for each probe, as well as a quality control report for each array. Differentially expressed genes were calculated using an Empirical Bayes modified T-statistic generated using the limma package[327] in R[††]. Genes that exhibited a $\log_2$ fold change > 1.25 (representing a fold change of 2.4x) and a false discovery rate (q) < 0.05 were considered to be differentially expressed.

4.3.6 Validation of microarray results by qPCR

The expression of six genes, shown by microarray analysis to be differentially expressed (target genes), was quantified using quantitative real-time polymerase chain reaction (qPCR). The genes selected for analysis, as well as the reference genes used, are shown on Table 4.2. The selected reference genes were chosen because they were shown to be expressed in all samples, and had minimal variation in expression levels across treatments according to microarray analysis.

[††] Microarray quality control analysis and generation of differentially expressed gene list was performed by Dr Wayne Young (AgResearch Grasslands).

Table 4.1 Microarray design

Slide and array positions of cyanine-3 and cyanine-5 labelled samples. A, Caco-2 cells in co-culture chamber in 5% CO_2; B, Caco-2 cells in co-culture chamber in anaerobic workstation. Samples loaded on to array 3 and 4 of slide 2 (duplicate samples) were not used for further downstream analysis.

Slide	*Array*	*Cyanine-3 labelled sample*	*Cyanine-5 labelled sample*
1	1	A3	B3
	2	B6	A5
	3	A1	B2
	4	B4	A6
2	1	B5	A4
	2	A2	B1
	3	B5	A4
	4	A3	B3

Table 4.2 Genes selected for qPCR analysis.

Genes selected for validation of microarray study by qPCR. Target genes were selected to include those that showed significant differential expression between treatments by microarray analysis. Reference genes were expressed in all samples, and the variation in expression levels across treatments was low and non-significant according to microarray analysis. Reactions were carried out using pre-designed and pre-validated PrimeTime primer/probe mixes indicated in the 'IDT assay' column.

Type	*Gene*	*Gene symbol*	*Transcript location*	*IDT assay*
Target gene	chemokine (C-X-C motif) receptor 4	*CXCR4*	NM_001008540	Hs.PT.56a. 27595676.g
	ankyrin repeat domain 1 (cardiac muscle)	*ANKRD1*	NM_014391	Hs.PT.56a. 20590239
	FBJ murine osteosarcoma viral oncogene homolog	*FOS*	NM_005252	Hs.PT.56a. 15540029
	zinc finger protein 226	*ZNF226*	NM_001032372	Hs.PT.56a. 2529721
	family with sequence similarity 101, member B	*FAM101B*	NM_182705	Hs.PT.56a. 38699899.g
	G0/G1switch 2	*G0S2*	NM_015714	Hs.PT.56a. 4027877.g
Reference gene	ribosomal protein S2	*RPS2*	NM_002952	Hs.PT.56a. 22843181
	ribosomal protein L23	*RPL23*	NM_000978	Hs.PT.56a. 14647700

For qPCR analysis, 500 ng of total RNA was reverse transcribed into cDNA using a High Capacity RNA-to-cDNA Kit (Applied Biosystems, Foster City, California, USA) as per to manufacturer's instructions. The reactions were incubated in a Mastercycler pro S thermal cycler (Eppendorf, North Ryde, New South Wales, Australia), and the cDNA was stored at -20°C prior to the determination of the expression levels of each gene. Expression levels of each gene were determined using pre-designed and pre-validated primer/probe mixes (PrimeTime qPCR Assays, 20x; Integrated DNA Technologies (IDT), Coralville, Iowa, USA; Table 4.2) and a Kapa Probe Fast qPCR kit (Kapa Biosystems, Woburn, Massachusetts, USA) on a Rotor-Gene 6000 real-time thermal cycler (Corbett Life Science, Concord, New South Wales, Australia).

All qPCR analyses (no-template controls and samples) were prepared as triplicate 10 μL reactions comprising a 9.0 μL aliquot of master mix (5.0 μL of Kapa Probe Fast Universal 2x qPCR Master Mix, 0.5 μL of PrimeTime qPCR assay for the gene of interest, 3.5 μL of nuclease-free water), and 1 μL of cDNA (at a 1 in 10 dilution in nuclease-free water). The thermal profile used was an initial enzyme activation step (95°C, 3 minutes) followed by 40 cycles of denaturation (95°C, 3 seconds) and annealing/extension/acquisition (60°C, 30 seconds). The data were normalised to the reference genes and analysed for expression level changes using Relative Expression Software Tool (REST) software (version 2.0.13; Qiagen). Correlation between microarray and qPCR results was tested by Spearman rho correlation analysis in R.

4.3.7 Ingenuity pathway and functional analysis

Differentially expressed genes were clustered into functional groups and pathways using Ingenuity Pathway Analysis (IPA; version 7.1; Ingenuity Systems Inc., Redwood City, California, USA; www.ingenuity.com.). IPA is a bioinformatics tool which correlates genes with biological functions, pathways and networks in the Ingenuity Knowledge Base, a repository of biological interactions and functional annotations curated from the literature. The dataset containing the list of differentially expressed gene identifiers and corresponding expression values was uploaded into IPA, and each identifier was mapped to its corresponding object in the Ingenuity Knowledge Base.

Genes were overlaid onto a global molecular network developed from information contained in the Ingenuity Knowledge Base, and networks were algorithmically generated based on their connectivity. The networks were assigned a score based on a hypergeometric test, representing the degree of relevance to the genes in the dataset.

The IPA functional analysis was used to identify biological functions that were most significantly over-represented among genes in the dataset. Differentially expressed genes associated with biological functions in the Ingenuity Knowledge Base were considered for the analysis. Right-tailed Fisher's exact test was used to calculate a P-value determining the probability that each biological function assigned to that dataset is due to chance alone.

The IPA canonical pathway analysis identified pathways in the IPA library that were most significantly over-represented among the list of differentially expressed genes. A P-value was calculated using the Fischer's exact test determining the probability that the association between the genes in the dataset the canonical pathway is explained by chance alone.

The IPA transcription factor analysis identified transcription factors that can explain observed gene expression changes. Given the observed differential expression of a gene (increased or decreased), a Z-score was used to predict the activation state of upstream transcription factors by the regulation direction (activating or inhibiting) associated with the relationship from the transcription factor to the gene.

4.3.8 Gene ontology analysis‡‡

The GOstats package[328] in R was used to identify biological processes from the Gene Ontology (GO) Consortium database over-represented in the differentially expressed genes list. The analysis used a hypergeometric test where biological processes were considered over-represented if genes within the dataset were associated with a biological process in greater proportion than would be expected through chance alone.

‡‡ Gene ontology analysis was carried out by Dr Wayne Young (AgResearch Grasslands).

4.3.9 Generation of heatmaps[§§]

Heatmaps were generated using the heatmap.2 command in R. A false colour heatmap of gene expression was created by hierarchical clustering of log-transformed microarray signal intensities for the genes showing the top 2% coefficient of variation across all samples.

The Kyoto Encyclopaedia of Genes and Genomes (KEGG) database is a knowledge base that maps genes and gene products to biological pathways of cellular processes such as metabolic processes and signal transduction cascades drawn from the published literature[329]. A heatmap of the expression of genes within KEGG pathways was created by hierarchical clustering of the mean signal intensity of the genes within each pathway, for the KEGG pathways showing the top 25% coefficient variation across all samples.

4.4 RESULTS

4.4.1 Differentially expressed genes

Global gene expression analysis was used to identify key differences in gene expression between Caco-2 cells cultured in the apical anaerobic model and those cultured under standard conditions for 12 hours. The expression levels of 1803 genes were altered ($q < 0.05$); 1159 genes had increased expression, and 644 genes had decreased expression in the apical anaerobic model. Figure 4.3 shows a heatmap of the microarray signal intensity levels for the genes showing the top 2% of variation across samples, which illustrates that the gene expression profiles across samples clustered by treatment group.

The qPCR results confirmed the direction of fold change for the six genes measured, and the P-values showed a significant fold change ($P < 0.05$) for all genes measured, except *FAM101B* which showed a trend towards significance ($P < 0.10$) (Table 4.3). Furthermore, fold change between microarray and qPCR results for the six genes showed a significant correlation (Spearman rho = 0.77) supporting the validity of the microarray results.

[§§] Heatmaps were generated by Dr Wayne Young (AgResearch Grasslands).

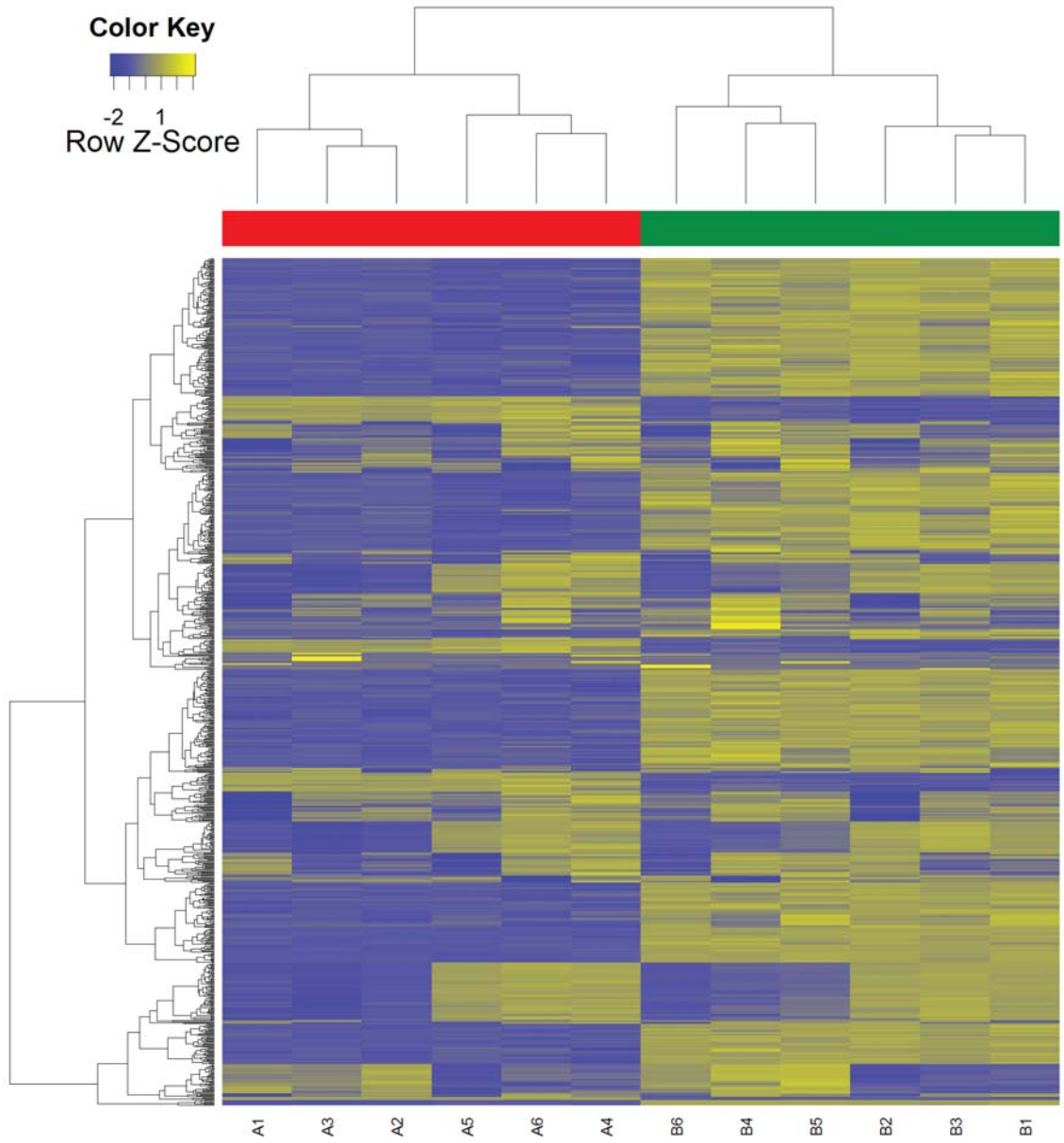

Figure 4.3 Heatmap of gene expression levels in Caco-2 cells cultured in the apical anaerobic environment or the co-culture chamber in a 5% CO_2 incubator.

Heatmap showing the expression levels of genes showing the top 2% variation across samples. Individual genes are represented by rows with samples in columns (A, Caco-2 cells in co-culture chamber in 5% CO_2; B, Caco-2 cells in co-culture chamber in anaerobic workstation). Heatmap colours indicates probe signal intensities, expressed as a standardised score with a mean of zero and standard deviation of one, with blue indicating a scaled value less than zero (decreased expression) and yellow indicating a scaled value greater than zero (increased expression). Dendrograms show clustering of samples and genes based on similarity of gene expression profiles between samples (columns), and similarity of expression for each gene across samples (rows). Colour blocks above the heatmap represent the treatment groups (red, Caco-2 cells in co-culture chamber in 5% CO_2; green, Caco-2 cells in co-culture chamber in anaerobic workstation).

Table 4.3 Validation of microarray results by qPCR.

Gene expression fold change and P-value (for qPCR data) or *q* (for microarray data) for the six genes validated using qPCR analysis. Fold change value indicates fold difference in expression between treatments; a positive value indicates higher expression level in Caco-2 cells grown in the apical anaerobic environment (compared to Caco-2 cells in the co-culture chamber in a 5% CO_2 incubator), and a negative value indicates a lower expression level.

Gene	*qPCR*		*Microarray*	
	Fold change	*P-value*	*Fold change*	q
CXCR4	3.07	<0.001	36.58	<0.001
ANKRD1	6.86	<0.001	25.69	<0.001
FOS	6.74	<0.001	14.12	<0.001
ZFN226	-4.46	0.001	-3.82	<0.001
FAM101B	-1.52	0.094	-5.21	<0.001
G0S2	-4.81	0.001	-5.42	<0.001

4.4.2 Biological functions associated with differentially expressed genes

A log fold change cut-off of 1.25 (fold change approximately 2.38) was applied to reduce the number of differentially expressed genes to approximately 1000 (691 genes had increased expression and 239 genes had decreased expression), and the data were analysed using IPA.

The IPA functional analysis identified the biological functions that were most significantly over-represented among the list of differentially expressed genes. Based on the expression direction of the differentially expressed genes, 31 biological functions (grouped into 20 IPA categories) were predicted to be induced (Table 4.4), while three biological functions (grouped into three IPA categories) were predicted to be suppressed (Table 4.5) in Caco-2 cells cultured in the apical anaerobic model compared to those cultured in standard conditions for 12 hours.

The most significantly modulated functions included 'cell survival', where 65 of the 99 genes involved had an expression direction consistent with cell survival. The functions 'proliferation of cells', 'cell cycle progression' and 'mitosis' were also predicted to be induced. The 'G2 phase' and 'G2/M phase' functions were predicted to be suppressed, which together with the induced 'cell cycle progression' function, was consistent with a shortening of the G2/M phase and thus faster cell renewal. Furthermore, the function 'cell death of epithelial cells' was not significantly modulated.

Gene expression was also consistent with induced 'development of blood vessels', 'accumulation of blood cells' and 'cell movement' functions, which are potential mechanisms for obtaining more oxygen. Functional analysis also indicated an increase in 'accumulation of leukocytes' functions in the apical anaerobic model compared to Caco-2 cells cultured in standard conditions, implicating immune cell trafficking and local inflammatory responses.

Hypergeometric testing using the GO stats package[328] identified 808 GO biological processes significantly over-represented among the list of differentially expressed genes, the top 50 of which are shown on Table 4.6. Many GO biological

Table 4.4 Key IPA biological functions predicted to be induced in Caco-2 cells in the apical anaerobic environment (compared to Caco-2 cells in the co-culture chamber in a 5% CO_2 incubator).

The P-value was calculated using the right-tailed Fisher Exact Test by considering the number of differentially expressed genes that participate in the function, and the total number of genes that are known to be associated with that function in the Ingenuity Knowledge Base. Given the observed differential regulation of a gene (up or down), the Z-score was used to determine the activation state of the biological function by the direction of effect associated with the relationship from the gene to the function. An absolute Z-score of ≥ 2 was considered significant (function activated if Z-score ≥ 2; inhibited if Z-score ≤ -2). 'Genes' indicates the number of differentially expressed genes associated with the function. *denotes functions that appear in more than one category.

Category	*Function*	*P-value*	*Z-score*	*Genes*
Cell Death	apoptosis of kidney cell lines	1.11E-04	2.284	21
	cell survival	5.47E-11	2.606	99
Cancer	cancer	5.48E-19	2.902	262
	metastasis	2.66E-07	2.937	46
	metastasis of tumour	2.47E-04	2.226	13
	neoplasia	3.45E-18	2.97	264
	non-Hodgkin's disease*	2.34E-07	2.364	33
Cellular Growth and Proliferation	proliferation of tumour cell lines	3.79E-07	2.124	70
	proliferation of tumour cells*	7.36E-04	2.011	20
Cellular Development	differentiation of osteoclasts*	2.70E-06	2.095	20
Haematological System Development and Function	accumulation of blood cells*	1.10E-05	2.142	25
	accumulation of leukocytes*	1.28E-04	2.391	22
	accumulation of mononuclear leukocytes*	7.34E-04	2.457	12
Cellular Movement	cell movement	3.74E-10	2.02	137
	cell movement of tumour cell lines	7.82E-06	2.355	51
	invasion of cells	1.31E-09	2.63	61
	invasion of tumour cell lines	6.19E-07	2.355	42
	migration of tumour cell lines	2.62E-05	2.35	40
Tissue Development	accumulation of blood cells*	1.10E-05	2.142	25
	accumulation of cells	7.35E-05	2.656	28
	accumulation of leukocytes*	1.28E-04	2.391	22

Category	*Function*	*P-value*	*Z-score*	*Genes*
	accumulation of mononuclear leukocytes*	7.34E-04	2.457	12
	adhesion of tumour cell lines*	3.12E-04	2.135	22
	differentiation of osteoclasts*	2.70E-06	2.095	20
Cell Cycle	cell cycle progression	1.94E-09	2.587	88
	mitogenesis	1.33E-04	2.545	18
	mitosis	3.18E-04	2.325	35
Organismal Development	development of blood vessel*	1.05E-08	2.452	64
	vasculogenesis*	1.55E-07	2.635	55
Connective Tissue Development and Function	differentiation of osteoclasts*	2.70E-06	2.095	20
Cardiovascular System Development and Function	angiogenesis	2.47E-05	2.768	47
	development of blood vessel*	1.05E-08	2.452	64
	vasculogenesis*	1.55E-07	2.635	55
Skeletal and Muscular System Development and Function	differentiation of osteoclasts*	2.70E-06	2.095	20
Cellular Function and Maintenance	autophagy of cells*	1.12E-03	2.562	17
	cellular homeostasis	2.14E-05	2.169	90
Inflammatory Response	accumulation of leukocytes*	1.28E-04	2.391	22
	accumulation of mononuclear leukocytes*	7.34E-04	2.457	12
Lymphoid Tissue Structure and Development	development of lymphatic system component	1.39E-04	2.072	30
Cell Morphology	autophagy of cells*	1.12E-03	2.562	17
Hematological Disease	non-Hodgkin's disease*	2.34E-07	2.364	33
Immune Cell Trafficking	accumulation of leukocytes*	1.28E-04	2.391	22
	accumulation of mononuclear leukocytes*	7.34E-04	2.457	12
Cell-To-Cell Signaling and Interaction	adhesion of tumor cell lines*	3.12E-04	2.135	22
Tumor Morphology	proliferation of tumor cells*	7.36E-04	2.011	20

Table 4.5 Key IPA biological functions predicted to be supressed in Caco-2 cells in the apical anaerobic environment (compared to Caco-2 cells in the co-culture chamber in a 5% CO_2 incubator).

The P-value was calculated using the right-tailed Fisher Exact Test by considering the number of differentially expressed genes that participate in the function, and the total number of genes that are known to be associated with that function in the Ingenuity Knowledge Base. Given the observed differential regulation of a gene (up or down), the Z-score was used to determine the activation state of the biological function by the direction of effect associated with the relationship from the gene to the function. An absolute Z-score of ≥ 2 was considered significant (function activated if Z-score ≥ 2; inhibited if Z-score ≤ -2). 'Genes' indicated the number of differentially expressed genes associated with the function.

Category	*Function*	*P-Value*	*Z-score*	*Genes*
Cell Death	cell death of skin	1.01E-03	-2.056	10
Cancer	G2 phase	6.94E-05	-2.451	23
	G2/M phase	2.86E-04	-2.991	18

Table 4.6 Gene ontology biological processes over-represented in differentially expressed genes from Caco-2 cells cultured in an apical anaerobic environment for 12 hours (compared to Caco-2 cells in the co-culture chamber in a 5% CO_2 incubator).

The 50 most significantly over-represented biological processes are shown. 'P-value' indicates significance of over-representation. 'Exp Count' indicates the expected number of differentially expressed genes associated with the biological process through chance alone, while 'Count' indicates the actual number of expressed genes. 'Size' indicates the total number of genes in the genome associated with the biological process

GO ID	*Term*	*P-value*	*Exp Count*	*Count*	*Size*
GO:0044237	cellular metabolic process	<0.001	513	625	7431
GO:0008152	metabolic process	<0.001	582	687	8439
GO:0009987	cellular process	<0.001	802	875	11620
GO:0006915	apoptosis	<0.001	78	136	1133
GO:0012501	programmed cell death	<0.001	79	136	1141
GO:0044260	cellular macromolecule metabolic process	<0.001	393	487	5699
GO:0008219	cell death	<0.001	86	144	1250
GO:0016265	death	<0.001	86	144	1253
GO:0044238	primary metabolic process	<0.001	526	615	7629
GO:0051716	cellular response to stimulus	<0.001	76	124	1102
GO:0042221	response to chemical stimulus	<0.001	105	159	1516
GO:0042981	regulation of apoptosis	<0.001	61	105	889
GO:0010941	regulation of cell death	<0.001	62	106	904
GO:0043067	regulation of programmed cell death	<0.001	62	105	897
GO:0043170	macromolecule metabolic process	<0.001	433	514	6274
GO:0010033	response to organic substance	<0.001	62	105	903
GO:0008283	cell proliferation	<0.001	81	128	1168
GO:0048523	negative regulation of cellular process	<0.001	131	188	1895
GO:0034641	cellular nitrogen compound metabolic process	<0.001	316	391	4584
GO:0033554	cellular response to stress	<0.001	48	85	698
GO:0006807	nitrogen compound metabolic process	<0.001	324	398	4698

GO ID	*Term*	*P-value*	*Exp Count*	*Count*	*Size*
GO:0050794	regulation of cellular process	<0.001	430	506	6236
GO:0051098	regulation of binding	<0.001	15	36	211
GO:0048522	positive regulation of cellular process	<0.001	141	196	2042
GO:0031325	positive regulation of cellular metabolic process	<0.001	69	110	999
GO:0042127	regulation of cell proliferation	<0.001	59	97	852
GO:0009893	positive regulation of metabolic process	<0.001	73	114	1052
GO:0043687	post-translational protein modification	<0.001	104	152	1509
GO:0048008	platelet-derived growth factor receptor signaling pathway	<0.001	2	10	22
GO:0006793	phosphorus metabolic process	<0.001	90	135	1308
GO:0006796	phosphate metabolic process	<0.001	90	135	1308
GO:0048519	negative regulation of biological process	<0.001	142	196	2064
GO:0043066	negative regulation of apoptosis	<0.001	28	55	404
GO:0060548	negative regulation of cell death	<0.001	29	56	415
GO:0090304	nucleic acid metabolic process	<0.001	257	322	3724
GO:0043069	negative regulation of programmed cell death	<0.001	28	55	409
GO:0042326	negative regulation of phosphorylation	<0.001	4	16	59
GO:0009891	positive regulation of biosynthetic process	<0.001	52	87	759
GO:0019222	regulation of metabolic process	<0.001	280	345	4060
GO:0048518	positive regulation of biological process	<0.001	155	208	2243
GO:0006916	anti-apoptosis	<0.001	16	37	236
GO:0006950	response to stress	<0.001	131	181	1905
GO:0050789	regulation of biological process	<0.001	454	523	6579
GO:0051101	regulation of DNA binding	<0.001	11	29	166
GO:0009892	negative regulation of metabolic process	<0.001	61	97	889

GO ID	*Term*	*P-value*	*Exp Count*	*Count*	*Size*
GO:0010629	negative regulation of gene expression	<0.001	40	69	573
GO:0006139	nucleobase, nucleoside, nucleotide and nucleic acid metabolic process	<0.001	296	360	4294
GO:0010563	negative regulation of phosphorus metabolic process	<0.001	4	16	63
GO:0045936	negative regulation of phosphate metabolic process	<0.001	4	16	63
GO:0006464	protein modification process	<0.001	122	169	1768

processes share similarities with the IPA biological functions, such as ‘cell death’ and ‘cell proliferation’, and ‘cellular processes’ (Table 4.6), which include ‘cell adhesion’, ‘cell communication’, ‘cell cycle’, and ‘cell junction organisation’. GO processes shared with IPA biological functions (not shown in Table 4.6) include ‘blood vessel development’ and ‘immune response-’ related functions. Other GO processes included ‘response to stress’, and ‘metabolic process’, which include ‘cellular metabolic process’ and ‘nitrogen compound metabolic process’.

4.4.3 Biological interaction networks associated with differentially expressed genes

Differentially expressed genes were examined for networks of biological interaction relationships using IPA. Twenty five networks were identified; of these the network with the highest ranked score is shown in Figure 4.4. The genes in this biological network were associated with the IPA biological functions ‘Cancer’, ‘Cellular Development’ and ‘Cellular Growth and Proliferation’. As shown in Figure 4.4, the up-regulated vascular endothelial growth factor *(Vegf)* gene is an important node in the interaction network. Other important nodes in the network included the glycoprotein hormones follicle stimulating hormone *(FSH)*, luteinising hormone *(Lh)* and choriogonadotropin *(hCGΔ)*, which were not differentially expressed.

4.4.4 KEGG pathway clustering

Hierarchical clustering of KEGG pathways showed that pathway expression profiles were similar between samples of the same treatment group (Figure 4.5). Pathways also grouped into several distinct clusters based on similarity of expression across samples, such as immune system related pathways (cluster that includes ‘NOD-like receptor signalling pathway’ and ‘B cell receptor signalling pathway’), DNA replication and repair pathways (cluster that includes ‘DNA replication’ and ‘mismatch repair’), metabolism (cluster that includes ‘steroid biosynthesis’ and ‘porphyrin and chlorophyll metabolism’) and signal transduction pathways (cluster that includes ‘mTOR signalling pathway’ and ‘VEGF signalling pathway’). KEGG pathways showing the top 25% variation in gene expression across samples were also related to cancer (e.g. ‘bladder cancer’, ‘thyroid cancer’) and cell communication (e.g. ‘tight junctions’, ‘adherens junctions’).

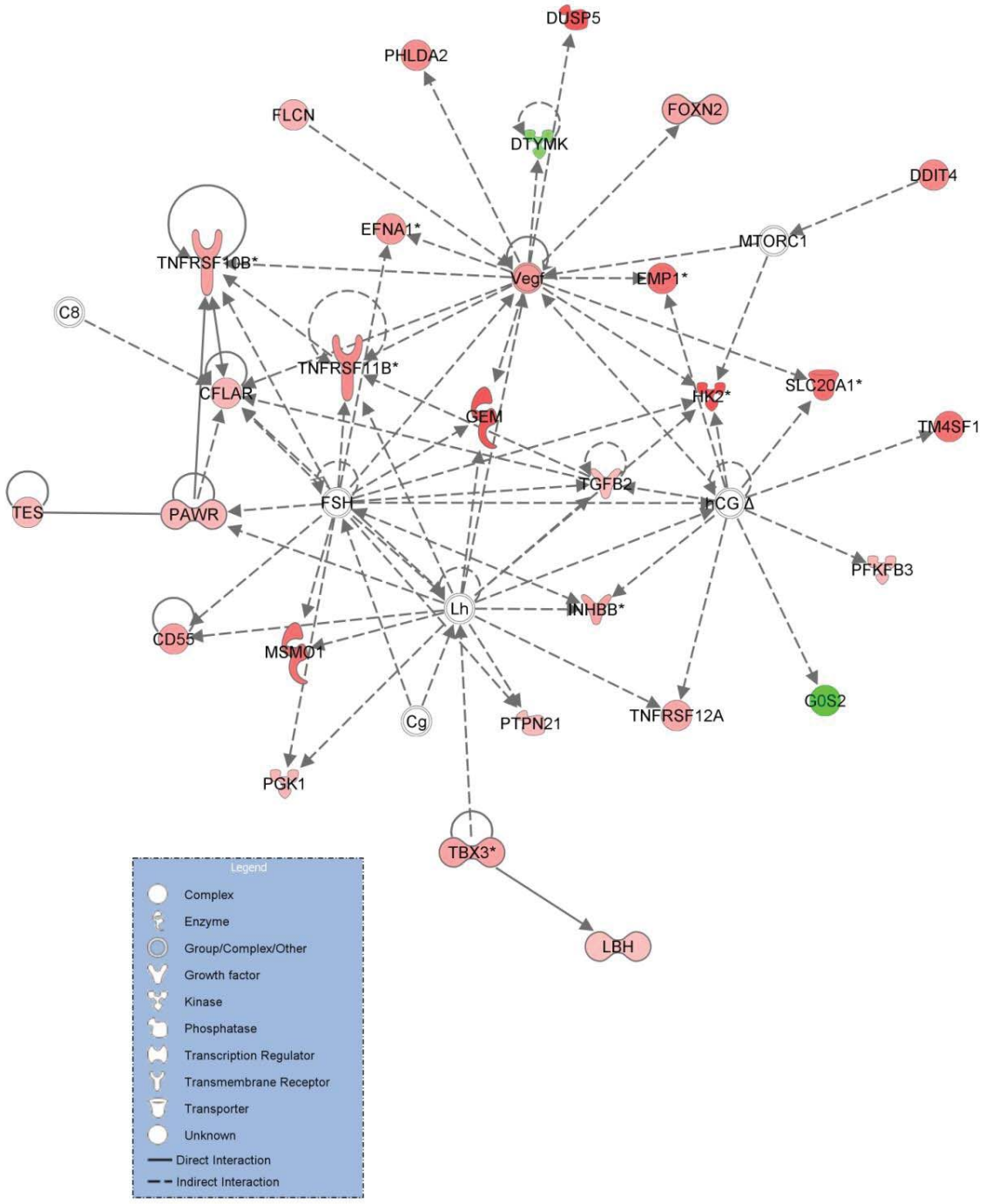

Figure 4.4 Network of differentially expressed genes in Caco-2 cells in the apical anaerobic environment (compared to Caco-2 cells in the co-culture chamber in a 5% CO_2 incubator).

Genes are represented by nodes and interactions represented by edges. Genes with increased expression in Caco-2 cells grown in the apical anaerobic environment (compared to Caco-2 cells in the co-culture chamber in a 5% CO_2 incubator) are depicted in shades of red, genes with decreased expression in shades of green. Intensity of colour indicates degree of fold change, with greater intensity signifying higher expression level. Node shape indicates functional class of gene product as indicated in legend.

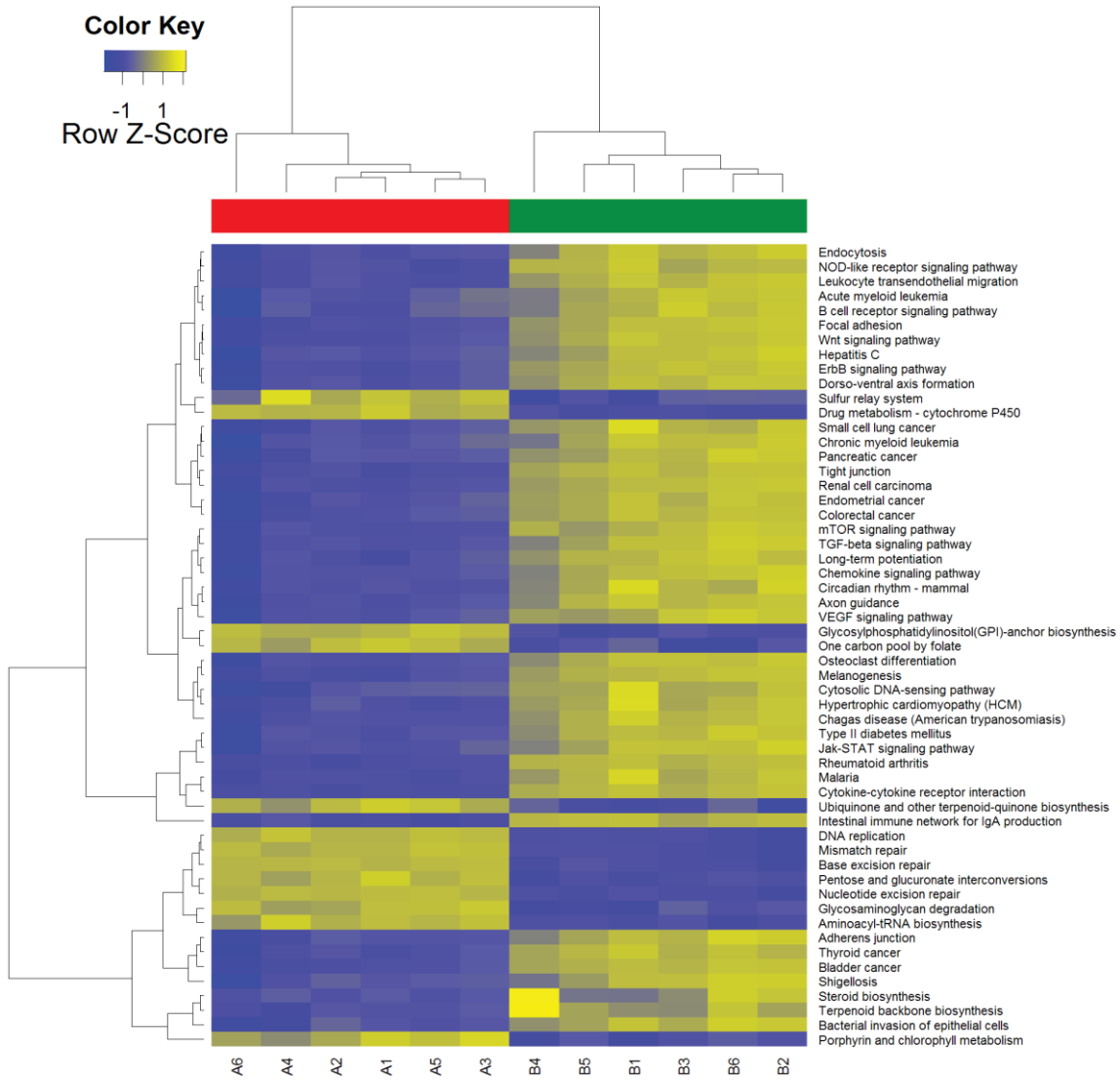

Figure 4.5 KEGG average expression heatmap for Caco-2 cells cultured in the apical anaerobic environment or the co-culture chamber in a 5% CO_2 incubator.

Heatmap showing the mean microarray expression levels of all genes within the listed KEGG pathways. Heatmap colours indicate mean signal intensities for each pathway, expressed as a standardised score with a mean of zero and standard deviation of one, with blue indicating a scaled value less than zero (decreased expression) and yellow indicating a scaled value greater than zero (increased expression). KEGG pathways are represented by rows with samples in columns (A, Caco-2 cells in co-culture chamber in 5% CO_2; B, Caco-2 cells in co-culture chamber in anaerobic workstation). Only the KEGG pathways with the top 25% variation in mean expression across all samples are shown. Dendrograms show clustering of samples and pathways based on similarity of pathway expression profiles between samples (columns), and similarity of expression for each pathway across samples (rows). Colour blocks above the heatmap represent the treatment groups (red, Caco-2 cells in co-culture chamber in 5% CO_2; green, Caco-2 cells in co-culture chamber in anaerobic workstation).

4.4.5 Ingenuity pathway analysis

The IPA canonical pathway analysis identified curated pathways in the IPA library that were most significantly over-represented among genes in the dataset. Table 4.7 lists 54 canonical pathways enriched with differentially expressed genes in Caco-2 cells cultured in the apical anaerobic conditions for 12 hours compared to those cultured in standard conditions, as calculated by IPA ($P < 0.05$).

The most significantly modulated pathway was the NF-E2-Related Factor 2 (NRF2)-mediated stress response pathway, where 20 genes out of the 191 genes which map to the pathway were differentially expressed (Figure 4.6). The observed increased expression of genes in this pathway is consistent with defence against damage caused by oxidative stress and maintenance of cellular redox homeostasis[330].

Also of particular note was the TJ signalling pathway where 12 genes out of the 163 genes which map to the pathway were differentially expressed (Figure 4.7). All of these genes had increased expression in Caco-2 cells grown in the apical anaerobic environment compared to Caco-2 cells in the co-culture chamber in a 5% CO_2 incubator, suggesting a strengthening of TJ integrity in the apical anaerobic model.

Other modulated pathways included tumour necrosis factor receptor (TNFR) signalling where genes coding for the anti-apoptotic protein cellular inhibitor of apoptosis protein (cIAP), and jun proto-oncogene (cJun) and FBJ murine osteosarcoma viral oncogene homolog (cFos), all of which lead to cell survival, had increased expression levels, while expression of genes involved in the apoptotic caspase cascade were unchanged (Figure 4.8). Inflammatory and anti-inflammatory pathways such as IL-6 (Figure 4.9), IL-17A and IL-10 signalling were also enriched with differentially expressed genes. Furthermore, genes encoding for negative regulators of NF-κB signalling, such as A20 and inhibitor of IκB, had increased expression as illustrated in the 'TNFR signalling' and 'death receptor signalling' canonical pathways.

4.4.6 Ingenuity upstream regulator analysis

Based on the changes in gene expression, IPA predicted 6 transcription factors to have increased activity, and 8 transcription factors to have decreased activity in Caco-2 cells

Table 4.7 IPA canonical pathways enriched with differentially expressed genes from Caco-2 cells cultured in an apical anaerobic environment for 12 hours (compared to Caco-2 cells in the co-culture chamber in a 5% CO_2 incubator).

Fisher's exact test was used to calculate a P-value determining the probability that the association between the differentially expressed genes and the canonical pathway is explained by chance alone. The ratio indicates the number of differentially expressed genes that map to the pathway divided by the total number of genes that map to the canonical pathway.

Canonical Pathway	*P-value*	*Ratio*
NRF2-mediated Oxidative Stress Response	0.00005	0.1050
ATM Signalling	0.00056	0.1530
TNFR2 Signalling	0.00091	0.1760
Role of Macrophages, Fibroblasts and Endothelial Cells in Rheumatoid Arthritis	0.00095	0.0719
RAR Activation	0.00158	0.0856
Role of IL-17A in Arthritis	0.00174	0.1270
TNFR1 Signalling	0.00324	0.1320
IL-17A Signalling in Gastric Cells	0.00339	0.2000
IL-6 Signalling	0.00347	0.0968
Role of Osteoblasts, Osteoclasts and Chondrocytes in Rheumatoid Arthritis	0.00447	0.0753
Colorectal Cancer Metastasis Signalling	0.00447	0.0739
p53 Signalling	0.00562	0.1040
Lymphotoxin β Receptor Signalling	0.00708	0.1150
Fructose and Mannose Metabolism	0.00776	0.0448
TGF-β Signalling	0.00794	0.1010
ILK Signalling	0.00813	0.0781
Circadian Rhythm Signalling	0.00891	0.1430
Polyamine Regulation in Colon Cancer	0.01047	0.1380
Death Receptor Signalling	0.01047	0.1080
Glucocorticoid Receptor Signalling	0.01047	0.0646
Induction of Apoptosis by HIV1	0.01148	0.1060
Hepatic Fibrosis / Hepatic Stellate Cell Activation	0.01202	0.0816
Molecular Mechanisms of Cancer	0.01288	0.0608
PPAR Signalling	0.01318	0.0849
Role of Tissue Factor in Cancer	0.01349	0.0877

Canonical Pathway	*P-value*	*Ratio*
Regulation of IL-2 Expression in Activated and Anergic T Lymphocytes	0.01413	0.0899
IL-17A Signalling in Fibroblasts	0.01479	0.1250
Hypoxia Signalling in the Cardiovascular System	0.01479	0.1080
Role of IL-17A in Psoriasis	0.01549	0.2310
HMGB1 Signalling	0.01622	0.0900
Mouse Embryonic Stem Cell Pluripotency	0.01820	0.0909
Role of JAK family kinases in IL-6-type Cytokine Signalling	0.01950	0.1480
April Mediated Signalling	0.02042	0.1160
Ovarian Cancer Signalling	0.02089	0.0775
IL-10 Signalling	0.02188	0.0897
MIF Regulation of Innate Immunity	0.02291	0.1000
Tight Junction Signalling	0.02399	0.0736
Cholecystokinin/Gastrin-mediated Signalling	0.02455	0.0849
HIF1α Signalling	0.02455	0.0841
Aryl Hydrocarbon Receptor Signalling	0.02455	0.0692
B Cell Activating Factor Signalling	0.02512	0.1110
Role of IL-17F in Allergic Inflammatory Airway Diseases	0.02512	0.1090
Retinoic acid Mediated Apoptosis Signalling	0.02512	0.0882
Neuregulin Signalling	0.02630	0.0784
Small Cell Lung Cancer Signalling	0.02884	0.0787
Corticotropin Releasing Hormone Signalling	0.03631	0.0662
ERK5 Signalling	0.03981	0.0938
Airway Pathology in Chronic Obstructive Pulmonary Disease	0.04169	0.2220
T Cell Receptor Signalling	0.04365	0.0734
ERK/MAPK Signalling	0.04365	0.0637
Glycolysis/Gluconeogenesis	0.04467	0.0538
CD40 Signalling	0.04571	0.0857
Wnt/β-catenin Signalling	0.04571	0.0698
TWEAK Signalling	0.04786	0.1030

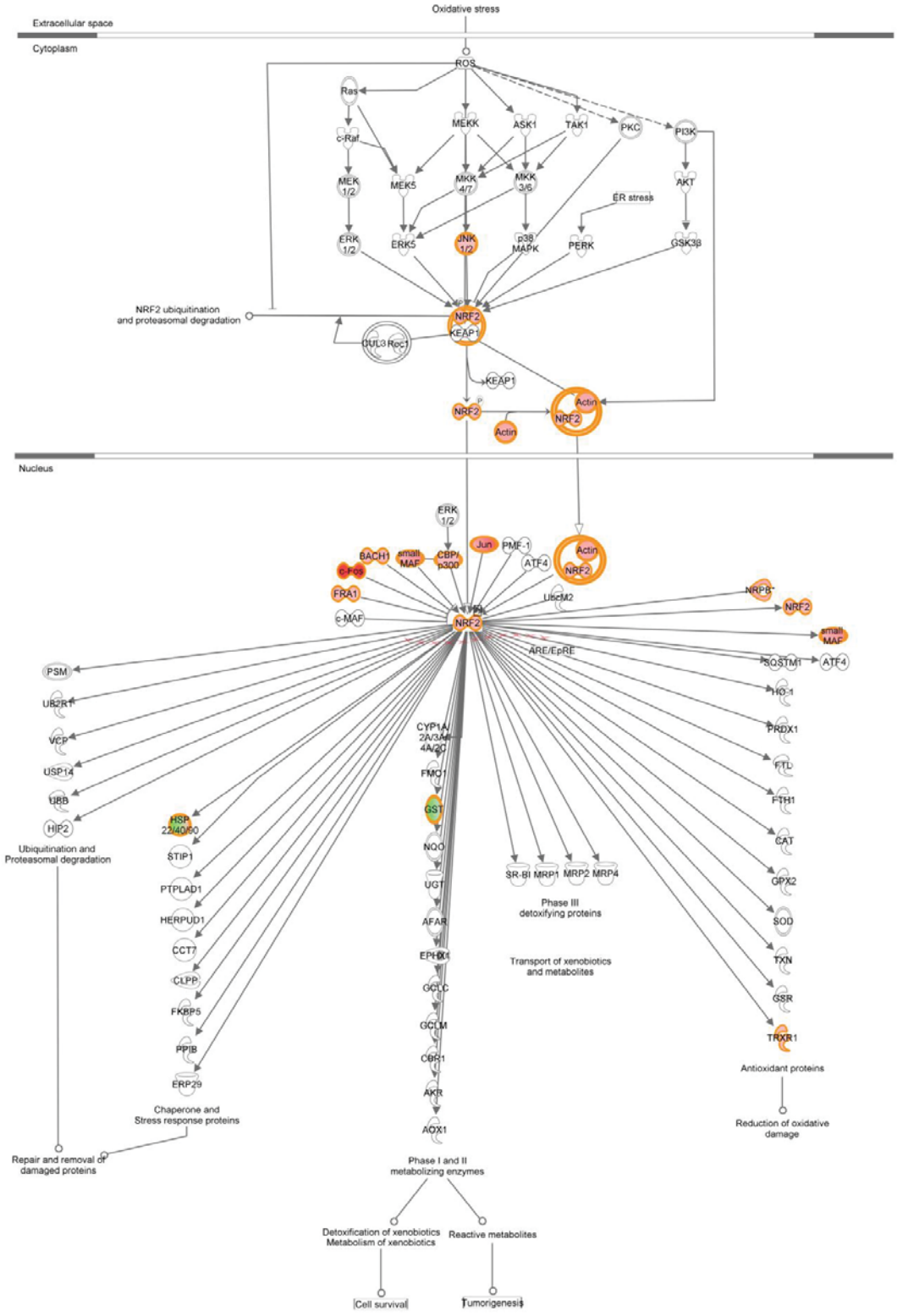

Figure 4.6 Ingenuity pathway for NRF2-mediated oxidative stress response.

Transcriptional information was projected onto the pathway; genes with increased expression in Caco-2 cells grown in the apical anaerobic environment (compared to Caco-2 cells in the co-culture chamber in a 5% CO_2 incubator) are depicted in shades of red, genes with decreased expression in shades of green. Intensity of colour indicates degree of fold change, with greater intensity signifying higher expression level.

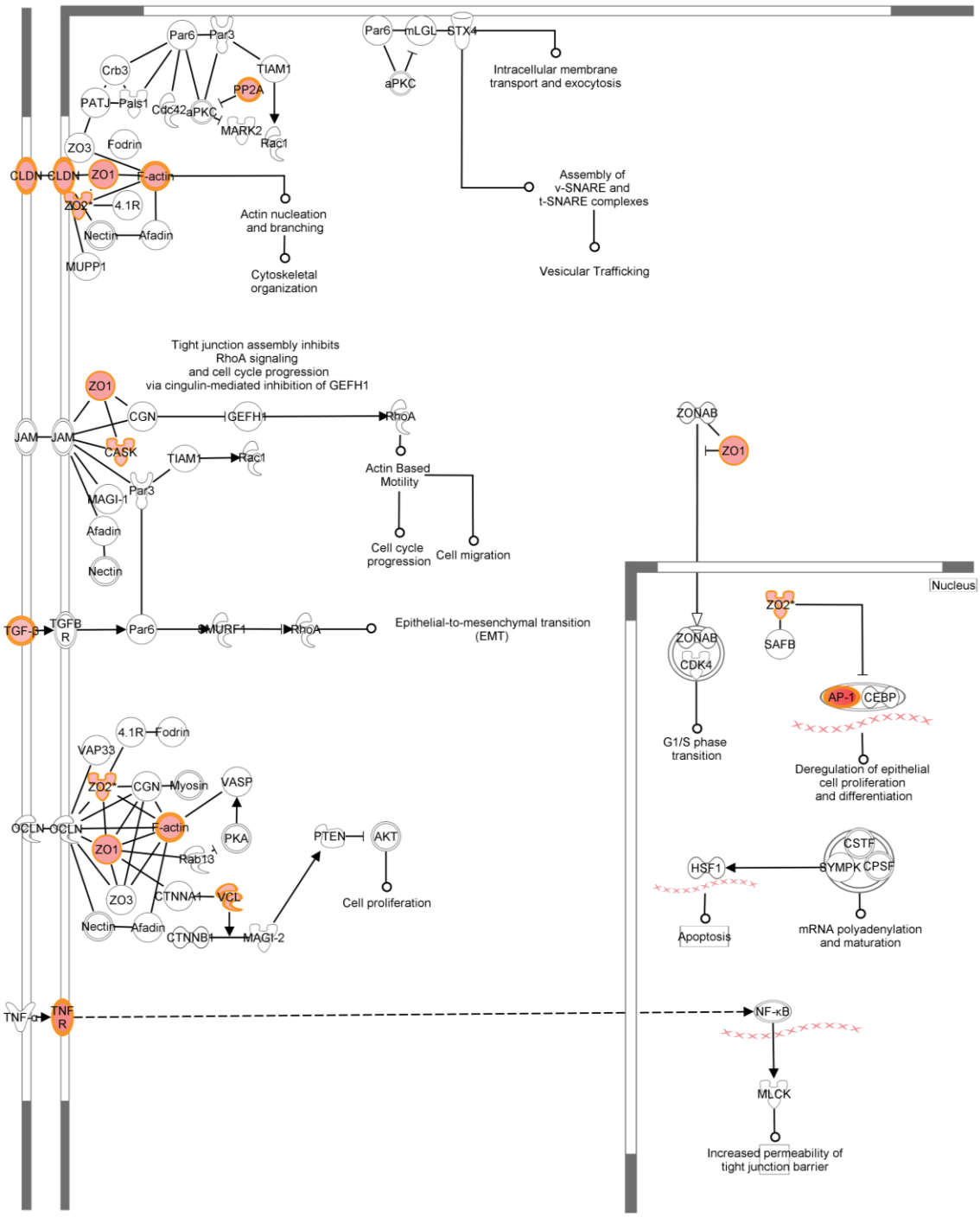

Figure 4.7 Ingenuity pathway for TJ signalling.

Transcriptional information was projected onto the pathway; genes with increased expression in Caco-2 cells grown in the apical anaerobic environment (compared to Caco-2 cells in the co-culture chamber in a 5% CO_2 incubator) are depicted in shades of red. Intensity of colour indicates degree of fold change, with greater intensity signifying higher expression level.

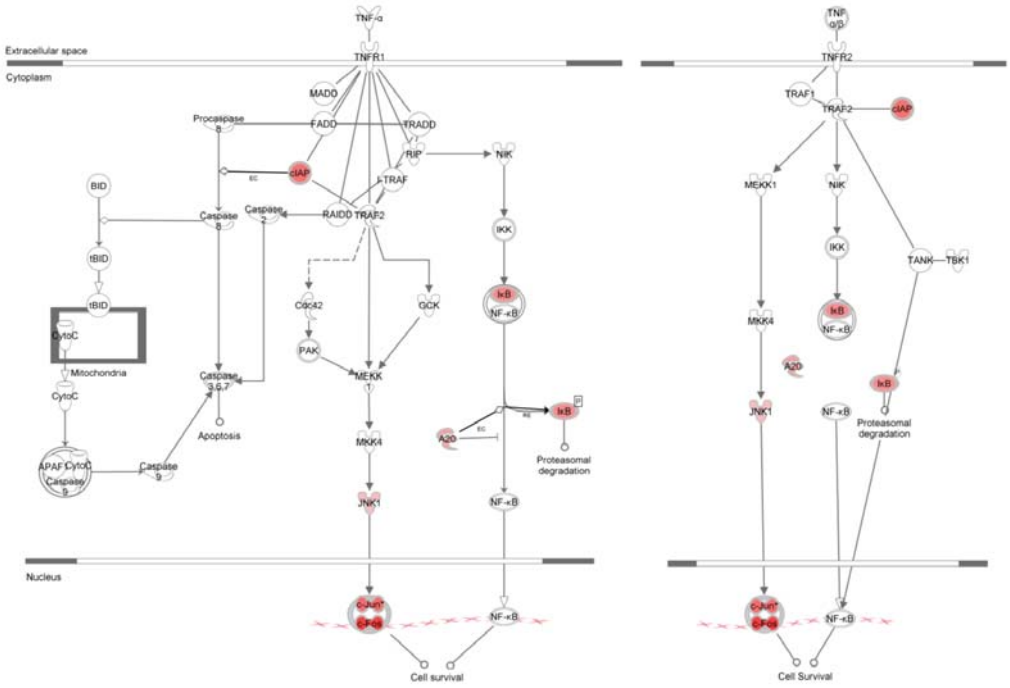

Figure 4.8 Ingenuity pathways for TNFR1 and TNFR2 signalling.

Transcriptional information was projected onto the pathway; genes with increased expression in Caco-2 cells grown in the apical anaerobic environment (compared to Caco-2 cells in the co-culture chamber in a 5% CO_2 incubator) are depicted in shades of red. Intensity of colour indicates degree of fold change, with greater intensity signifying higher expression level.

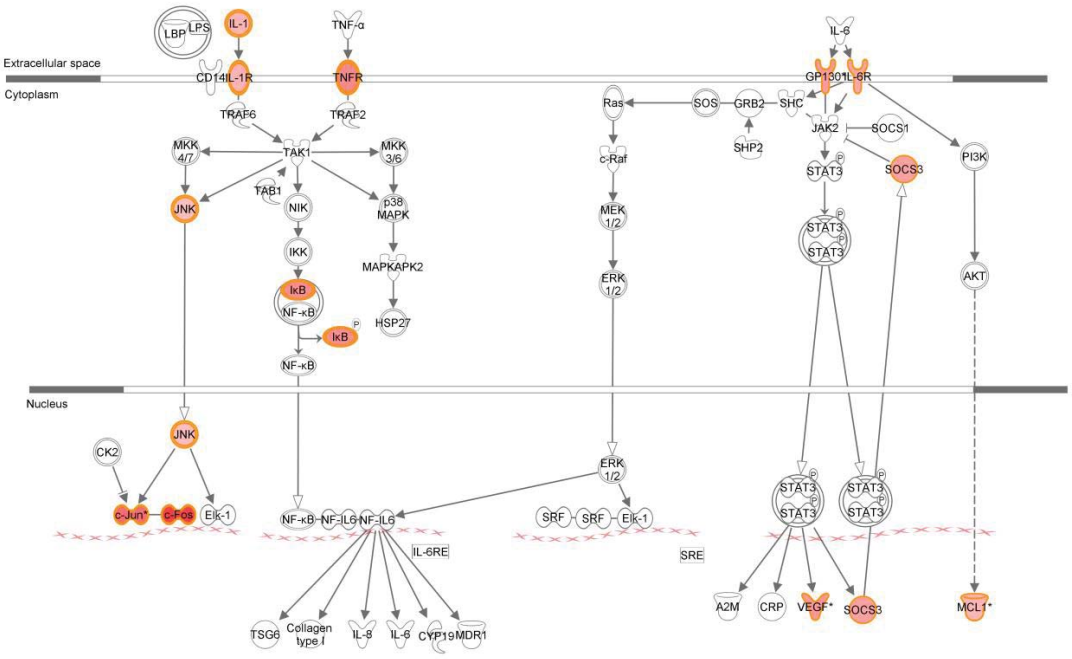

Figure 4.9 Ingenuity pathway for IL6.

Transcriptional information was projected onto the pathway; genes with increased expression in Caco-2 cells grown in the apical anaerobic environment (compared to Caco-2 cells in the co-culture chamber in a 5% CO_2 incubator) are depicted in shades of red. Intensity of colour indicates degree of fold change, with greater intensity signifying higher expression level.

cultured in the apical anaerobic environment for 12 hours, compared to cells cultured under standard conditions (Table 4.8). Transcription factors with predicted increased activity included hypoxia-inducible factor (HIF)1α and P53, known to regulate gene expression during hypoxic conditions[331] (Figure 4.10). None of the genes coding for the transcription factors listed in Figure 4.10 showed a change in expression (except for MYC, 1.596 log fold change). Overall the gene expression changes suggest that the Caco-2 cells in the apical anaerobic model had adapted to survive in an atmosphere of lower oxygen compared to cells cultured in a conventional system.

Table 4.8 Predicted activation state of transcription factors in Caco-2 cells cultured in an apical anaerobic environment for 12 hours (compared to Caco-2 cells in the co-culture chamber in a 5% CO_2 incubator).

The P-value was calculated by the Fischer's Exact test and indicates the statistical significance of differentially expressed genes that are downstream of the transcription factor. Given the observed differential expression of a gene (increased or decreased), the Z-score was used to determine the activation state of upstream transcription factors by the regulation direction associated with the relationship from the transcription factor to the gene. An absolute Z-score of ≥ 2 was considered significant (transcription factor activated if Z-score ≥ 2; inhibited if Z-score ≤ -2).

Predicted Activation State	*Transcription Factor*	*Z-score*	*P-value*
Activated	TP53 (includes EG:22059)	3.892	2.08E-10
	PDX1 (includes EG:18609)	3.246	1.71E-07
	HIF1A	2.868	2.01E-13
	CREB1	2.727	1.26E-17
	FOXL2	2.528	4.97E-08
	CDKN2A	2.37	1.09E-02
Inhibited	HNF4A	-2.031	1.22E-01
	MEOX2	-2.045	1.50E-07
	TCF3	-2.084	3.81E-02
	RXRA	-2.103	6.71E-03
	HSF1 (includes EG:15499)	-2.127	5.31E-02
	MYCN	-2.268	1.96E-01
	KLF2	-2.394	3.95E-05
	MYC	-2.484	7.18E-04

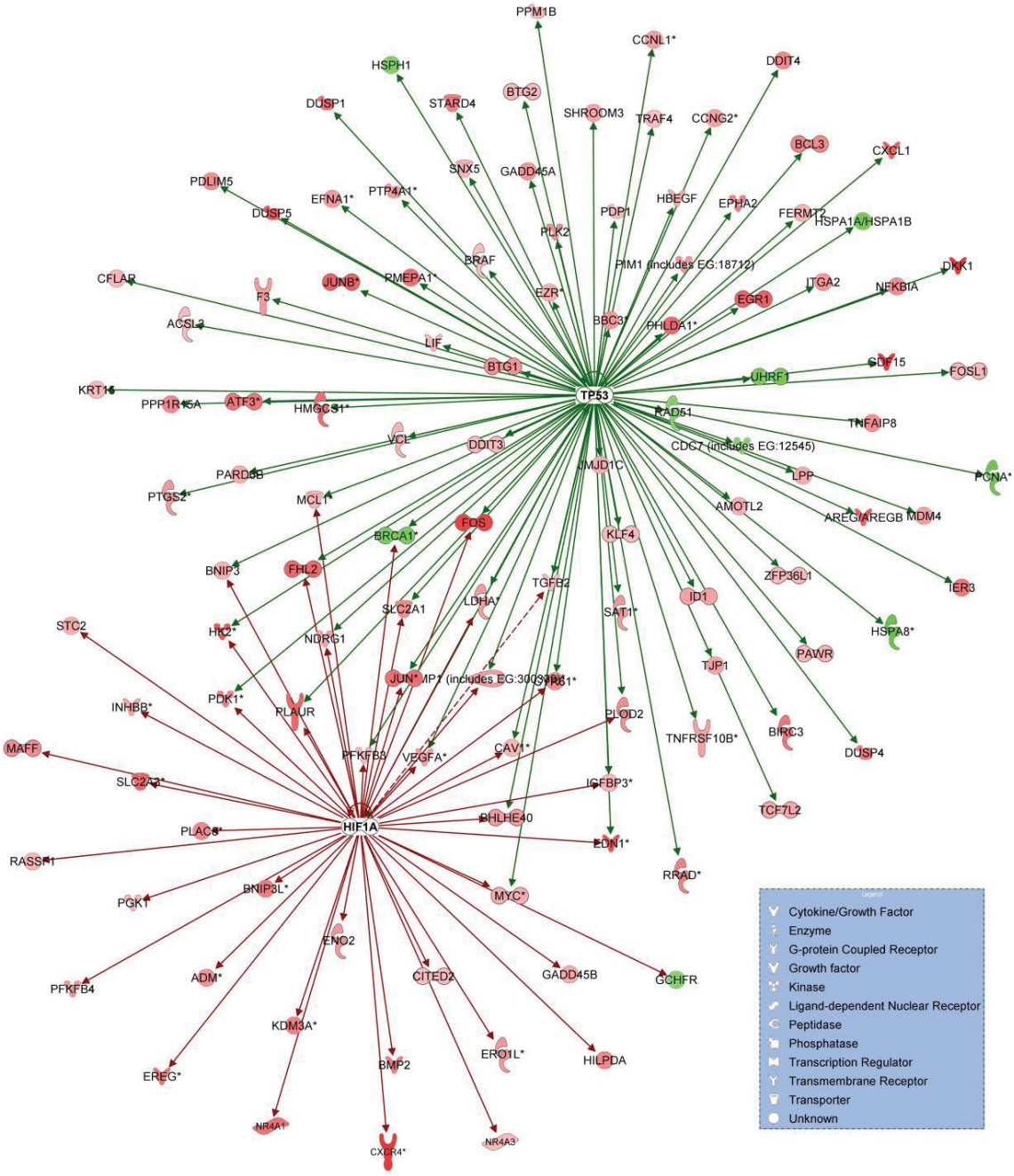

Figure 4.10 Network of differentially expressed genes regulated by P53 and HIF1A in Caco-2 cells cultured in an apical anaerobic environment for 12 hours (compared to Caco-2 cells in the co-culture chamber in a 5% CO_2 incubator).

Genes with increased expression in Caco-2 cells grown in the apical anaerobic environment (compared to Caco-2 cells in the co-culture chamber in a 5% CO_2 incubator) are depicted in shades of red, genes with decreased expression in shades of green. Intensity of colour indicates degree of fold change, with greater intensity signifying higher expression level. Shapes indicate functional class of gene products as indicated in legend.

4.5 DISCUSSION

Global gene expression analysis showed that gene expression in Caco-2 cells cultured in an apical anaerobic environment for 12 hours was consistent with the upregulation of cell survival and proliferation in reduced oxygen conditions, compared to Caco-2 cells in the co-culture chamber in a 5% CO_2 incubator, suggesting an adaptation to a lower supply of oxygen in the apical anaerobic model. These results are consistent with the Caco-2 being viable and maintaining an intact epithelial barrier as discussed in the previous chapter, further supporting the validity of the apical anaerobic model.

The results from the IPA transcription factor analysis infer that the Caco-2 cells in the apical anaerobic model received sufficient oxygen to avoid apoptosis for 12 hours or more. Insufficient level of oxygen is known to increase the protein abundance and activity of P53, leading to P53-dependent apoptosis in cells (reviewed by Sermeus and Michiels (2011)[331]). Hypoxia-induced P53-dependent apoptosis involves cytochrome *c* release and the consequent activation of caspase-9 and caspase-3. While Caco-2 gene expression in the apical anaerobic model was consistent with increased P53 activity, gene expression of cytochrome *c* and caspase was unchanged. This is consistent with there being no difference in viability in Caco-2 cells in the apical anaerobic model compared to a conventional Transwell system. The gene expression data fit the model proposed by Sermeus and Michiels (2011)[331], where under severe or sustained hypoxia, increased P53 protein coupled with decreased HIF1 activity leads to cell cycle arrest and apoptosis, but under mild hypoxic conditions HIF1α stabilisation allows cells to adapt to the reduced oxygen atmosphere.

The transcription factor HIF1α, predicted to be have increased activity in the apical anaerobic model, is highly unstable in the presence of oxygen, but activated in conditions of hypoxia though oxygen-dependent enzymatic hydroxylation of specific amino-acid residues[332]. Upon activation, HIF1 induces genes whose products allow cells to adapt to low levels of oxygen, including genes responsible for glucose transport and glucose metabolism, enabling cells to maintain sufficient levels of ATP[323]. HIF1 also induces transcription of genes involved in cell migration and vasculogenesis consistent with biological functions predicted by IPA analysis[332,333].

The adaptation of Caco-2 cells to survive is also evident in the IPA biological functions predicted to be increased in the apical anaerobic model, for example functions such as 'cell survival' and 'proliferation of cells'. While it may be argued that the IPA function 'apoptosis of kidney cell lines' was predicted to be increased, thus suggesting a decrease in cell viability, the functions 'cell death of epithelial cells' and 'apoptosis of epithelial cell lines' were not predicted to be altered. In addition, the functions 'cell cycle progression' and 'mitosis' were also predicted to be increased, while the 'G2 phase' function was predicted to be decreased, consistent with faster cell renewal. This is further evident in the IPA biological interaction network constructed using differentially expressed genes, whose associated biological functions were 'Cancer', 'Cellular Development' and 'Cellular Growth and Proliferation'. *Vegf,* an important node in the interaction network, is also associated with cell proliferation[334] and survival[335] functions, and is regulated by hypoxia[336]. The other important nodes in the network, namely the Lh, FSH and CG complexes, have been shown to regulate in part the expression and localisation of VEGF[337,338].

It is well known that supply of oxygen to tissue is largely dependent on vascularisation and vasodilation at the site of the tissue. Consistent with this, IPA functional analysis indicated an increased 'development of blood vessels' and 'accumulation of blood cells'. Gene expression was also consistent with increased 'cell movement' functions, which is also a potential mechanism of obtaining more oxygen. Further, *vegf* from the IPA interaction network is also associated with cell migration. The activation of the HIF1 transcription factor also increases transcription of genes involved in cell migration and vasculogenesis consistent with the predicted Ingenuity biological functions[332,333]. Thus, as indicated above, the transcriptomic data suggest that the Caco-2 cells in the apical anaerobic model have adapted to an atmosphere of lower oxygen compared to cells cultured in a conventional system, but receive sufficient oxygen to avoid apoptosis for 12 hours or more.

Many of the GO biological processes enriched with differentially expressed genes are similar to the predicted IPA biological functions (for example 'cell proliferation', 'cell cycle' and 'blood vessel development') thus verifying that the cells have adapted to survive in an atmosphere of reduced oxygen. Similarly, the GO process 'response to stress' includes, among others, processes such as 'response to anoxia and hypoxia'. Other GO processes enriched in the apical anaerobic model included

'metabolic processes' and 'cellular processes' (the top 2 ranked processes) and their descendent 'cellular metabolic processes'. Changes in genes involved in metabolic processes suggest a metabolic adaptation of the Caco-2 cells in the apical anaerobic environment. Cellular oxygen demand is dependent on cell metabolism, thus an adaptation to reduced levels of oxygen requires the downregulation of metabolic demand[306]. Thus the observed changes to metabolic processes maybe an adaptation to the reduced oxygen in the apical anaerobic model.

The 'NRF2-mediated oxidative stress response' pathway was the most significant IPA canonical pathway enriched with genes from the dataset. Mitochondria are known to release reactive oxygen species (ROS) during periods of low oxygen and thereby increase oxidative stress[339]. Thus the NRF2 pathway may be activated in Caco-2 cells in the apical anaerobic model in response to this, as it is capable of causing a broad and coordinated set of responses against oxidative stress[340]. On the other hand, products of many of the genes upregulated in the NRF pathway are also known to inhibit NRF function.

The TNFR pathways were also enriched with differentially expressed genes from the dataset. The TNFR pathways are involved in sending both cell death and cell survival signals. The expression of genes in the apical anaerobic model within both the TNFR-1 and TNFR-2 pathways were consistent with cell survival. TNF family members are also known to play important roles in several physiological processes including cell proliferation, apoptosis and induction of immune responses[341].

The changes in gene expression observed in the apical anaerobic model are similar to those observed in tumour cells. This is illustrated by the IPA functional analysis where the top ranked biological function is 'cancer'. Tumour cells are usually exposed to a hypoxic environment due to the lack of blood vessels in proliferating tumours[323]. Nonetheless, tumour cells have adapted several mechanisms to survive in a low oxygen environment. The genes involved in many of the biological functions and GO processes represented in the dataset, such as cell survival, vasculogenesis, apoptosis and cell adhesion, are commonly also upregulated in tumour cells exposed to hypoxic environments in response to HIF1[323]. The activation of the *vegf* in the interaction network, for example, is also observed in tumour cells, as a means of increasing vasculogenesis to improve oxygen and nutrient availability[323]. Further, the metabolism of cancer cells, in the presence of low oxygen, is known to shift from oxidative

phosphorylation to the oxygen independent metabolism of glycolysis[342]. Interestingly, this shift is regulated by several transcription factors, which among others includes HIF-1 and p53 predicted to be activated in Caco-2 cells in the apical anaerobic model, and MYC, the gene expression of which was increased in Caco-2 cells in the apical anaerobic model. In light of the above, it could be hypothesised that Caco-2 cells in the apical anaerobic environment utilised glycolysis to ensure their viability.

As described in Chapter 3, the Caco-2 cells in the apical anaerobic model maintained an intact and well-formed junctional barrier. On the contrary, increased permeability and reduced TJ protein expression is usually observed in hypoxic and oxidative stress conditions[343,344]. Consistent with the well-formed TJ barrier, the Ingenuity pathway for TJ signalling was enriched with genes from the dataset, and the expression direction of the genes indicated formation of junctional complexes. Under hypoxic conditions the intestinal barrier is known to be dysregulated by the activation of inflammatory cascades such as hypoxia-elicited tumour necrosis factor-alpha (TNF-α), which synergises with pro-inflammatory mediators, such as IFN-γ, leading to increased TJ permeability and intestinal inflammation[283]. A common factor in the promoter sites of hypoxia-induced inflammatory genes is the cAMP response element (CRE), which binds to the transcription factor CRE-binding protein (CREB) during physiological conditions repressing transcription of the inflammatory genes[345]. Under hypoxic conditions, however, CREB is degraded, and its repressor function is lost. Activation of NF-κB (which similar to HIF1α and P53 contains redox sensitive cysteine residues at its DNA binding sites[346]) together with the degradation of CREB is key in the induction of inflammation in response to hypoxia. In the apical anaerobic model, however, consistent with the intact intestinal barrier, CREB is predicted to have increased activation (suggesting it is unlikely that CREB is degraded), while NF-κB was not predicted to have an altered activation state (consistent with increased expression levels of IκB, inhibitor of NF-κB).

Global gene expression analysis also implicated the regulation of several immune-related functions and pathways in the apical anaerobic model. The Ingenuity pathway for IL-6, for example, was enriched with genes from the dataset, and gene expression was consistent with activation of downstream processes. Further, the HIF1 transcription factor, predicted to be activated, is known to co-ordinate the induction of TLR2 and TLR6 (even though global gene expression analysis did not indicate a

difference in TLR expression). Therefore, while it is well known that commensal and probiotic strains of bacteria exert immunomodulatory effects on Caco-2 cells[210,257] and other cell lines[254,256], it is possible that the immune responses of Caco-2 cells in the apical anaerobic model would differ compared to those cultured under conventional conditions.

In conclusion, gene expression in Caco-2 cells cultured in the apical anaerobic model (compared to Caco-2 cells cultured under standard conditions) was consistent with the upregulation of cell survival and proliferation in reduced oxygen conditions, showing the viability of the monolayer, and suggesting its adaptation to a lower supply of oxygen in the apical anaerobic model. The adaptation of this model can be likened to that of proliferating cancer cells in a tumour mass where oxygen supply is scarce. Caco-2 cells, as a cell line derived from colorectal cancer, may be well suited to grow in a low oxygen atmosphere, and possibly utilise the glycolysis pathway for ATP production.

Overall these data, together with the data from the previous chapter, support the viability of the Caco-2 cell monolayer, and the integrity of the TJ barrier, thus supporting the validity of this novel apical anaerobic model. This model is therefore suitable for the study of regulation of barrier integrity by commensal intestinal bacteria. For example, while probiotic bacteria, such as strains of *L. plantarum*, are known to increase *in vitro*[192] and *in vivo*[193] abundance of TJ proteins, and alter expression of genes involved in TJ formation *in vitro*[192], a few studies also suggest that obligate commensal anaerobes such as *B. thetaiotaomicron* regulate intestinal barrier integrity *in vitro*[201]. This reductionist *in vitro* model can be used to gain insights into the mechanisms of crosstalk between the anaerobic commensal bacteria and intestinal cells. A better understanding of the underlying mechanisms will enable the development of strategies to improve intestinal barrier function, and in turn reduce the risk of intestinal and systemic disorders in susceptible individuals[5].

Chapter 5:

Interactions between an obligate anaerobic bacterium and Caco-2 cells in an apical anaerobic model of the intestinal barrier

5.1 INTRODUCTION

The intestinal tract is inhabited by 10^{14} microbes (the intestinal microbiota), over tenfold the number of cells that make up the human body[18], dominated by an estimated 500-1000 different bacterial species[13]. The microbiome (collective genome of all microbes that reside in and on humans) is estimated to contain over 100-times the number of genes in the human genome[149,347]. It is becoming increasingly evident that these bacteria, including their metabolites are a key mediator in the regulation of intestinal barrier function, as well as playing functional roles in immunomodulation, host metabolism, pathogen evasion, and even the development and maturation of the intestine[1,151]. However, over 90% of the intestinal microbiota is composed of obligate anaerobes[19,150]. Due to the difficulty in culturing obligate anaerobic bacteria with intestinal cells, much of the research on the modulation of intestinal barrier function by bacteria has focussed predominantly on oxygen-tolerant bacteria[193,195,197].

The obligate anaerobe *F. prausnitzii* is a major member of the Firmicutes, a dominant phylum of the intestinal microbiota[173], and is considered one of the most abundant representatives of the human faecal microbiota[348,349]. However *F. prausnitzii* has decreased prevalence in mucosa-associated microbiota of patients with IBD[15,350,351] and coeliac disease[16] where intestinal barrier integrity is known to be compromised[7,8]. Similarly, in a culture-independent study characterising bacterial communities in patients with IBD, sequences representative of *F. prausnitzii* as well as several other cultured commensal anaerobes including *B. thetaiotaomicron*, were found to be depleted in patients with IBD[17]. It is therefore plausible, that *F. prausnitzii* and other commensal anaerobic bacteria are important in the regulation of the intestinal barrier.

In vitro only the culture supernatant of *F. prausnitzii*, and not the UV-killed bacteria or bacterial fractions, was able to reduce secretion of the pro-inflammatory cytokine IL-8 by Caco-2 cells[257]. This suggests that the bioactive component is a secreted metabolite or a factor released into the growth medium during anaerobic growth. The apical anaerobic model of the intestinal barrier, developed and validated in the work described in the previous chapters of this dissertation, serves as a useful platform to study the crosstalk between obligate anaerobic bacteria and intestinal epithelial cells, as it provides an environment suitable for the survival of obligate

anaerobes such as *F. prausnitzii*, while ensuring the viability and barrier integrity of the Caco-2 cell monolayer.

5.2 HYPOTHESIS AND AIMS

The hypothesis of the study reported here was that obligate anaerobic bacteria exert differential effects on epithelial cells based on whether or not the bacterial cells are viable.

The first aim was to demonstrate that the apical anaerobic model can be used to study interactions between live obligate anaerobic bacteria and Caco-2 cells. The obligate anaerobe *F. prausnitzii* was used for this purpose. Furthermore, the facultative anaerobe *L. rhamnosus* was also used for comparison, as this strain has been shown to influence barrier function in intestinal cell lines, and would survive in the anaerobic apical environment. The viability of bacterial cells was assessed to ensure *F. prausnitzii* could survive in the apical anaerobic model.

The second aim was to assess the effects of *F. prausnitzii* on intestinal barrier integrity. TEER and small molecule permeability across the Caco-2 monlayers were determined at regular intervals in the presence of the bacterium.

The third aim was to examine the effect of *F. prausnitzii* on intestinal epithelial cell gene expression. The intention was to allow a better understanding of molecular changes that occur in Caco-2 cells in response to bacteria in the apical anaerobic model.

To determine if the effects exerted on Caco-2 cells by viable *F. prausnitzii* differed to the effects exerted by non-viable *F. prausnitzii* cells, Caco-2 cells were also co-cultured with UV-killed *F. prausnitzii* cells and compared to Caco-2 cells co-cultured with viable *F. prausnitzii* cells. If the effects of viable *F. prausnitzii* cells were different to that of non-viable cells, this would illustrate the importance of a system that allows for live obligate anaerobic bacteria to be co-cultured with intestinal cells *in vitro*.

5.3 METHODS

5.3.1 Culture of epithelial cells

Caco-2 cells were cultured on to cell culture inserts (refer to section 3.3.1.1) which were transferred in to the co-culture chamber (refer to section 3.3.1.2) and exposed to an anaerobic environment on the apical side (refer to section 3.3.1.3). For all experiments described in this chapter, where Caco-2 cells were cultured in the co-culture chamber, the cell culture medium was prepared by mixing 49.5 mL of M199 with 500 μL of NEAA.

5.3.2 Culture of bacteria

5.3.2.1 *Faecalibacterium prausnitzii* cell culture

F. prausnitzii DSM17677[301] was obtained from Deutsche Sammlung von Mikroorganismen und Zellkulturen (DSMZ) microorganism culture collection and cultured anaerobically in brain-heart infusion (BHI) broth at 37°C using Hungate culture tubes (16 mm diameter, 125 mm long; BellCo glass, Vineland, New Jersey, USA) sealed with butyl rubber stoppers. BHI broth was prepared as described in section 5.3.3.1. The bacteria were inoculated either using a sterile syringe flushed with anaerobic CO_2, or by opening the Hungate tubes inside an anaerobic workstation (Concept Plus, Ruskinn Technology Ltd) containing an atmosphere of 10% CO_2, 10% H_2 in N_2. Bacterial stocks were maintained at -80°C as described in section 5.3.4.1.

5.3.2.2 *Lactobacillus rhamnosus* cell culture

L. rhamnosus HN001 was obtained from the Culture Collection of the Fonterra Research Centre, Palmerston North, New Zealand. Bacteria were cultured on Man, Rogosa and Sharpe (MRS) agar (section 5.3.3.3) or in MRS broth (section 5.3.3.2), at 37°C in a 5% CO_2 incubator. Bacterial stocks were maintained at -80°C as described in section 5.3.4.2.

5.3.3 Preparation of bacterial culture medium

5.3.3.1 Anaerobic BHI broth

All components listed in Table 5.1, except for L-cysteine and vitamin K solution, were dissolved in 1 L of distilled H_2O. The solution was boiled to eliminate DO and aid the dissolving of components. The solution was allowed to cool in an ice-water bath while being bubbled with oxygen-free CO_2. Once cooled to room temperature, L-cysteine and vitamin K were added, and the pH of the solution adjusted to 7.0 ± 0.2 using NaOH, while maintaining the stream of CO_2. The solution was dispensed into the Hungate tubes filled with oxygen-free CO_2 in 10 mL aliquots using a pipette flushed with oxygen-free CO_2. The tubes were sealed with butyl rubber stoppers and perforated plastic caps with a headspace of 100% CO_2, and autoclaved on the same day at 121°C and 15 psi for 20 minutes.

5.3.3.2 MRS broth

MRS broth was prepared by mixing 55 g of lactobacilli MRS Broth powder (Acumedia manufacturers, Michigan, USA) in 1 L of distilled H_2O. The solution was heated to aid the dissolving of the powder, and once cooled, dispensed into the Hungate tubes, covered with plastic caps, and autoclaved at 121°C and 15 psi for 20 minutes.

5.3.3.3 Anaerobic BHI agar

Anaerobic BHI broth was prepared as described in section 5.3.3.1, but without the addition of L-cysteine, in a high pressure Shott bottle (SCHOTT AG, Mainz, Germany). Bacteriological Agar (Oxoid, Hampshire, UK) was added to the medium (1.5 % (w/v)) while being bubbled with oxygen-free CO_2, and the bottle was sealed with a butyl rubber stopper and perforated Shott cap, prior to being autoclaved at 121°C and 15 psi for 20 minutes. The agar was poured on to Petri dishes inside an anaerobic workstation. Once set, the plates were stored in plastic bags inside the anaerobic workstation for no more than 3 days.

Table 5.1 Components of the modified brain-heart infusion medium.

Media components and volumes required to prepare 1 L of modified BHI medium.

Media component	*Volume*
BHI powder (Becton Dickinson)	37 g
Yeast extract (Becton Dickinson)	5 g
0.05% (w/v) haemin, prepared in 1N NaOH (Sigma-Aldrich)	10 mL
0.5% (v/v) vitamin K solution, prepared in 95% EtOH (Sigma-Aldrich)	1 mL
L-cysteine (Sigma-Aldrich)	2 g
Distilled H_2O	1 L

5.3.3.4 MRS agar

MRS broth was prepared as described in section 5.3.3.2 with 1.5% (w/v) of Bacteriological Agar. The agar solution was allowed to set in Petri dishes after being autoclaved, and stored at 4°C.

5.3.4 Long term storage of cultures

Frozen stocks of *F. prausnitzii* and *L. rhamnosus* were maintained at -80°C in DMSO (5.3.4.1) and glycerol (5.3.4.2) respectively.

5.3.4.1 Preservation with DMSO

An anaerobic solution of 50% DMSO was prepared as follows. All components listed in Table 5.2 except L-cysteine were mixed thoroughly. The solution was boiled to eliminate DO, and cooled on an ice-water bath while being bubbled with oxygen-free CO_2. Once cooled to room temperature, the L-cysteine was added, and the solution was dispensed into Hungate tubes, sealed and sterilised as described in section 5.3.3.1. This solution was injected into the viable culture of bacteria using a sterile syringe flushed with anaerobic CO_2, to a final concentration of 10% (v/v) (5% DMSO in final mixture), and the culture was kept at -20°C overnight, following which it was stored at -80°C. Frozen stocks were subjected to no more than five freeze-thaw cycles.

5.3.4.2 Preservation with glycerol

Freezing medium was prepared by mixing 5.5 g of MRS powder to 66 mL of water and adding 33 mL of glycerol and mixing thoroughly. 1 mL aliquots were prepared in cryogenic vials and autoclaved at 121°C and 15 psi for 20 minutes. Two to three fresh colonies of *L. rhamnosus* were added per vial, mixed well, and frozen at -80°C.

5.3.5 Enumeration of bacteria

5.3.5.1 Counting chamber

A 20 µL sample of the bacterial suspension was mixed with 980 µL of PBS (1:50 dilution) and loaded on to a Petroff-Hausser counting chamber. The counting chamber

Table 5.2 Components of the 50% DMSO solution.

Solution components and volumes required to prepare 1 L of 50% DMSO solution.

Solution component	*Volume*
Salt solution A*	170 mL
Salt solution 2B*	170 mL
DMSO	500 mL
$NaHCO_3$	5 g
L-cysteine	0.5 g
0.1% w/v resazurin	2 drops
Distilled H_2O	80 mL

*Salt solution A contained 6 g/L NaCl, 1.5 g/L $(NH_4)_2SO_4$, 3 g/L KH_2PO_4, 0.79 g/L $CaCl_2.H_2O$ and 1.2 g/L of $MgSO_4.7H_2O$; Salt solution B contained either 6 g/L K_2HPO_4 or 7.86 g/L $K_2HPO_4.H_2O$.

was 0.02 mm deep and etched with two grid systems which consisting of 25 larger squares, each of which was divided into 16 smaller squares. The number of bacteria was counted for 4 large squares using a phase contrast microscope. To determine the number of bacteria per mL in the counting chamber, the average number of bacteria per square was multiplied by 1.25×10^6. This number was multiplied by 50 to take into account the 1:50 dilution, and calculate the concentration of bacteria in the undiluted suspension.

5.3.5.2 Colony-forming units

The bacterial suspension was diluted by factors of 10 in a 96 well microtitre plate by adding 20 μL of the previous dilution to 180 μL of anaerobic PBS and mixing carefully inside the anaerobic workstation. Anaerobic BHI agar plates (section 5.3.3.3) were divided into 4 quadrants, each of which corresponded to a single dilution factor. For each sample of bacterial suspension, 3 drops of 20 μL from each dilution was placed on the appropriate quadrant. The agar plates were incubated for 24 to 48 hours upside down inside the anaerobic workstation until bacterial colonies were visible. In quadrants where the total number of colonies per drop of sample was between 10-100, the number of colonies was counted, and multiplied by the appropriate dilution factor to determine the total number of colony-forming units (CFUs)/mL. A quadrant containing 10-100 colonies per spot was chosen because this range was considered statistically valid and easy to count. If less than 10 colonies were present, errors in dilution technique or presence of contaminants could affect the final count, whereas if more than a 100 colonies were present, multiple colonies would be indistinguishable.

5.3.6 16S rRNA gene sequencing

The identity of the bacterial strains used in this study was confirmed based on their 16S rRNA gene sequences. For each strain, genomic DNA was isolated (5.3.6.1), and the 16S rRNA gene amplified (5.3.6.2) and sequenced (5.3.6.3), following which the trace was compared with known bacterial sequences.

5.3.6.1 DNA isolation

DNA was isolated from approximately 3 mL of overnight bacterial culture using a phenol:chloroform extraction method[352]. Cultures were harvested by centrifuging 1.7 mL aliquots at 12000 x g for 5 minutes, and resuspending the resulting cell pellets in

350 µL TE buffer (100 mM Tris-HCl (pH 8), 10 mM EDTA). A 5 µL volume of RNase (10 mg/mL; Sigma-Aldrich) and 50 µL of lysozyme (100 mg/mL, prepared in 10mM Tris-HCl (pH8); Sigma-Aldrich) was added to the cell suspension to facilitate cell lysis and the subsequent degradation of RNA. This solution was incubated for 30 minutes at 37°C, while gently inverting the tube every 10 minutes to facilitate mixing, following which 50 µL of proteinase K (5 mg/mL; Sigma-Aldrich) was added, and the solution was incubated at 52°C for 30 minutes to facilitate degradation of cellular protein and inactivation of nucleases. Subsequently, 50 µL of 10% (w/v) SDS was added and the solution incubated at 52°C for approximately 15 minutes until the solution cleared and became uniform in consistency. A 500 µL volume of phenol:chloroform:iso amyl alcohol (25:24:1) was added to the cleared cell suspension. The solution was mixed by inversion before precipitated protein and other organic material was pelleted by centrifugation at 12000 x g for 15 minutes. The upper aqueous layer containing the nucleic acids was transferred to a new 1.7 mL tube and mixed with a further 500 µl phenol:chloroform:iso amyl alcohol (25:24:1) and centrifuged as described above. The upper aqueous layer was transferred to a new 1.7 mL tube and the DNA precipitated by gently mixing with 1 mL 100% isopropanol. DNA was pelleted by centrifugation at 12000 x g for 10 minutes and the supernatant decanted. The DNA pellet was washed with 1 mL of 70% ethanol. After centrifugation at 12000 x g for 5 minutes, the ethanol was decanted and the remaining ethanol evaporated by air drying the tube for 15 minutes. The DNA pellet was dissolved in 200 µL of autoclaved distilled water at 4°C overnight, after which the DNA was quantified using a NanoDrop, and stored at -20°C until needed.

5.3.6.2 Polymerase chain reaction

Polymerase chain reaction (PCR) was performed in 50 µL reactions in a Hybaid PX2 thermal cycler (Thermo Fisher Scientific). PCR primers (Table 5.3) were diluted to a final concentration of 10 pmol/µL. PCR reactions were prepared in 0.2 mL thin wall PCR tubes by mixing 27.8 µL of autoclaved distilled water, 5 µL taq buffer, 5 µL Mg (25 mM), 0.2 µL taq (5 U/µL) and 5 µL dNTP (2 mM) together with 1 µL each of forward and reverse primers. The PCR conditions were an initial denaturation step (94°C, 4 minutes) followed by 35 cycles of denaturation (94°C, 4 minutes), annealing (50°C, 30 seconds), and extension (72°C, 1 minute), followed by a final extension (72°C, 10 minutes). The PCR products were examined by agarose gel electrophoresis

and purified using the Roche High Pure PCR purification kit (Roche, Basel, Switzerland) as per the manufacturer's protocol for 'Purification of PCR Products in Solution after Amplification'. After purification DNA in the PCR product was quantified using a NanoDrop.

5.3.6.3 DNA sequencing

DNA sequencing reactions were prepared by mixing approximately 30 ng of DNA with 3.2 pmol of forward or reverse primer (Table 5.3), and with autoclaved distilled water to a volume of 15 μL. Sequencing reactions were conducted by the Allan Wilson Centre for Genome Sequencing Service (Massey University, NZ). This service included fluorescent labelling of PCR products using the BigDye™ Terminator Version 3.1, a ready Reaction Cycle Sequencing kit cycle by sequencing PCR, subsequent removal of unincorporated fluorescent ddNTPs by cleanup and precipitation of products and capillary separation on an ABI3730 Genetic Analyzer (Applied Biosystems). Results were returned as sequencing trace files.

The forward and reverse sequences were manually checked and aligned using Vector NTI ContigExpress software (Version 11; Life Technologies), and the consensus sequence was compared using the National Center for Biotechnology Information (NCBI) nucleotide Basic Local Alignment Search (BLASTN) tool to NCBI nucleotide collection (nr/nt) database[353].

5.3.7 Bacterial growth measurement

Two hundred μL each of 24-hour-old primary broth cultures of *F. prausnitzii* and *L. rhamnosus* were used to inoculate triplicate Hungate tubes of BHI or MRS broth respectively. The initial optical density (OD) of the Hungate tubes was taken using an OD600 DiluPhotometer spectrophotometer (Implen, München, Germany) at a wavelength of 600 nm. The Hungate tubes were incubated at 37°C and the OD_{600} was measured at 2 hour intervals over 24 hours. Where the OD_{600} reached the maximum capacity of the spectrophotometer (2.00), 200 μL of the broth was added to a DiluCell DC10 cuvette (Implen). Due to the design of the cuvette, the lightpath of the spectrophotometer was reduced from 10 mm (standard cuvette) to 1.0 mm, and thus, according to the Beer-Lambert-Law, this results in a 'virtual dilution' of the sample by a

Table 5.3 Oligonucleotide sequences used for 16S sequence analysis

Primer	*Name*	*Sequence*	*Reference*
Forward	27F	GAG TTT GAT CMT GGC TCA G	Modified from Lane (1991)[354]
Reverse	1492R	GGY TAC CTT GTT ACG ACT T	Lane (1991)[354]

factor of 10. While this inconsistency did not allow for a continuous growth curve to be plotted, it enabled the detection of the stationary phase of the growth curve. OD_{600} readings taken using DiluCell cuvettes were multiplied by a factor of 10.

5.3.8 Epithelial and bacterial cell co-culture

5.3.8.1 Preparation of bacterial cultures

16-hour-old secondary cultures of *F. prausnitzii* (section 5.3.8.1.1) and *L. rhamnosus* (section 5.3.8.1.2) were pelleted by centrifugation at 2492 x g for 6 minutes (11180/13190 rotor, Sigma 3-18K centrifuge) and resuspended in anaerobic cell culture medium inside an anaerobic workstation (Concept Plus). The amount of bacteria in the solution was estimated by quantifying the bacterial cells in a Petroff-Hauser chamber (section 5.3.5.1). Using this estimate, bacterial solutions were further resuspended to a desired concentration in anaerobic cell culture medium.

5.3.8.1.1 Preparation of *Faecalibacterium prausnitzii*

A frozen culture of *F. prausnitzii* (section 5.3.3.4) was warmed to 37°C in a water bath, and 200 µL inoculated in to 10 mL of anaerobic BHI broth (section 5.3.3.1). The inoculated tubes (primary culture) were incubated for 24 hours at 37°C, after which 200 µL was inoculated in to 10 mL of fresh anaerobic BHI broth (secondary culture).

5.3.8.1.2 Preparation of *Lactobacillus rhamnosus*

Frozen cultures of *L. rhamnosus* (section 5.3.3.4) were regenerated by streaking onto MRS agar plates (5.3.3.3) and incubating at 37°C in a 50% CO_2 incubator for 24-48 hours. A single colony was used to inoculate 10 mL MRS broth (section 5.3.3.2) which was incubated at 37°C in a 50% CO_2 for 24 hours (primary culture). Two hundred µL of primary culture was inoculated into 10 mL of fresh MRS broth (secondary culture).

5.3.8.1.3 Preparation of UV-killed *Faecalibacterium prausnitzii*

F. prausnitzii culture from section 5.3.8.1.1 was added at a volume of approximately 1.1 mL per well to a 6 well microtitre plate. The plate was placed on ice directly below a UV lamp and exposed to UVC radiation for 15 minutes to ensure that the bacterial cells were rendered non-viable. This method was verified to be effective by assessing the bacterial survival by determining CFU/mL as described in section 5.3.5.2.

5.3.8.2 Preparation of epithelial cells

The TEER of 14 day-old Caco-2 cell monolayers was checked (refer to section 2.3.4.2) to ensure the cells formed an effective epithelial barrier. Only monolayers which gave a resistance of over 300 Ω were used for co-culture experiments. The cell culture medium was removed from the Transwell insert and well, and replaced with cell culture medium prepared as described in section 5.3.1. The plates were incubated overnight at 37°C in a 5% CO_2 incubator. This step was necessary to ensure that cells were free of antibiotics and FBS so as not to inhibit bacterial growth or induce overgrowth of bacteria respectively.

5.3.8.3 Establishing co-culture

The Caco-2 cell monolayers (section 5.3.8.2) were exposed to an apical anaerobic environment in the co-culture chamber as described in section 3.3.1.3. Once inside the anaerobic workstation, the medium in the apical compartment of the co-culture chamber was replaced with the appropriate bacterial sample prepared as described in section 5.3.8.1. Unless otherwise mentioned, bacteria were seeded at a multiplicity of infection (MOI) of 100 (a cell culture insert was determined to have approximately 6 x 10^5 Caco-2 cells at confluence; thus 6 x 10^7 bacteria were seeded onto each inset).

5.3.9 Estimating bacterial viability

Bacterial survival following incubation with Caco-2 cells was assessed by determining CFU/mL as described in section 5.3.5.2. To detect any bacteria that were associated with the Caco-2 cells (either attached or internalised), and hence not represented in the cell culture media, the Caco-2 cells were lysed with an anaerobic solution of 1% triton-X. Treatments were compared using a general ANOVA in GenStat, and statistical difference was declared between two treatments when the difference in means was greater than the LSD at 5%.

5.3.10 TEER assay

Caco-2 cell monolayers were co-cultured with *F. prausnitzii, L. rhamnosus,* UV-killed *F. prausnitzii* or control cell culture medium (without bacteria) over 8 hours in the apical anaerobic model, and TEER of the monolayers were measured (n = 3 per treatment) during this time as described in section 3.3.7. The time frame of 8 hours was

chosen based on previous studies on the effects of bacteria on intestinal barrier integrity *in vitro*, where beneficial effects of bacteria or their metabolites were observed between 2-6 hours of co-culture[191,193,195,196].

TEER was measured approximately 30 minutes prior to, and immediately after, adding bacterial treatments. The change in TEER for each insert was calculated based on the TEER at the time point immediately prior to adding the treatment (henceforth known as the initial TEER). The experiment was repeated three times and the data were combined (total n = 9 per treatment). Only inserts where the initial TEER was between 500 $\Omega.cm^2$ and 4000 $\Omega.cm^2$, as measured by the CellZscope controller, were considered for statistical analysis, as TEER values outside this range are usually indicative of an erroneous reading. Furthermore, if the TEER rose above 4000 $\Omega.cm^2$ at any time point, the insert was also excluded from further analysis, as this indicates erroneous variability in the electrode or electrode connection. Treatments were compared using repeated measurements ANOVA in R and statistical difference was declared between two treatments for a given time point where the difference in means was greater than the LSD at 5%.

5.3.11 ^{3}H-mannitol bioassay

Caco-2 cell monolayers were co-cultured with *F. prausnitzii, L. rhamnosus,* UV-killed *F. prausnitzii* or control cell culture medium (without bacteria) over 8 hours in the apical anaerobic model, and paracellular permeability of the monolayers were measured during this time using the ^{3}H-mannitol bioassay as described in section 3.3.8 (n = 3 per treatment). The treatments were prepared as follows. Bacteria cultures were prepared at dilutions of 6 x 10^7 bacteria/mL as described in section 5.3.8.1. ^{3}H-mannitol in 90% ethanol (American Radiolabelled Chemicals) was diluted in anaerobic cell culture medium to an activity of approximately 2.25 x 10^5 Bq/mL. This solution of ^{3}H-mannitol was mixed with the bacterial suspension to a final activity of approximately 9.25 x 10^4 Bq/mL and 3.53 x 10^7 bacteria/mL (i.e. 6 x 10^7 bacteria in 1.7 mL). The amount of ^{3}H-mannitol that crossed the Caco-2 cell monolayer from the apical to the basal side was determined at 0, 2, 4, 6 and 8 hours. The experiment was carried out two times, and the data were combined (total n = 6 per treatment). Treatments were compared using repeated measurements ANOVA in GenStat using data which were square-root-transformed to stabilise variance. Statistical difference was declared between two

treatments for a given time point where the difference in means was greater than the LSD at 5%.

5.3.12 Global gene expression analysis

Caco-2 cell monolayers were co-cultured with *F. prausnitzii*, *L. rhamnosus*, UV-killed *F. prausnitzii* or control cell culture medium (without bacteria) for four hours in the apical anaerobic model (n = 3 per treatment). At the end of the incubation period, RNAprotect Cell Reagent (Qiagen) was added at a volume of approximately nine times the volume of the apical medium to lyse the Caco-2 cells and stabilise the RNA. RNA was isolated from each Caco-2 cell monolayer (section **Error! Reference source not found.**), and stored frozen at -80°C until needed. The experiment was carried out 2 times (total n = 6 per treatment), and the global gene expression profiles of the Caco-2 cells were analysed using Agilent Technologies 44k whole human genome oligonucleotide arrays (refer to section 4.3.5).

5.3.12.1 Experimental design

A 'reference' design was chosen for the microarray analysis, as the number of treatment groups in this experiment precluded a 'loop' design as used in the previous study (Chapter 4). Unlike the loop design which directly compared differential gene expression in two treatment groups, the reference design indirectly compares various treatment groups by comparing all samples to a universal reference sample[355]. Figure 5.1 graphically illustrates the two experimental designs for an experiment comprising four treatment groups. In a reference design, because treatments are not compared directly, the variance of the log fold change for a given gene will be higher than in a loop design, denoting lower statistical power[355]. However, as illustrated in Figure 5.1, where more than two treatment groups exist, the loop design becomes overly complex and requires a large number of arrays.

RNA abundance for all samples was therefore compared to a common reference cDNA that was prepared in one large pool from total RNA extracted from untreated Caco-2 cells harvested from a T125 cell culture flask. Amplified cDNA from each sample was labelled with cyanine-3, and hybridised to one array, along with cyanine-5 labelled reference cDNA. The slide and array positions were systematically chosen such

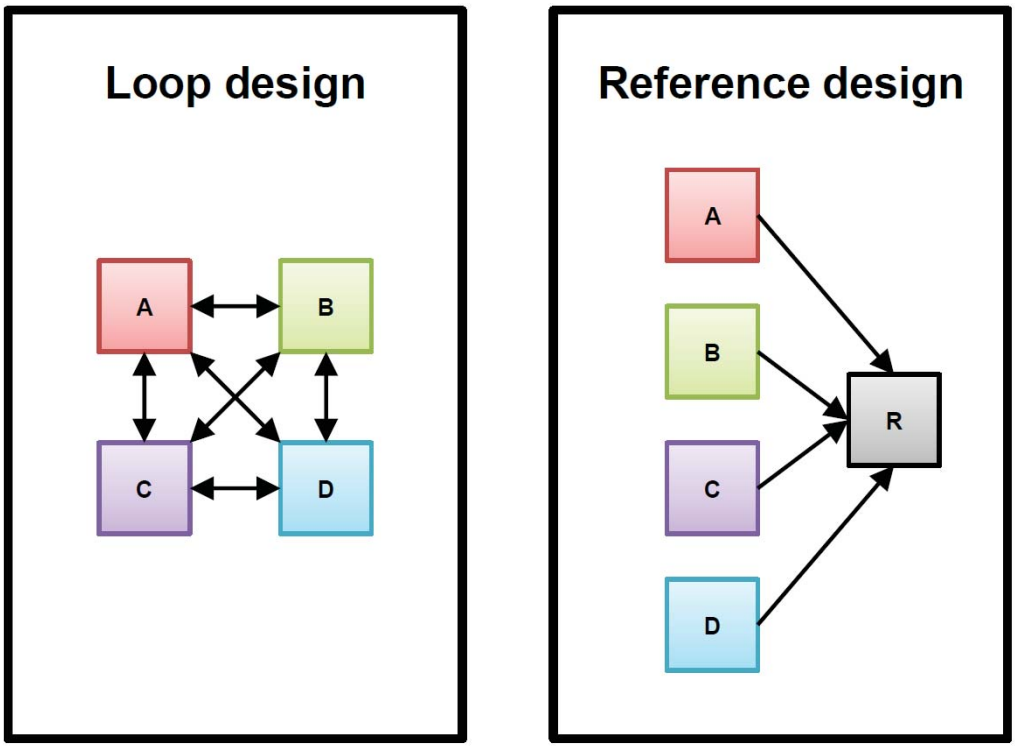

Figure 5.1 Design choices for the microarray experiment.

Two possible designs that compare gene expression in four treatment groups 'A', 'B', 'C' and 'D' are shown; R, reference. In a loop design, the differential expression of genes between two samples is measured directly on the same array. For any particular gene, the log fold change between treatment 'A' and 'B', for example, is calculated as $\log_2(A/B)$ for that gene[355]. In a reference design, expression levels of samples are measured in separate arrays. In this case the $\log_2$ fold change is the difference of two independent log ratios from the equation $\log_2(A/B) = \log_2(A/R) - \log_2(B/R)$ [355]. If the variance for one independent log ratio is σ^2, then the variance of the difference of two log ratios is $2\sigma^2$. Thus the variance of the log fold change for a given gene will be higher in a reference design, compared to a loop design.

that each slide received one sample from each treatment group, and samples from a given treatment were not placed on the same array position in more than two slides. Samples were randomly allocated to slides. The slide and array positions of the cyanine-3 labelled samples are shown in Table 5.4.

5.3.12.2 RNA isolation

Total RNA was extracted from the Caco-2 cells, and purified following quality control checks as described in section 4.3.3. However, an RNeasy mini plus kit (Qiagen) was used in the place of a standard RNeasy kit for RNA isolation, as this contained the necessary spin columns for a DNA elimination step which resulted in RNA of higher purity.

5.3.12.3 Gene expression analysis[***]

Differentially expressed genes were calculated as described in section 4.3.5. Genes that exhibited a fold change > 2 and $q < 0.05$ were determined to be differentially expressed. The programme Venny[356] was used to generate Venn diagrams showing the number of differentially expressed genes each treatment comparison had in common. IPA was used to cluster differentially expressed genes into functional groups and pathways, generate biological interaction networks, and predict upstream transcription regulators to explain the observed changes in gene expression (as described in section 4.3.7).

In addition, the R package 'Prediction Analysis of Microarrays for R' (pamr) was used to select genes that best differentiated the treatment groups from one another based on a 'shrunken centroids'[357] method. This subset of genes was subsequently analysed by principal component analysis (PCA) and hierarchical clustering, and visualised as a false colour heatmap.

To validate the microarray results, the expression of five genes, shown to be differentially expressed between Caco-2 cells treated with *F. prausnitzii* and Caco-2 cells treated with UV-killed *F. prausnitzii* were quantified using qPCR as described in

[***] Calculation of differentially expressed genes, class prediction of gene expression profiles in pamr, generation of the heatmap, and principal component analysis were performed by Dr Wayne Young (AgResearch Grasslands).

Table 5.4 Microarray design

Slide and array positions of cyanine-3 labelled samples. A, Caco-2 cells treated with *F. prausnitzii*; B, Caco-2 cells treated with *L. rhamnosus*; C, Caco-2 cells treated with UV-killed *F. prausnitzii*; D, Caco-2 cells with no treatment. RNA for samples labelled 1-3, and 4-6 for isolated from two different runs of the experiment.

Slide	*Array 1*	*Array 2*	*Array 3*	*Array 4*
1	A4	B3	C6	D5
2	B1	C1	D2	A6
3	C5	D3	A3	B4
4	D4	A1	B5	C4
5	A2	D1	C2	B6
6	B2	C3	D6	A5

section 4.3.6. The genes selected for analysis, as well as the reference genes used, are shown on Table 5.5. The selected reference genes were chosen because they were shown to be expressed in all samples, and had minimal variation in expression levels across treatments according to microarray analysis. Correlation between microarray and qPCR results was tested by Spearman rho correlation analysis in R.

5.4 RESULTS

5.4.1 Confirmation of bacterial strains

The identities of *F. prausnitzii* and *L. rhamnosus* were confirmed by comparing their 16S rRNA gene sequences with known bacterial sequences in the NCBI nucleotide collection database. The trace of *F. prausnitzii* produced a significant alignment with the sequence of 'Butyrate-producing bacterium A2-165 16S rRNA gene', which provided the highest sequence identity (98%) of all sequences not from an 'uncultured clone'. As A2-165 is the strain designation for *F. prausnitzii* DSM17677, the identity of this strain was confirmed. Of the top 20 sequences which produced significant alignment with the 16S trace of *L. rhamnosus*, 17 sequences were that of the 16S rRNA gene of *L. rhamnosus*. The other 3 sequences were that of the 16S rRNA gene of 2 *Lactobacillus* species and an uncultured clone. Thus the sequence identity of this strain was confirmed as *L. rhamnosus*.

5.4.2 Growth Curve

The growth curve (Figure 5.2) indicated that *L. rhamnosus* reached stationary phase between 10 and 12 hours, while *F. prausnitzii* reached stationary phase between 12 and 14 hours. However, when *F. prausnitzii* cultures were allowed to grow undisturbed (i.e. OD not measured at the 2-10 hour time points), the OD consistently reached its maximum (approximately 1.1), within a 12 hour period. Based on these data, the 12 hour old secondary cultures of bacteria were deemed to be at stationary phase, and prepared for co-culture experiments.

Table 5.5 Genes selected for qPCR analysis.

Genes selected for validation of microarray study by qPCR. Target genes were selected to include those that showed significant differential expression between Caco-2 cells treated with *F. prausnitzii* and Caco-2 cells treated with UV-killed *F. prausnitzii* by microarray analysis. Reference genes were expressed in all samples, and the variation in expression levels across treatments was low and non-significant according to microarray analysis. Reactions were carried out using pre-designed and pre-validated PrimeTime primer/probe mixes indicated in the 'IDT assay' column.

Type	*Gene*	*Gene symbol*	*Transcript location*	*IDT assay*
Target gene	serpin peptidase inhibitor, clade A	*SERPINA3*	NM_001085	Hs.PT.56a. 15580605
	chemokine (C-C motif) ligand 20	*CCL20*	NM_004591	Hs.PT.56a. 19355926
	interleukin 8	*IL8*	NM_000584	Hs.PT.56a. 39926886.g
	heparin-binding EGF-like growth factor	*HBEGF*	NM_001945	Hs.PT.56a. 2450091
	sprouty-related, EVH1 domain containing protein 1	*SPRED1*	NM_152594	Hs.PT.56a. 24271959
Reference gene	ribosomal protein S2	*RPS2*	NM_002952	Hs.PT.56a. 22843181
	glyceraldehyde-3-phosphate dehydrogenase	*GAPDH*	NM_002046	Hs.PT.39a. 22214836

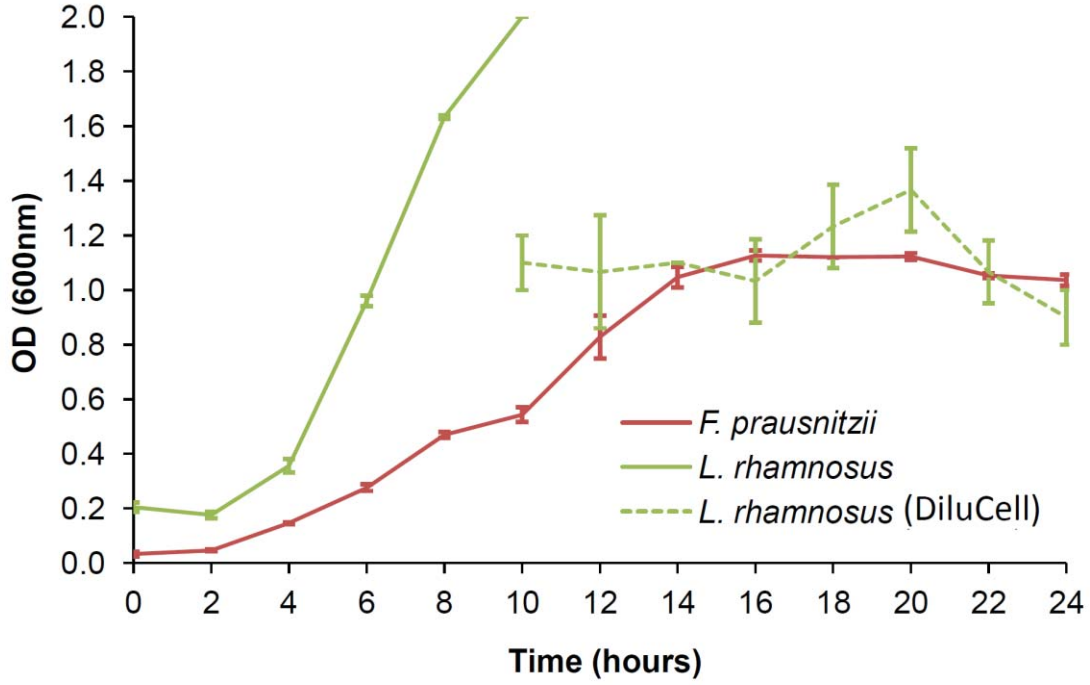

Figure 5.2 Growth curves for *F. prausnitzii* and *L. rhamnosus*.

Each growth curve shows the mean (+/- SEM) OD over time (n = 3). *F. prausnitzii* was cultured in anaerobic BHI broth at 37°C in Hungate culture tubes sealed with butyl rubber stoppers. *L. rhamnosus* was cultured in MRS broth at 37°C, 5% CO_2. When the OD of the *L. rhamnosus* sample reached the maximum capacity of the spectrophotometer, the OD was measured in a DiluCell cuvette which virtually diluted the sample by a factor of 10. The *L. rhamnosus* (DiluCell) curve shows the mean OD read by the spectrophotometer multiplied by a factor of 10.

5.4.3 Viability of bacteria in the apical anaerobic model

First, the ability of bacteria to survive and grow in anaerobic cell culture medium, with or without FBS, was determined by comparing the CFU before and after incubation at 37°C inside an anaerobic workstation for 12 hours. The number of CFU had not dropped after the 12 hour incubation (Figure 5.3).

The viability of *F. prausnitzii* and *L. rhamnosus* in the apical anaerobic model was then determined by comparing the CFU before and after 8 hours of co-culture of Caco-2 cells in the anaerobic apical environment. *F. prausnitzii* was found to be almost solely in the cell culture medium, while significant amounts of *L. rhamnosus* were present both in the cell culture medium and the Caco-2 cell lysate, indicating that in an anaerobic environment *L. rhamnosus*, but not *F. prausnitzii*, attaches to Caco-2 cells (Figure 5.4a). In the apical anaerobic model, the total *F. prausnitzii* CFU (in cell culture medium and cell lysate) reduced by less than 1 log after an 8 hour incubation. When cultured in cell culture medium at 37°C under standard atmospheric conditions however, the *F. prausnitzii* CFU reduced by over 4 logs within 30 minutes (Figure 5.4b). The total *L. rhamnosus* CFU was not altered after 8 hours in the apical anaerobic model.

5.4.4 Effect of bacteria on TEER

The effect of live *F. prausnitzii*, UV-killed *F. prausnitzii*, and *L. rhamnosus* on intestinal barrier integrity was measured using the TEER assay (Figure 5.5). All treatments and the control (cell culture medium without bacteria) resulted in an immediate drop in TEER. The TEER tended to recover over the next 4 hours, and then decrease slightly over the remaining 4 hours. While none of the treatments differed significantly from each other at any time point, the TEER of Caco-2 cells treated with bacterial cells consistently recovered faster than Caco-2 cells treated with control cell culture medium in each experiment.

5.4.5 Effect of bacteria on ^{3}H-mannitol permeability

Changes in small molecule permeability across Caco-2 cell monolayers in in response to live *F. prausnitzii*, UV-killed *F. prausnitzii*, and *L. rhamnosus* was measured using

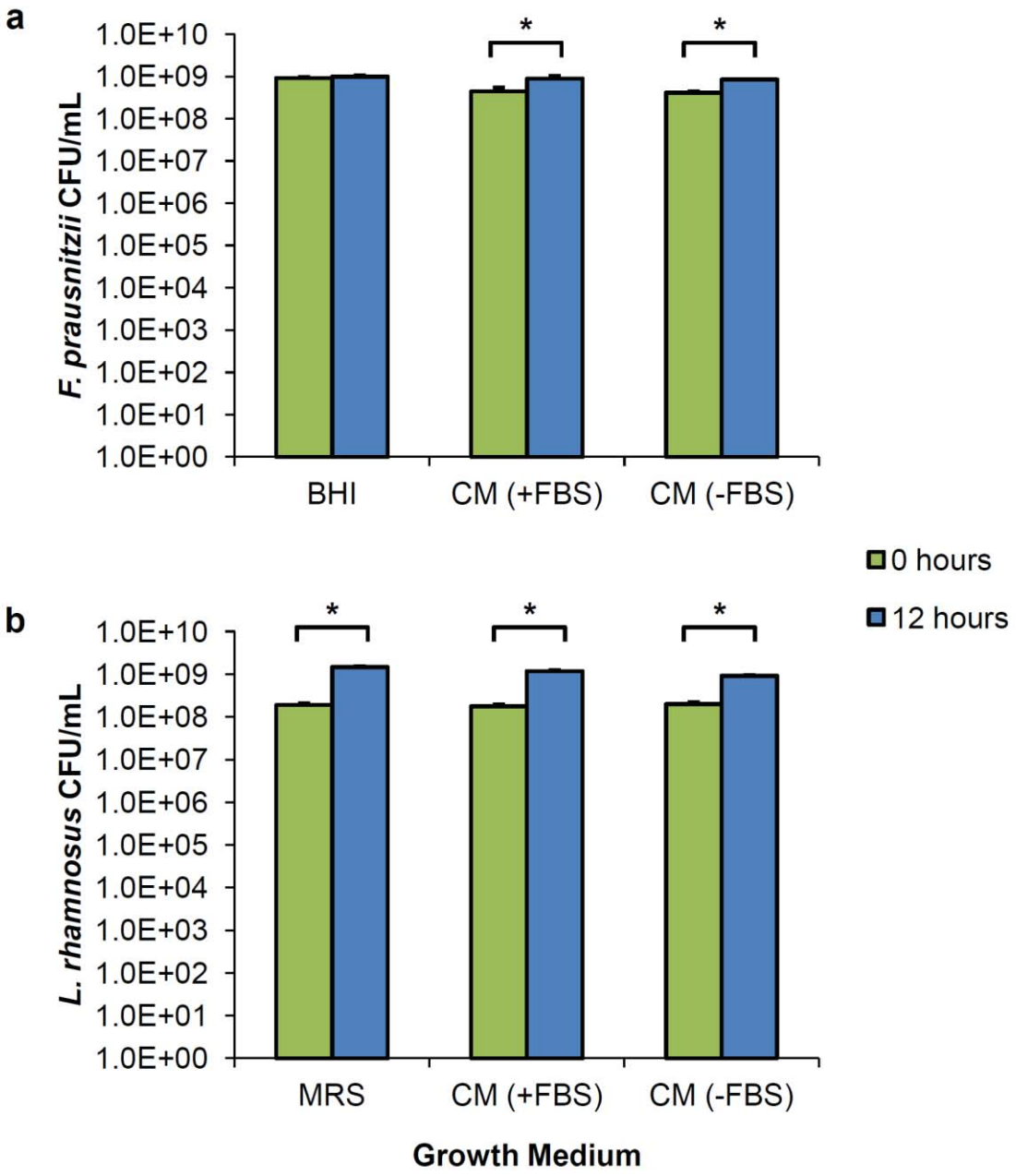

Figure 5.3 Viability of bacteria in the anaerobic cell culture medium.

Graphs show mean (+/- SEM; n = 3) CFU/mL of *F. prausnitzii* (a) and *L. rhamnosus* (b) at 0 and 12 hours grown in anaerobic cell culture medium or BHI or MRS broth. CM, anaerobic cell culture medium with (+) or without (-) FBS. * $P < 0.05$.

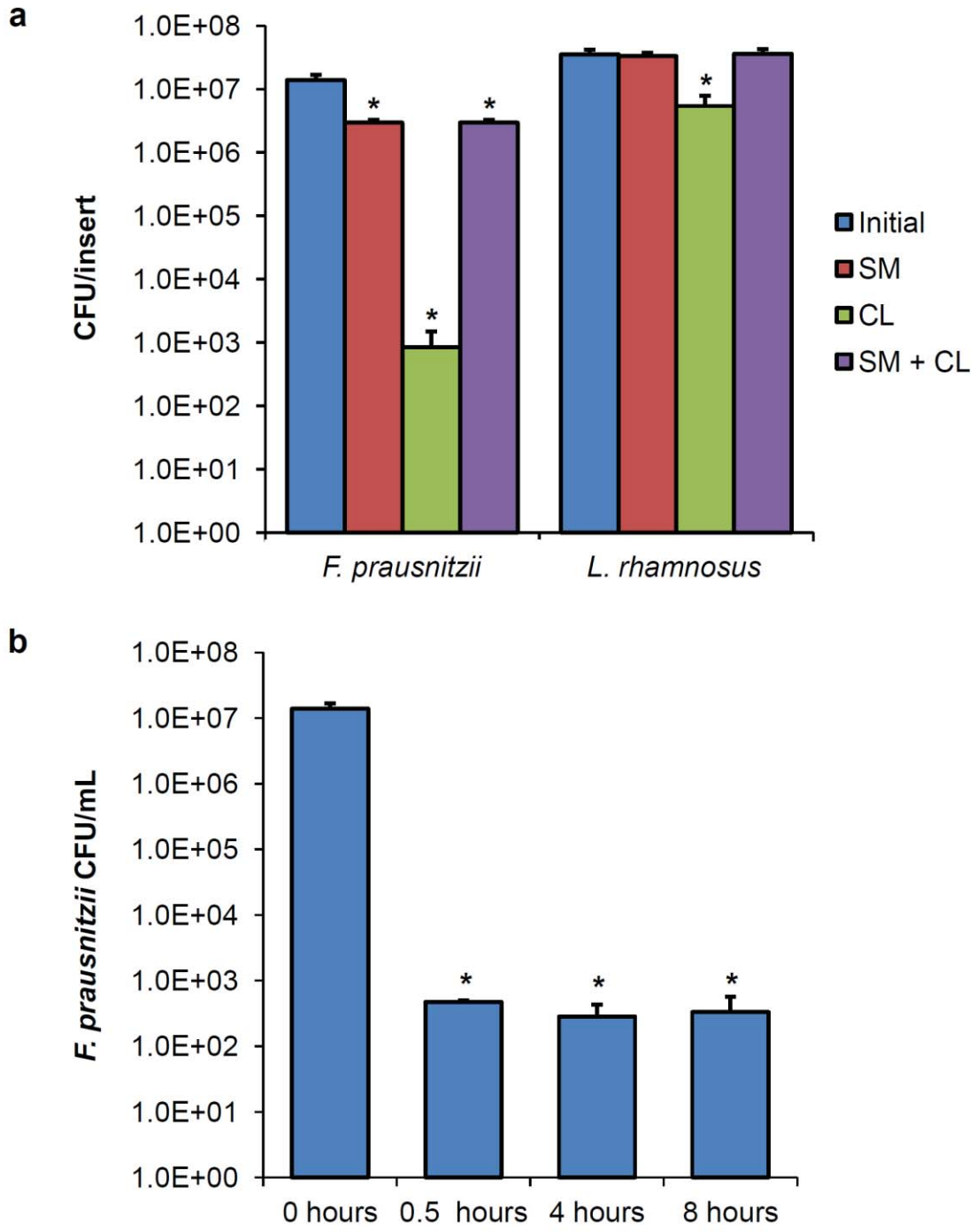

Figure 5.4 Bacterial viability in the apical anaerobic environment and standard atmospheric conditions.

(a) Amount of bacteria added to the apical compartment (initial), and the amount of bacteria present after 12 hours in the cell culture medium (spent media; SM), cell lysate (CL), and in total (SM + CL). Graphs show mean (+/- SEM) CFU per insert (n = 6; 2 experiments, 3 samples per treatment per experiment). (b) Viability of *F. prausnitzii* prior to and on exposure to standard atmospheric conditions for 0.5, 4 and 8 hours. Graphs show mean (+/- SEM) CFU per insert (n = 3). * P > 0.05 compared to initial/ 0 hours.

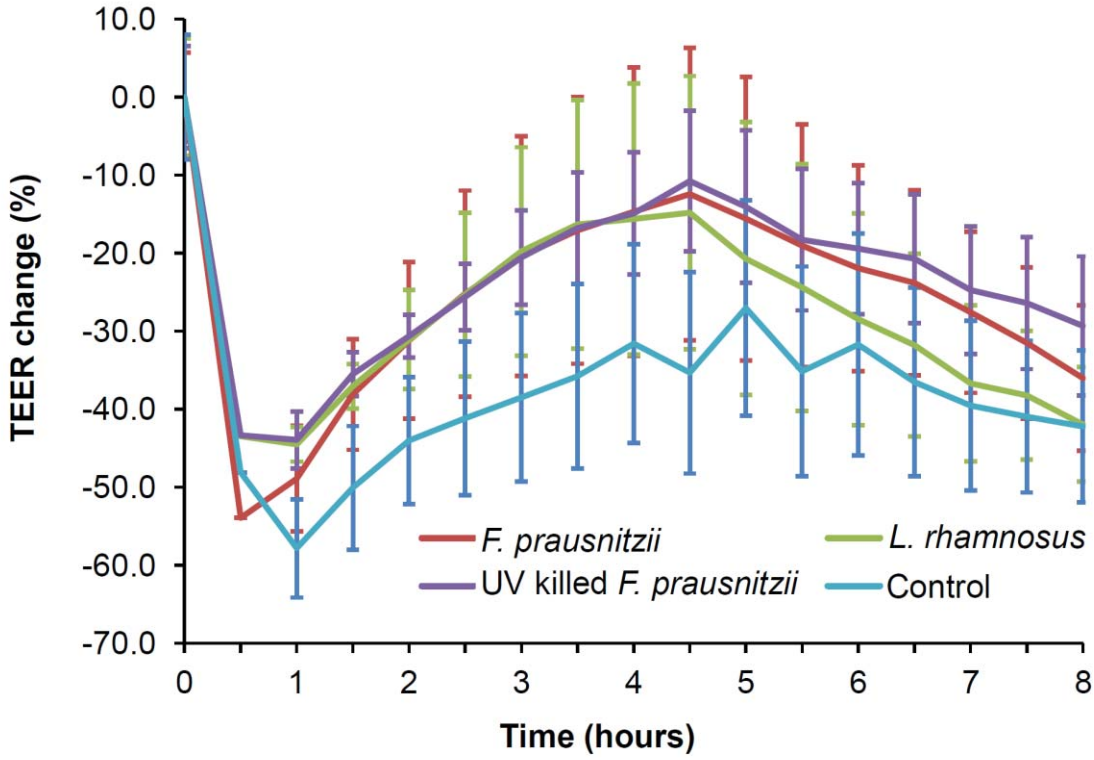

Figure 5.5 Effect of bacteria on TEER across Caco-2 cell monolayers in the apical anaerobic model over time.

Change in TEER across Caco-2 cell monolayers co-cultured with *F. prausnitzii*, *L. rhamnosus*, UV-killed *F. prausnitzii* or no bacteria in an apical anaerobic environment. The graph shows the mean (+/- SEM) change in TEER (*F. prausnitzii* and *L. rhamnosus*: n = 5, UV-killed *F. prausnitzii* and control: n = 6; 3 experiments, 1-3 samples per treatment per experiment). The mean TEER did not differ between treatments at any time point.

the ^{3}H-mannitol bioassay (Figure 5.6). Approximately 15% of mannitol crossed over from the apical to the basal compartment within 2 hours where Caco-2 cells had been treated with *L. rhamnosus*, while it was less than 5% for all other treatment groups even at the 8 hour time point. The amount of ^{3}H-mannitol in the basal compartment was significantly higher in Caco-2 cells treated with *L. rhamnosus* compared with the control at each time point. None of the other treatment groups differed from the control at the 95% confidence level, except for Caco-2 cells treated with live *F. prausnitzii* which had more mannitol pass through from the apical to the basal compartment at the 8 hour time point compared to the control.

5.4.6 Differentially expressed genes

Global gene expression analysis was used to identify key differences in gene expression between Caco-2 cells co-cultured with *F. prausnitzii, L. rhamnosus,* UV-killed *F. prausnitzii* or cell culture medium only (i.e. untreated) for 4 hours. The number of genes where the expression level was altered is shown in Table 5.6 for each treatment comparison. The qPCR results confirmed the direction of fold change for the five genes measured in the *F. prausnitzii* vs. UV-killed *F. prausnitzii* comparison (Table 5.7). Furthermore, fold change between microarray and qPCR results showed a strong correlation (Spearman rho = 0.90) supporting the validity of the microarray results.

The largest difference in gene expression was seen between Caco-2 cells co-cultured with *F. prausnitzii* and untreated Caco-2 cells, where 61 genes had decreased in expression in Caco-2 cells treated with *F. prausnitzii*. On the contrary, only 4 genes were differentially expressed between Caco-2 cells co-cultured with *L. rhamnosus* and untreated Caco-2 cells. Thus comparisons between Caco-2 cells co-cultured with *L. rhamnosus* and untreated Caco-2 cells were not considered for pathway analysis.

Three genes were shared in common within differentially expressed genes between Caco-2 cells co-cultured with *F. prausnitzii* compared to Caco-2 cells treated with UV-killed *F. prausnitzii,* and Caco-2 cells co-cultured with *F. prausnitzii, L. rhamnosus,* or UV-killed *F. prausnitzii* compared to untreated Caco-2 cells (Figure 5.7). The largest overlap in differentially expressed genes was found between Caco-2 co-cultured with *F. prausnitzii* compared with untreated Caco-2 cells and Caco-2 cells treated with *F. prausnitzii* compared with Caco-2 cells treated with UV-killed *F.*

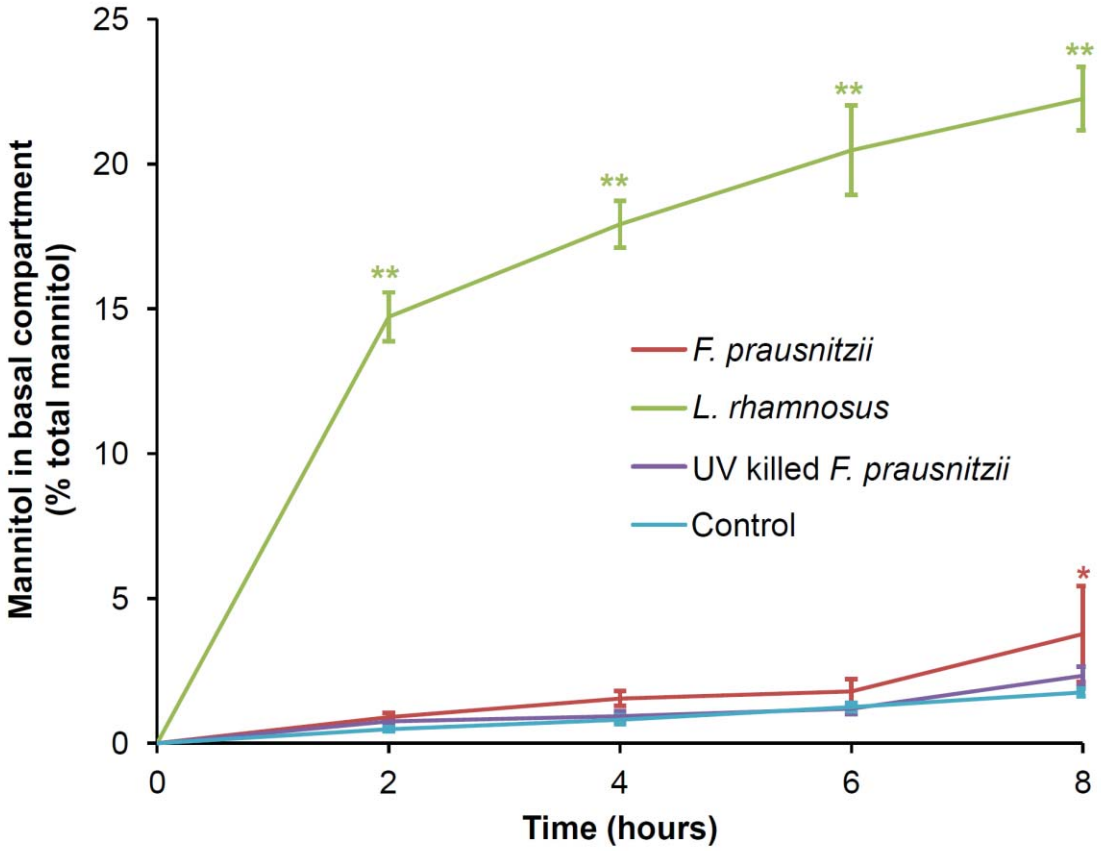

Figure 5.6 Effect of bacteria on permeability of Caco-2 cell monolayers in the apical anaerobic model.

Permeability of ^{3}H-mannitol across Caco-2 cell monolayers co-cultured with *F. prausnitzii*, *L. rhamnosus*, UV-killed *F. prausnitzii* or no bacteria. The graph shows the mean (+/- SEM) % of ^{3}H-mannitol in the cell culture insert that crossed the Caco-2 cell monolayer to the chamber well (n = 6; 2 experiments, 3 samples per treatment per experiment). * $P < 0.05$, ** $P < 0.01$, compared to control.

Table 5.6 Numbers of genes differentially expressed by the Caco-2 cells.

Number of differentially expressed genes in Caco-2 cells co-cultured with bacteria for 4 hours (fold change > 2, q < 0.05). 'Increased expression' indicates the number of genes more highly expressed in the first treatment in the comparison, 'Decreased expression' indicates the number of genes more highly expressed in the second treatment of the comparison (Fp, *F. prausnitzii*; Lr, *L. rhamnosus*; UV Fp, UV-killed *F. prausnitzii*; NB, no treatment).

Comparison	*Increased expression*	*Decreased expression*
Fp vs. Lr	0	38
Fp vs. UV Fp	5	40
Fp vs. NB	0	61
Lr vs. UV Fp	15	2
Lr vs. NB	0	4
UV Fp vs. NB	0	24

Table 5.7 Validation of microarray results by qPCR.

Gene expression fold change and P-value (for qPCR data) or *q* (for microarray data) for the five genes validated using qPCR analysis. Fold change value indicates fold difference in expression between treatments; a positive value indicates higher expression level in Caco-2 cells treated with *F. prausnitzii* (compared to Caco-2 cells treated with UV-killed *F. prausnitzii*), and a negative value indicates a lower expression level.

Gene	*qPCR*		*Microarray*	
	Fold change	*P-value*	*Fold change*	q
SERPINA3	-4.46	0.001	-2.98	<0.001
CCL20	-3.57	0.001	-4.59	<0.001
IL8	-2.51	0.001	-2.84	<0.001
HBEGF	2.48	<0.001	2.39	<0.001
SPRED1	2.12	0.001	2.05	0.002

prausnitzii. The highest number of unique differentially expressed genes was found in the comparison between Caco-2 cells treated with *F. prausnitzii* and untreated Caco-2 cells.

Figure 5.8 shows a heatmap of the gene expression, which clearly illustrates that gene expression across samples clustered by treatment group. However, gene expression of Caco-2 cells co-cultured with *L. rhamnosus* also tended to cluster with that of Caco-2 cells co-cultured with UV-killed *F. prausnitzii* (samples 1-3), and no bacteria (samples 4-6). This strongly suggests a difference in gene expression between the two runs of the experiment for the *L. rhamnosus* treated samples. This difference is further illustrated by the PCA profiles (Figure 5.9), where the Caco-2 cells treated with *F. prausnitzii*, UV-killed *F. prausnitzii* or no bacteria, group into individual clusters, but samples from the *L. rhamnosus* treatment forms two distinct clusters based on the two individual runs of the experiment, and samples 4 to 6 overlap with the samples that were not treated with bacteria.

5.4.7 Biological interaction networks

Differentially expressed genes were examined for networks of biological interaction relationships using IPA. The highest ranked interaction network generated from differentially expressed genes between Caco-2 cells treated with *F. prausnitzii* and untreated Caco-2 cells (score = 31) is shown in Figure 5.10. This interaction network was associated with the IPA biological functions 'Cell Signalling', 'Humoral Immune Response', and 'Protein Synthesis'. The interaction network generated from differentially expressed genes between Caco-2 cells treated with UV-killed *F. prausnitzii* and untreated Caco-2 cells (score = 26; Figure 5.11), was associated with the biological functions 'Cellular Movement', 'Hematological System Development and Function' and 'Immune Cell Trafficking'. When comparing Caco-2 cells treated with *F. prausnitzii* and Caco-2 cells treated with UV-killed *F. prausnitzii*, the highest ranked interaction network (score = 27) was also associated with the functions 'Cellular Movement' and 'Immune Cell Trafficking', as well as 'Cell-to-Cell Signalling and Interaction' (Figure 5.12). The interaction network generated from differentially expressed genes between Caco-2 cells treated with *L. rhamnosus* and untreated Caco-2

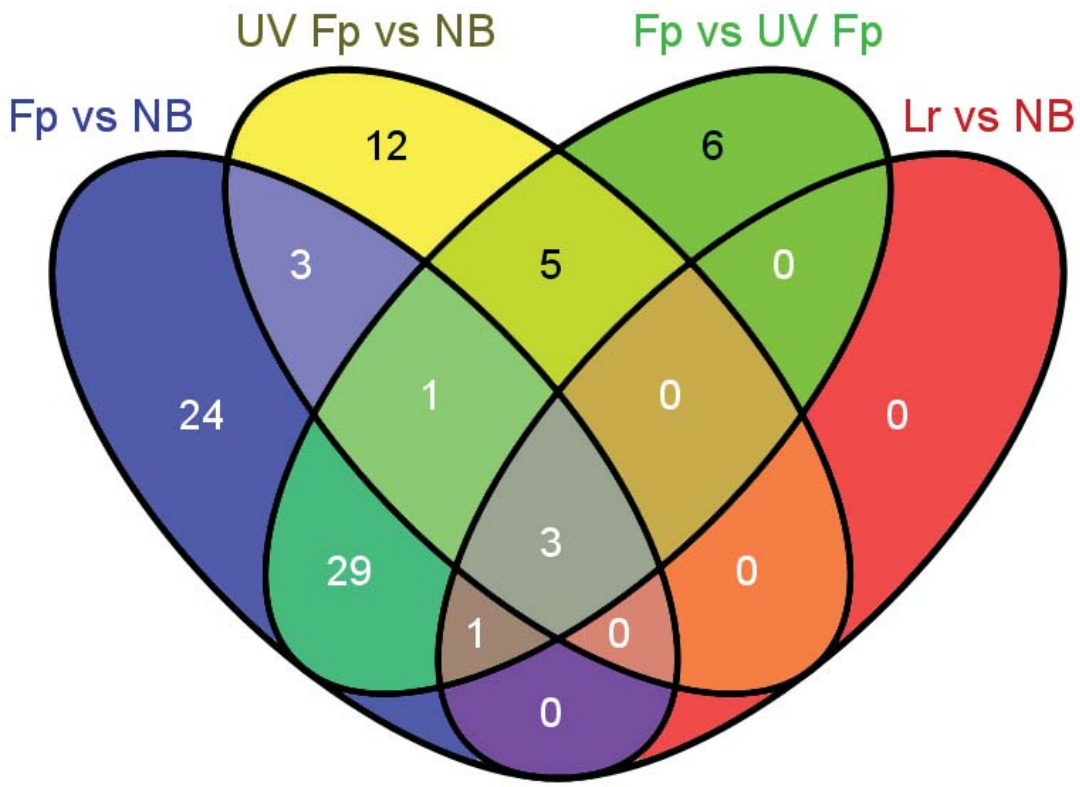

Figure 5.7 Numbers of shared and unique differentially expressed genes by Caco-2 cells treated with various bacteria.

Venn diagram showing the number of differentially expressed genes for each comparison and how many were shared between each comparison (Fp, *F. prausnitzii*; NB, no treatment; UV Fp, UV-killed *F. prausnitzii*; Lr, *L. rhamnosus*).

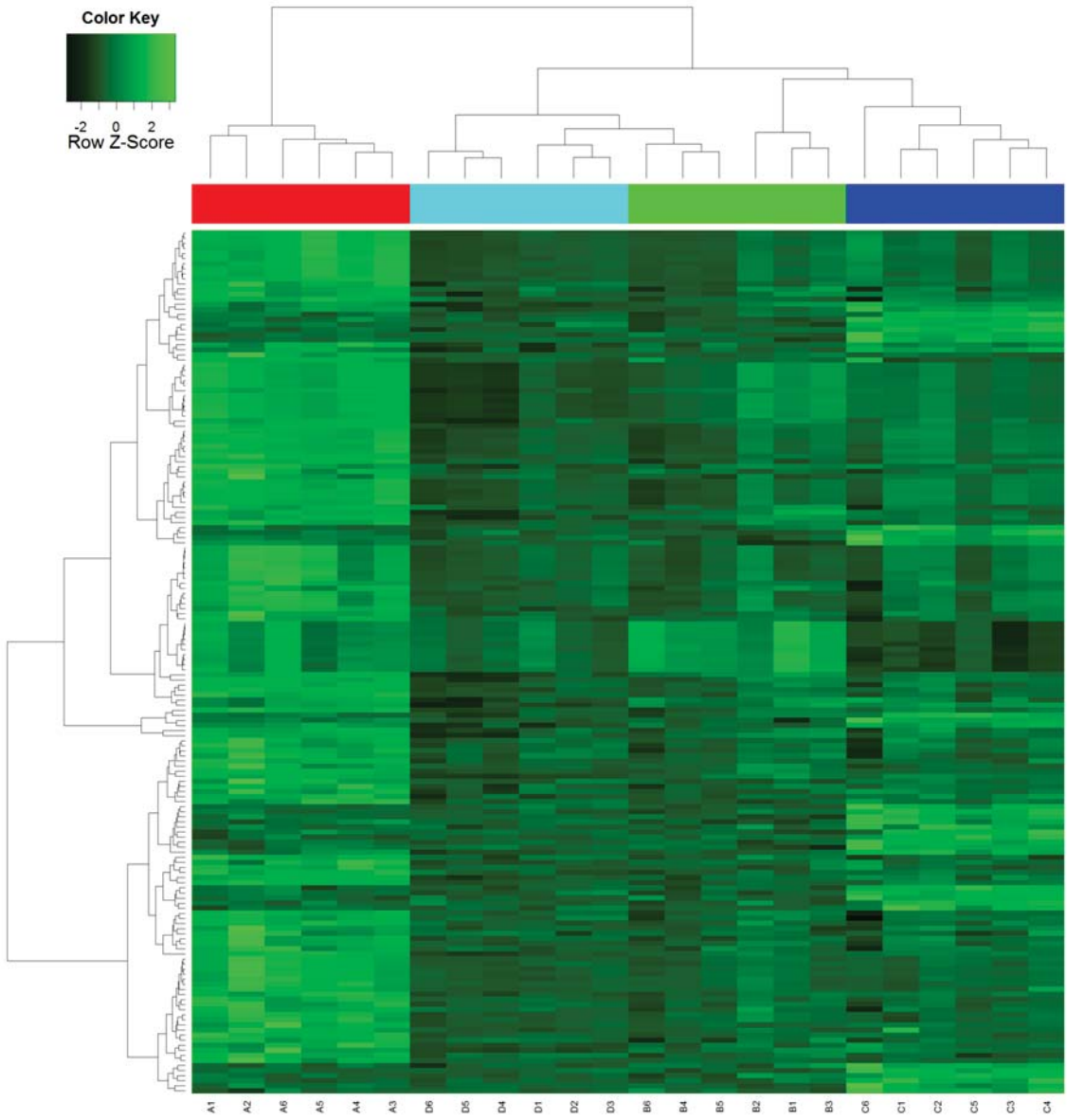

Figure 5.8 Heatmap of gene expression levels in Caco-2 cells treated with various bacteria.

Heatmap showing the expression levels of genes, predicted by pamr to characterise treatment groups, across samples. Individual genes are represented by rows with samples in columns (A, *F. prausnitzii*; B, *L. rhamnosus*; C, UV-killed *F. prausnitzii*; D, no treatment; RNA for samples labelled 1-3, and 4-6 were isolated from two different runs of the experiment). Heatmap colours indicate expression of genes relative to reference RNA, expressed as a standardised score with a mean of zero and standard deviation of one, with black indicating a scaled value less than zero (decreased expression) and green indicating a scaled value greater than zero (increased expression). Dendrograms show clustering of samples and genes based on similarity of gene expression profiles between samples (columns), and similarity of expression for each gene across samples (rows). Colour blocks above the heatmap represent the treatment groups (red, *F. prausnitzii*; green, *L. rhamnosus*; dark blue, UV-killed *F. prausnitzii*; light blue, no treatment).

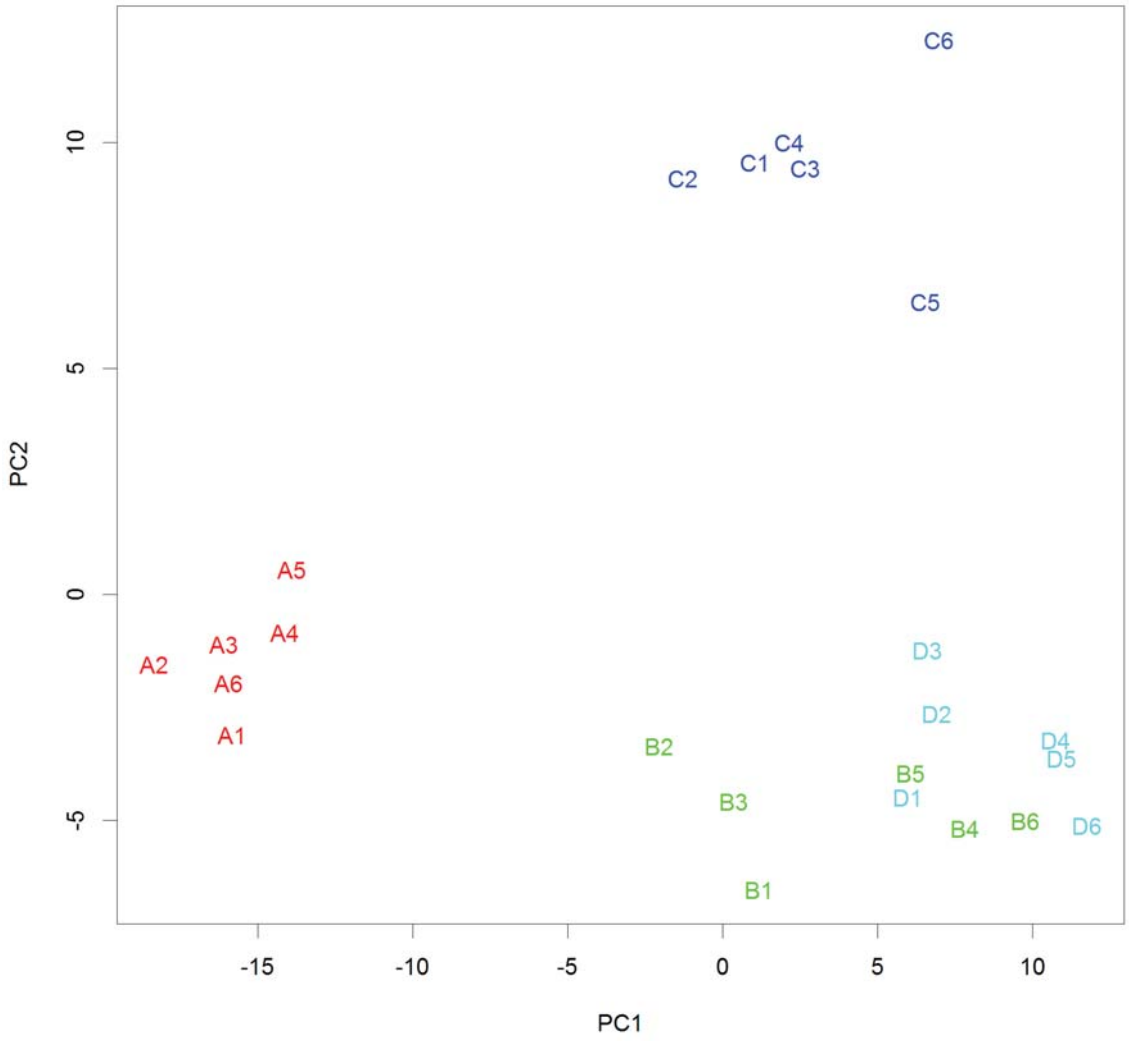

Figure 5.9 Principal component analysis profile of gene expression by Caco-2 cells treated with various bacteria.

PCA plot of expression profiles of genes predicted by pamr to characterise treatment groups. Each data point indicates a gene expression profile from one sample. A, *F. prausnitzii*; B, *L. rhamnosus*; C, UV-killed *F. prausnitzii*; D, no treatment. RNA for samples labelled 1-3, and 4-6 were isolated from two different runs of the experiment.

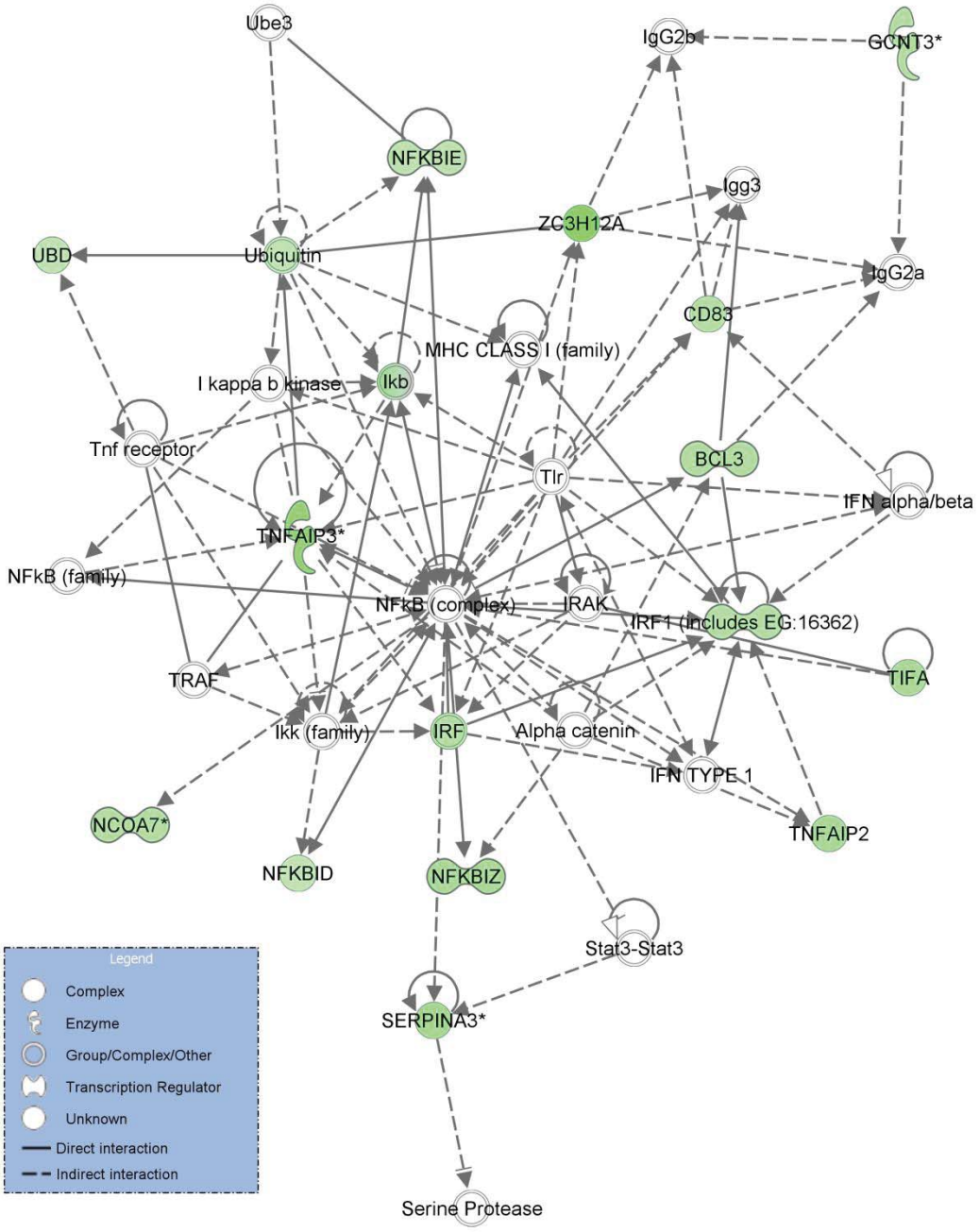

Figure 5.10 Network of differentially expressed genes in Caco-2 co-cultured with *F. prausnitzii* (compared to Caco-2 cells not treated with bacteria).

Genes are represented by nodes and interactions represented by edges. Genes with decreased expression in Caco-2 cells treated with *F. prausnitzii* (compared to Caco-2 cells not treated with bacteria) are depicted in shades of green. Intensity of colour indicates degree of fold change, with greater intensity signifying higher expression level. Node shape indicates functional class of gene product as indicated in legend.

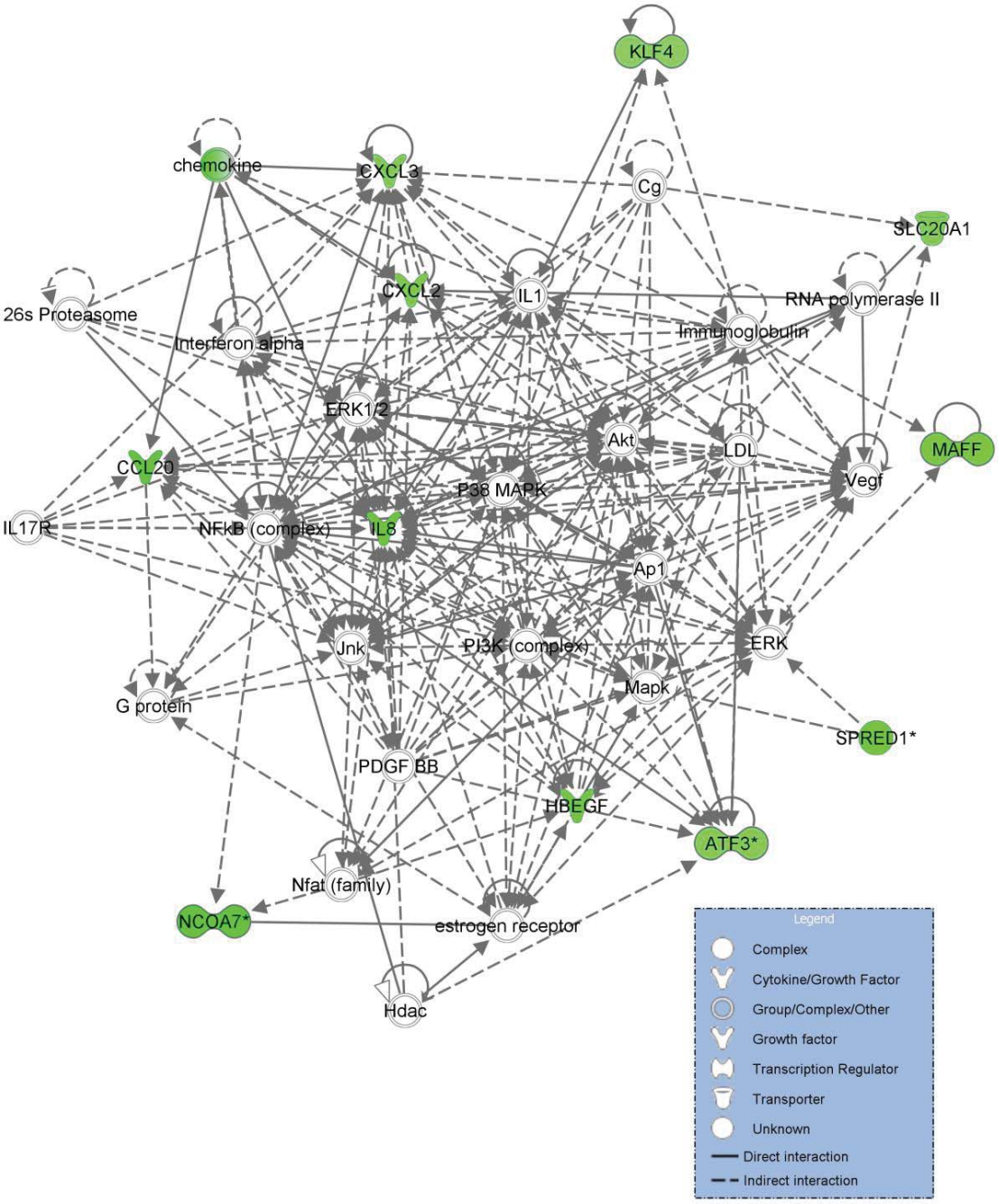

Figure 5.11 Network of differentially expressed genes in Caco-2 co-cultured with UV-killed *F. prausnitzii* (compared to Caco-2 cells not treated with bacteria).

Genes are represented by nodes and interactions represented by edges. Genes with decreased expression in Caco-2 cells treated with UV-killed *F. prausnitzii* (compared to Caco-2 cells not treated with bacteria) are depicted in shades of green. Intensity of colour indicates degree of fold change, with greater intensity signifying higher expression level. Node shape indicates functional class of gene product as indicated in legend.

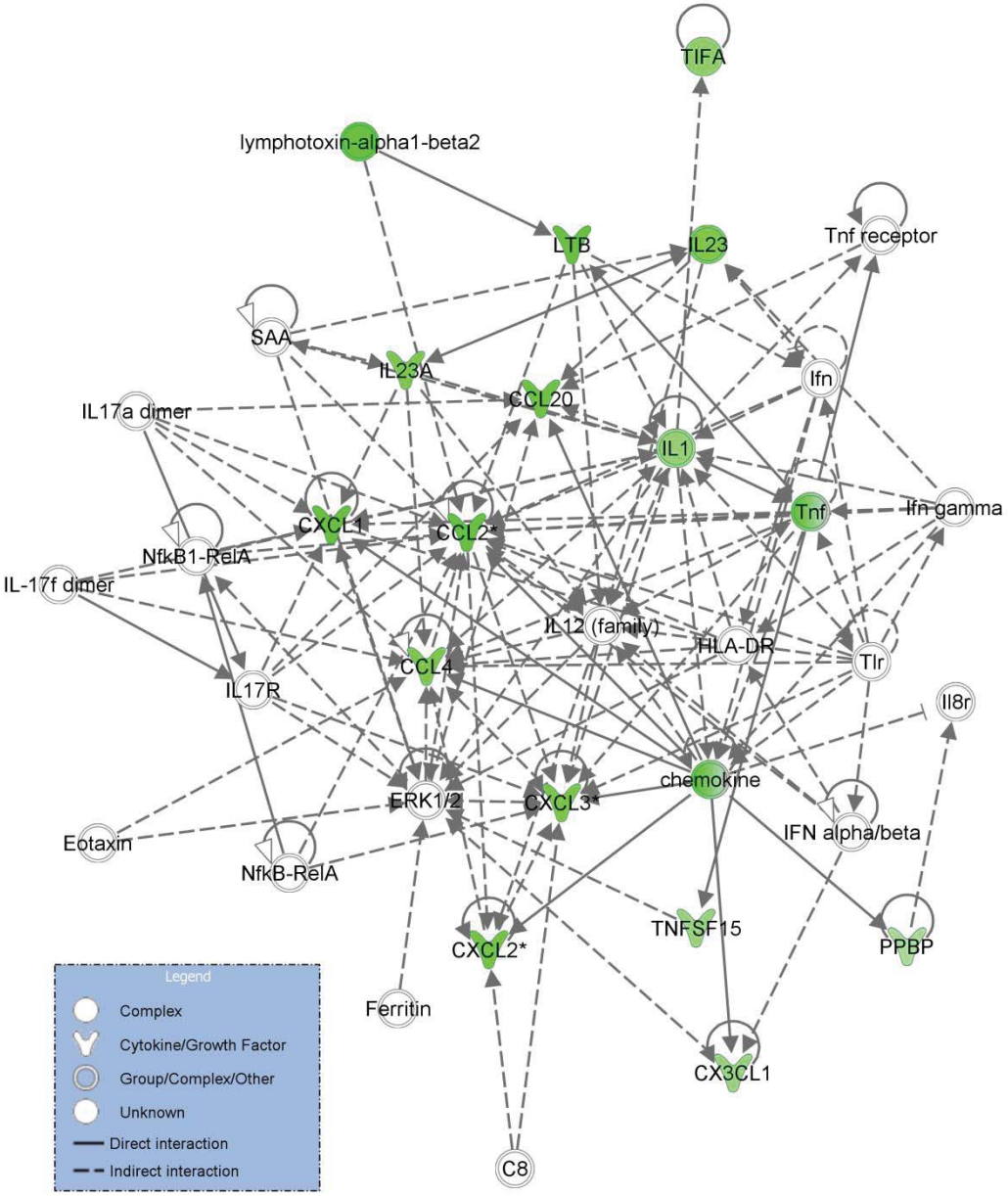

Figure 5.12 Network of differentially expressed genes in Caco-2 co-cultured with *F. prausnitzii* (compared to Caco-2 cells treated with UV-killed *F. prausnitzii*).

Genes are represented by nodes and interactions represented by edges. Genes with decreased expression in Caco-2 cells treated with *F. prausnitzii* (compared to Caco-2 cells treated with UV-killed *F. prausnitzii*) are depicted in shades of green. Intensity of colour indicates degree of fold change, with greater intensity signifying higher expression level. Node shape indicates functional class of gene product as indicated in legend.

cells (score = 9; Figure 5.13), was associated with the biological functions 'Infectious Disease', 'Inflammatory Response' and 'Cardiovascular System Development and Function'.

5.4.8 Biological functions associated with differentially expressed genes

The IPA functional analysis identified the biological functions that were most significantly over-represented among the list of differentially expressed genes. In Caco-2 cells co-cultured with *F. prausnitzii*, compared with Caco-2 cells not treated with bacteria, six biological functions (grouped into eight functional categories) were predicted to be increased, while 139 biological functions (grouped into 28 functional categories) were predicted to be decreased, based on the expression direction of the differentially expressed genes (Table 5.8). Functions predicted to be decreased largely belonged to the 'inflammatory response' and 'immune cell trafficking' categories, while predicted decreased functions belonged to the 'infectious disease' and 'cellular growth and proliferation' categories.

Caco-2 cells co-cultured with UV-killed *F. prausnitzii* were only predicted to have two and four biological functions increased and decreased respectively compared to untreated Caco-2 cells (Table 5.9). Similar to cells treated with live bacteria, the predicted increased and decreased functions belonged to the 'cellular growth and proliferation' and 'immune cell trafficking' categories respectively. However, unlike in Caco-2 cells co-cultured with live *F. prausnitzii*, the functions predicted to be increased were associated with the 'inflammatory response' category.

Compared with Caco-2 cells co-cultured with UV-killed *F. prausnitzii*, Caco-2 cells co-cultured with live *F. prausnitzii* had two biological functions increased (grouped into six functional categories) and 112 biological functions decreased (grouped into 31 functional categories) (Table 5.10). Many of these functions are similar to those of the first comparison (Table 5.8) indicating that the effect of UV-killed *F. prasunitzii* on Caco-2 was minimal compared to the effect of live *F. prausnitzii*.

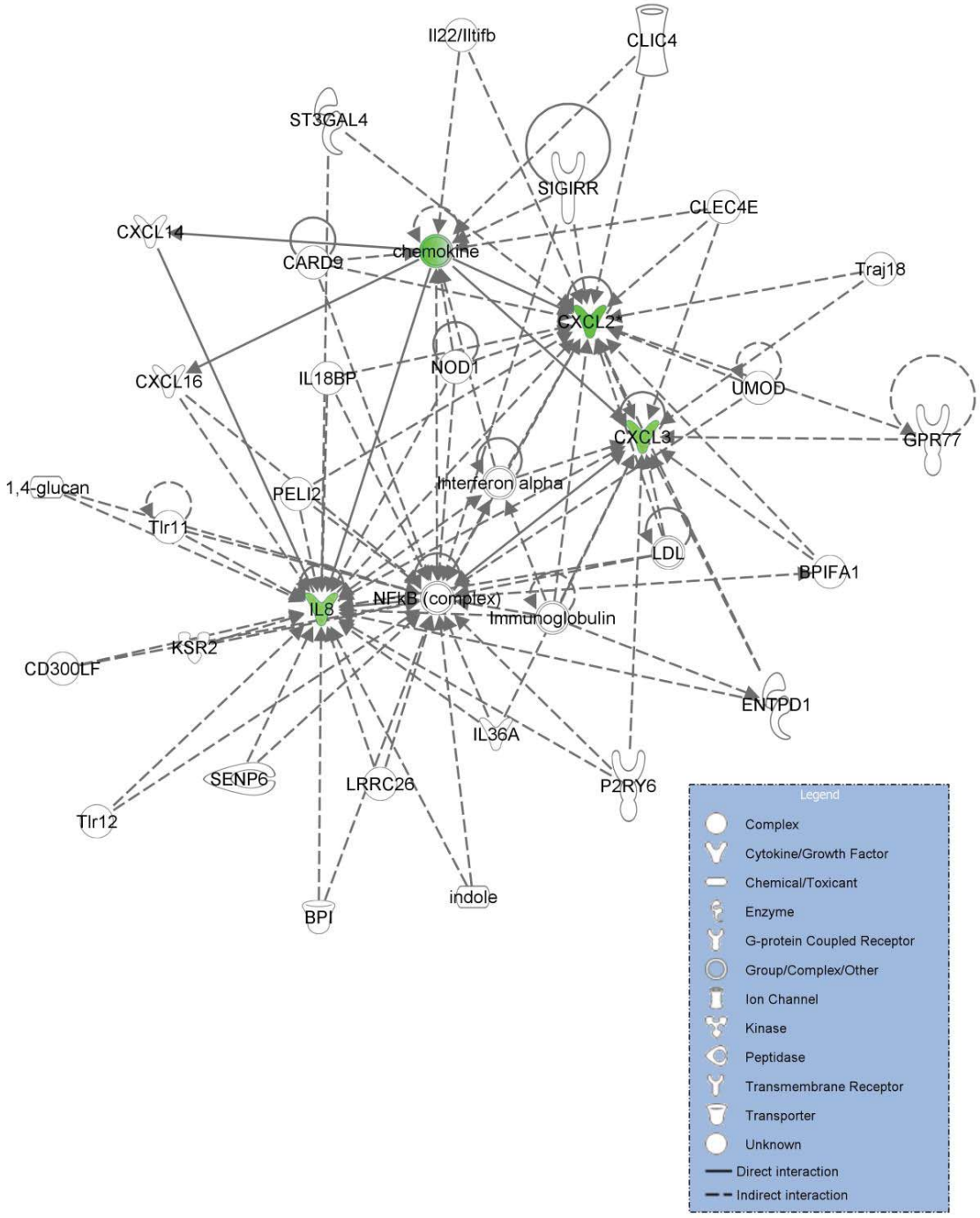

Figure 5.13 Network of differentially expressed genes in Caco-2 co-cultured with *L. rhamnosus* (compared to Caco-2 cells not treated with bacteria).

Genes are represented by nodes and interactions represented by edges. Genes with decreased expression in Caco-2 cells treated with *L. rhamnosus* (compared to Caco-2 cells not treated with bacteria) are depicted in shades of green. Intensity of colour indicates degree of fold change, with greater intensity signifying higher expression level. Node shape indicates functional class of gene product as indicated in legend.

Table 5.8 Key biological functions predicted to be increased or decreased in Caco-2 cells co-cultured with *F. prausnitzii* (compared to Caco-2 cells not treated with bacteria).

The P-value was calculated using the right-tailed Fisher Exact Test by considering the number of differentially expressed genes that participate in the function, and the total number of genes that are known to be associated with that function in the Ingenuity Knowledge Base. Given the observed differential regulation of a gene (up or down), the Z-score was used to determine the activation state of the biological function by the direction of effect associated with the relationship from the gene to the function. An absolute Z-score of ≥ 2 was considered significant (function activated if Z-score ≥ 2; inhibited if Z-score ≤ -2). Only the top 20 'decreased' functions (based on P-value) are shown. 'Genes' indicates the number of differentially expressed genes associated with the function.

Predicted activation	*Function*	*P-value*	*Z-score*	*Genes*
Increased	bacterial infection	<0.001	2.145	18
	infection of mammalia	<0.001	2.841	13
	proliferation of myeloid progenitor cells	<0.001	2.449	6
	organismal death	<0.001	2.458	22
	quantity of Single positive thymocytes	<0.001	2.236	5
	parasitic infection	<0.001	2.183	6
Decreased	recruitment of monocytes	<0.001	-2.395	10
	cell movement of neutrophils	<0.001	-3.284	16
	recruitment of neutrophils	<0.001	-2.492	13
	attraction of leukocytes	<0.001	-3.092	10
	inflammatory response	<0.001	-2.807	22
	attraction of phagocytes	<0.001	-2.958	9
	recruitment of phagocytes	<0.001	-2.846	14
	mobilization of leukocytes	<0.001	-2.952	9
	recruitment of mononuclear leukocytes	<0.001	-3.228	11
	mobilization of myeloid cells	<0.001	-2.791	8
	cell movement of myeloid cells	<0.001	-3.319	19
	leukocyte migration	<0.001	-2.891	23
	cell movement of phagocytes	<0.001	-3.254	19
	migration of granulocytes	<0.001	-2.893	12
	chemotaxis of myeloid cells	<0.001	-3.185	15
	recruitment of lymphocytes	<0.001	-2.920	10

Predicted activation	*Function*	*P-value*	*Z-score*	*Genes*
	recruitment of leukocytes	<0.001	-3.113	15
	chemotaxis of phagocytes	<0.001	-3.045	15
	attraction of myeloid cells	<0.001	-2.803	8
	chemoattraction of phagocytes	<0.001	-2.759	8

Table 5.9 Key biological functions predicted to be increased or decreased in Caco-2 cells co-cultured with UV-killed *F. prausnitzii* (compared to Caco-2 cells not treated with bacteria).

The P-value was calculated using the right-tailed Fisher Exact Test by considering the number of differentially expressed genes that participate in the function, and the total number of genes that are known to be associated with that function in the Ingenuity Knowledge Base. Given the observed differential regulation of a gene (up or down), the Z-score was used to determine the activation state of the biological function by the direction of effect associated with the relationship from the gene to the function. An absolute Z-score of ≥ 2 was considered significant (function activated if Z-score ≥ 2; inhibited if Z-score ≤ -2). Genes indicated the number of differentially expressed genes associated with the function.

Predicted activation	*Function*	*P-value*	*Z-score*	*Genes*
Increased	proliferation of lymphatic system cells	<0.001	2.000	4
	proliferation of immune cells	0.028	2.000	4
Decreased	quantity of leukocytes	<0.001	-2.155	9
	chemotaxis of cells	0.001	-2.227	5
	transcription of RNA	0.007	-2.061	8
	migration of cells	0.013	-2.006	7

Table 5.10 Key biological functions predicted to be increased or decreased in Caco-2 cells co-cultured with *F. prausnitzii* (compared to Caco-2 treated with UV-killed *F. prausnitzii*).

The P-value was calculated using the right-tailed Fisher Exact Test by considering the number of differentially expressed genes that participate in the function, and the total number of genes that are known to be associated with that function in the Ingenuity Knowledge Base. Given the observed differential regulation of a gene (up or down), the Z-score was used to determine the activation state of the biological function by the direction of effect associated with the relationship from the gene to the function. An absolute Z-score of ≥ 2 was considered significant (function activated if Z-score ≥ 2; inhibited if Z-score ≤ -2). Only the top 20 'decreased' functions (based on P-value) are shown. Genes indicated the number of differentially expressed genes associated with the function.

Predicted activation	*Function*	*P-value*	*Z-score*	*Genes*
Increased	infection of mammalia	<0.001	2.107	9
	proliferation of myeloid progenitor cells	<0.001	2.000	4
Decreased	cell movement of neutrophils	<0.001	-3.191	15
	chemotaxis of myeloid cells	<0.001	-3.217	15
	chemotaxis of phagocytes	<0.001	-3.226	15
	cell movement of myeloid cells	<0.001	-3.247	18
	cell movement of phagocytes	<0.001	-3.217	18
	chemotaxis of neutrophils	<0.001	-3.197	12
	attraction of cells	<0.001	-2.954	10
	chemotaxis of cells	<0.001	-3.017	17
	recruitment of monocytes	<0.001	-2.177	8
	attraction of leukocytes	<0.001	-2.926	9
	stimulation of cells	<0.001	-2.554	14
	chemoattraction of cells	<0.001	-2.770	9
	cell movement of leukocytes	<0.001	-2.907	19
	migration of granulocytes	<0.001	-2.837	11
	attraction of phagocytes	<0.001	-2.780	8
	attraction of myeloid cells	<0.001	-2.620	7
	chemoattraction of phagocytes	<0.001	-2.584	7
	recruitment of mononuclear leukocytes	<0.001	-2.924	9
	recruitment of phagocytes	<0.001	-2.699	11
	migration of neutrophils	<0.001	-2.507	9

5.4.9 Ingenuity pathway analysis

The IPA canonical pathway analysis identified curated pathways in the IPA library that were most significantly over-represented among genes in the dataset. For Caco-2 cells co-cultured with *F. prausnitzii* (compared with untreated Caco-2 cells) 159 pathways were identified, the top 20 of which are shown in Table 5.11. Many of these pathways involved IL-17A signalling, for example 'differential regulation of cytokine production in intestinal epithelial cells IL-17A and IL-17F' (shown in Figure 5.14), 'IL-17A signalling in gastric cells' and the most significant pathway by P-value 'role of IL-17A in arthritis'. For Caco-2 cells co-cultured with *L. rhamnosus* (compared with untreated Caco-2 cells) 21 pathways were significantly over-represented among genes in the dataset, the top 20 of which are shown in Table 5.12. For Caco-2 cells co-cultured with UV-killed *F. prausnitzii* (compared with untreated Caco-2 cells) only 12 pathways were significantly over-represented among genes in the dataset (Table 5.13). Seven pathways were common between those listed in the above mentioned tables, including many IL-17A associated pathways, such as those mentioned above, 'TREM1 signalling' (shown in Figure 5.15) and 'glucocorticoid receptor signalling'.

Many (105) canonical pathways were enriched with differentially expressed genes from Caco-2 cells co-cultured with *F. prausnitzii* compared to Caco-2 treated with UV-killed *F. prausnitzii*, the top 20 of which are shown in Table 5.14. Four pathways were found to be in common between those listed in Table 5.11, and Table 5.14, which included 'differential regulation of cytokine production in macrophages and T helper cells by IL-17A and IL-17F', 'differential regulation of cytokine production in intestinal epithelial cells by IL-17A and IL-17F' (Figure 5.14), and 'dendritic cell maturation' (Figure 5.16), which suggests that the regulation of these pathways was significantly different between Caco-2 cells co-cultured with live *F. prausnitzii*, and Caco-2 cells co-cultured with UV-killed *F. prausnitzii*. Also of particular note were the canonical pathways for 'TREM1 signalling' (Figure 5.15) and 'IL-8 signalling' (Figure 5.17).

Table 5.11 Canonical pathways enriched with differentially expressed genes from Caco-2 cells co-cultured with *F. prausnitzii* (compared to Caco-2 cells not treated with bacteria).

Fisher's exact test was used to calculate a P-value determining the probability that the association between the differentially expressed genes and the canonical pathway is explained by chance alone. The ratio indicates the number of differentially expressed genes that map to the pathway divided by the total number of genes that map to the canonical pathway. Only the top 20 pathways (based on P-value) are shown.

Ingenuity Canonical Pathways	*P-value*	*Ratio*
Role of IL-17A in Arthritis	<0.001	0.127
TREM1 Signalling	<0.001	0.099
Role of Hypercytokinemia/hyperchemokinemia in the Pathogenesis of Influenza	<0.001	0.136
Differential Regulation of Cytokine Production in Macrophages and T Helper Cells by IL-17A and IL-17F	<0.001	0.278
Role of IL-17F in Allergic Inflammatory Airway Diseases	<0.001	0.125
Differential Regulation of Cytokine Production in Intestinal Epithelial Cells by IL-17A and IL-17F	<0.001	0.217
Glucocorticoid Receptor Signalling	<0.001	0.034
IL-17A Signalling in Gastric Cells	<0.001	0.200
TNFR2 Signalling	<0.001	0.152
Role of IL-17A in Psoriasis	<0.001	0.308
Dendritic Cell Maturation	<0.001	0.039
IL-17A Signalling in Fibroblasts	<0.001	0.125
Communication between Innate and Adaptive Immune Cells	<0.001	0.055
TNFR1 Signalling	<0.001	0.096
Role of Macrophages, Fibroblasts and Endothelial Cells in Rheumatoid Arthritis	<0.001	0.027
Type I Diabetes Mellitus Signalling	<0.001	0.050
Death Receptor Signalling	<0.001	0.078
Airway Pathology in Chronic Obstructive Pulmonary Disease	<0.001	0.333
Induction of Apoptosis by HIV1	<0.001	0.077
IL-17A Signalling in Airway Cells	<0.001	0.069

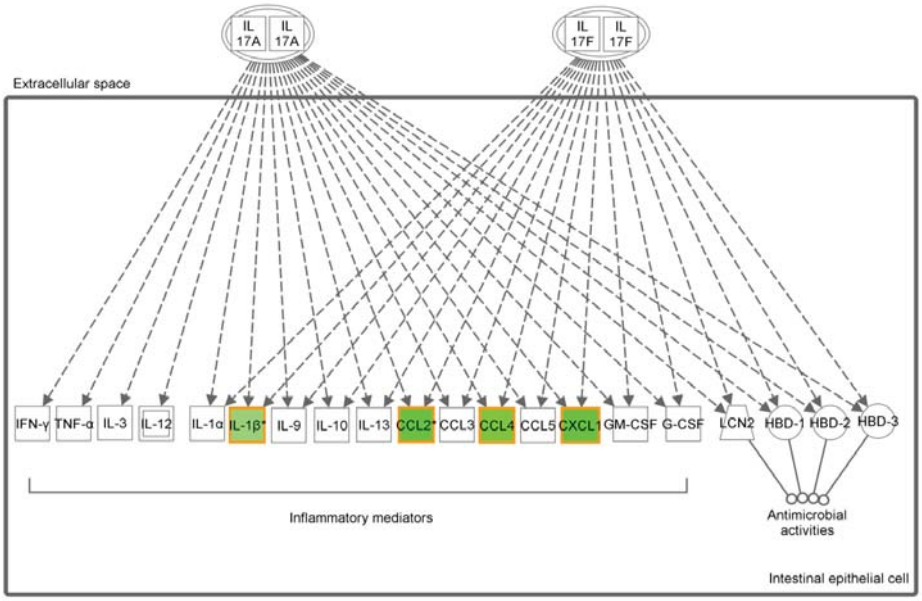

Figure 5.14 Ingenuity pathway for 'Differential Regulation of Cytokine Production in Intestinal Epithelial Cells by IL-17A and IL-17F'.

Transcriptional information was projected on to the pathway; genes with decreased expression in Caco-2 cells co-cultured with *F. prausnitzii* compared to Caco-2 treated with UV-killed *F. prausnitzii* are depicted in shades of green. Intensity of colour indicates degree of fold change, with greater intensity signifying higher expression level.

Table 5.12 Canonical pathways enriched with differentially expressed genes from Caco-2 cells co-cultured with *L. rhamnosus* (compared to Caco-2 cells not treated with bacteria).

Fisher's exact test was used to calculate a P-value determining the probability that the association between the differentially expressed genes and the canonical pathway is explained by chance alone. The ratio indicates the number of differentially expressed genes that map to the pathway divided by the total number of genes that map to the canonical pathway. Only the top 20 pathways (based on P-value) are shown.

Ingenuity Canonical Pathways	*P-value*	*Ratio*
Airway Pathology in Chronic Obstructive Pulmonary Disease	<0.001	0.222
Role of IL-17A in Psoriasis	<0.001	0.154
Role of IL-17A in Arthritis	<0.001	0.032
TREM1 Signalling	<0.001	0.028
Hepatic Fibrosis / Hepatic Stellate Cell Activation	<0.001	0.014
Glucocorticoid Receptor Signalling	0.001	0.007
IL-17A Signalling in Gastric Cells	0.006	0.040
Hematopoiesis from Pluripotent Stem Cells	0.008	0.016
Role of Hypercytokinemia/hyperchemokinemia in the Pathogenesis of Influenza	0.009	0.023
Role of IL-17F in Allergic Inflammatory Airway Diseases	0.010	0.021
Role of Cytokines in Mediating Communication between Immune Cells	0.011	0.018
IL-17A Signaling in Airway Cells	0.015	0.014
IL-17 Signaling	0.017	0.014
Communication between Innate and Adaptive Immune Cells	0.017	0.009
Bladder Cancer Signaling	0.020	0.011
HMGB1 Signaling	0.022	0.010
Role of Tissue Factor in Cancer	0.025	0.009
Atherosclerosis Signaling	0.027	0.007
IL-6 Signaling	0.028	0.008
Hepatic Cholestasis	0.032	0.006

Table 5.13 Canonical pathways enriched with differentially expressed genes from Caco-2 cells co-cultured with UV-killed *F. prausnitzii* (compared to Caco-2 cells not treated with bacteria).

Fisher's exact test was used to calculate a P-value determining the probability that the association between the differentially expressed genes and the canonical pathway is explained by chance alone. The ratio indicates the number of differentially expressed genes that map to the pathway divided by the total number of genes that map to the canonical pathway. Only pathways where P <0.05 are shown.

Ingenuity Canonical Pathways	*P-value*	*Ratio*
Role of IL-17A in Psoriasis	<0.001	0.231
Airway Pathology in Chronic Obstructive Pulmonary Disease	<0.001	0.222
Role of IL-17A in Arthritis	<0.001	0.048
IL-17A Signaling in Gastric Cells	0.001	0.080
TREM1 Signaling	0.003	0.028
Threonine Degradation II	0.003	0.111
IL-17A Signaling in Airway Cells	0.004	0.028
Role of Tissue Factor in Cancer	0.010	0.018
Hepatic Fibrosis / Hepatic Stellate Cell Activation	0.016	0.014
IL-8 Signaling	0.028	0.010
Hematopoiesis from Pluripotent Stem Cells	0.047	0.016
Glucocorticoid Receptor Signaling	0.050	0.007

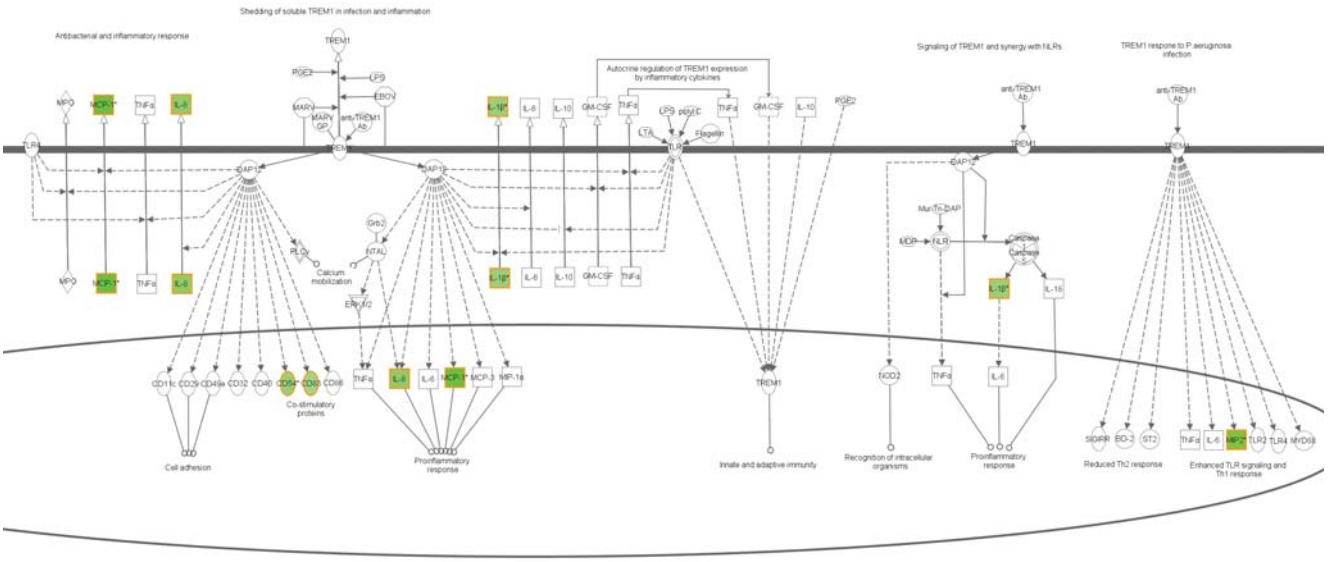

Figure 5.15 Ingenuity pathway for 'TREM1 Signalling'.

Transcriptional information was projected on to the pathway; genes with decreased expression in Caco-2 cells co-cultured with *F. prausnitzii* compared with Caco-2 treated with UV-killed *F. prausnitzii* are depicted in shades of green. Intensity of colour indicates degree of fold change, with greater intensity signifying higher expression level.

Table 5.14 Canonical pathways enriched with differentially expressed genes from Caco-2 cells co-cultured with *F. prausnitzii* (compared to Caco-2 treated with UV-killed *F. prausnitzii*).

Fisher's exact test was used to calculate a P-value determining the probability that the association between the differentially expressed genes and the canonical pathway is explained by chance alone. The ratio indicates the number of differentially expressed genes that map to the pathway divided by the total number of genes that map to the canonical pathway. Only the top 20 pathways (based on P-value) are shown.

Ingenuity Canonical Pathways	*P-value*	*Ratio*
Role of IL-17A in Arthritis	<0.001	0.095
TREM1 Signaling	<0.001	0.085
Role of IL-17A in Psoriasis	<0.001	0.308
Role of IL-17F in Allergic Inflammatory Airway Diseases	<0.001	0.104
Differential Regulation of Cytokine Production in Macrophages and T Helper Cells by IL-17A and IL-17F	<0.001	0.222
Differential Regulation of Cytokine Production in Intestinal Epithelial Cells by IL-17A and IL-17F	<0.001	0.174
Hepatic Fibrosis / Hepatic Stellate Cell Activation	<0.001	0.041
Role of Hypercytokinaemia/hyperchemokinaemia in the Pathogenesis of Influenza	<0.001	0.091
Glucocorticoid Receptor Signaling	<0.001	0.024
IL-17A Signaling in Gastric Cells	<0.001	0.120
IL-17 Signaling	<0.001	0.054
Communication between Innate and Adaptive Immune Cells	<0.001	0.037
Dendritic Cell Maturation	<0.001	0.024
Role of Macrophages, Fibroblasts and Endothelial Cells in Rheumatoid Arthritis	<0.001	0.018
Airway Pathology in Chronic Obstructive Pulmonary Disease	<0.001	0.222
Role of Tissue Factor in Cancer	<0.001	0.035
Atherosclerosis Signaling	<0.001	0.029
Role of Cytokines in Mediating Communication between Immune Cells	<0.001	0.055
IL-17A Signaling in Airway Cells	0.001	0.042
Altered T Cell and B Cell Signaling in Rheumatoid Arthritis	0.002	0.033

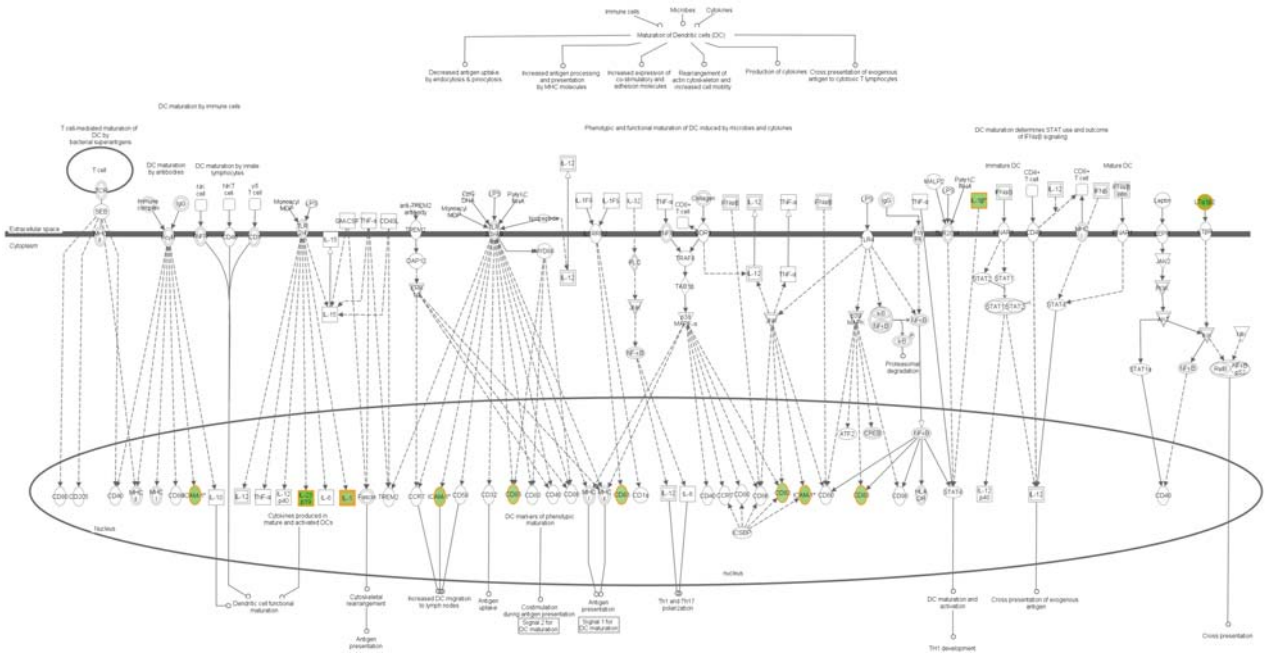

Figure 5.16 Ingenuity pathway for 'Dendritic Cell Maturation'.

Transcriptional information was projected on to the pathway; genes with decreased expression in Caco-2 cells co-cultured with *F. prausnitzii* compared to Caco-2 treated with UV-killed *F. prausnitzii* are depicted in shades of green. Intensity of colour indicates degree of fold change, with greater intensity signifying higher expression level.

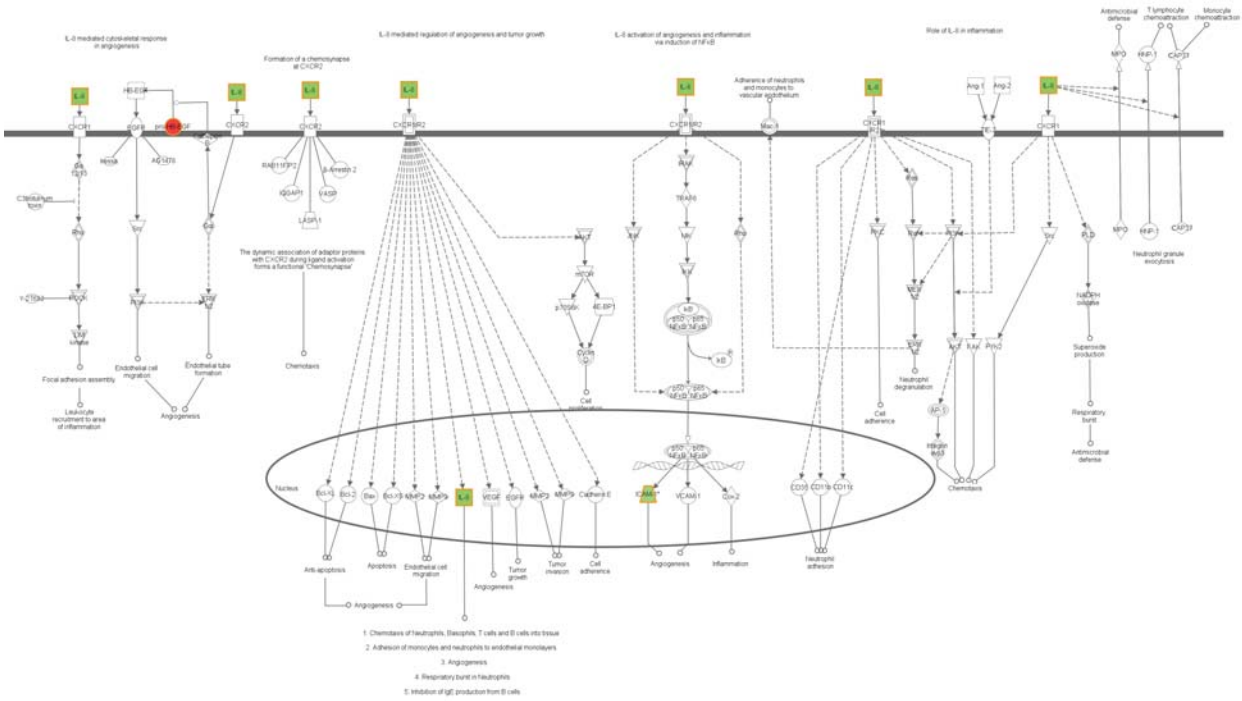

Figure 5.17 Ingenuity pathway for 'IL-8 Signalling'.

Transcriptional information was projected on to the pathway; genes with increased expression in Caco-2 cells co-cultured with *F. prausnitzii* compared to Caco-2 treated with UV-killed *F. prausnitzii* are depicted in shades of red, genes with decreased expression in shades of green. Intensity of colour indicates degree of fold change, with greater intensity signifying higher expression level.

5.4.10 Ingenuity upstream regulator analysis

Based on the changes in gene expression, IPA upstream analysis predicted the activation state of upstream transcription regulators such as transcription factors, cytokines and kinase inhibitors. In Caco-2 cells co-cultured with *F. prausnitzii* (compared to untreated Caco-2 cells), 92 transcription regulators were predicted to be activated while 214 transcription regulators were predicted to be inhibited, (the top 20 of each are shown in Table 5.15). The most significant transcription regulator (by P-value) predicted to be activated was the IL-10 cytokine, while the most significant transcription regulator predicted to be inhibited was the NF-κB transcription factor complex. These predictions strongly suggest that Caco-2 cells co-cultured with live *F. prausnitzii* exhibit an anti-inflammatory profile. Other molecules involved in the NF-κB pathway such as the MYD88 and NFκB1 were also predicted to be inhibited, along with pro-inflammatory cytokines such as IL-1 and TNF. The transmembrane receptors, TLR7 and TLR4 were also predicted to be 'inhibited'.

In Caco-2 cells co-cultured with UV-killed *F. prausnitzii* (compared to untreated Caco-2 cells), seven transcription regulators were predicted to be activated, while 22 were predicted to be inhibited (all regulators found to be activated and the top 20 inhibited regulators are shown in Table 5.16). The most significant transcription regulators (by P-value) predicted to be activated and inhibited was the transcription factor mesenchyme homeobox 2 (MEOX2) transcription factor, and the TLR5 transmembrane receptor, respectively. The transcription regulators predicted to be activated and inhibited in Caco-2 cells co-cultured with UV-killed *F. prausnitzii* (compared to untreated Caco-2 cells) were a subset of those predicted to be activated and inhibited in Caco-2 cells co-cultured with live *F. prausnitzii* (compared to untreated Caco-2 cells), respectively. The only exceptions were TREM1 and the hepatocyte growth factor (HGF) predicted to be inhibited in Caco-2 cells co-cultured with UV-killed *F. prausnitzii*.

Compared to Caco-2 cells co-cultured with UV-killed *F. prausnitzii*, 49 transcription regulators were predicted to be activated, and 139 transcription regulators were predicted to be inhibited in Caco-2 cells co-cultured with live *F. prausnitzii* (the top 20 of each are shown on Table 5.17). With the exception of two transcription

Table 5.15 Predicted activation state of transcription regulators in Caco-2 cells co-cultured with *F. prausnitzii* (compared to Caco-2 cells not treated with bacteria).

The P-value was calculated by the Fisher's Exact test and indicates the statistical significance of differentially expressed genes that are downstream of the regulator. Given the observed differential expression of a gene (up or down), the Z-score was used to determine the activation state of the upstream regulator by the regulation direction associated with the relationship from the regulator to the gene. An absolute Z-score of ≥ 2 was considered significant (regulator activated if Z-score ≥ 2; inhibited if Z-score ≤ -2).Only the 20 most significant regulators (based on P value) predicted to be activated and inhibited are shown. * denotes molecules the gene expression of which was different in Caco-2 cells co-cultured with *F. prausnitzii* (compared to Caco-2 cells not treated with bacteria).

Predicted Activation State	*Regulator*	*Molecule Type*	*Z-score*	*P-value*
Activated	IL-10	cytokine	2.520	<0.001
	pyrrolidine dithiocarbamate	chemical reagent	3.402	<0.001
	LY294002	chemical - kinase inhibitor	4.357	<0.001
	SB203580	chemical - kinase inhibitor	4.221	<0.001
	dexamethasone	chemical drug	2.150	<0.001
	Bay 11-7082	chemical - kinase inhibitor	3.261	<0.001
	etanercept	biologic drug	3.111	<0.001
	SP600125	chemical - kinase inhibitor	3.547	<0.001
	U0126	chemical - kinase inhibitor	3.991	<0.001
	wortmannin	chemical - kinase inhibitor	2.276	<0.001
	PS-1145	chemical - kinase inhibitor	2.779	<0.001
	resveratrol	chemical drug	2.447	<0.001
	Alpha catenin	group	3.434	<0.001
	SR 144528	chemical reagent	2.018	<0.001
	PD98059	chemical - kinase inhibitor	3.804	<0.001
	simvastatin	chemical drug	2.779	<0.001
	VIP	other	2.507	<0.001
	epigallocatechin-gallate	chemical drug	3.363	<0.001
	benzyloxycarbonyl-Leu-Leu-Leu aldehyde	chemical - protease inhibitor	2.515	<0.001

Predicted Activation State	*Regulator*	*Molecule Type*	*Z-score*	*P-value*
	genistein	chemical drug	3.115	<0.001
Inhibited	NFkB (complex)	complex	-5.989	<0.001
	poly rI:rC-RNA	chemical reagent	-4.883	<0.001
	IL-1B*	cytokine	-4.981	<0.001
	TNF*	cytokine	-6.052	<0.001
	IRAK4	kinase	-2.134	<0.001
	lipopolysaccharide	chemical drug	-5.936	<0.001
	RELA	transcription regulator	-4.515	<0.001
	IL-1A	cytokine	-4.688	<0.001
	NFKB1	transcription regulator	-3.023	<0.001
	resiquimod	chemical drug	-3.254	<0.001
	MYD88	other	-4.322	<0.001
	CD40LG	cytokine	-3.622	<0.001
	IKBKB	kinase	-3.881	<0.001
	TRADD	other	-3.592	<0.001
	IFNG (includes EG:15978)	cytokine	-4.988	<0.001
	TLR7	transmembrane receptor	-3.931	<0.001
	REL	transcription regulator	-2.439	<0.001
	TICAM1	other	-3.692	<0.001
	TLR4	transmembrane receptor	-4.040	<0.001
	C5	cytokine	-3.154	<0.001

Table 5.16 Predicted activation state of transcription regulators in Caco-2 cells co-cultured with UV-killed *F. prausnitzii* (compared to Caco-2 cells not treated with bacteria).

The P-value was calculated by the Fisher's Exact test and indicates the statistical significance of differentially expressed genes that are downstream of the regulator. Given the observed differential expression of a gene (up or down), the Z-score was used to determine the activation state of the upstream regulator by the regulation direction associated with the relationship from the regulator to the gene. An absolute Z-score of ≥ 2 was considered significant (regulator activated if Z-score ≥ 2; inhibited if Z-score ≤ -2). Only the 20 most significant regulators (based on P value) predicted to be inhibited are shown.

Predicted Activation State	*Regulator*	*Molecule Type*	*Z-score*	*P-value*
Activated	MEOX2	transcription regulator	2.236	<0.001
	S100A6	transporter	2.000	<0.001
	PD98059	chemical - kinase inhibitor	2.406	<0.001
	SB203580	chemical - kinase inhibitor	2.162	<0.001
	U0126	chemical - kinase inhibitor	2.211	<0.001
	LY294002	chemical - kinase inhibitor	2.176	<0.001
	dexamethasone	chemical drug	2.216	0.003
Inhibited	TLR5	transmembrane receptor	-2.205	<0.001
	TREM1	other	-2.600	<0.001
	poly rI:rC-RNA	chemical reagent	-2.717	<0.001
	leukotriene D4	chemical - endogenous mammalian	-2.183	<0.001
	FOXL2	transcription regulator	-2.216	<0.001
	tributyrin	chemical drug	-2.219	<0.001
	TLR7	transmembrane receptor	-2.208	<0.001
	mycophenolic acid	chemical drug	-2.236	<0.001
	IL-17A	cytokine	-2.226	<0.001
	camptothecin	chemical toxicant	-2.236	<0.001
	hydrogen peroxide	chemical - endogenous mammalian	-2.404	<0.001
	E. coli B4 lipopolysaccharide	chemical toxicant	-2.182	<0.001
	IFNG (includes EG:15978)	cytokine	-2.596	<0.001

Predicted Activation State	*Regulator*	*Molecule Type*	*Z-score*	*P-value*
	TNF	cytokine	-2.960	<0.001
	IL-1B	cytokine	-2.532	<0.001
	F2	peptidase	-2.156	<0.001
	lipopolysaccharide	chemical drug	-2.915	<0.001
	HGF	growth factor	-2.170	<0.001
	NFkB (complex)	complex	-2.396	<0.001

Table 5.17 Predicted activation state of transcription regulators in Caco-2 cells co-cultured with *F. prausnitzii* (compared to Caco-2 treated with UV-killed *F. prausnitzii*).

The P-value was calculated by the Fisher's Exact test and indicates the statistical significance of differentially expressed genes that are downstream of the regulator. Given the observed differential expression of a gene (up or down), the Z-score was used to determine the activation state of the upstream regulator by the regulation direction associated with the relationship from the regulator to the gene. An absolute Z-score of ≥ 2 was considered significant (regulator activated if Z-score ≥ 2; inhibited if Z-score ≤ -2).Only the 20 most significant regulators (based on P value) predicted to be activated and inhibited are shown. * denotes molecules whose gene expression was different in Caco-2 cells co-cultured with *F. prausnitzii* compared to Caco-2 treated with UV-killed *F. prausnitzii*.

Predicted Activation State	*Regulator*	*Molecule Type*	*Z-score*	*P-value*
Activated	MEOX2	transcription regulator	2.714	<0.001
	Bay 11-7082	chemical - kinase inhibitor	2.960	<0.001
	etanercept	biologic drug	2.779	<0.001
	SB203580	chemical - kinase inhibitor	3.618	<0.001
	pyrrolidine dithiocarbamate	chemical reagent	3.094	<0.001
	U0126	chemical - kinase inhibitor	3.009	<0.001
	LY294002	chemical - kinase inhibitor	3.233	<0.001
	IL-10	cytokine	3.072	<0.001
	PS-1145	chemical - kinase inhibitor	2.408	<0.001
	PD98059	chemical - kinase inhibitor	3.100	<0.001
	simvastatin	chemical drug	2.882	<0.001
	aspirin	chemical drug	2.155	<0.001
	SP600125	chemical - kinase inhibitor	2.811	<0.001
	apigenin	chemical - endogenous non-mammalian	2.621	<0.001
	HMOX1	enzyme	2.602	<0.001
	resveratrol	chemical drug	2.929	<0.001
	PP2/AG1879 tyrosine kinase inhibitor	chemical - kinase inhibitor	2.586	<0.001
	TNFAIP3*	enzyme	2.396	<0.001
	IL-1RN	cytokine	2.061	<0.001
	AG490	chemical - kinase inhibitor	2.592	<0.001

Predicted Activation State	*Regulator*	*Molecule Type*	*Z-score*	*P-value*
Inhibited	NFkB (complex)	complex	-4.720	<0.001
	IL-1B*	cytokine	-3.981	<0.001
	IL-1A	cytokine	-4.130	<0.001
	TNF	cytokine	-4.825	<0.001
	IKBKB	kinase	-4.030	<0.001
	poly rI:rC-RNA	chemical reagent	-3.959	<0.001
	RELA	transcription regulator	-3.931	<0.001
	resiquimod	chemical drug	-2.065	<0.001
	Ni2+	chemical reagent	-3.157	<0.001
	NFKB1	transcription regulator	-2.629	<0.001
	IL-17A	cytokine	-3.151	<0.001
	TRADD	other	-3.162	<0.001
	E.coli lipopolysaccharide	chemical - endogenous non-mammalian	-3.240	<0.001
	CD40LG	cytokine	-3.541	<0.001
	MYD88	other	-3.504	<0.001
	F2	peptidase	-3.411	<0.001
	TLR7	transmembrane receptor	-3.261	<0.001
	peptidoglycan	chemical - endogenous non-mammalian	-3.250	<0.001
	lipopolysaccharide	chemical drug	-4.496	<0.001
	Fibrinogen	complex	-2.536	<0.001

regulators predicted to be activated ('TNFAIP3' and 'carbon monoxide'), and seven transcription regulators predicted to be inhibited ('ATP', 'IFI16', 'MAPK9', 'BCL2', 'KRAS', 'Cg', and 'Ca^{2+}'), all other elements were a subset of the respective group of transcription regulators predicted to be activated or inhibited in Caco-2 cells co-cultured with *F. prausnitzii* compared to untreated Caco-2 cells. This suggests that live *F. prausnitzii* have much more profound effects on Caco-2 cells than non-viable (UV-killed) *F. prausnitzii.*

5.5 DISCUSSION

The results reported in this chapter demonstrate that the apical anaerobic model can be used to study interactions between a live commensal obligate anaerobe and intestinal epithelial cells. *F. prausnitzii* is known to survive in an aerobic atmosphere for less than two minutes[301]. In support of this, the viability of *F. prausnitzii* was shown to drop by over four logs when cultured for 30 minutes in an aerobic atmosphere. This loss in viability was reduced to one log for *F. prausnitzii* co-cultured with Caco-2 cells for 8 hours in the apical anaerobic model. The ^{3}H-mannitol bioassay and global gene expression analysis showed that live *F. prausnitzii* exert greater effects on Caco-2 cells than dead *F. prausnitzii*, thus demonstrating the usefulness of a physiologically relevant co-culture system which allows obligate anaerobic bacteria to remain viable for the duration of the co-culture experiment.

The TEER assay did not show any differences in barrier integrity between Caco-2 cells treated with or without bacteria at the 95% confidence level. The *L. rhamnosus* HN001 strain has previously been shown to increase TEER in Caco-2 cells (compared to Caco-2 cells without bacteria) within 4 hours of co-culture in standard (aerobic) cell culture conditions[196]. However, this effect could not be replicated in Caco-2 cells co-cultured with *L. rhamnosus* in the co-culture chamber inside a 5% CO_2 incubator (data not shown). This may have been due to differences in TEER measuring equipment used, Caco-2 cell culture conditions, or the MOI used.

On the other hand, the ^{3}H-mannitol bioassay indicated an increase in paracellular permeability across Caco-2 cell monolayers co-cultured with *L. rhamnosus*. This is contrary to the expected barrier enhancing properties of *L. rhamnosus* HN001 as indicated by its effect on TEER[196]. However, paracellular permeability and TEER are

thought to be regulated by different TJ proteins and via independent mechanisms[53], and thus it is possible for certain compounds to have opposing effects on TEER and paracellular permeability. Furthermore, facultative anaerobes such as *L. rhamnosus* switch from aerobic to anaerobic respiration in the absence of oxygen, thus altering the metabolism and the potential influence on Caco-2 cells. The observed increase in paracellular permeability caused by *L. rhamnosus* may be specific to anaerobically cultured *L. rhamnosus*, and warrants further investigation comparing the effects of aerobically and anaerobically cultured strains of *L. rhamnosus* on Caco-2 cells. No differences were observed between Caco-2 cell monolayers co-cultured with live or UV-killed *F. prausnitzii* over the first 6 hours. However, by the 8-hour time point, *F. prausnitzii* were shown to have increased paracellular permeability compared to Caco-2 cell monolayers co-cultured with UV-killed *F. prausnitzii* or without bacteria, and as such suggests that live *F. prausnitzii* may have a greater influence on intestinal epithelial cell function than non-viable bacteria.

A 4-hour incubation time was chosen for the microarray experiment as opposed to the 8-hour incubation carried out for the barrier integrity assays because transcriptional changes occur much more rapidly than phenotypical changes in cells. Furthermore, several studies have identified significant changes in gene expression in intestinal epithelial monolayers treated with bacteria for as low as 2 or 0.5 hours[256]. Recently it was also shown that *Lactobacillus acidophilus* increased the expression of genes in immune related pathways in Caco-2 cells following a shorter incubation time of 1 hour compared with longer incubation times of 4 or 8 hours[358]. Thus, as both *L. rhamnosus*[359] and *F. prausnitzii*[257] are known to influence immune related pathways in the intestinal epithelial cells, a shorter incubation time than 8 hours was considered appropriate for the analysis of global gene expression.

Gene expression analysis identified live *F. prausnitzii* as having the greatest effect on the number of differentially expressed Caco-2 cell genes, and *L. rhamnosus* as having the least effect. The observed smaller effect of *L. rhamnosus* may have been due to variation in the effect of the bacteria over the two different runs of the experiment, as shown by the PCA plot. Live *F. prausnitzii* showed a more profound effect on the number of differentially expressed Caco-2 cell genes than UV-killed *F. prausnitzii*, indicating that anaerobic bacteria exert different effects on intestinal epithelial cells depending if they are alive or non-viable. Similarly, it has previously been shown that

F. prausnitzii supernatant reduced secretion of the pro-inflammatory cytokine IL-8 in Caco-2 cells whereas UV-killed bacteria and bacterial fractions had no effect[257].

The NF-κB complex was the central node in the biological interaction network generated from differentially expressed genes between Caco-2 cells treated with *F. prausnitzii* and untreated Caco-2 cells. Most of the other nodes, including ubiquitin, IκB, and IKK, were also largely related to the NF-κB pathway. In the biological interaction network generated from differentially expressed genes between Caco-2 cells treated with UV-killed *F. prausnitzii* and untreated Caco-2 cells, NF-κB was an important node, but was not the central node of the network. Further, unlike in the case of live bacteria, other NF-κB-related molecules were absent from this network. NF-κB is considered a master switch for many of the genes involved in the innate immune response. For example activation of NF-κB leads to increased secretion of cytokines, which attract macrophages, neutrophils, and various growth factors which aid proliferation of immune cells[130]. Under homeostatic conditions, localisation of NF-κB from the cytoplasm into the nucleus is prevented by IκB. However, under pathological conditions, IKK phosphorylates IκB, targeting it for degradation by means of ubiquitination. This in turn frees NF-κB to enter the nucleus and initiate transcription of NF-κB responsive genes[132].

F. prausnitzii is thought to secrete an as yet unidentified substance capable of decreasing NF-κB activation, as the bacterial supernatant, but not UV-killed bacterial cells, was able to inhibit the NF-κB pathway in Caco-2 cells[257]. Further, *F. prausnitzii* or its supernatant has also been shown to induce secretion of the anti-inflammatory cytokine IL-10 *in vivo*. Consistent with this, the top upstream transcription regulators predicted to be 'activated' or 'inhibited' by *F. prausnitzii* in Caco-2 cells (compared to Caco-2 cells not treated with bacteria) were IL-10 and NF-κB respectively. IL-10 was not predicted to be activated by UV-killed *F, prausnitzii* cells (compared to Caco-2 cells not treated with bacteria), and while NF-κB was predicted to be inhibited, the Z-score, and rank by P-value was less than that of Caco-2 cells co-cultured with live *F. prausnitzii*.

Another important node in the biological interaction network generated from differentially expressed genes between Caco-2 cells treated with *F. prausnitzii* and untreated Caco-2 cells was the down regulated 'IFN regulatory factor (IRF)1'. The

related ‘IRF’ (also showing decreased expression) was also a node in this network. The IRF family of transcription factors are involved in regulating the expression of IFNs, a family of pro-inflammatory cytokines. None of the above mentioned molecules were present in the biological interaction network generated from differentially expressed genes between Caco-2 cells co-cultured with UV-killed *F. prausnitzii* and untreated Caco-2 cells. However, the activity of the pro-inflammatory cytokine IFNγ and TNFα were predicted to be supressed in both Caco-2 cells co-cultured with live or UV-killed *F. prausnitzii* (compared to Caco-2 cell not treated with bacteria). Nonetheless, overall the data suggest that viable *F. prausnitzii* cells may exert more profound anti-inflammatory effects on intestinal epithelial cells *in vitro* than non-viable UV-killed *F. prausnitzii*.

Another node present in the biological interaction network generated from differentially expressed genes between Caco-2 cells treated with *F. prausnitzii* and Caco-2 cells treated with UV-killed *F. prausnitzii* or no bacteria was ‘TLR’. TLRs are a family of type I transmembrane receptors, expressed on the surface of intestinal epithelial cells as well as on specialised antigen presenting cells such as dendritic cells in the lamina propria and play a crucial role in immune activation and the innate response[360]. When activated, TLR interacts with various adaptor proteins that recruit protein kinases in a cascade that ultimately activates transcription factors such as NF-κB (reviewed in Krishnan *et al.* (2007)[361]). The activity of ‘TLR’ was predicted to be inhibited in Caco-2 cells co-cultured with *F. prausnitzii* compared with Caco-2 cells co-cultured with UV-killed *F. prausnitzii*. Similarly, the activity of MyD88, an example of the above mentioned adaptor proteins, was also predicted to be decreased. Moreover, IRAK-4, an example of the above mentioned protein kinases, was predicted to be inhibited in Caco-2 cells by live but not UV-killed *F. prausnitzii*. These results suggest that compared with UV-killed *F. prausnitzii*, viable *F. prausnitzii* cells are able to downregulate innate signalling pathways involving TLR and MyD88.

Of the canonical pathways in the IPA library that were significantly over-represented among the list of differentially expressed genes between Caco-2 cells cultured with live and UV-killed bacteria, a large number were not related to intestinal epithelial cells, such as ‘TREM1 signalling’, where TREM (triggering receptor expressed on myeloid cells) is a cell surface receptor selectively on neutrophils, monocytes and macrophages, and ‘dendritic cell maturation’, a pathway specific to

dendritic cells. However, one exception was the pathway 'differential regulation of cytokine production in intestinal epithelial cells by IL-17A and IL-17F'. These pathways are involved in cytokine signalling and the cellular immune response. IL-17A and IL-17F are cytokines, which in the intestine act as ligands, important in the immune response, and produce a range of cytokines and chemokines. TREM signalling leads to the activation of NF-κB and the production of cytokines. DC are present in the intestine and have been implicated both in the maintenance of and tolerance towards commensals and the generation of immune response against pathogens[136]. These cells have two major functions, which are to acquire antigens and stimulate lymphocytes. Antigens are acquired by 'immature' DC. However, inflammatory stimuli induce the maturation of these cells which go on to stimulate lymphocytes. The direction of gene expression indicates downregulation of these pathways, suggesting that viable *F. prausnitzii* have an increased anti-inflammatory effect compared to non-viable *F. prausnitzii*. However, further investigation is required to determine if *F. prausnitzii* does indeed have the above mentioned effects on non-epithelial cell types.

The immunomodulatory properties of *F. prausnitzii* could also be attributed to bacterial metabolites produced by only viable bacterial cells. For example, *F. prausnitzii* are known to produce several short chain fatty acids (SCFAs) through the fermentation of dietary fibre, of which the most thoroughly investigated is butyrate[301]. Butyrate has been reported to have anti-inflammatory effects, and is effective in reducing symptoms of inflammatory diseases of the intestine[362]. One of the best known anti-inflammatory mechanisms of butyrate is the suppression of NF-κB activation[363], which is also implied by the IPA biological interaction network analysis and IPA upstream analysis of differentially expressed genes in Caco-2 cells co-cultured with *F. prausnitzii* compared with Caco-2 cells co-cultured with UV-killed *F. prausnitzii* or not treated with bacteria. However, butyrate is also known to regulate TJ related proteins such as occludin, and ZO-1, and thereby increase intestinal epithelial barrier integrity[222]. As the TEER, mannitol flux, or gene expression data do not suggest that *F. prausnitzii* improves intestinal barrier integrity, it is unlikely that these bacteria produce significant amounts of butyrate in the cell culture medium in the apical anaerobic co-culture model. Further, *F. prausnitzii* did not grow in the apical anaerobic co-culture model, and substrates required for fermentation of dietary fibre were not added to the anaerobic cell culture medium, suggesting it is unlikely that *F. prausnitzii* would have produced any

SCFAs. This could be further investigated by analysing the amount of SCFAs produced by *F. prausnitzii* in the anaerobic cell culture medium (e.g. using high performance liquid chromatography), and aiding the production of SCFAs in this growth medium through supplementation with additional substrates, or co-culturing the bacteria at exponential phase rather than stationary phase.

F. prausnitzii loses a log viability in the apical anaerobic model. This may be due to that fact that the bacterium is grown in a culture medium not optimised for its growth, in the presence of epithelial cells which potentially competes for nutrients, or due to the presence of a low level oxygen in the culture medium. Supplementation of the apical cell culture medium, for example with acetate or riboflavin, may potentially also improve the viability of *F. prausnitzii* in the apical anaerobic environment. Acetate has been shown to be necessary for the growth of *F. prausnitzii*[301]. Several strains of *F. prausnitzii* have also been shown to utilise apple pectin and uronic acid for growth[364]. Recent studies have shown that, in low oxygen levels, *F. prausnitzii* uses riboflavin to shuttle electrons extracellularly to oxygen, and that this electron shuttling strongly stimulates the growth of *F. prausnitzii*[303,365]. Improved viability of *F. prausnitzii* in the apical anaerobic model may reveal additional mechanisms through which *F. prausnitzii* influence epithelial cell function.

As discussed above live *F. prausnitzii* exerted greater and more profound effects on Caco-2 cells compared to UV-killed *F. prausnitzii*, many of which were more akin to the effects of bacteria on intestinal epithelial cells *in vivo*. Inside the human intestinal tract, the vast majority of bacterial cells would be viable; thus the effects of the live obligate anaerobes, as assessed by the apical anaerobic co-culture model, may be more representative of the physiological effects of anaerobic commensal bacteria, than non-viable bacteria co-cultured with intestinal epithelial cells under conventional cell culture conditions.

Chapter 6:

General discussion

6.1 BACKGROUND

This project was part of a wider research programme which builds on the assertion that "health is the future of food", and aims to understand how food nutrients and constituents, both in terms of their nutritional value as well as their impact beyond simple nutrition, influence intestinal function, and hence health. As described in Chapter 1, the human intestine is a complex ecosystem consisting of various types of human intestinal cells and microbial cells, which undergo a molecular 'crosstalk' essential for the proper regulation and functionality of the intestinal barrier. While much research has been carried out to investigate how microbes and their metabolites mediate this molecular crosstalk, the vast majority of *in vitro* studies have focussed on oxygen-tolerant microbes. However, over 90% of the commensal intestinal bacteria are obligate anaerobes, some of which are extremely oxygen sensitive and technically challenging to co-culture with human cells in conventional *in vitro* cell culture models. A major aim of the work presented in this dissertation was to develop and validate a method to overcome this limitation (Chapters 2 to 5).

A better understanding of the regulation of barrier function will assist the development of foods that confer substantiated health and wellness benefits. The research presented in this dissertation was directed at the establishment of protocols and validation of a unique *in vitro* model of the intestinal barrier, representative of the physiological conditions of the intestine. The model can be used to gain insights into the mechanisms of crosstalk between commensal obligate anaerobic bacteria and intestinal cells, and new knowledge generated using this model will assist in the development of strategies to improve intestinal barrier function using food.

6.2 SUMMARY OF RESULTS

The studies recorded in this dissertation underpin the development of an apical anaerobic model of the human intestinal barrier which allows polarised intestinal cells to remain viable when exposed to an anaerobic environment on the apical side. This model was designed specifically to investigate the interactions between commensal obligate anaerobes and intestinal epithelial cells, with a focus on the regulation of the intestinal barrier. The model utilised a dual-environment co-culture chamber, which,

when placed inside an anaerobic workstation, allowed Caco-2 cell monolayers to be exposed to an anaerobic environment on the apical (luminal) side, while maintaining an aerobic basal side to prevent hypoxia.

At 12 hours of incubation, the DO content in the medium of the apical compartment of the co-culture chamber was almost undetectable, while in the basal compartment DO was over 75% saturation, showing that the chamber maintained an anaerobic apical compartment, and that oxygen tension in the basal compartment was not depleted, thus supporting the validity of the use of this model over 12 hours. The Caco-2 cells in the apical anaerobic model remained viable and maintained features characteristic of intestinal epithelial cells, while global changes in gene expression levels also suggested that these cells had adapted to survive in an atmosphere of lower oxygen compared to cells cultured in a conventional system. Further, the Caco-2 cells maintained a polarised monolayer with intact TJ over the 12 hour period, indicating that the model was suitable for investigating interactions between obligate anaerobes and polarised intestinal epithelial cells.

The apical anaerobic model was used to investigate interactions between the commensal anaerobe *F. prausnitzii* and intestinal cells. While the viability of *F. prausnitzii* dropped by four logs after 30 minutes in aerobic conditions, this loss in viability was reduced to one log for *F. prausnitzii* co-cultured with Caco-2 cells in the apical anaerobic model for 12 hours. To demonstrate the usefulness of the model, the effects of live vs. dead *F. prausnitzii* (which cannot be maintained viable in conventional cell culture models) on intestinal barrier function and epithelial cell gene expression was investigated.

Each well of the prototype co-culture chamber was equipped with a pair of electrodes for automated measurement of TEER, and a port sealed with a septum for sampling of basal medium for measuring molecule permeability. These features allowed the effects of bacteria on intestinal barrier integrity to be investigated. The TEER assay did not show any effect of viable or non-viable *F. prausnitzii* on Caco-2 cell monolayers, while viable *F. prausnitzii* were shown to increase small molecule permeability after 8 hours of co-culture compared with non-viable *F. prausnitzii*. Global gene expression analysis also showed that *F. prausnitzii* cells exert different effects on Caco-2 cells when it is alive, compared to when it is dead, highlighting the need for a

co-culture system that allows obligate anaerobic bacteria to be cultured with epithelial cell monolayers.

6.3 GENERAL DISCUSSION

6.3.1 Development

The physical component of the intestinal barrier is a single layer of epithelial cells that separates the luminal contents from the inside of the body. TJ seal the paracellular space between epithelial cells while providing selective permeability to fluids, electrolytes and small molecules. In the apical anaerobic model described in this dissertation, Caco-2 cells were used to model the intestinal epithelial barrier, as they are known to form a confluent monolayers with intact TJ and spontaneously differentiate to polarised small intestine enterocyte-like cells, characterised by an apical brush border[228].

The TJ of the polarised monolayer is an important component of this model. For example, the modulation of TJ is an important mechanism through which the intestinal barrier is regulated by commensal intestinal bacteria and food components in the human intestine[59]. Furthermore, as TJ seal the paracellular space between the epithelial cells[366], it will ensure that minimal oxygen diffuses from the basal through to the apical compartment, thus maintaining the dual environment in the co-culture chamber. Although HT29 cells can be induced to differentiate by means of various chemicals, unlike Caco-2 cells they do not differentiate spontaneously under normal culture conditions[229]. While T84 cells do differentiate spontaneously, their brush border is not as well developed as Caco-2 cells and their morphology is characteristic of colonic crypt cells[238].

Despite the common use of differentiated Caco-2 cell monolayers as a model of the human intestinal epithelium, these cells have inherent limitations due to their tumour origin, and may not always be representative of human intestinal cells *in vivo*. For example, Caco-2 cells exhibit physiological and biochemical properties of small intestine absorptive enterocytes although they were derived from a human colon[228]. These include the expression of hydrolase enzymes associated with the brush border of small intestinal enterocytes, and the foetal, but not adult, human colon. Certain features of Caco-2 cells are also representative of other cytotypes. For example, ion conductivity

and permeability of Caco-2 cells resemble cells found in the colonic crypt[275]. Nonetheless Caco-2 remains one of the most widely used models of the intestinal epithelium and is well characterised, and easily maintained.

The human intestine is covered by a layer of mucus. The mucus layer in the colon has two distinct layers, an inner layer, which is seemingly sterile and attached to the underlying mucosa[115,116,117], and an upper layer which contains mucins, cell debris and bacteria[115]. In contrast, the small intestine, which is resembled by the Caco-2 cell line, is thought to be covered by a thin discontinuous layer of mucus[120], and thus may be the main region of the human intestine where most of the host-microbe interactions take place.

The apical anaerobic model makes use of a 2-dimensional Transwell (microporous membrane) system, which facilitates basolateral feeding of cells, similar to the *in vivo* setting where epithelial cells obtain nutrients from the underlying blood vessels[244]. In the apical anaerobic model, the microporous membrane separates the apical anaerobic atmosphere from the basal aerobic environment. Here the model is more similar to the *in vivo* setting because it also mimics epithelial cells receiving oxygen from the underlying capillaries.

More complex systems, such as 3-dimensional models[367], and miniature intestines on microchips[368,369], have also been developed, although it can be argued that these models are still a work in progress[370]. One such model utilised an absorbent polymer gel to build micro-scale scaffolding, representing the intestinal villi, on to which Caco-2 cells were seeded[367]. More recently, a model that mimics peristalsis was developed[369]. This model is composed of a microchip with microfluidic channels lined by Caco-2 cells, and utilises vacuum chambers to mimic peristalsis. TEER measurements were also possible using electrode wires connected to a voltohmmeter. Further, this model allowed for co-culture with the facultative anaerobe *L. rhamnosus* for extended periods (over a week), without compromising the viability of the human or bacterial cells. Another similar microfluidic model developed by Kim *et al.* (2010)[368] facilitated the co-culture of the epithelial cell line HeLa with both commensal and pathogenic bacteria (both facultative anaerobic strains) in independent compartments, to allow study of the subsequent pathogen colonisation and the effect of the commensal environment. Such models reflect a complex physiology akin to *in vivo* models, while at the same time providing the advantages of an *in vitro* model, such as allowing control

over conditions influencing variability. These models could potentially be further developed to facilitate co-culture with commensal anaerobic bacteria.

The apical anaerobic model described in this dissertation made use of the well-studied and characterised Caco-2 cell line, and the Transwell co-culture system. A custom built co-culture chamber facilitated the separation of the apical and basal environments of the polarised monolayer, which allowed for an anaerobic apical environment. Compared to existing models, the apical anaerobic model offers the advantages of simplicity, and automated measurements of epithelial barrier integrity, which once validated could be suitable for the study of the regulation of barrier integrity by commensal anaerobic intestinal bacteria.

6.3.2 Validation

It is crucial that the apical anaerobic model, as with all newly developed models, be sufficiently validated prior to its application. This required firstly that the model be shown to maintain an anaerobic apical environment and an aerobic basal environment for the duration of the experiment, and secondly that the cells remain viable in the altered atmosphere. Finally, because the apical anaerobic model was developed with the main intention of studying interactions with intestinal bacteria, and the regulation of intestinal barrier function, the polarisation and TJ integrity of the Caco-2 cell monolayer was of utmost importance. Other features of Caco-2 cells, such as the expression and activity of brush border enzymes (digestive enzymes), membrane transporters, and nuclear receptors (such as vitamin receptors) were not studied. However, if the apical anaerobic model would be used in alternative applications, such as in the study of active transport of food compounds, or as a model of drug metabolism, it is recommended that the features of the Caco-2 cell monolayer relevant to the application be characterised in the anaerobic apical environment.

As discussed in section 6.3.1, the region of the human intestinal tract represented by Caco-2 cells is unclear. While derived from a human colon, they express brush border enzymes associated with the small intestine[228], and ion permeability akin to colonic crypt cells[275]. Thus when validating the apical anaerobic model, Caco-2 cells were not compared with *in vivo* or *ex vivo* tissue. Instead, Caco-2 cells cultured in the anaerobic apical environment were compared with Caco-2 cells cultured on microporous membranes under conventional cell culture conditions.

As described in Chapter 3, this newly developed model was able to maintain an apical anaerobic environment for 12 hours. Caco-2 cells in the apical anaerobic model remained viable during this time. Studies of intestinal barrier integrity showed that TJ integrity was also preserved, contrary to previous studies which have observed hypoxia induced loss of epithelial barrier function[283,284], and increased epithelial permeability and decreased TEER in Caco-2 cells[285].

Many functional characteristics of the Caco-2 cell line are affected by various factors, including passage number, composition of the cell culture medium, and the type of membrane on which the cells are seeded[269]. Caco-2 cells obtained from different laboratories also show functional differences[371]. Given these observations, it was plausible that culturing Caco-2 cells in an anaerobic apical environment would influence its functional characteristics.

Global gene expression analysis was used to reveal key differences in gene expression and ascertain possible functional differences between Caco-2 cells grown in the apical anaerobic model and those grown under conventional conditions. As the Caco-2 cells in the apical anaerobic model are arguably more representative of the physiological conditions in the intestine than cells cultured under standard cell culture conditions, it was hypothesised that altered functional characteristics may cause these cells to be more similar to epithelial cells in the human intestine. This however was not reflected in the data. Instead, gene expression profiles were consistent with increased cell survival and proliferation in reduced oxygen conditions, suggesting an adaptation of the Caco-2 cells in the apical anaerobic model to a lower supply of oxygen. The adaptation of this model can be likened to that of proliferating cancer cells in a tumour mass where oxygen supply is scarce[323]. Thus it could be argued that the functional characteristics of the Caco-2 cells in the apical anaerobic model may be more similar to that of the colorectal cancer cells the cell line was derived from, rather than normal intestinal cells under physiological conditions. Nonetheless, as discussed in Chapter 4, the gene expression data supported the phenotypical data showing the viability of the Caco-2 cell monolayer, and the integrity of the TJ barrier, thus supporting the validity of this novel apical anaerobic model of the intestinal barrier.

6.3.3 Application

As demonstrated in Chapter 5, the apical anaerobic model could be used to co-culture a commensal obligate anaerobe with Caco-2 cells. The viability of the anaerobe *F. prausnitzii* dropped by one log in the apical anaerobic model after 8 hours of co-culture, whereas it was shown to drop by over four logs after 30 minutes in an aerobic environment. Using the TEER electrodes and sampling ports built into the co-culture chamber, it was possible to measure the effect of the bacteria on intestinal epithelial barrier integrity by means of the TEER and ^{3}H-mannitol bioassay. Furthermore, RNA was extracted from the Caco-2 cells to identify changes in gene expression in response to bacteria.

Apart from studies of barrier integrity, the apical anaerobic model could have been used to measure the production of immune mediators and chemokines by Caco-2 cells in response to the obligate anaerobe[372]. Changes in the immune phenotype would indicate if and how *F. prausnitzii* modulate immune pathways in host cells, and help confirm putative biological pathways and networks identified through global gene expression analysis.

One major limitation of the apical anaerobic model was that while it improved the survival rate of the obligate anaerobe compared to an aerobic environment, some loss of viability of the obligate anaerobe was observed. As illustrated by previous studies, the metabolites secreted by (viable) bacteria can regulate intestinal cell signalling pathways[257,373]. While global gene expression analysis suggested differences in the regulation of biological functions and pathways by non-viable and viable bacterial cells, a better survival of the 'viable' bacteria may have revealed more subtle, and a greater number of differences between the treatments. Furthermore, if the anaerobes were able to grow in the apical anaerobic model, they may have exerted additional effects. This hypothesis is in light of studies such as where the ability of pathogenic *Salmonella* to enter host cells *in vitro* was dependent on the growth phase of the bacterium[374].

Further research is needed to improve the survival of obligate anaerobes, and if possible allow them to grow, in the apical anaerobic model. Culturing of obligate anaerobes is technically challenging[375], and culturing anaerobes in a newly developed model is likely to pose additional complications, and will require further method

development. In the study described in Chapter 5, the anaerobe *F. prausnitzii* was cultured in cell culture medium devoid of oxygen. However, as shown in Chapter 3, a small amount of DO may be present in the apical compartment of the chamber, which may affect the metabolism of *F. prausnitzii*. If so, the addition of a reducing agent, such as glucose or cysteine, to the apical culture medium, may aid in improving anaerobe survival[375]. Furthermore, supplementing the apical culture medium with substrates specifically shown to aid the growth of the obligate anaerobe of interest (for example acetate[301] or riboflavin[365] shown to aid the growth of *F. prausnitzii*) may promote the survival or growth of the obligate anaerobe in the apical anaerobic co-culture model. Supplementation of the culture medium could potentially also affect the Caco-2 cells. Thus these effects should be determined and accounted for when designing co-culture experiments.

The apical anaerobic model of the intestinal barrier could potentially be used to screen for commensal obligate anaerobes that confer beneficial effects on intestinal barrier function. Once identified, the model can be used to test the extent of these effects (e.g. co-culture bacteria at various MOIs, and/or different phases of growth) and dissect the mechanisms-of-action through which the bacteria exert these effects (e.g. compare the effects of different bacterial fractions, or mutant strains with known gene deletions). In addition to live bacteria, the apical anaerobic model can be used to test effects of common bacterial constituents, such as lipopolysaccharide, or TLR antagonists, on Caco-2 cells in an anaerobic apical environment. These effects may be different to that of Caco-2 cells in conventional conditions, and the data may help dissect potential mechanisms-of-action of bacteria in the apical anaerobic model. However, as previously discussed, the apical anaerobic model, as with all *in vitro* models, has its limitations, and the data generated may not be representative of the *in vivo* situation. Thus when drawing conclusions based on experiments carried out using the apical anaerobic model, these limitations should be considered, and it is recommended that the beneficial effects of the bacteria also be tested *in vivo*.

6.4 FUTURE PERSPECTIVES

6.4.1 Improving the co-culture chamber design

The design of the co-culture chamber utilised in the apical anaerobic model allows for the aerobic environment of the chamber well to be separated from the anaerobic environment of the anaerobic workstation. While this design allows for Caco-2 cells to be cultured in an anaerobic apical environment for at least 12 hours, and the TEER electrodes and sampling ports, aid the measurement of barrier integrity, further modifications were considered to improve the versatility and ease-of-use of the co-culture chamber.

Currently each chamber lid can hold either a pressure release valve, or a rubber septum, sealing the sampling port. Future prototypes should allow for both a sampling port sealed with a septum, and a valve which allows for more convenient setting up of the co-culture chamber. Furthermore, while the current design of the chamber includes a top electrode plate, this does not serve the same purpose as the lid of a multi-well cell culture plate. Thus, future prototypes should integrate a secondary lid that can be placed over the top electrode plate, and thus help maintain the sterility in the apical compartment of the chamber when being transferred between the cell culture hood, 5% CO_2 incubator and anaerobic workstation.

Future prototypes of the apical anaerobic model could be miniaturised. The current design contains a 50 mL chamber well, and the chamber lids act as adaptors for 12 mm (4.67 cm^2) cell culture inserts. As discussed in Chapter 2, the relatively large volume of medium was used to ensure that sufficient DO was available for the Caco-2 cells, while the large insert size (which equates to a high number of cells in the Caco-2 cell monolayer), ensured a sufficient RNA yield for the gene expression studies carried out in Chapters 4 and 5. However a smaller cell culture insert could be substituted for most experiments, which would allow for a smaller co-culture chamber. Further, as shown in Chapter 3, the DO in the basal compartment of the co-culture chamber had reduced by less than 25% after 12 hours, suggesting that a lower volume of basal medium may be sufficient for Caco-2 cell survival and maintenance of barrier integrity. If a smaller cell culture insert was used as described above, each well in the co-culture chamber would contain fewer Caco-2 cells, resulting in a smaller DO demand. Thus the size of the basal compartment, and hence the chamber could be considerably reduced.

During the validation of the co-culture chamber model, methods of introducing oxygen to the basal compartment were investigated to ensure that the Caco-2 cells had sufficient oxygen available to sustain their viability and barrier integrity. One method involved the modification of the chamber base with six individual channels, each of which would allow fresh aerobic medium to flow through, and replace the contents of each chamber well. However, the possibility of a simpler and more feasible method was also explored, where the existing sampling port would be converted into an 'oxygen port'. In this method, a gas line would run through the rubber septum of the sampling port through to the basal compartment of the chamber, thus allowing the basal medium to be perfused with aerobic gas. These methods would have been further developed if the validation of the model proved that the current method was insufficient to ensure epithelial cell viability in the apical anaerobic model.

6.4.2 Creating a physiological intestinal environment

As previously discussed, reductionist *in vitro* cell culture models present many advantages over *in vivo* models. However, these models lack the complexity and dynamic nature of an *in vivo* system. Although it may be argued that an *in vitro* model could never be an *in vivo* alternative, as discussed below, models such as the apical anaerobic model can be developed further to better represent the *in vivo* situation.

One major difference between the apical anaerobic model and the *in vivo* situation is the absence of mucus. As described in Chapter 1, the mucus layer which overlays the intestinal epithelium, is the first anatomical site at which the host encounters bacteria. The mucus layer plays an important role in the attachment of bacteria[376], and the physicochemical properties of the mucus layer influence the rate of diffusion to the epithelium[377]. Moreover, while the apical anaerobic model is composed of solely enterocyte-like cells, the intestinal barrier contains various different types of cells, such goblet cells, endocrine cells, and M cells[378].

To overcome these limitations, co-cultures of two or more cell lines can be established in the apical anaerobic co-culture model. For example, some *in vitro* models of the intestinal barrier contain Caco-2 cells co-cultured with HT29-MTX cells, which represent mucus-secreting goblet cells. These cells modulate TJ geometry and 'tightness' and produce a mucus layer that covers the cell surface mimicking physiological conditions[2,248].

Epithelial-immune cell co-cultures are also routinely established to allow the investigation of immune cell mediation by intestinal bacteria and other components[253,254]. For example, several studies have also established *in vitro* models containing immature DC and Caco-2 cells[213,379]. As described in Chapter 1, DC are an important component of the intestinal barrier, and are able to sample luminal contents while maintaining TJ integrity[128].

The apical anaerobic model could potentially be developed into a more complex system that constitutes three intestinal cell types (epithelial, dendritic and goblet), and thus be more representative of the intestinal barrier than a single-cell-type model. Caco-2 cells could be co-cultured with goblet-like cells (e.g. as described in Hilgendorf *et al.* (2000)[248]), which would result in the development of a mucus layer in the anaerobic luminal environment. The DC could be seeded on the basal side of the semi permeable membrane as described in Rimoldi *et al.* (2004)[213], and as such would be cultured in the aerobic compartment of the co-culture chamber, ensuring its survival.

As a model which better represents physiological conditions, such a model would allow for more comprehensive investigation of the crosstalk between the barrier components that regulate barrier function. For example, assays could be carried out to determine if epithelial cells influence DC responses in the apical anaerobic model; for example by assessing DC translocation across the epithelial cell monolayer in response to intestinal epithelial derived factors. Furthermore, the effect on commensal anaerobic bacteria on the DC immune phenotype could also be investigated.

6.4.3 Future applications of the apical anaerobic model

While the apical anaerobic model was designed specifically to investigate the effects of obligate anaerobic bacteria and intestinal epithelial cells, it could also be used to study the effects of facultative anaerobic bacteria. Commensal facultative anaerobes, and facultative anaerobic probiotic bacteria, though able to survive under aerobic conditions, also survive under anaerobic conditions in the human intestinal tract. Thus facultative anaerobes cultured in the apical anaerobic model are in an environment more similar to the conditions in the intestine than conventional cell culture models in a solely aerobic environment.

In order to survive in both aerobic and anaerobic environments, facultative anaerobes are able to fluctuate between aerobic respiration, anaerobic respiration and fermentation[380]. Thus the physiology of the facultative anaerobe is considerably altered depending on its environment. Gene expression analysis of the facultative anaerobe *E. coli* revealed profound changes in the transcription profile within 5 minutes of transition from an anaerobic to aerobic environment, and biological pathways such as 'peroxide stress management', 'methionine biosynthesis', and 'oxygen-dependent putrescine degradation' were suggested to be involved[304]. Another study showed that exposure of EHEC O157:NM to anaerobic conditions leads to the transcription of *sfpA*, a gene encoding for fimbriae[381]. Although fimbriae were absent in this strain of EHEC under standard aerobic conditions, exposure to an anaerobic environment led to the expression of fimbriae and subsequently enhanced adherence of EHEC to intestinal epithelial cells *in vitro*.

In light of the above examples, the effects of facultative anaerobes on intestinal epithelial cells are likely to differ based on whether the bacteria are in a conventional aerobic environment or an anaerobic environment. As facultative anaerobes cultured in the apical anaerobic model would be in an environment more similar to the conditions found in the intestine, the effects of the bacteria in this model are more likely to be representative of the *in vivo* situation than in conventional cell culture models.

Another application of the apical anaerobic model is the study of the effects of dietary components on intestinal epithelial cells. As discussed in Chapter 1, dietary components, including whole food extracts, proteins and amino acids have been shown to directly affect the integrity of the intestinal barrier. However, as illustrated by the studies described in Chapter 1, most of the investigations carried out *in vitro* have been on intestinal epithelial cells cultured under conventional conditions. Thus *in vitro* investigation of the effect of dietary components on the intestinal barrier may be warranted in the apical anaerobic model.

In addition to their direct effects, interactions of food components with commensal intestinal bacteria are also known to be important in the regulation of the intestinal barrier[222,223]. Furthermore, dietary components can aid intestinal barrier function by negating the effects of pathogenic bacteria. For example, human milk oligosaccharides inhibit the adhesion of intestinal pathogens such as *E. coli* and *Vibrio cholerae* to Caco-2 cells[224]. *In vitro* studies of epithelial cells co-cultured with food and

bacteria are also important in determining the regulation of various other aspects of intestinal epithelial cells; for example probiotic strains of *E. coli* and *Lactobacillus salivarius* have been shown to enhance calcium uptake, possibly through influencing calcium transport mechanisms, in Caco-2 cells[382]. An advantage of using the apical anaerobic model to study the effect of food components includes the ability to co-culture commensal and/or pathogenic intestinal bacteria, including obligate anaerobes, in a physiological intestinal environment, previously not possible using conventional cell culture models.

6.5 CONCLUSIONS

The establishment and validation of a new *in vitro* model of the intestinal barrier, designed to allow investigation of the interactions between commensal obligate anaerobic bacteria and the intestinal epithelium, has been described. This model enables polarised intestinal cells to remain viable when exposed to an apical anaerobic environment. Because the intestinal cells were exposed to an anaerobic environment on the apical (luminal) side, this model is arguably more representative of the physiological conditions of the intestine than conventional models in a solely aerobic environment. Using the commensal anaerobe *F. prausnitzii* it was demonstrated that viable anaerobes exerted greater and more profound effects on intestinal cells compared to non-viable anaerobes usually studied in conventional cell culture models. Many of these were more akin to the effects of bacteria on intestinal epithelial cells *in vivo*, arguing for the need for this apical anaerobic model.

Further research is needed to ensure a better survival rate and growth of the obligate anaerobes in the apical anaerobic model, which could result in the generation of more physiologically relevant data. Furthermore, the apical anaerobic model could be developed to include multiple cell types, including immune cells, and a mucus layer. The apical anaerobic model could also be used to study the effects of facultative anaerobic bacteria (such as probiotics) on intestinal cells; and as the bacteria will be in an *in vitro* environment more similar to the intestinal lumen than conventional cell culture models, the bacterial metabolites and their affects could potentially be more representative of the *in vivo* situation.

However, the potential drawbacks of the apical anaerobic model should not be overlooked. Importantly, because the human intestinal cells used were from a tumour-origin, and are in a lower-oxygen atmosphere, arguably more representative of the tumour environment, it may not be appropriate to extrapolate data generated using this model to the *in vivo* situation. Thus, when drawing any and all conclusions using this model, the limitations of the model should be first considered.

Nonetheless the apical anaerobic model offers the advantages of simplicity and automated measurements of epithelial barrier integrity in a dual-environment suitable for the culture of both obligate anaerobic bacteria and human intestinal cells. As such this model is a valuable tool to advance knowledge and provide an understanding of the mechanisms of crosstalk between commensal anaerobic bacteria and human intestinal cells important in the regulation of intestinal barrier function.

APPENDICES

Appendix I Engineers' drawings of the co-culture chamber

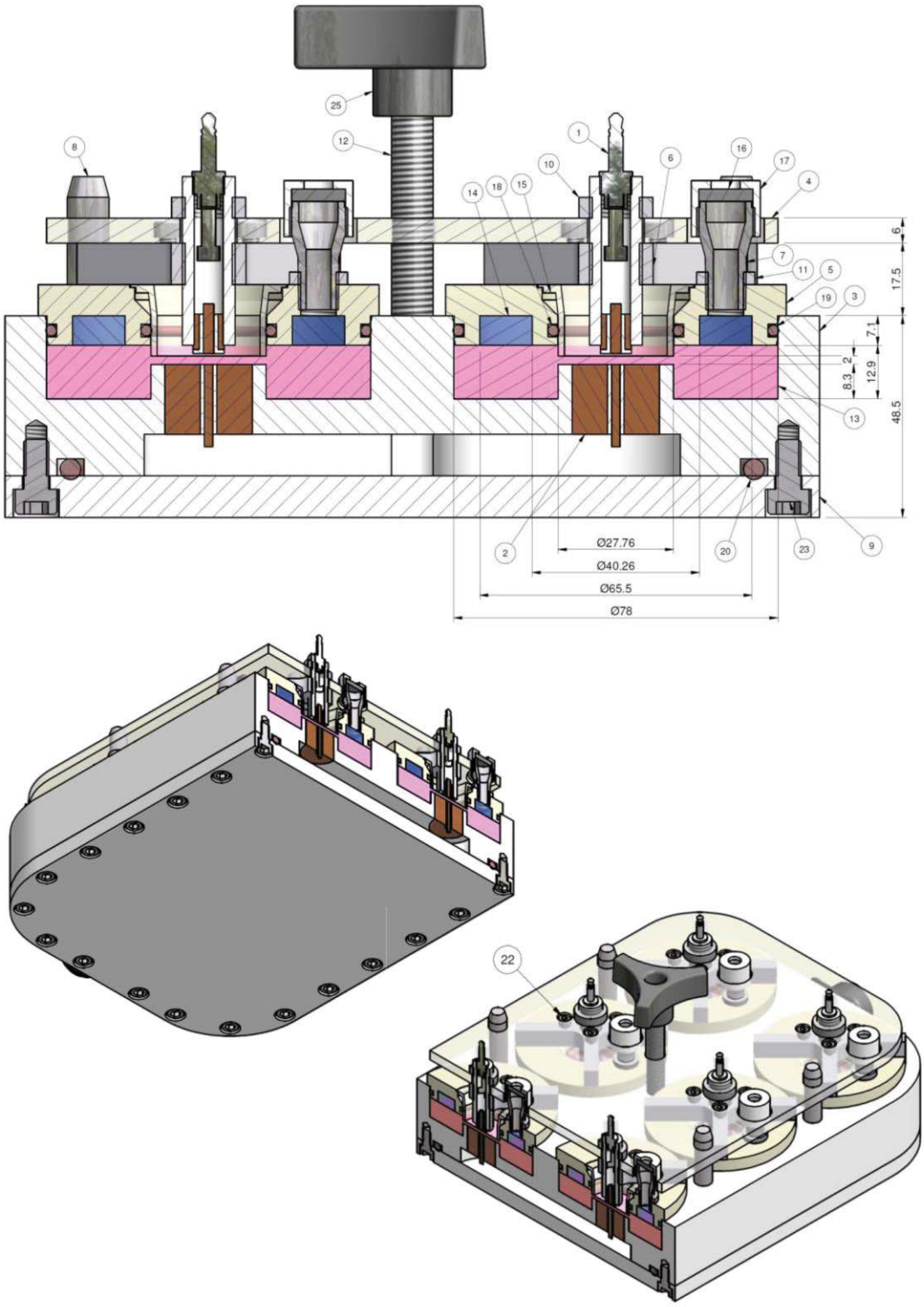

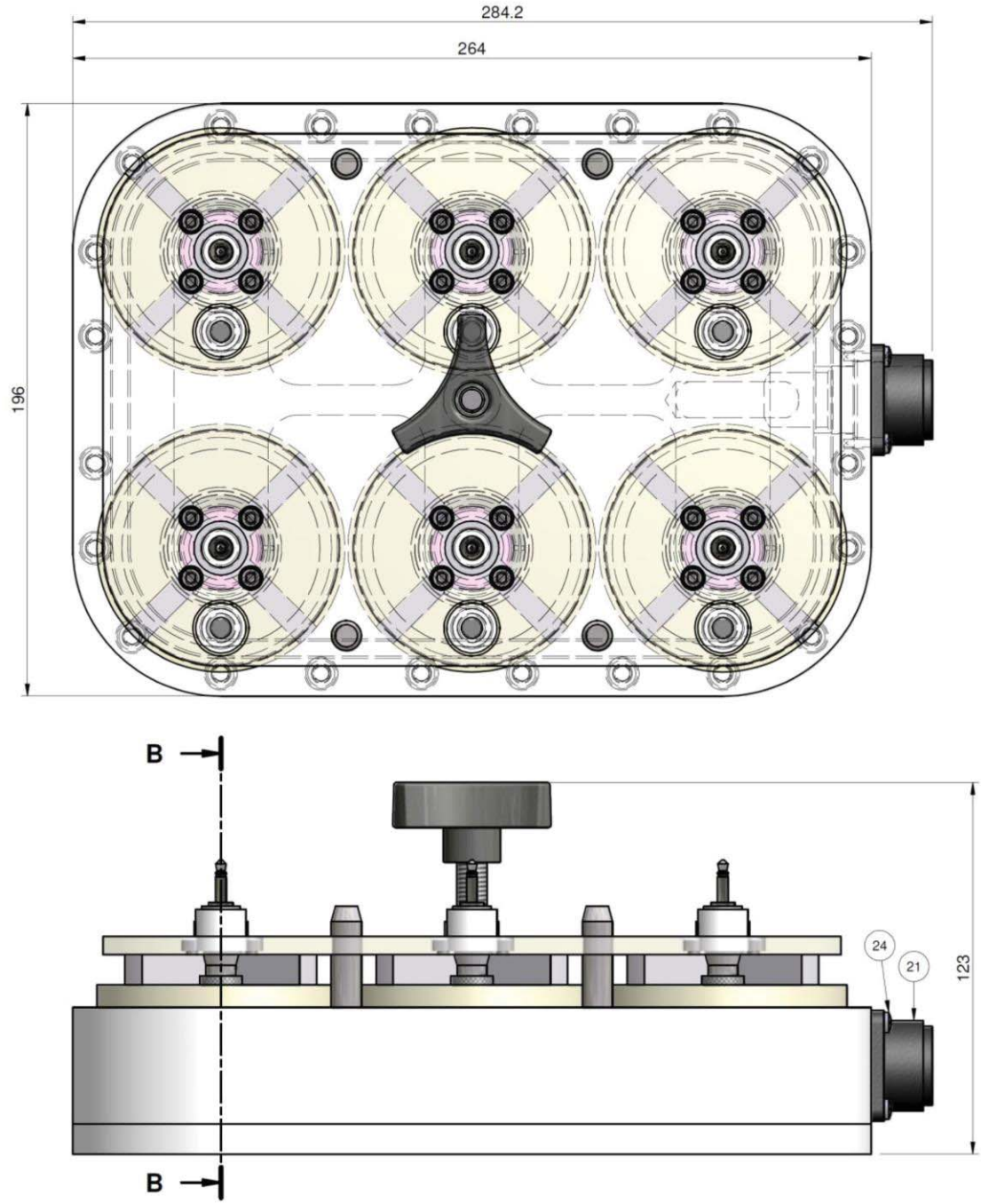
284.2
264
196
B
B
24
21
123

Item	*Description*
1	Top Electrode Assembly
2	Bottom Electrode Assembly
3	Chamber
4	Chamber Lid
5	Chamber Seal
6	Top Electrode Holder
7	Septum Adaptor
8	Lid Location Pin
9	Chamber Base
10	Top Electrode Lock Nut
11	Septum Adaptor Lock Nut
12	Handle Stud
13	Cell Culture Medium
14	Air
15	Insert
16	Septum
17	Labco Exetainer
18	Seal Inner O-Ring - Size BS121 - Silicone Rubber
19	Seal Outer O-Ring - Size BS150 - Silicone Rubber
20	Base O-Ring - 5mm Cord Dia - Silicone Rubber
21	Amphenol C16-3 Panel Plug
22	Socket Head Cap Screw - M4x0.7P x 10 - 316 Stainless
23	Socket Head Cap Screw - M6x1P x 12 - 316 Stainless
24	6 x 0.500" Pan Pozi Self Tapper - SS 4
25	Tri Knob M10

Appendix II FACSCalibur instruments for DNA content analysis

Detectors/Amps:

Param	*Detector*	*Voltage*	*AmpGain*	*Mode*
P1	FSC	E-1	2.13	Lin
P2	SSC	293	1.00	Lin
P3	FL1	659	1.00	Lin
P4	FL2	327	1.00	Lin
P5	FL3	650	1.00	Lin
P6	FL2-A		1.00	Lin
P7	FL2-W		1.00	Lin

Threshold:

Primary Parameter: FSC
Value: 39

Secondary Parameter: None

Compensation:

FL1 - 0.0 % FL2
FL2 - 0.0 % FL1
FL2 - 0.0 % FL3

Appendix III Settings for confocal microscope

Dimensions

Dimension	*Logical Size*	*Physical Length*	*Physical Origin*
X	1024	387.50 µm	0.00 µm
Y	1024	387.50 µm	0.00 µm

Scanner Settings

ScanMode	xyz
Pinhole [m]	67.9 µm
Pinhole [airy]	1.00
Size-Width	387.5 µm
Size-Height	387.5 µm
Size-Depth	0.0
StepSize	0.04 µm
Voxel-Width	378.8 nm
Voxel-Height	378.8 nm
Voxel-Depth	0.0 nm
Zoom	1.0
Scan-Direction	1
SequentialMode	0
Frame-Accumulation	1
Frame-Average	1
Line-Average	8
Resolution	8 bits
Channels	2
Format-Width	1024 pixels
Format-Height	1024 pixels
Sections	1

Hardware Settings

AOTF (405)	35 %
AOTF (458)	0 %
AOTF (476)	0 %
AOTF (488)	0 %
AOTF (496)	0 %
AOTF (514)	0 %

AOTF (561)	25 %
AOTF (633)	0 %
PMT 1	Active
PMT 1 (Offs.)	-0.13333333333334 %
PMT 1 (HV)	663.3 Volt
PMT 1 (HV_Unit)	V
PMT 1 (Preamp)	Standard
PMT 2	Inactive
PMT 3	Active
PMT 3 (Offs.)	-1.07333333333334 %
PMT 3 (HV)	562.0 Volt
PMT 3 (HV_Unit)	V
PMT 3 (Preamp)	Standard
PMT Trans	Inactive
UV Lens FW	Lens 40x/1.25 Oil
Laser (405 Diode, UV)	405 nm
Laser (Argon, visible)	458 nm
Laser (Argon, visible) (Power)	20 %
Laser (DPSS 561, visible)	561 nm
Laser (HeNe 633, visible)	633 nm
Scan Field Rotation	0 degrees
Scan Speed	400 Hz
Objective	HCX PL APO lambda blue 40.0x1.25 OIL UV
Numerical aperture (Obj.)	1.25
Refraction index	1.52
Emission bandwidth PMT 1: begin - end	419.0nm - 500.8nm
Emission bandwidth PMT 3: begin - end	570.6nm - 672.3nm

Sequential Setting Nr.1 (Occludin channel)

Target Slider	Target Park
UV Lens Wheel	Lens 40x/1.25 Oil
PMT 1 (418.961038961039nm - 500.779220779221nm)	Active, Gain: 663, Offset: 0
PMT 2 (500.909090909091nm - 543.766233766234nm)	Inactive, Gain: 550, Offset: 0
PMT 3 (570.584415584415nm - 672.337662337663nm)	Active, Gain: 562, Offset: -1
Transmission	Inactive, Gain: 246, Offset: 0
Laser Line UV(405)	35 %
Laser Line Visible(458)	0 %
Laser Line Visible(476)	0 %
Laser Line Visible(488)	0 %
Laser Line Visible(496)	0 %
Laser Line Visible(514)	0 %

Laser Line Visible(561)	25 %
Laser Line Visible(633)	0 %

Sequential Setting Nr.2 (ZO-1 channel)

Target Slider	Target Park
UV Lens Wheel	Lens 40x/1.25 Oil
PMT 1 (422.077922077922nm - 474.285714285714nm) Inactive, Gain: 707, Offset: 0	
PMT 2 (500.909090909091nm - 570.259740259741nm) Active, Gain: 690, Offset: 0	
PMT 3 (585.38961038961nm - 699.155844155844nm) Inactive, Gain: 629, Offset: 0	
Transmission	Inactive, Gain: 246, Offset: 0
Laser Line UV(405)	0 %
Laser Line Visible(458)	0 %
Laser Line Visible(476)	0 %
Laser Line Visible(488)	100 %
Laser Line Visible(496)	0 %
Laser Line Visible(514)	0 %
Laser Line Visible(561)	0 %
Laser Line Visible(633)	0 %

REFERENCES

1. Sekirov, I., Russell, S.L., Antunes, L.C. & Finlay, B.B. Gut microbiota in health and disease. *Physiol Rev* **90**, 859-904 (2010).
2. Lievin-Le Moal, V. & Servin, A.L. The front line of enteric host defense against unwelcome intrusion of harmful microorganisms: mucins, antimicrobial peptides, and microbiota. *Clin Microbiol Rev* **19**, 315-337 (2006).
3. Didierlaurent, A., Sirard, J.-C., Kraehenbuhl, J.-P. & Neutra, M.R. How the gut senses its content. *Cell Microbiol* **4**, 61-72 (2002).
4. Farhadi, A., Banan, A., Fields, J. & Keshavarzian, A. Intestinal barrier: an interface between health and disease. *J Gastroenterol Hepatol* **18**, 479-497 (2003).
5. Liu, Z., Li, N. & Neu, J. Tight junctions, leaky intestines, and pediatric diseases. *Acta Paediatr* **94**, 386-393 (2005).
6. Arrieta, M.C., Bistritz, L. & Meddings, J.B. Alterations in intestinal permeability. *Gut* **55**, 1512-1520 (2006).
7. Vogelsang, H., Schwarzenhofer, M. & Oberhuber, G. Changes in Gastrointestinal Permeability in Celiac Disease. *Dig Dis* **16**, 333-336 (1998).
8. Suenaert, P., Bulteel, V., Lemmens, L., Noman, M., Geypens, B., Van Assche, G., Geboes, K., Ceuppens, J.L. & Rutgeerts, P. Anti-tumor necrosis factor treatment restores the gut barrier in Crohn's disease. *Am J Gastroenterol* **97**, 2000-2004 (2002).
9. Camilleri, M., Madsen, K., Spiller, R., Greenwood-Van Meerveld, B. & Verne, G.N. Intestinal barrier function in health and gastrointestinal disease. *Neurogastroenterol Motil* **24**, 503-512 (2012).
10. Damci, T., Nuhoglu, I., Devranoglu, G., Osar, Z., Demir, M. & Ilkova, H. Increased intestinal permeability as a cause of fluctuating postprandial blood glucose levels in Type 1 diabetic patients. *Eur J Clin Invest* **33**, 397-401 (2003).
11. Yacyshyn, B., Meddings, J., Sadowski, D. & Bowen-Yacyshyn, M.B. Multiple sclerosis patients have peripheral blood CD45RO+ B cells and increased intestinal permeability. *Dig Dis Sci* **41**, 2493-2498 (1996).
12. McCracken, V.J. & Lorenz, R.G. The gastrointestinal ecosystem: a precarious alliance among epithelium, immunity and microbiota. *Cell Microbiol* **3**, 1-11 (2001).
13. Rajilic-Stojanovic, M., Smidt, H., de Vos, W.M., Rajilic-Stojanovic, M., Smidt, H. & de Vos, W.M. Diversity of the human gastrointestinal tract microbiota revisited. *Environ Microbiol* **9**, 2125-2136 (2007).
14. Wells, J.M., Rossi, O., Meijerink, M. & van Baarlen, P. Epithelial crosstalk at the microbiota–mucosal interface. *Proc Natl Acad Sci U S A* **108**, 4607 (2011).
15. Mondot, S., Kang, S., Furet, J.P., Aguirre de Carcer, D., McSweeney, C., Morrison, M., Marteau, P., Dore, J. & Leclerc, M. Highlighting new phylogenetic specificities of Crohn's disease microbiota. *Inflamm Bowel Dis* **17**, 185-192 (2011).

16. De Palma, G., Nadal, I., Medina, M., Donat, E., Ribes-Koninckx, C., Calabuig, M. & Sanz, Y. Intestinal dysbiosis and reduced immunoglobulin-coated bacteria associated with coeliac disease in children. *BMC Microbiol* **10**, 63 (2010).

17. Frank, D.N., St Amand, A.L., Feldman, R.A., Boedeker, E.C., Harpaz, N. & Pace, N.R. Molecular-phylogenetic characterization of microbial community imbalances in human inflammatory bowel diseases. *Proc Natl Acad Sci U S A* **104**, 13780-13785 (2007).

18. Ley, R.E., Peterson, D.A. & Gordon, J.I. Ecological and evolutionary forces shaping microbial diversity in the human intestine. *Cell* **124**, 837-848 (2006).

19. Ramakrishna, B.S. The normal bacterial flora of the human intestine and its regulation. *J Clin Gastroenterol* **41**, S2-S6 (2007).

20. Deplancke, B. & Gaskins, H.R. Microbial modulation of innate defense: goblet cells and the intestinal mucus layer. *Am J Clin Nutr* **73**, 1131S-1141S (2001).

21. Macpherson, A.J. & Uhr, T. Induction of protective IgA by intestinal dendritic cells carrying commensal bacteria. *Science* **303**, 1662-1665 (2004).

22. Hollander, D. Crohn's disease, TNF-alpha, and the leaky gut. The chicken or the egg? *Am J Gastroenterol* **97**, 1867-1868 (2002).

23. Turner, J.R. Intestinal mucosal barrier function in health and disease. *Nat Rev Immunol* **9**, 799-809 (2009).

24. Watts, T., Berti, I., Sapone, A., Gerarduzzi, T., Not, T., Zielke, R. & Fasano, A. Role of the intestinal tight junction modulator zonulin in the pathogenesis of type I diabetes in BB diabetic-prone rats. *Proc Natl Acad Sci U S A* **102**, 2916-2921 (2005).

25. Hooper, L.V. Do symbiotic bacteria subvert host immunity? *Nat Rev Microbiol* **7**, 367-374 (2009).

26. Davin, J.C., Forget, P. & Mahieu, P.R. Increased intestinal permeability to (51 Cr) EDTA is correlated with IgA immune complex-plasma levels in children with IgA-associated nephropathies. *Acta Paediatr Scand* **77**, 118-124 (1988).

27. Wigg, A.J., Roberts-Thomson, I.C., Dymock, R.B., McCarthy, P.J., Grose, R.H. & Cummins, A.G. The role of small intestinal bacterial overgrowth, intestinal permeability, endotoxaemia, and tumour necrosis factor alpha in the pathogenesis of non-alcoholic steatohepatitis. *Gut* **48**, 206-211 (2001).

28. Mullin, J., Valenzano, M., Verrecchio, J. & Kothari, R. Age- and diet-related increase in transepithelial colon permeability of Fischer 344 rats. *Dig Dis Sci.* **47**, 2262-2270. (2002).

29. Ma, T.Y., Hollander, D., Dadufalza, V. & Krugliak, P. Effect of aging and caloric restriction on intestinal permeability. *Exp Gerontol* **27**, 321-333 (1992).

30. Saweirs, W.M., Andrews, D.J. & Low-Beer, T.S. The double sugar test of intestinal permeability in the elderly. *Age Ageing* **14**, 312-315 (1985).

31. Saunders, P.R., Kosecka, U., McKay, D.M. & Perdue, M.H. Acute stressors stimulate ion secretion and increase epithelial permeability in rat intestine. *Am J Physiol* **267**, G794-799 (1994).

32. van der Flier, L.G. & Clevers, H. Stem cells, self-renewal, and differentiation in the intestinal epithelium. *Annu Rev Physiol* **71**, 241-260 (2009).

33. Louvard, D., Kedinger, M. & Hauri, H.P. The differentiating intestinal epithelial cell: establishment and maintenance of functions through interactions between cellular structures. *Annu Rev Cell Biol* **8**, 157-195 (1992).

34. Farquhar, M.G. & Palade, G.E. Junctional complexes in various epithelia. *J Cell Biol* **17**, 375-412 (1963).

35. Shen, L. & Turner, J.R. Role of epithelial cells in initiation and propagation of intestinal inflammation. Eliminating the static: tight junction dynamics exposed. *Am J Physiol Gastrointest Liver Physiol* **290**, G577-582 (2006).

36. Perez-Moreno, M. & Fuchs, E. Catenins: keeping cells from getting their signals crossed. *Dev Cell* **11**, 601-612 (2006).

37. Madara, J.L. Intestinal absorptive cell tight junctions are linked to cytoskeleton. *Am J Physiol* **253**, C171-175 (1987).

38. Garrod, D. & Chidgey, M. Desmosome structure, composition and function. *Biochim Biophys Acta* **1778**, 572-587 (2008).

39. Sosinsky, G.E. & Nicholson, B.J. Structural organization of gap junction channels. *Biochim Biophys Acta* **1711**, 99-125 (2005).

40. Banan, A., Choudhary, S., Zhang, Y., Fields, J.Z. & Keshavarzian, A. Ethanol-induced barrier dysfunction and its prevention by growth factors in human intestinal monolayers: evidence for oxidative and cytoskeletal mechanisms. *J Pharmacol Exp Ther* **291**, 1075-1085 (1999).

41. Powell, D.W. Barrier function of epithelia. *Am J Physiol Gastrointest Liver Physiol* **241**, G275-288 (1981).

42. Fasano, A. Novel approaches for oral delivery of macromolecules. *J Pharm Sci* **87**, 1351-1356 (1998).

43. Van Itallie, C.M., Holmes, J., Bridges, A., Gookin, J.L., Coccaro, M.R., Proctor, W., Colegio, O.R. & Anderson, J.M. The density of small tight junction pores varies among cell types and is increased by expression of claudin-2. *J Cell Sci* **121**, 298-305 (2008).

44. Chiba, H., Osanai, M., Murata, M., Kojima, T. & Sawada, N. Transmembrane proteins of tight junctions. *Biochim Biophys Acta* **1778**, 588-600 (2008).

45. Fanning, A.S., Jameson, B.J., Jesaitis, L.A. & Anderson, J.M. The tight junction protein ZO-1 establishes a link between the transmembrane protein occludin and the actin cytoskeleton. *J Biol Chem* **273**, 29745-29753 (1998).

46. Furuse, M. Molecular basis of the core structure of tight junctions. *Cold Spring Harb Perspect Biol* **2**, a002907 (2010).

47. Furuse, M., Fujita, K., Hiiragi, T., Fujimoto, K. & Tsukita, S. Claudin-1 and -2: novel integral membrane proteins localizing at tight junctions with no sequence similarity to occludin. *J Cell Biol* **141**, 1539-1550 (1998).

48. Furuse, M., Hirase, T., Itoh, M., Nagafuchi, A., Yonemura, S., Tsukita, S. & Tsukita, S. Occludin: a novel integral membrane protein localizing at tight junctions. *J Cell Biol* **123**, 1777-1788 (1993).

49. Ikenouchi, J., Furuse, M., Furuse, K., Sasaki, H., Tsukita, S. & Tsukita, S. Tricellulin constitutes a novel barrier at tricellular contacts of epithelial cells. *J Cell Biol* **171**, 939-945 (2005).

50. Balda, M.S. & Matter, K. Transmembrane proteins of tight junctions. *Semin Cell Dev Biol* **11**, 281-289 (2000).

51. Furuse, M., Sasaki, H., Fujimoto, K. & Tsukita, S. A single gene product, claudin-1 or -2, reconstitutes tight junction strands and recruits occludin in fibroblasts. *J Cell Biol* **143**, 391-401 (1998).

52. Bücker, R., Schumann, M., Amasheh, S. & Schulzke, J.-D. Claudins in Intestinal Function and Disease in *Current Topics in Membranes*, Vol. Volume 65. (ed. A.S.L. Yu) 195-227 (Academic Press, Burlington, MA; 2010).

53. Balda, M.S., Whitney, J.A., Flores, C., González, S., Cereijido, M. & Matter, K. Functional dissociation of paracellular permeability and transepithelial electrical resistance and disruption of the apical-basolateral intramembrane diffusion barrier by expression of a mutant tight junction membrane protein. *J Cell Biol* **134**, 1031-1049 (1996).

54. Bazzoni, G. The JAM family of junctional adhesion molecules. *Curr Opin Cell Biol* **15**, 525-530 (2003).

55. Martin-Padura, I., Lostaglio, S., Schneemann, M., Williams, L., Romano, M., Fruscella, P., Panzeri, C., Stoppacciaro, A., Ruco, L., Villa, A., Simmons, D. & Dejana, E. Junctional adhesion molecule, a novel member of the immunoglobulin superfamily that distributes at intercellular junctions and modulates monocyte transmigration. *J Cell Biol* **142**, 117-127 (1998).

56. Cohen, C.J., Shieh, J.T., Pickles, R.J., Okegawa, T., Hsieh, J.T. & Bergelson, J.M. The coxsackievirus and adenovirus receptor is a transmembrane component of the tight junction. *Proc Natl Acad Sci U S A* **98**, 15191-15196 (2001).

57. Bazzoni, G., Martinez-Estrada, O.M., Orsenigo, F., Cordenonsi, M., Citi, S. & Dejana, E. Interaction of junctional adhesion molecule with the tight junction components ZO-1, cingulin, and occludin. *J Biol Chem* **275**, 20520-20526 (2000).

58. Liu, Y., Nusrat, A., Schnell, F.J., Reaves, T.A., Walsh, S., Pochet, M. & Parkos, C.A. Human junction adhesion molecule regulates tight junction resealing in epithelia. *J Cell Sci* **113 (Pt 13)**, 2363-2374 (2000).

59. Ulluwishewa, D., Anderson, R.C., McNabb, W.C., Moughan, P.J., Wells, J.M. & Roy, N.C. Regulation of tight junction permeability by intestinal bacteria and dietary components. *J Nutr* **141**, 769-776 (2011).

60. Fanning, A.S. & Anderson, J.M. PDZ domains: fundamental building blocks in the organization of protein complexes at the plasma membrane. *J Clin Invest* **103**, 767-772 (1999).

61. Itoh, M., Furuse, M., Morita, K., Kubota, K., Saitou, M. & Tsukita, S. Direct binding of three tight junction-associated MAGUKs, ZO-1, ZO-2, and ZO-3, with the COOH termini of claudins. *J Cell Biol* **147**, 1351-1363 (1999).

62. Utepbergenov, D.I., Fanning, A.S. & Anderson, J.M. Dimerization of the scaffolding protein ZO-1 through the second PDZ domain. *J Biol Chem* **281**, 24671-24677 (2006).

63. Itoh, M., Sasaki, H., Furuse, M., Ozaki, H., Kita, T. & Tsukita, S. Junctional adhesion molecule (JAM) binds to PAR-3: a possible mechanism for the recruitment of PAR-3 to tight junctions. *J Cell Biol* **154**, 491-497 (2001).

64. Fanning, A.S., Ma, T.Y. & Anderson, J.M. Isolation and functional characterization of the actin binding region in the tight junction protein ZO-1. *FASEB J* **16**, 1835-1837 (2002).

65. Linnemann, T., Geyer, M., Jaitner, B.K., Block, C., Kalbitzer, H.R., Wittinghofer, A. & Herrmann, C. Thermodynamic and kinetic characterization of the interaction between the Ras binding domain of AF6 and members of the Ras subfamily. *J Biol Chem* **274**, 13556-13562 (1999).

66. Stevenson, B.R., Anderson, J.M., Braun, I.D. & Mooseker, M.S. Phosphorylation of the tight-junction protein ZO-1 in two strains of Madin-Darby canine kidney cells which differ in transepithelial resistance. *Biochem J* **263**, 597-599 (1989).

67. Findley, M.K. & Koval, M. Regulation and roles for claudin-family tight junction proteins. *IUBMB Life* **61**, 431-437 (2009).

68. Wong, V. Phosphorylation of occludin correlates with occludin localization and function at the tight junction. *Am J Physiol* **273**, C1859-1867 (1997).

69. Farhadi, A., Keshavarzian, A., Ranjbaran, Z., Fields, J.Z. & Banan, A. The role of protein kinase C isoforms in modulating injury and repair of the intestinal barrier. *J Pharmacol Exp Ther* **316**, 1-7 (2006).

70. Song, J.C., Hanson, C.M., Tsai, V., Farokhzad, O.C., Lotz, M. & Matthews, J.B. Regulation of epithelial transport and barrier function by distinct protein kinase C isoforms. *Am J Physiol Cell Physiol* **281**, C649-661 (2001).

71. Cario, E., Gerken, G. & Podolsky, D.K. Toll-like receptor 2 enhances ZO-1-associated intestinal epithelial barrier integrity via protein kinase C. *Gastroenterology* **127**, 224-238 (2004).

72. Plotnikov, A., Zehorai, E., Procaccia, S. & Seger, R. The MAPK cascades: Signaling components, nuclear roles and mechanisms of nuclear translocation. *Biochim Biophys Acta* (2010).

73. Johnson, G.L. & Lapadat, R. Mitogen-activated protein kinase pathways mediated by ERK, JNK, and p38 protein kinases. *Science* **298**, 1911-1912 (2002).

74. Basuroy, S., Seth, A., Elias, B., Naren, A.P. & Rao, R. MAPK interacts with occludin and mediates EGF-induced prevention of tight junction disruption by hydrogen peroxide. *Biochem J* **393**, 69-77 (2006).

75. Turner, J.R., Rill, B.K., Carlson, S.L., Carnes, D., Kerner, R., Mrsny, R.J. & Madara, J.L. Physiological regulation of epithelial tight junctions is associated with myosin light-chain phosphorylation. *Am J Physiol* **273**, C1378-1385 (1997).

76. Scott, K.G., Meddings, J.B., Kirk, D.R., Lees-Miller, S.P. & Buret, A.G. Intestinal infection with Giardia spp. reduces epithelial barrier function in a myosin light chain kinase-dependent fashion. *Gastroenterology* **123**, 1179-1190 (2002).

77. Shen, L., Black, E.D., Witkowski, E.D., Lencer, W.I., Guerriero, V., Schneeberger, E.E. & Turner, J.R. Myosin light chain phosphorylation regulates barrier function by remodeling tight junction structure. *J Cell Sci* **119**, 2095-2106 (2006).

78. Nusrat, A., Giry, M., Turner, J.R., Colgan, S.P., Parkos, C.A., Carnes, D., Lemichez, E., Boquet, P. & Madara, J.L. Rho protein regulates tight junctions and perijunctional actin organization in polarized epithelia. *Proc Natl Acad Sci U S A* **92**, 10629-10633 (1995).

79. Kimura, K., Ito, M., Amano, M., Chihara, K., Fukata, Y., Nakafuku, M., Yamamori, B., Feng, J., Nakano, T., Okawa, K., Iwamatsu, A. & Kaibuchi, K. Regulation of myosin phosphatase by Rho and Rho-associated kinase (Rho-kinase). *Science* **273**, 245-248 (1996).

80. Walsh, S.V., Hopkins, A.M., Chen, J., Narumiya, S., Parkos, C.A. & Nusrat, A. Rho kinase regulates tight junction function and is necessary for tight junction assembly in polarized intestinal epithelia. *Gastroenterology* **121**, 566-579 (2001).

81. Bruewer, M., Hopkins, A.M., Hobert, M.E., Nusrat, A. & Madara, J.L. RhoA, Rac1, and Cdc42 exert distinct effects on epithelial barrier via selective structural and biochemical modulation of junctional proteins and F-actin. *Am J Physiol Cell Physiol* **287**, C327-335 (2004).

82. Drago, S., El Asmar, R., Di Pierro, M., Grazia Clemente, M., Tripathi, A., Sapone, A., Thakar, M., Iacono, G., Carroccio, A., D'Agate, C., Not, T., Zampini, L., Catassi, C. & Fasano, A. Gliadin, zonulin and gut permeability: Effects on celiac and non-celiac intestinal mucosa and intestinal cell lines. *Scand J Gastroenterol* **41**, 408-419 (2006).

83. Wang, W., Uzzau, S., Goldblum, S.E. & Fasano, A. Human zonulin, a potential modulator of intestinal tight junctions. *J Cell Sci* **113 Pt 24**, 4435-4440 (2000).

84. Clemente, M.G., De Virgiliis, S., Kang, J.S., Macatagney, R., Musu, M.P., Di Pierro, M.R., Drago, S., Congia, M. & Fasano, A. Early effects of gliadin on enterocyte intracellular signalling involved in intestinal barrier function. *Gut* **52**, 218-223 (2003).

85. Lammers, K.M., Lu, R., Brownley, J., Lu, B., Gerard, C., Thomas, K., Rallabhandi, P., Shea-Donohue, T., Tamiz, A., Alkan, S., Netzel-Arnett, S., Antalis, T., Vogel, S.N. & Fasano, A. Gliadin induces an increase in intestinal permeability and zonulin release by binding to the chemokine receptor CXCR3. *Gastroenterology* **135**, 194-204 e193 (2008).

86. Hashimoto, K., Matsunaga, N. & Shimizu, M. Effect of vegetable extracts on the transepithelial permeability of the human intestinal Caco-2 cell monolayer. *Biosci Biotechnol Biochem* **58**, 1345-1346 (1994).

87. Jensen-Jarolim, E., Gajdzik, L., Haberl, I., Kraft, D., Scheiner, O. & Graf, J. Hot spices influence permeability of human intestinal epithelial monolayers. *J Nutr* **128**, 577-581 (1998).

88. Hashimoto, K., Kawagishi, H., Nakayama, T. & Shimizu, M. Effect of capsianoside, a diterpene glycoside, on tight-junctional permeability. *Biochim Biophys Acta* **2**, 281-290 (1997).

89. Konish, Y. Modulations of food-derived substances on intestinal permeability in Caco-2 cell monolayers. *Biosci Biotechnol Biochem* **67**, 2297-2299 (2003).

90. Mine, Y. & Zhang, J.W. Surfactants enhance the tight-junction permeability of food allergens in human intestinal epithelial Caco-2 cells. *Int Arch Allergy Immunol* **130**, 135-142 (2003).

91. Narai, A., Arai, S. & Shimizu, M. Rapid decrease in transepithelial electrical resistance of human intestinal Caco-2 cell monolayers by cytotoxic membrane perturbents. *Toxicol In Vitro* **11**, 347-354 (1997).

92. Shi, X. & Gisolfi, C.V. Paracellular transport of water and carbohydrates during intestinal perfusion of protamine in the rat. *Am J Med Sci* **311**, 107-112 (1996).

93. Sadowski, D.C. & Meddings, J.B. Luminal nutrients alter tight-junction permeability in the rat jejunum: an in vivo perfusion model. *Can J Physiol Pharmacol* **71**, 835-839 (1993).

94. Yasumatsu, H. & Tanabe, S. The casein peptide Asn-Pro-Trp-Asp-Gln enforces the intestinal tight junction partly by increasing occludin expression in Caco-2 cells. *Br J Nutr* **104**, 951-956 (2010).

95. Visser, J.T., Lammers, K., Hoogendijk, A., Boer, M.W., Brugman, S., Beijer-Liefers, S., Zandvoort, A., Harmsen, H., Welling, G., Stellaard, F., Bos, N.A., Fasano, A. & Rozing, J. Restoration of impaired intestinal barrier function by the hydrolysed casein diet contributes to the prevention of type 1 diabetes in the diabetes-prone BioBreeding rat. *Diab tologia* **53**, 2621-2628 (2010).

96. Hashimoto, K., Nakayama, T. & Shimizu, M. Effects of beta-lactoglobulin on the tight-junctional stability of Caco-2-SF monolayer. *Biosci Biotechnol Biochem* **62**, 1819-1821 (1998).

97. Madara, J.L. & Carlson, S. Supraphysiologic L-tryptophan elicits cytoskeletal and macromolecular permeability alterations in hamster small intestinal epithelium in vitro. *J Clin Invest* **87**, 454-462 (1991).

98. Li, N., DeMarco, V.G., West, C.M. & Neu, J. Glutamine supports recovery from loss of transepithelial resistance and increase of permeability induced by media change in Caco-2 cells. *J Nutr Biochem* **14**, 401-408 (2003).

99. Li, N., Lewis, P., Samuelson, D., Liboni, K. & Neu, J. Glutamine regulates Caco-2 cell tight junction proteins. *Am J Physiol Gastrointest Liver Physiol* **287**, G726-733 (2004).

100. Rhoads, J.M., Argenzio, R.A., Chen, W., Rippe, R.A., Westwick, J.K., Cox, A.D., Berschneider, H.M. & Brenner, D.A. L-glutamine stimulates intestinal cell proliferation and activates mitogen-activated protein kinases. *Am J Physiol* **272**, G943-953 (1997).

101. Finamore, A., Massimi, M., Conti Devirgiliis, L. & Mengheri, E. Zinc deficiency induces membrane barrier damage and increases neutrophil transmigration in Caco-2 cells. *J Nutr* **138**, 1664-1670 (2008).

102. Lindmark, T., Kimura, Y. & Artursson, P. Absorption enhancement through intracellular regulation of tight junction permeability by medium chain fatty acids in Caco-2 cells. *J Pharmacol Exp Ther* **284**, 362-369 (1998).

103. Usami, M., Komurasaki, T., Hanada, A., Kinoshita, K. & Ohata, A. Effect of gamma-linolenic acid or docosahexaenoic acid on tight junction permeability in intestinal monolayer cells and their mechanism by protein kinase C activation and/or eicosanoid formation. *Nutrition* **19**, 150-156 (2003).

104. Usami, M., Muraki, K., Iwamoto, M., Ohata, A., Matsushita, E. & Miki, A. Effect of eicosapentaenoic acid (EPA) on tight junction permeability in intestinal monolayer cells. *Clin Nutr* **20**, 351-359 (2001).

105. Soderholm, J.D., Oman, H., Blomquist, L., Veen, J., Lindmark, T. & Olaison, G. Reversible increase in tight junction permeability to macromolecules in rat ileal mucosa in vitro by sodium caprate, a constituent of milk fat. *Dig Dis Sci* **43**, 1547-1552 (1998).

106. Roche, H.M., Terres, A.M., Black, I.B., Gibney, M.J. & Kelleher, D. Fatty acids and epithelial permeability: effect of conjugated linoleic acid in Caco-2 cells. *Gut* **48**, 797-802 (2001).

107. Thanou, M., Verhoef, J.C. & Junginger, H.E. Oral drug absorption enhancement by chitosan and its derivatives. *Adv Drug Deliv Rev* **52**, 117-126 (2001).

108. Schipper, N.G., Olsson, S., Hoogstraate, J.A., deBoer, A.G., Varum, K.M. & Artursson, P. Chitosans as absorption enhancers for poorly absorbable drugs 2: mechanism of absorption enhancement. *Pharm Res* **14**, 923-929 (1997).

109. Amasheh, M., Schlichter, S., Amasheh, S., Mankertz, J., Zeitz, M., Fromm, M. & Schulzke, J.D. Quercetin enhances epithelial barrier function and increases claudin-4 expression in Caco-2 cells. *J Nutr* **138**, 1067-1073 (2008).

110. Suzuki, T. & Hara, H. Quercetin enhances intestinal barrier function through the assembly of zonula occludens-2, occludin, and claudin-1 and the expression of claudin-4 in Caco-2 cells. *J Nutr* **139**, 965-974 (2009).

111. Watson, J.L., Ansari, S., Cameron, H., Wang, A., Akhtar, M. & McKay, D.M. Green tea polyphenol (-)-epigallocatechin gallate blocks epithelial barrier dysfunction provoked by IFN-gamma but not by IL-4. *Am J Physiol Gastrointest Liver Physiol* **287**, G954-961 (2004).

112. Schmitz, H., Fromm, M., Bentzel, C.J., Scholz, P., Detjen, K., Mankertz, J., Bode, H., Epple, H.J., Riecken, E.O. & Schulzke, J.D. Tumor necrosis factor-alpha (TNFalpha) regulates the epithelial barrier in the human intestinal cell line HT-29/B6. *J Cell Sci* **112 (Pt 1)**, 137-146 (1999).

113. Sansonetti, P.J. War and peace at mucosal surfaces. *Nat Rev Immunol* **4**, 953-964 (2004).

114. McGuckin, M.A., Eri, R., Simms, L.A., Florin, T.H.J. & Radford-Smith, G. Intestinal Barrier Dysfunction in Inflammatory Bowel Diseases. *Inflamm Bowel Dis* **15**, 100-113 (2009).

115. Matsuo, K., Ota, H., Akamatsu, T., Sugiyama, A. & Katsuyama, T. Histochemistry of the surface mucous gel layer of the human colon. *Gut* **40**, 782-789 (1997).

116. van der Waaij, L.A., Harmsen, H.J., Madjipour, M., Kroese, F.G., Zwiers, M., van Dullemen, H.M., de Boer, N.K., Welling, G.W. & Jansen, P.L. Bacterial population analysis of human colon and terminal ileum biopsies with 16S

rRNA-based fluorescent probes: commensal bacteria live in suspension and have no direct contact with epithelial cells. *Inflamm Bowel Dis* **11**, 865-871 (2005).

117. Swidsinski, A., Sydora, B.C., Doerffel, Y., Loening-Baucke, V., Vaneechoutte, M., Lupicki, M., Scholze, J., Lochs, H. & Dieleman, L.A. Viscosity gradient within the mucus layer determines the mucosal barrier function and the spatial organization of the intestinal microbiota. *Inflamm Bowel Dis* **13**, 963-970 (2007).

118. Forstner, J.F., Oliver, M.G. & Sylvester, F.A. Production, structure, and biologic relevance of gastrointestinal mucins in *Infections of the gastrointestinal tract*. (eds. M.J. Blaser, P.D. Smith, J.I. Ravdin, H.B. Greenberg & R.L. Guerrant) (Raven Press, New York; 1995).

119. Barnett, A.M., Roy, N.C., McNabb, W.C. & Cookson, A.L. The interactions between endogenous bacteria, dietary components and the mucus layer of the large bowel. *Food Funct* **3**, 690-699 (2012).

120. Atuma, C., Strugala, V., Allen, A. & Holm, L. The adherent gastrointestinal mucus gel layer: thickness and physical state in vivo. *Am J Physiol Gastrointest Liver Physiol* **280**, G922-929 (2001).

121. Pullan, R.D., Thomas, G.A., Rhodes, M., Newcombe, R.G., Williams, G.T., Allen, A. & Rhodes, J. Thickness of adherent mucus gel on colonic mucosa in humans and its relevance to colitis. *Gut* **35**, 353-359 (1994).

122. Szentkuti, L., Riedesel, H., Enss, M.L., Gaertner, K. & Von Engelhardt, W. Pre-epithelial mucus layer in the colon of conventional and germ-free rats. *Histochem J* **22**, 491-497 (1990).

123. Enss, M.L., Grosse-Siestrup, H., Schmidt-Wittig, U. & Gartner, K. Changes in colonic mucins of germfree rats in response to the introduction of a "normal" rat microbial flora. Rat colonic mucin. *J Exp Anim Sci* **35**, 110-119 (1992).

124. Kandori, H., Hirayama, K., Takeda, M. & Doi, K. Histochemical, lectin-histochemical and morphometrical characteristics of intestinal goblet cells of germfree and conventional mice. *Exp Anim* **45**, 155-160 (1996).

125. Meslin, J.C., Fontaine, N. & Andrieux, C. Variation of mucin distribution in the rat intestine, caecum and colon: effect of the bacterial flora. *Comp Biochem Physiol A Mol Integr Physiol* **123**, 235-239 (1999).

126. Mowat, A.M. Anatomical basis of tolerance and immunity to intestinal antigens. *Nat Rev Immunol* **3**, 331-341 (2003).

127. Miller, H., Zhang, J., Kuolee, R., Patel, G.B. & Chen, W. Intestinal M cells: the fallible sentinels? *World J Gastroenterol* **13**, 1477-1486 (2007).

128. Rescigno, M., Urbano, M., Valzasina, B., Francolini, M., Rotta, G., Bonasio, R., Granucci, F., Kraehenbuhl, J.P. & Ricciardi-Castagnoli, P. Dendritic cells express tight junction proteins and penetrate gut epithelial monolayers to sample bacteria. *Nat Immunol* **2**, 361-367 (2001).

129. Medzhitov, R. & Janeway, C.A., Jr. Decoding the patterns of self and nonself by the innate immune system. *Science* **296**, 298-300 (2002).

130. Magalhaes, J.G., Tattoli, I., Girardin, S.E., Magalhaes, J.G., Tattoli, I. & Girardin, S.E. The intestinal epithelial barrier: how to distinguish between the microbial flora and pathogens. *Semin Immunol* **19**, 106-115 (2007).

131. Bhavsar, A.P., Guttman, J.A. & Finlay, B.B. Manipulation of host-cell pathways by bacterial pathogens. *Nature* **449**, 827-834 (2007).

132. Perkins, N.D. Post-translational modifications regulating the activity and function of the nuclear factor kappa B pathway. *Oncogene* **25**, 6717-6730 (2006).

133. Baumgart, D.C. & Carding, S.R. Inflammatory bowel disease: cause and immunobiology. *Lancet* **369**, 1627-1640 (2007).

134. Hayden, M.S., West, A.P. & Ghosh, S. NF-kappaB and the immune response. *Oncogene* **25**, 6758-6780 (2006).

135. Pestka, S., Krause, C.D. & Walter, M.R. Interferons, interferon-like cytokines, and their receptors. *Immunol Rev* **202**, 8-32 (2004).

136. Coombes, J.L. & Powrie, F. Dendritic cells in intestinal immune regulation. *Nat Rev Immunol* **8**, 435-446 (2008).

137. Nagler-Anderson, C. Man the barrier! Strategic defences in the intestinal mucosa. *Nat Rev Immunol* **1**, 59-67 (2001).

138. Stagg, A.J., Hart, A.L., Knight, S.C. & Kamm, M.A. The dendritic cell: Its role in intestinal inflammation and relationship with gut bacteria. *Gut* **52**, 1522-1529 (2003).

139. Mora, J.R., Iwata, M., Eksteen, B., Song, S.Y., Junt, T., Senman, B., Otipoby, K.L., Yokota, A., Takeuchi, H., Ricciardi-Castagnoli, P., Rajewsky, K., Adams, D.H. & von Andrian, U.H. Generation of gut-homing IgA-secreting B cells by intestinal dendritic cells. *Science* **314**, 1157-1160 (2006).

140. Johansson, C. & Kelsall, B.L. Phenotype and function of intestinal dendritic cells. *Semin Immunol* **17**, 284-294 (2005).

141. Niess, J.H., Brand, S., Gu, X., Landsman, L., Jung, S., McCormick, B.A., Vyas, J.M., Boes, M., Ploegh, H.L., Fox, J.G., Littman, D.R. & Reinecker, H.C. CX3CR1-mediated dendritic cell access to the intestinal lumen and bacterial clearance. *Science* **307**, 254-258 (2005).

142. Iwasaki, A. & Kelsall, B.L. Freshly isolated Peyer's patch, but not spleen, dendritic cells produce interleukin 10 and induce the differentiation of T helper type 2 cells. *J Exp Med* **190**, 229-239 (1999).

143. Chieppa, M., Rescigno, M., Huang, A.Y. & Germain, R.N. Dynamic imaging of dendritic cell extension into the small bowel lumen in response to epithelial cell TLR engagement. *J Exp Med* **203**, 2841-2852 (2006).

144. Vallon-Eberhard, A., Landsman, L., Yogev, N., Verrier, B. & Jung, S. Transepithelial pathogen uptake into the small intestinal lamina propria. *J Immunol* **176**, 2465-2469 (2006).

145. Rescigno, M., Rotta, G., Valzasina, B. & Ricciardi-Castagnoli, P. Dendritic cells shuttle microbes across gut epithelial monolayers. *Immunobiology* **204**, 572-581 (2001).

146. Iwasaki, A. in Annual Review of Immunology, Vol. 25 381-418 (2007).

147. Chirdo, F.G., Millington, O.R., Beacock-Sharp, H. & Mowat, A.M. Immunomodulatory dendritic cells in intestinal lamina propria. *Eur J Immunol* **35**, 1831-1840 (2005).

148. Rimoldi, M., Chieppa, M., Salucci, V., Avogadri, F., Sonzogni, A., Sampietro, G.M., Nespoli, A., Viale, G., Allavena, P. & Rescigno, M. Intestinal immune homeostasis is regulated by the crosstalk between epithelial cells and dendritic cells. *Nat Immunol* **6**, 507-514 (2005).

149. Xu, J. & Gordon, J.I. Inaugural Article: Honor thy symbionts. *Proc Natl Acad Sci U S A* **100**, 10452-10459 (2003).

150. Eckburg, P.B., Bik, E.M., Bernstein, C.N., Purdom, E., Dethlefsen, L., Sargent, M., Gill, S.R., Nelson, K.E. & Relman, D.A. Diversity of the human intestinal microbial flora. *Science* **308**, 1635-1638 (2005).

151. O'Hara, A.M. & Shanahan, F. The gut flora as a forgotten organ. *EMBO Rep* **7**, 688-693 (2006).

152. Satokari, R., Gronroos, T., Laitinen, K., Salminen, S. & Isolauri, E. *Bifidobacterium* and *Lactobacillus* DNA in the human placenta. *Lett Appl Microbiol* **48**, 8-12 (2009).

153. Jimenez, E., Fernandez, L., Marin, M.L., Martin, R., Odriozola, J.M., Nueno-Palop, C., Narbad, A., Olivares, M., Xaus, J. & Rodriguez, J.M. Isolation of commensal bacteria from umbilical cord blood of healthy neonates born by cesarean section. *Curr Microbiol* **51**, 270-274 (2005).

154. Rotimi, V.O. & Duerden, B.I. The development of the bacterial flora in normal neonates. *J Med Microbiol* **14**, 51-62 (1981).

155. Caicedo, R.A., Schanler, R.J., Li, N. & Neu, J. The developing intestinal ecosystem: implications for the neonate. *Pediatr Res* **58**, 625-628 (2005).

156. Bezirtzoglou, E., Romond, M.B. & Romond, C. Modulation of Clostridium perfringens intestinal colonization in infants delivered by caesarean section. *Infection* **17**, 232-236 (1989).

157. Grönlund, M.M., Lehtonen, O.P., Eerola, E. & Kero, P. Fecal microflora in healthy infants born by different methods of delivery: Permanent changes in intestinal flora after cesarean delivery. *J Pediatr Gastroenterol Nutr* **28**, 19-25 (1999).

158. Bezirtzoglou, E. The intestinal microflora during the first weeks of life. *Anaerobe* **3**, 173-177 (1997).

159. Zoetendal, E.G., Akkermans, A.D.L., Akkermans-van Vliet, W.M., De Visser, J.A.G.M. & De Vos, W.M. The host genotype affects the bacterial community in the human gastrointestinal tract. *Microb Ecol Health Dis* **13**, 129-134 (2001).

160. Hayashi, H., Sakamoto, M. & Benno, Y. Fecal microbial diversity in a strict vegetarian as determined by molecular analysis and cultivation. *Microbiol Immunol* **46**, 819-831 (2002).

161. Finegold, S.M., Sutter, V.L., Sugihara, P.T., Elder, H.A., Lehmann, S.M. & Phillips, R.L. Fecal microbial flora in Seventh Day Adventist populations and control subjects. *Am J Clin Nutr* **30**, 1781-1792 (1977).

162. Mueller, S., Saunier, K., Hanisch, C., Norin, E., Alm, L., Midtvedt, T., Cresci, A., Silvi, S., Orpianesi, C., Verdenelli, M.C., Clavel, T., Koebnick, C., Zunft, H.J., Dore, J. & Blaut, M. Differences in fecal microbiota in different European study populations in relation to age, gender, and country: a cross-sectional study. *Appl Environ Microbiol* **72**, 1027-1033 (2006).

163. Mai, V. & Morris, J.G., Jr. Colonic bacterial flora: changing understandings in the molecular age. *J Nutr* **134**, 459-464 (2004).

164. Manson, J.M., Rauch, M. & Gilmore, M.S. The commensal microbiology of the gastrointestinal tract. *Adv Exp Med Biol* **635**, 15-28 (2008).

165. Frank, D.N. & Pace, N.R. Gastrointestinal microbiology enters the metagenomics era. *Curr Opin Gastroenterol* **24**, 4-10 (2008).

166. Bik, E.M., Eckburg, P.B., Gill, S.R., Nelson, K.E., Purdom, E.A., Francois, F., Perez-Perez, G., Blaser, M.J. & Relman, D.A. Molecular analysis of the bacterial microbiota in the human stomach. *Proc Natl Acad Sci U S A* **103**, 732-737 (2006).

167. Villarreal, M.R. File: Digestive system diagram en.svg (2007) Retrieved 16 April 2009, from http://commons.wikimedia.org/wiki/File:Digestive_system_diagram_en.svg

168. Dethlefsen, L., McFall-Ngai, M. & Relman, D.A. An ecological and evolutionary perspective on human-microbe mutualism and disease. *Nature* **449**, 811-818 (2007).

169. Sonnenburg, J.L., Angenent, L.T. & Gordon, J.I. Getting a grip on things: how do communities of bacterial symbionts become established in our intestine? *Nat Immunol* **5**, 569-573 (2004).

170. Hayashi, H., Sakamoto, M., Kitahara, M. & Benno, Y. Molecular analysis of fecal microbiota in elderly individuals using 16S rDNA library and T-RFLP. *Microbiol Immunol* **47**, 557-570 (2003).

171. Backhed, F., Ley, R.E., Sonnenburg, J.L., Peterson, D.A. & Gordon, J.I. Host-bacterial mutualism in the human intestine. *Science* **307**, 1915-1920 (2005).

172. Ley, R.E., Turnbaugh, P.J., Klein, S. & Gordon, J.I. Microbial ecology: human gut microbes associated with obesity. *Nature* **444**, 1022-1023 (2006).

173. Duncan, S.H., Louis, P. & Flint, H.J. Cultivable bacterial diversity from the human colon. *Lett Appl Microbiol* **44**, 343-350 (2007).

174. Shanahan, F. The host-microbe interface within the gut. *Best practice & research. Clinical gastroenterology.* **16**, 915-931 (2002).

175. Gill, S.R., Pop, M., Deboy, R.T., Eckburg, P.B., Turnbaugh, P.J., Samuel, B.S., Gordon, J.I., Relman, D.A., Fraser-Liggett, C.M. & Nelson, K.E. Metagenomic analysis of the human distal gut microbiome. *Science* **312**, 1355-1359 (2006).

176. Hooper, L.V., Wong, M.H., Thelin, A., Hansson, L., Falk, P.G. & Gordon, J.I. Molecular analysis of commensal host-microbial relationships in the intestine. *Science* **291**, 881-884 (2001).

177. Hill, M.J. Intestinal flora and endogenous vitamin synthesis. *Eur J Cancer Prev* **6 Suppl 1**, S43-45 (1997).

178. Guarner, F. & Malagelada, J.R. Gut flora in health and disease. *Lancet* **361**, 512-519 (2003).

179. Roper, J., Francois, F., Shue, P.L., Mourad, M.S., Pei, Z., Olivares de Perez, A.Z., Perez-Perez, G.I., Tseng, C.H. & Blaser, M.J. Leptin and ghrelin in relation to Helicobacter pylori status in adult males. *J Clin Endocrinol Metab* **93**, 2350-2357 (2008).

180. Alam, M., Midtvedt, T. & Uribe, A. Differential cell kinetics in the ileum and colon of germfree rats. *Scand J Gastroenterol* **29**, 445-451 (1994).

181. Frankel, W.L., Zhang, W., Singh, A., Klurfeld, D.M., Don, S., Sakata, T., Modlin, I. & Rombeau, J.L. Mediation of the trophic effects of short-chain fatty acids on the rat jejunum and colon. *Gastroenterology* **106**, 375-380 (1994).

182. Stappenbeck, T.S., Hooper, L.V. & Gordon, J.I. Developmental regulation of intestinal angiogenesis by indigenous microbes via Paneth cells. *Proc Natl Acad Sci U S A* **99**, 15451-15455 (2002).

183. Brook, I. Bacterial interference. *Crit Rev Microbiol* **25**, 155-172 (1999).

184. Bernet, M.F., Brassart, D., Neeser, J.R. & Servin, A.L. Lactobacillus acidophilus LA 1 binds to cultured human intestinal cell lines and inhibits cell attachment and cell invasion by enterovirulent bacteria. *Gut* **35**, 483-489 (1994).

185. Hooper, L.V., Xu, J., Falk, P.G., Midtvedt, T. & Gordon, J.I. A molecular sensor that allows a gut commensal to control its nutrient foundation in a competitive ecosystem. *Proc Natl Acad Sci U S A* **96**, 9833-9838 (1999).

186. Madsen, K., Cornish, A., Soper, P., McKaigney, C., Jijon, H., Yachimec, C., Doyle, J., Jewell, L. & De Simone, C. Probiotic bacteria enhance murine and human intestinal epithelial barrier function. *Gastroenterology* **121**, 580-591 (2001).

187. Gupta, P., Andrew, H., Kirschner, B.S. & Guandalini, S. Is lactobacillus GG helpful in children with Crohn's disease? Results of a preliminary, open-label study. *J Pediatr Gastroenterol Nutr* **31**, 453-457 (2000).

188. Zareie, M., Johnson-Henry, K., Jury, J., Yang, P.C., Ngan, B.Y., McKay, D.M., Soderholm, J.D., Perdue, M.H. & Sherman, P.M. Probiotics prevent bacterial translocation and improve intestinal barrier function in rats following chronic psychological stress. *Gut* **55**, 1553-1560 (2006).

189. Zyrek, A.A., Cichon, C., Helms, S., Enders, C., Sonnenborn, U. & Schmidt, M.A. Molecular mechanisms underlying the probiotic effects of *Escherichia coli* Nissle 1917 involve ZO-2 and PKCzeta redistribution resulting in tight junction and epithelial barrier repair. *Cell Microbiol* **9**, 804-816 (2007).

190. Ukena, S.N., Singh, A., Dringenberg, U., Engelhardt, R., Seidler, U., Hansen, W., Bleich, A., Bruder, D., Franzke, A., Rogler, G., Suerbaum, S., Buer, J., Gunzer, F. & Westendorf, A.M. Probiotic *Escherichia coli* Nissle 1917 inhibits leaky gut by enhancing mucosal integrity. *PLoS ONE* **2**, e1308 (2007).

191. Ewaschuk, J.B., Diaz, H., Meddings, L., Diederichs, B., Dmytrash, A., Backer, J., Looijer-van Langen, M. & Madsen, K.L. Secreted bioactive factors from *Bifidobacterium infantis* enhance epithelial cell barrier function. *Am J Physiol Gastrointest Liver Physiol* **295**, G1025-1034 (2008).

192. Anderson, R.C., Cookson, A.L., McNabb, W.C., Park, Z., McCann, M.J., Kelly, W.J. & Roy, N.C. *Lactobacillus plantarum* MB452 enhances the function of the intestinal barrier by increasing the expression levels of genes involved in tight junction formation. *BMC Microbiol* **10**, 316 (2010).

193. Karczewski, J., Troost, F.J., Konings, I., Dekker, J., Kleerebezem, M., Brummer, R.J. & Wells, J.M. Regulation of human epithelial tight junction proteins by *Lactobacillus plantarum in vivo* and protective effects on the epithelial barrier. *Am J Physiol Gastrointest Liver Physiol* **298**, G851-859 (2010).

194. Cario, E., Gerken, G. & Podolsky, D.K. Toll-like receptor 2 controls mucosal inflammation by regulating epithelial barrier function. *Gastroenterology* **132**, 1359-1374 (2007).

195. Qin, H., Zhang, Z., Hang, X. & Jiang, Y. *L. plantarum* prevents enteroinvasive Escherichia coli-induced tight junction proteins changes in intestinal epithelial cells. *BMC Microbiol* **9**, 63 (2009).

196. Anderson, R.C., Cookson, A.L., McNabb, W.C., Kelly, W.J. & Roy, N.C. *Lactobacillus plantarum* DSM 2648 is a potential probiotic that enhances intestinal barrier function. *FEMS Microbiol Lett* **309**, 184-192 (2010).

197. Putaala, H., Salusjarvi, T., Nordstrom, M., Saarinen, M., Ouwehand, A.C., Bech Hansen, E. & Rautonen, N. Effect of four probiotic strains and *Escherichia coli* O157:H7 on tight junction integrity and cyclo-oxygenase expression. *Res Microbiol* **159**, 692-698 (2008).

198. Hardt, W.D. & Galan, J.E. A secreted *Salmonella* protein with homology to an avirulence determinant of plant pathogenic bacteria. *Proc Natl Acad Sci U S A* **94**, 9887-9892 (1997).

199. Liao, A.P., Petrof, E.O., Kuppireddi, S., Zhao, Y., Xia, Y., Claud, E.C. & Sun, J. *Salmonella* type III effector AvrA stabilizes cell tight junctions to inhibit inflammation in intestinal epithelial cells. *PLoS ONE* **3**, e2369 (2008).

200. Trivedi, K., Barrett, K.E. & Resta-Lenert, S.C. Probiotic inhibition of the entry of enteroinvasive *E. coli* into human intestinal epithelial cells involves both Rho-dependent and independent pathways. *Gastroenterology* **124**, A106 (2003).

201. Resta-Lenert, S. & Barrett, K.E. Probiotics and commensals reverse TNF-alpha- and IFN-gamma-induced dysfunction in human intestinal epithelial cells. *Gastroenterology* **130**, 731-746 (2006).

202. Ghadimi, D., Vrese, M.D., Heller, K.J. & Schrezenmeir, J. Effect of natural commensal-origin DNA on toll-like receptor 9 (TLR9) signaling cascade, chemokine IL-8 expression, and barrier integritiy of polarized intestinal epithelial cells. *Inflamm Bowel Dis* (2009).

203. Hacker, J. & Carniel, E. Ecological fitness, genomic islands and bacterial pathogenicity. A Darwinian view of the evolution of microbes. *EMBO Rep* **2**, 376-381 (2001).

204. Gruenheid, S. & Finlay, B.B. Crowd control: quorum sensing in pathogenic E. coli. *Trends Microbiol* **8**, 442-443 (2000).

205. Swidsinski, A., Ladhoff, A., Pernthaler, A., Swidsinski, S., Loening-Baucke, V., Ortner, M., Weber, J., Hoffmann, U., Schreiber, S., Dietel, M. & Lochs, H.

Mucosal flora in inflammatory bowel disease. *Gastroenterology* **122**, 44-54 (2002).

206. Hornef, M.W., Frisan, T., Vandewalle, A., Normark, S. & Richter-Dahlfors, A. Toll-like receptor 4 resides in the Golgi apparatus and colocalizes with internalized lipopolysaccharide in intestinal epithelial cells. *J Exp Med* **195**, 559-570 (2002).

207. Gewirtz, A.T., Navas, T.A., Lyons, S., Godowski, P.J. & Madara, J.L. Cutting edge: bacterial flagellin activates basolaterally expressed TLR5 to induce epithelial proinflammatory gene expression. *J Immunol* **167**, 1882-1885 (2001).

208. Bambou, J.C., Giraud, A., Menard, S., Begue, B., Rakotobe, S., Heyman, M., Taddei, F., Cerf-Bensussan, N. & Gaboriau-Routhiau, V. In vitro and ex vivo activation of the TLR5 signaling pathway in intestinal epithelial cells by a commensal *Escherichia coli* strain. *J Biol Chem* **279**, 42984-42992 (2004).

209. Neish, A.S., Gewirtz, A.T., Zeng, H., Young, A.N., Hobert, M.E., Karmali, V., Rao, A.S. & Madara, J.L. Prokaryotic regulation of epithelial responses by inhibition of IkappaB-alpha ubiquitination. *Science* **289**, 1560-1563 (2000).

210. Kelly, D., Campbell, J.I., King, T.P., Grant, G., Jansson, E.A., Coutts, A.G., Pettersson, S. & Conway, S. Commensal anaerobic gut bacteria attenuate inflammation by regulating nuclear-cytoplasmic shuttling of PPAR-gamma and RelA. *Nat Immunol* **5**, 104-112 (2004).

211. van Baarlen, P., Troost, F.J., van Hemert, S., van der Meer, C., de Vos, W.M., de Groot, P.J., Hooiveld, G.J., Brummer, R.J. & Kleerebezem, M. Differential NF-kappaB pathways induction by *Lactobacillus plantarum* in the duodenum of healthy humans correlating with immune tolerance. *Proc Natl Acad Sci U S A* **106**, 2371-2376 (2009).

212. Beg, A.A. ComPPARtmentalizing NF-κB in the gut. *Nat Immunol* **5**, 14-16 (2004).

213. Rimoldi, M., Chieppa, M., Vulcano, M., Allavena, P. & Rescigno, M. Intestinal epithelial cells control dendritic cell function. *Ann N Y Acad Sci* **1029**, 66-74 (2004).

214. Harris, S.G., Padilla, J., Koumas, L., Ray, D. & Phipps, R.P. Prostaglandins as modulators of immunity. *Trends Immunol* **23**, 144-150 (2002).

215. Hilkens, C.M., Snijders, A., Snijdewint, F.G., Wierenga, E.A. & Kapsenberg, M.L. Modulation of T-cell cytokine secretion by accessory cell-derived products. *Eur Respir J Suppl* **22**, 90s-94s (1996).

216. Kalinski, P., Vieira, P.L., Schuitemaker, J.H., de Jong, E.C. & Kapsenberg, M.L. Prostaglandin E(2) is a selective inducer of interleukin-12 p40 (IL-12p40) production and an inhibitor of bioactive IL-12p70 heterodimer. *Blood* **97**, 3466-3469 (2001).

217. Allakhverdi, Z., Comeau, M.R., Jessup, H.K., Yoon, B.R., Brewer, A., Chartier, S., Paquette, N., Ziegler, S.F., Sarfati, M. & Delespesse, G. Thymic stromal lymphopoietin is released by human epithelial cells in response to microbes, trauma, or inflammation and potently activates mast cells. *J Exp Med* **204**, 253-258 (2007).

218. Dignass, A.U. & Podolsky, D.K. Cytokine modulation of intestinal epithelial cell restitution: central role of transforming growth factor beta. *Gastroenterology* **105**, 1323-1332 (1993).

219. Fujita, S., Seino, K., Sato, K., Sato, Y., Eizumi, K., Yamashita, N., Taniguchi, M. & Sato, K. Regulatory dendritic cells act as regulators of acute lethal systemic inflammatory response. *Blood* **107**, 3656-3664 (2006).

220. Smythies, L.E., Sellers, M., Clements, R.H., Mosteller-Barnum, M., Meng, G., Benjamin, W.H., Orenstein, J.M. & Smith, P.D. Human intestinal macrophages display profound inflammatory anergy despite avid phagocytic and bacteriocidal activity. *J Clin Invest* **115**, 66-75 (2005).

221. Di Cagno, R., Mazzacane, F., Rizzello, C.G., Vincentini, O., Silano, M., Giuliani, G., De Angelis, M. & Gobbetti, M. Synthesis of isoflavone aglycones and equol in soy milks fermented by food-related lactic acid bacteria and their effect on human intestinal Caco-2 cells. *J Agric Food Chem* **58**, 10338-10346 (2010).

222. Peng, L., Li, Z.R., Green, R.S., Holzman, I.R. & Lin, J. Butyrate enhances the intestinal barrier by facilitating tight junction assembly via activation of AMP-activated protein kinase in Caco-2 cell monolayers. *J Nutr* **139**, 1619-1625 (2009).

223. Gibson, G.R. Fibre and effects on probiotics (the prebiotic concept). *Clin Nutr* **1**, 25-31 (2004).

224. Coppa, G.V., Zampini, L., Galeazzi, T., Facinelli, B., Ferrante, L., Capretti, R. & Orazio, G. Human milk oligosaccharides inhibit the adhesion to Caco-2 cells of diarrheal pathogens: *Escherichia coli*, *Vibrio cholerae*, and *Salmonella fyris*. *Pediatr Res* **59**, 377-382 (2006).

225. Langerholc, T., Maragkoudakis, P.A., Wollgast, J., Gradisnik, L. & Cencic, A. Novel and established intestinal cell line models - An indispensable tool in food science and nutrition. *Trends in Food Science &Technology* **22, Supplement 1**, S11-S20 (2011).

226. Evans, G.S., Flint, N. & Potten, C.S. Primary cultures for studies of cell regulation and physiology in intestinal epithelium. *Annu Rev Physiol* **56**, 399-417 (1994).

227. Dexter, D.L. & Hager, J.C. Maturation-induction of tumor cells using a human colon carcinoma model. *Cancer* **45**, 1178-1184 (1980).

228. Pinto, M., Robine Leon, S. & Appay, M.D. Enterocyte-like differentiation and polarization of the human colon carcinoma cell line Caco-2 in culture. *Biol Cell* **47**, 323-330 (1983).

229. Pinto, M., Appay, M., Simon-Assmann, P., Chevalier, G., Dracopoli, N., Fogh, J. & Zweibaum, A. Enterocytic differentiation of cultured human colon cancer cells by replacement of glucose by galactose in the medium. *Biol Cell* **44**, 193-196 (1982).

230. Nanthakumar, N.N., Fusunyan, R.D., Sanderson, I. & Walker, W.A. Inflammation in the developing human intestine: A possible pathophysiologic contribution to necrotizing enterocolitis. *Proc Natl Acad Sci U S A* **97**, 6043-6048 (2000).

231. Cencic, A. & Langerholc, T. Functional cell models of the gut and their applications in food microbiology--a review. *Int J Food Microbiol* **141 Suppl 1**, S4-14 (2010).

232. Jones, N., Perdue, M.H., Sherman, P.M. & McKay, D.M. Bacterial interactions with host epithelium in vitro. *Methods Mol Biol* **188**, 383-400 (2002).

233. Grajek, W. & Olejnik, A. Epithelial cell cultures in vitro as a model to study functional properties of food. *Pol J Food Nutr Sci* **13**, 5-24 (2004).

234. Le Ferrec, E., Chesne, C., Artusson, P., Brayden, D., Fabre, G., Gires, P., Guillou, F., Rousset, M., Rubas, W. & Scarino, M.L. In vitro models of the intestinal barrier. The report and recommendations of ECVAM Workshop 46. European Centre for the Validation of Alternative methods. *Altern Lab Anim* **29**, 649-668 (2001).

235. Gaush, C.R., Hard, W.L. & Smith, T.F. Characterization of an established line of canine kidney cells (MDCK). *Proc Soc Exp Biol Med* **122**, 931-935 (1966).

236. Cho, M.J., Thompson, D.P., Cramer, C.T., Vidmar, T.J. & Scieszka, J.F. The Madin Darby canine kidney (MDCK) epithelial cell monolayer as a model cellular transport barrier. *Pharm Res* **6**, 71-77 (1989).

237. Lesuffleur, T., Barbat, A., Dussaulx, E. & Zweibaum, A. Growth adaptation to methotrexate of HT-29 human colon carcinoma cells is associated with their ability to differentiate into columnar absorptive and mucus-secreting cells. *Cancer Res* **50**, 6334-6343 (1990).

238. Dharmsathaphorn, K., McRoberts, J., Mandel, K., Tisdale, L. & Masui, H. A human colonic tumor cell line that maintains vectorial electrolyte transport. *Am J Physiol Gastrointest Liver Physiol* **246**, G204 (1984).

239. Tompkins, W.A., Watrach, A.M., Schmale, J.D., Schultz, R.M. & Harris, J.A. Cultural and antigenic properties of newly established cell strains derived from adenocarcinomas of the human colon and rectum. *J Natl Cancer Inst* **52**, 1101-1110 (1974).

240. Chen, T.R., Dorotinsky, C.S., McGuire, L.J., Macy, M.L. & Hay, R.J. DLD-1 and HCT-15 cell lines derived separately from colorectal carcinomas have totally different chromosome changes but the same genetic origin. *Cancer Genet Cytogenet* **81**, 103-108 (1995).

241. Sambruy, Y., Ferruzza, S., Ranaldi, G. & De Angelis, I. Intestinal cell culture models: applications in toxicology and pharmacology. *Cell Biol Toxicol* **17**, 301-317 (2001).

242. Chantret, I., Barbat, A., Dussaulx, E., Brattain, M.G. & Zweibaum, A. Epithelial polarity, villin expression, and enterocytic differentiation of cultured human colon carcinoma cells: a survey of twenty cell lines. *Cancer Res* **48**, 1936-1942 (1988).

243. Hidalgo, I.J., Raub, T.J. & Borchardt, R.T. Characterization of the human colon carcinoma cell line (Caco-2) as a model system for intestinal epithelial permeability. *Gastroenterology* **96**, 736-749 (1989).

244. McCormick, B.A. The use of transepithelial models to examine host-pathogen interactions. *Curr Opin Microbiol* **6**, 77-81 (2003).

245. Philpott, D.J., McKay, D.M., Sherman, P.M. & Perdue, M.H. Infection of T84 cells with enteropathogenic *Escherichia coli* alters barrier and transport functions. *Am J Physiol* **270**, G634-645 (1996).

246. Collington, G.K., Booth, I.W. & Knutton, S. Rapid modulation of electrolyte transport in Caco-2 cell monolayers by enteropathogenic *Escherichia coli* (EPEC) infection. *Gut* **42**, 200-207 (1998).

247. Song, F., Ito, K., Denning, T.L., Kuninger, D., Papaconstantinou, J., Gourley, W., Klimpel, G., Balish, E., Hokanson, J. & Ernst, P.B. Expression of the neutrophil chemokine KC in the colon of mice with enterocolitis and by intestinal epithelial cell lines: effects of flora and proinflammatory cytokines. *J Immunol* **162**, 2275-2280 (1999).

248. Hilgendorf, C., Spahn-Langguth, H., Regardh, C.G., Lipka, E., Amidon, G.L. & Langguth, P. Caco-2 versus Caco-2/HT29-MTX co-cultured cell lines: permeabilities via diffusion, inside- and outside-directed carrier-mediated transport. *J Pharm Sci* **89**, 63-75 (2000).

249. Mahler, G.J., Shuler, M.L. & Glahn, R.P. Characterization of Caco-2 and HT29-MTX cocultures in an in vitro digestion/cell culture model used to predict iron bioavailability. *J Nutr Biochem* **20**, 494-502 (2009).

250. Walter, E., Janich, S., Roessler, B.J., Hilfinger, J.M. & Amidon, G.L. HT29-MTX/Caco-2 cocultures as an in vitro model for the intestinal epithelium: In vitro-in vivo correlation with permeability data from rats and humans. *J Pharm Sci* **85**, 1070-1076 (1996).

251. Pontier, C., Pachot, J., Botham, R., Lenfant, B. & Arnaud, P. HT29-MTX and Caco-2/TC7 monolayers as predictive models for human intestinal absorption: role of the mucus layer. *J Pharm Sci* **90**, 1608-1619 (2001).

252. O'Neill, D.W. & Bhardwaj, N. Differentiation of peripheral blood monocytes into dendritic cells. *Current protocols in immunology* **Chapter 22**, Unit 22F 24 (2005).

253. McKay, D.M. & Perdue, M.H. Establishing epithelial-immune cell co-cultures. Effects on epithelial ion transport and permeability. *Methods Mol Biol* **188**, 359-371 (2002).

254. Zoumpopoulou, G., Tsakalidou, E., Dewulf, J., Pot, B. & Grangette, C. Differential crosstalk between epithelial cells, dendritic cells and bacteria in a co-culture model. *Int J Food Microbiol* **131**, 40-51 (2009).

255. Dingle, T., Mulvey, G.L., Humphries, R.M. & Armstrong, G.D. A real-time quantitative PCR assay for evaluating *Clostridium difficile* adherence to differentiated intestinal Caco-2 cells. *J Med Microbiol* **59**, 920-924 (2010).

256. O'Hara, A.M., O'Regan, P., Fanning, A., O'Mahony, C., Macsharry, J., Lyons, A., Bienenstock, J., O'Mahony, L. & Shanahan, F. Functional modulation of human intestinal epithelial cell responses by *Bifidobacterium infantis* and *Lactobacillus salivarius*. *Immunology* **118**, 202-215 (2006).

257. Sokol, H., Pigneur, B., Watterlot, L., Lakhdari, O., Bermudez-Humaran, L.G., Gratadoux, J.J., Blugeon, S., Bridonneau, C., Furet, J.P., Corthier, G., Grangette, C., Vasquez, N., Pochart, P., Trugnan, G., Thomas, G., Blottiere, H.M., Dore, J., Marteau, P., Seksik, P. & Langella, P. *Faecalibacterium prausnitzii* is an anti-

inflammatory commensal bacterium identified by gut microbiota analysis of Crohn disease patients. *Proc Natl Acad Sci U S A* **105**, 16731-16736 (2008).

258. Cottet, S., Corthesy-Theulaz, I., Spertini, F. & Corthesy, B. Microaerophilic conditions permit to mimic in vitro events occurring during in vivo *Helicobacter pylori* infection and to identify Rho/Ras-associated proteins in cellular signaling. *J Biol Chem* **277**, 33978-33986 (2002).

259. Mills, D.C., Gundogdu, O., Elmi, A., Bajaj-Elliott, M., Taylor, P.W., Wren, B.W. & Dorrell, N. Increase in *Campylobacter jejuni* invasion of intestinal epithelial cells under low-oxygen coculture conditions that reflect the in vivo environment. *Infect Immun* **80**, 1690-1698 (2012).

260. Schüller, S. & Phillips, A.D. Microaerobic conditions enhance type III secretion and adherence of enterohaemorrhagic *Escherichia coli* to polarized human intestinal epithelial cells. *Environ Microbiol* **12**, 2426-2435 (2010).

261. Laube, B., Winkler, S., Ladstetter, B., Scheller, T. & Schwarz, L.R. Establishment of a novel in vitro system for studying the interaction of xenobiotic metabolism of liver and intestinal microflora. *Arch Toxicol* **74**, 379-387 (2000).

262. Rosenfeldt, V., Benfeldt, E., Valerius, N.H., Paerregaard, A. & Michaelsen, K.F. Effect of probiotics on gastrointestinal symptoms and small intestinal permeability in children with atopic dermatitis. *J Pediatr* **145**, 612-616 (2004).

263. Briske-Anderson, M.J., Finley, J.W. & Newman, S.M. The influence of culture time and passage number on the morphological and physiological development of Caco-2 cells. *Proc Soc Exp Biol Med* **214**, 248-257 (1997).

264. Hubatsch, I., Ragnarsson, E.G. & Artursson, P. Determination of drug permeability and prediction of drug absorption in Caco-2 monolayers. *Nat Protoc* **2**, 2111-2119 (2007).

265. Masters, J.R. & Stacey, G.N. Changing medium and passaging cell lines. *Nat Protoc* **2**, 2276-2284 (2007).

266. Simione, F.P. Thermo Scientific Nalgene and Nunc Cryopreservation Guide (2009) Retrieved 03/12/12, from http://www.atcc.org/Portals/1/Pdf/Cryopreservation_Technical_Manual.pdf

267. Foster, K.A., Avery, M.L., Yazdanian, M. & Audus, K.L. Characterization of the Calu-3 cell line as a tool to screen pulmonary drug delivery. *Int J Pharm* **208**, 1-11 (2000).

268. EVOM2 Epithelial Voltohmmeter Instruction Manual (2011) Retrieved 03/10/12, from http://www.wpiinc.com/clientuploads/pdf/EVOM2_IM.pdf

269. Sambuy, Y., De Angelis, I., Ranaldi, G., Scarino, M.L., Stammati, A. & Zucco, F. The Caco-2 cell line as a model of the intestinal barrier: influence of cell and culture-related factors on Caco-2 cell functional characteristics. *Cell Biol Toxicol* **21**, 1-26 (2005).

270. Vachon, P.H. & Beaulieu, J.F. Transient mosaic patterns of morphological and functional differentiation in the Caco-2 cell line. *Gastroenterology* **103**, 414-423 (1992).

271. Seki, T., Harada, S., Hosoya, O., Morimoto, K. & Juni, K. Evaluation of the establishment of a tight junction in Caco-2 cell monolayers using a pore permeation model involving two different sizes. *Biol Pharm Bull* **31**, 163-166 (2008).

272. Delie, F. & Rubas, W. A human colonic cell line sharing similarities with enterocytes as a model to examine oral absorption: advantages and limitations of the Caco-2 model. *Crit Rev Ther Drug Carrier Syst* **14**, 221-286 (1997).

273. Behrens, I. & Kissel, T. Do cell culture conditions influence the carrier-mediated transport of peptides in Caco-2 cell monolayers? *Eur J Pharm Sci* **19**, 433-442 (2003).

274. Yu, H. & Sinko, P.J. Influence of the microporous substratum and hydrodynamics on resistances to drug transport in cell culture systems: calculation of intrinsic transport parameters. *J Pharm Sci* **86**, 1448-1457 (1997).

275. Grasset, E., Pinto, M., Dussaulx, E., Zweibaum, A. & Desjeux, J.F. Epithelial properties of human colonic carcinoma cell line Caco-2: electrical parameters. *Am J Physiol* **247**, C260-267 (1984).

276. Rimoldi, M., Chieppa, M., Larghi, P., Vulcano, M., Allavena, P. & Rescigno, M. Monocyte-derived dendritic cells activated by bacteria or by bacteria-stimulated epithelial cells are functionally different. *Blood* **106**, 2818-2826 (2005).

277. Tucker, S.P., Melsen, L.R. & Compans, R.W. Migration of polarized epithelial cells through permeable membrane substrates of defined pore size. *Eur J Cell Biol* **58**, 280-290 (1992).

278. Fahmy, B. & Cormier, S.A. Copper oxide nanoparticles induce oxidative stress and cytotoxicity in airway epithelial cells. *Toxicol In Vitro* **23**, 1365-1371 (2009).

279. Brinster, R.L. & Cross, P.C. Effect of copper on the preimplantation mouse embryo. *Nature* **238**, 398-399 (1972).

280. Stoehr, L.C., Gonzalez, E., Stampfl, A., Casals, E., Duschl, A., Puntes, V. & Oostingh, G.J. Shape matters: effects of silver nanospheres and wires on human alveolar epithelial cells. *Particle and Fibre Toxicology* **8**, 1-15 (2011).

281. Chopra, I. The increasing use of silver-based products as antimicrobial agents: a useful development or a cause for concern? *J Antimicrob Chemother* **59**, 587-590 (2007).

282. Veltman, K., Hummel, S., Cichon, C., Sonnenborn, U. & Schmidt, M.A. Identification of Specific miRNAs Targeting Proteins of the Apical Junctional Complex that Simulate the Probiotic Effect of *E. coli* Nissle 1917 on T84 Epithelial Cells. *Int J Biochem Cell Biol* (2011).

283. Taylor, C.T., Dzus, A.L. & Colgan, S.P. Autocrine regulation of epithelial permeability by hypoxia: role for polarized release of tumor necrosis factor alpha. *Gastroenterology* **114**, 657-668 (1998).

284. Friedman, G.B., Taylor, C.T., Parkos, C.A. & Colgan, S.P. Epithelial permeability induced by neutrophil transmigration is potentiated by hypoxia: role of intracellular cAMP. *J Cell Physiol* **176**, 76-84 (1998).

285. Xu, D.Z., Lu, Q., Kubicka, R. & Deitch, E.A. The effect of hypoxia/reoxygenation on the cellular function of intestinal epithelial cells. *J Trauma* **46**, 280-285 (1999).

286. Radtke, D.B., White, A.F., Davis, J.V. & Wilde, F.D. Correction Factors for Oxygen Solubility and Salinity in *US Geological Survey, Techniques of Water-Resources Investigations, Book 9*. (eds. F.D. Wilde, D.B. Radtke, J. Gibs & R.T. Iwatsubo) DO 27–DO 38 (Denver, CO; 1998).

287. Borenfreund, E. & Puerner, J.A. Toxicity determined in vitro by morphological alterations and neutral red absorption. *Toxicol Lett* **24**, 119-124 (1985).

288. Weyermann, J., Lochmann, D. & Zimmer, A. A practical note on the use of cytotoxicity assays. *Int J Pharm* **288**, 369-376 (2005).

289. Louis, K. & Siegel, A. Cell Viability Analysis Using Trypan Blue: Manual and Automated Methods in *Mammalian Cell Viability*, Vol. 740. (ed. M.J. Stoddart) 7-12 (Humana Press, 2011).

290. Ormerod, M. Analysis of DNA - general methods, Vol. 229. (2000).

291. Travis, S. & Menzies, I. Intestinal permeability: functional assessment and significance. *Clinical science (London, England: 1979)* **82**, 471 (1992).

292. Cleveland, W.S., Grosse, E. & Shyu, W.M. Local regression models in *Statistical Models in S*. (eds. J.M. Chambers & W. T.J. Hastie) (Chapman and Hall/CRC, 1992).

293. Coyne, C.B., Shen, L., Turner, J.R. & Bergelson, J.M. Coxsackievirus entry across epithelial tight junctions requires occludin and the small GTPases Rab34 and Rab5. *Cell Host Microbe* **2**, 181-192 (2007).

294. Tortora, G.J. & Derrickson, B.H. Introduction to the human body, Edn. 9. (Wiley, 2011).

295. Tygstrup, N., Winkler, K., Mellemgaard, K. & Andreassen, M. Determination of the hepatic arterial blood flow and oxygen supply in man by clamping the hepatic artery during surgery. *J Clin Invest* **41**, 447-454 (1962).

296. Sheridan, W.G., Lowndes, R.H. & Young, H.L. Intraoperative tissue oximetry in the human gastrointestinal tract. *Am J Surg* **159**, 314-319 (1990).

297. Colt, J. Computation of dissolved gas concentrations in water as functions of temperature, salinity, and pressure. (American Fisheries Society, 1984).

298. Rueckert, R.R. & Mueller, G.C. Effect of oxygen tension on HeLa cell growth. *Cancer Res* **20**, 944-949 (1960).

299. Lind Due, V., Bonde, J., Kann, T. & Perner, A. Extremely low oxygen tension in the rectal lumen of human subjects. *Acta Anaesthesiol Scand* **47**, 372 (2003).

300. Van den Abbeele, P., Van de Wiele, T., Verstraete, W. & Possemiers, S. The host selects mucosal and luminal associations of coevolved gut microorganisms: a novel concept. *FEMS Microbiol Rev* **35**, 681-704 (2011).

301. Duncan, S.H., Hold, G.L., Harmsen, H.J., Stewart, C.S. & Flint, H.J. Growth requirements and fermentation products of *Fusobacterium prausnitzii*, and a proposal to reclassify it as *Faecalibacterium prausnitzii* gen. nov., comb. nov. *Int J Syst Evol Microbiol* **52**, 2141-2146 (2002).

302. Swidsinski, A., Loening-Baucke, V., Verstraelen, H., Osowska, S. & Doerffel, Y. Biostructure of fecal microbiota in healthy subjects and patients with chronic idiopathic diarrhea. *Gastroenterology* **135**, 568-579 (2008).

303. Khan, M.T., Duncan, S.H., Stams, A.J., van Dijl, J.M., Flint, H.J. & Harmsen, H.J. The gut anaerobe *Faecalibacterium prausnitzii* uses an extracellular electron shuttle to grow at oxic-anoxic interphases. *ISME J* **6**, 1578-1585 (2012).

304. Partridge, J.D., Scott, C., Tang, Y., Poole, R.K. & Green, J. Escherichia coli transcriptome dynamics during the transition from anaerobic to aerobic conditions. *J Biol Chem* **281**, 27806-27815 (2006).

305. Hochachka, P.W. & Mommsen, T.P. Protons and anaerobiosis. *Science* **219**, 1391-1397 (1983).

306. Wheaton, W.W. & Chandel, N.S. Hypoxia. 2. Hypoxia regulates cellular metabolism. *Am J Physiol Cell Physiol* **300**, C385-393 (2011).

307. Repetto, G., del Peso, A. & Zurita, J.L. Neutral red uptake assay for the estimation of cell viability/cytotoxicity. *Nat Protoc* **3**, 1125-1131 (2008).

308. Reyes, F.J., Centelles, J.J., Lupiáñez, J.A. & Cascante, M. (2α,3β)-2,3-Dihydroxyolean-12-en-28-oic acid, a new natural triterpene from Olea europea, induces caspase dependent apoptosis selectively in colon adenocarcinoma cells. *FEBS Lett* **580**, 6302-6310 (2006).

309. Adnan, H., Quach, H., MacIntosh, K., Antenos, M. & Kirby, G.M. Low levels of GSTA1 expression are required for Caco-2 cell proliferation. *PLoS ONE* **7**, e51739 (2012).

310. Furuse, M., Furuse, K., Sasaki, H. & Tsukita, S. Conversion of zonulae occludentes from tight to leaky strand type by introducing claudin-2 into Madin-Darby canine kidney I cells. *J Cell Biol* **153**, 263-272 (2001).

311. Madara, J.L., Barenberg, D. & Carlson, S. Effects of cytochalasin D on occluding junctions of intestinal absorptive cells: further evidence that the cytoskeleton may influence paracellular permeability and junctional charge selectivity. *J Cell Biol* **102**, 2125-2136 (1986).

312. Unno, N., Menconi, M.J., Salzman, A.L., Smith, M., Hagen, S., Ge, Y., Ezzell, R.M. & Fink, M.P. Hyperpermeability and ATP depletion induced by chronic hypoxia or glycolytic inhibition in Caco-2BBe monolayers. *Am J Physiol* **270**, G1010-1021 (1996).

313. Shifflett, D.E., Clayburgh, D.R., Koutsouris, A., Turner, J.R. & Hecht, G.A. Enteropathogenic *E. coli* disrupts tight junction barrier function and structure in vivo. *Lab Invest* **85**, 1308-1324 (2005).

314. Clayburgh, D.R., Barrett, T.A., Tang, Y., Meddings, J.B., Van Eldik, L.J., Watterson, D.M., Clarke, L.L., Mrsny, R.J. & Turner, J.R. Epithelial myosin light chain kinase-dependent barrier dysfunction mediates T cell activation-induced diarrhea in vivo. *J Clin Invest* **115**, 2702-2715 (2005).

315. Ivanov, A.I., Nusrat, A. & Parkos, C.A. Endocytosis of epithelial apical junctional proteins by a clathrin-mediated pathway into a unique storage compartment. *Mol Biol Cell* **15**, 176-188 (2004).

316. Bruewer, M., Utech, M., Ivanov, A.I., Hopkins, A.M., Parkos, C.A. & Nusrat, A. Interferon-gamma induces internalization of epithelial tight junction proteins via a macropinocytosis-like process. *FASEB J* **19**, 923-933 (2005).

317. Saito, H., Motohashi, H., Mukai, M. & Inui, K. Cloning and characterization of a pH-sensing regulatory factor that modulates transport activity of the human H+/peptide cotransporter, PEPT1. *Biochem Biophys Res Commun* **237**, 577-582 (1997).

318. Hidalgo, I.J. & Borchardt, R.T. Transport of bile acids in a human intestinal epithelial cell line, Caco-2. *Biochim Biophys Acta* **1035**, 97-103 (1990).

319. Lampen, A., Bader, A., Bestmann, T., Winkler, M., Witte, L. & Borlak, J.T. Catalytic activities, protein- and mRNA-expression of cytochrome P450 isoenzymes in intestinal cell lines. *Xenobiotica* **28**, 429-441 (1998).

320. Baranczyk-Kuzma, A., Garren, J.A., Hidalgo, I.J. & Borchardt, R.T. Substrate specificity and some properties of phenol sulfotransferase from human intestinal Caco-2 cells. *Life Sci* **49**, 1197-1206 (1991).

321. Huin, C., Schohn, H., Hatier, R., Bentejac, M., Antunes, L., Plenat, F., Bugaut, M. & Dauca, M. Expression of peroxisome proliferator-activated receptors alpha and gamma in differentiating human colon carcinoma Caco-2 cells. *Biol Cell* **94**, 15-27 (2002).

322. Shimakura, J., Terada, T., Saito, H., Katsura, T. & Inui, K. Induction of intestinal peptide transporter 1 expression during fasting is mediated via peroxisome proliferator-activated receptor alpha. *Am J Physiol Gastrointest Liver Physiol* **291**, G851-856 (2006).

323. Brahimi-Horn, M.C. & Pouyssegur, J. Hypoxia in cancer cell metabolism and pH regulation. *Essays Biochem* **43**, 165-178 (2007).

324. Kuhlicke, J., Frick, J.S., Morote-Garcia, J.C., Rosenberger, P. & Eltzschig, H.K. Hypoxia inducible factor (HIF)-1 coordinates induction of Toll-like receptors TLR2 and TLR6 during hypoxia. *PLoS ONE* **2**, e1364 (2007).

325. Small intestine structure (2005) Retrieved 21 December 2012, from http://science.kennesaw.edu/~jdirnber/Bio2108/Lecture/LecPhysio/41-19-SmallIntestStruct-AL.gif

326. Babu, M.M. Introduction to microarray data analysis in *Computational Genomics: Theory and Application*. (ed. R.P. Grant) 225-249 (Horizon Bioscience, 2004).

327. Smyth, G.K. Linear models and empirical bayes methods for assessing differential expression in microarray experiments. *Stat Appl Genet Mol Biol* **3**, Article3 (2004).

328. Falcon, S. & Gentleman, R. Using GOstats to test gene lists for GO term association. *Bioinformatics* **23**, 257-258 (2007).

329. Kanehisa, M. & Goto, S. KEGG: kyoto encyclopedia of genes and genomes. *Nucleic Acids Res* **28**, 27-30 (2000).

330. Trachootham, D., Lu, W., Ogasawara, M.A., Nilsa, R.D. & Huang, P. Redox regulation of cell survival. *Antioxid Redox Signal* **10**, 1343-1374 (2008).

331. Sermeus, A. & Michiels, C. Reciprocal influence of the p53 and the hypoxic pathways. *Cell Death Dis* **2**, e164 (2011).

332. Schofield, C.J. & Ratcliffe, P.J. Oxygen sensing by HIF hydroxylases. *Nat Rev Mol Cell Biol* **5**, 343-354 (2004).

333. Manalo, D.J., Rowan, A., Lavoie, T., Natarajan, L., Kelly, B.D., Ye, S.Q., Garcia, J.G. & Semenza, G.L. Transcriptional regulation of vascular endothelial cell responses to hypoxia by HIF-1. *Blood* **105**, 659-669 (2005).

334. Zhang, H. & Issekutz, A.C. Down-modulation of monocyte transendothelial migration and endothelial adhesion molecule expression by fibroblast growth factor: reversal by the anti-angiogenic agent SU6668. *Am J Pathol* **160**, 2219-2230 (2002).

335. Martin, R., Lahlil, R., Damert, A., Miquerol, L., Nagy, A., Keller, G. & Hoang, T. SCL interacts with VEGF to suppress apoptosis at the onset of hematopoiesis. *Development* **131**, 693-702 (2004).

336. Aryee, D.N., Niedan, S., Kauer, M., Schwentner, R., Bennani-Baiti, I.M., Ban, J., Muehlbacher, K., Kreppel, M., Walker, R.L., Meltzer, P., Poremba, C., Kofler, R. & Kovar, H. in Cancer Research, Vol. 70 4015-4023 (2010).

337. Moncayo, H.E., Penz-Koza, A., Marth, C., Gastl, G., Herold, M. & Moncayo, R. Vascular endothelial growth factor in serum and in the follicular fluid of patients undergoing hormonal stimulation for in-vitro fertilization. *Hum Reprod* **13**, 3310-3314 (1998).

338. Anasti, J.N., Kalantaridou, S.N., Kimzey, L.M., George, M. & Nelson, L.M. Human follicle fluid vascular endothelial growth factor concentrations are correlated with luteinization in spontaneously developing follicles. *Hum Reprod* **13**, 1144-1147 (1998).

339. Guzy, R.D. & Schumacker, P.T. Oxygen sensing by mitochondria at complex III: the paradox of increased reactive oxygen species during hypoxia. *Exp Physiol* **91**, 807-819 (2006).

340. Miyata, T., Takizawa, S. & van Ypersele de Strihou, C. Hypoxia. 1. Intracellular sensors for oxygen and oxidative stress: novel therapeutic targets. *Am J Physiol Cell Physiol* **300**, C226-231 (2011).

341. Baud, V. & Karin, M. Signal transduction by tumor necrosis factor and its relatives. *Trends Cell Biol* **11**, 372-377 (2001).

342. Cairns, R.A., Harris, I.S. & Mak, T.W. Regulation of cancer cell metabolism. *Nat Rev Cancer* **11**, 85-95 (2011).

343. Fischer, S., Reinel, A., Wiesnet, M., Renz, D. & Schaper, W. Effect of hypoxia on the expression of tight junction proteins in endothelial and epithelial cells. *J Physiol* **539P**, 92P (2002).

344. John, L.J., Fromm, M. & Schulzke, J.D. Epithelial barriers in intestinal inflammation. *Antioxid Redox Signal* **15**, 1255-1270 (2011).

345. Taylor, C.T., Fueki, N., Agah, A., Hershberg, R.M. & Colgan, S.P. Critical role of cAMP response element binding protein expression in hypoxia-elicited induction of epithelial tumor necrosis factor-alpha. *J Biol Chem* **274**, 19447-19454 (1999).

346. Haddad, J.J. Antioxidant and prooxidant mechanisms in the regulation of redox(y)-sensitive transcription factors. *Cell Signal* **14**, 879-897 (2002).

347. Turnbaugh, P.J., Ley, R.E., Hamady, M., Fraser-Liggett, C.M., Knight, R. & Gordon, J.I. The human microbiome project. *Nature* **449**, 804-810 (2007).

348. Moore, W.E. & Moore, L.H. Intestinal floras of populations that have a high risk of colon cancer. *Appl Environ Microbiol* **61**, 3202-3207 (1995).

349. Cato, E.P., Salmon, C.W. & Moore, W. *Fusobacterium prausnitzii* (Hauduroy et al.) Moore and Holdeman: emended description and designation of neotype strain. *Int J Syst Bacteriol* **24**, 225-229 (1974).

350. Swidsinski, A., Loening-Baucke, V., Vaneechoutte, M. & Doerffel, Y. Active Crohn's disease and ulcerative colitis can be specifically diagnosed and monitored based on the biostructure of the fecal flora. *Inflamm Bowel Dis* **14**, 147-161 (2008).

351. Sokol, H., Seksik, P., Furet, J.P., Firmesse, O., Nion-Larmurier, I., Beaugerie, L., Cosnes, J., Corthier, G., Marteau, P. & Dore, J. Low counts of *Faecalibacterium prausnitzii* in colitis microbiota. *Inflamm Bowel Dis* **15**, 1183-1189 (2009).

352. Saito, H. & Miura, K.I. Preparation of Transforming Deoxyribonucleic Acid by Phenol Treatment. *Biochim Biophys Acta* **72**, 619-629 (1963).

353. Zhang, Z., Schwartz, S., Wagner, L. & Miller, W. A greedy algorithm for aligning DNA sequences. *J Comput Biol* **7**, 203-214 (2000).

354. Lane, D.J. 16S/23S rRNA sequencing in *Nucleic Acid Techniques in Bacterial Systematics*. (eds. E. Stackebrandt & M. Goodfellow) 115-175 (John Wiley & Son Ltd, New York; 1991).

355. Yang, Y.H. & Speed, T. Design issues for cDNA microarray experiments. *Nat Rev Genet* **3**, 579-588 (2002).

356. Oliveros, J.C. VENNY. An interactive tool for comparing lists with Venn Diagrams. *http://bioinfogp.cnb.csic.es/tools/venny/index.html*. (2007).

357. Tibshirani, R., Hastie, T., Narasimhan, B. & Chu, G. Diagnosis of multiple cancer types by shrunken centroids of gene expression. *Proc Natl Acad Sci U S A* **99**, 6567-6572 (2002).

358. O'Flaherty, S. & Klaenhammer, T.R. Influence of exposure time on gene expression by human intestinal epithelial cells exposed to *Lactobacillus acidophilus*. *Appl Environ Microbiol* **78**, 5028-5032 (2012).

359. Gill, H.S., Rutherfurd, K.J., Prasad, J. & Gopal, P.K. Enhancement of natural and acquired immunity by *Lactobacillus rhamnosus* (HN001), *Lactobacillus acidophilus* (HN017) and *Bifidobacterium lactis* (HN019). *Br J Nutr* **83**, 167-176 (2000).

360. Medzhitov, R. Toll-like receptors and innate immunity. *Nat Rev Immunol* **1**, 135-145 (2001).

361. Krishnan, J., Selvarajoo, K., Tsuchiya, M., Lee, G. & Choi, S. Toll-like receptor signal transduction. *Exp Mol Med* **39**, 421-438 (2007).

362. Di Sabatino, A., Morera, R., Ciccocioppo, R., Cazzola, P., Gotti, S., Tinozzi, F.P., Tinozzi, S. & Corazza, G.R. Oral butyrate for mildly to moderately active Crohn's disease. *Aliment Pharmacol Ther* **22**, 789-794 (2005).

363. Place, R.F., Noonan, E.J. & Giardina, C. HDAC inhibition prevents NF-kappa B activation by suppressing proteasome activity: down-regulation of proteasome subunit expression stabilizes I kappa B alpha. *Biochem Pharmacol* **70**, 394-406 (2005).

364. Lopez-Siles, M., Khan, T.M., Duncan, S.H., Harmsen, H.J., Garcia-Gil, L.J. & Flint, H.J. Cultured representatives of two major phylogroups of human colonic *Faecalibacterium prausnitzii* can utilize pectin, uronic acids, and host-derived substrates for growth. *Appl Environ Microbiol* **78**, 420-428 (2012).

365. Khan, M.T., Browne, W.R., van Dijl, J.M. & Harmsen, H.J. How can *Faecalibacterium prausnitzii* employ riboflavin for extracellular electron transfer? *Antioxid Redox Signal* **17**, 1433-1440 (2012).

366. Tsukita, S., Furuse, M. & Itoh, M. Multifunctional strands in tight junctions. *Nat Rev Mol Cell Biol* **2**, 285-293 (2001).

367. Sung, J.H., Yu, J., Luo, D., Shuler, M.L. & March, J.C. Microscale 3-D hydrogel scaffold for biomimetic gastrointestinal (GI) tract model. *Lab Chip* **11**, 389-392 (2011).

368. Kim, J., Hegde, M. & Jayaraman, A. Co-culture of epithelial cells and bacteria for investigating host-pathogen interactions. *Lab Chip* **10**, 43-50 (2010).

369. Kim, H.J., Huh, D., Hamilton, G. & Ingber, D.E. Human gut-on-a-chip inhabited by microbial flora that experiences intestinal peristalsis-like motions and flow. *Lab Chip* **20**, 20 (2012).

370. Baker, M. Tissue models: a living system on a chip. *Nature* **471**, 661-665 (2011).

371. Hayeshi, R., Hilgendorf, C., Artursson, P., Augustijns, P., Brodin, B., Dehertogh, P., Fisher, K., Fossati, L., Hovenkamp, E., Korjamo, T., Masungi, C., Maubon, N., Mols, R., Mullertz, A., Monkkonen, J., O'Driscoll, C., Oppers-Tiemissen, H.M., Ragnarsson, E.G., Rooseboom, M. & Ungell, A.L. Comparison of drug transporter gene expression and functionality in Caco-2 cells from 10 different laboratories. *Eur J Pharm Sci* **35**, 383-396 (2008).

372. Elshal, M.F. & McCoy, J.P. Multiplex bead array assays: Performance evaluation and comparison of sensitivity to ELISA. *Methods* **38**, 317-323 (2006).

373. Yan, F., Cao, H., Cover, T.L., Whitehead, R., Washington, M.K. & Polk, D.B. Soluble proteins produced by probiotic bacteria regulate intestinal epithelial cell survival and growth. *Gastroenterology* **132**, 562-575 (2007).

374. Lee, C.A. & Falkow, S. The ability of Salmonella to enter mammalian cells is affected by bacterial growth state. *Proc Natl Acad Sci U S A* **87**, 4304-4308 (1990).

375. Willis, A.T. Anaerobic culture methods in *Anaerobic Microbiology A Practical Approach*. (ed. P.N. Levett) 1-12 (IRL Press at Oxford University Press, New York; 1991).

376. Johansson, M.E., Phillipson, M., Petersson, J., Velcich, A., Holm, L. & Hansson, G.C. The inner of the two Muc2 mucin-dependent mucus layers in colon is devoid of bacteria. *Proc Natl Acad Sci U S A* **105**, 15064-15069 (2008).

377. Winne, D. Rat jejunum perfused in situ: effect of perfusion rate and intraluminal radius on absorption rate and effective unstirred layer thickness. *Naunyn Schmiedebergs Arch Pharmacol* **307**, 265-274 (1979).

378. Madara, J.L. & Trier, J.S. Functional Morphology of the Mucosa of the Small Intestine in *Physiology of the Gastrointestinal Tract*, Edn. 2nd Ed. (ed. R. Johnson) 1209-1249 (Raven Press, New York; 1987).

379. Butler, M., Ng, C.Y., van Heel, D.A., Lombardi, G., Lechler, R., Playford, R.J. & Ghosh, S. Modulation of dendritic cell phenotype and function in an in vitro model of the intestinal epithelium. *Eur J Immunol* **36**, 864-874 (2006).

380. Iuchi, S. & Weiner, L. Cellular and molecular physiology of Escherichia coli in the adaptation to aerobic environments. *J Biochem* **120**, 1055-1063 (1996).

381. Musken, A., Bielaszewska, M., Greune, L., Schweppe, C.H., Muthing, J., Schmidt, H., Schmidt, M.A., Karch, H. & Zhang, W. Anaerobic conditions promote expression of Sfp fimbriae and adherence of sorbitol-fermenting enterohemorrhagic Escherichia coli O157:NM to human intestinal epithelial cells. *Appl Environ Microbiol* **74**, 1087-1093 (2008).

382. Gilman, J. & Cashman, K.D. The effect of probiotic bacteria on transepithelial calcium transport and calcium uptake in human intestinal-like Caco-2 cells. *Curr Issues Intest Microbiol* **7**, 1-5 (2006).